IAEA TECDOC SERIES

Spent Fuel Performance Assessment and Research

Final Report of a Coordinated Research Project on Spent Fuel Performance Assessment and Research (SPAR-III) 2009–2014

IAEA
International Atomic Energy Agency

SPENT FUEL PERFORMANCE ASSESSMENT AND RESEARCH

The following States are Members of the International Atomic Energy Agency:

AFGHANISTAN	GERMANY	OMAN
ALBANIA	GHANA	PAKISTAN
ALGERIA	GREECE	PALAU
ANGOLA	GUATEMALA	PANAMA
ARGENTINA	GUYANA	PAPUA NEW GUINEA
ARMENIA	HAITI	PARAGUAY
AUSTRALIA	HOLY SEE	PERU
AUSTRIA	HONDURAS	PHILIPPINES
AZERBAIJAN	HUNGARY	POLAND
BAHAMAS	ICELAND	PORTUGAL
BAHRAIN	INDIA	QATAR
BANGLADESH	INDONESIA	REPUBLIC OF MOLDOVA
BELARUS	IRAN, ISLAMIC REPUBLIC OF	ROMANIA
BELGIUM	IRAQ	RUSSIAN FEDERATION
BELIZE	IRELAND	RWANDA
BENIN	ISRAEL	SAN MARINO
BOLIVIA, PLURINATIONAL STATE OF	ITALY	SAUDI ARABIA
	JAMAICA	SENEGAL
BOSNIA AND HERZEGOVINA	JAPAN	SERBIA
BOTSWANA	JORDAN	SEYCHELLES
BRAZIL	KAZAKHSTAN	SIERRA LEONE
BRUNEI DARUSSALAM	KENYA	SINGAPORE
BULGARIA	KOREA, REPUBLIC OF	SLOVAKIA
BURKINA FASO	KUWAIT	SLOVENIA
BURUNDI	KYRGYZSTAN	SOUTH AFRICA
CAMBODIA	LAO PEOPLE'S DEMOCRATIC REPUBLIC	SPAIN
CAMEROON		SRI LANKA
CANADA	LATVIA	SUDAN
CENTRAL AFRICAN REPUBLIC	LEBANON	SWAZILAND
	LESOTHO	SWEDEN
CHAD	LIBERIA	SWITZERLAND
CHILE	LIBYA	SYRIAN ARAB REPUBLIC
CHINA	LIECHTENSTEIN	TAJIKISTAN
COLOMBIA	LITHUANIA	THAILAND
CONGO	LUXEMBOURG	THE FORMER YUGOSLAV REPUBLIC OF MACEDONIA
COSTA RICA	MADAGASCAR	
CÔTE D'IVOIRE	MALAWI	TOGO
CROATIA	MALAYSIA	TRINIDAD AND TOBAGO
CUBA	MALI	TUNISIA
CYPRUS	MALTA	TURKEY
CZECH REPUBLIC	MARSHALL ISLANDS	UGANDA
DEMOCRATIC REPUBLIC OF THE CONGO	MAURITANIA	UKRAINE
	MAURITIUS	UNITED ARAB EMIRATES
DENMARK	MEXICO	UNITED KINGDOM OF GREAT BRITAIN AND NORTHERN IRELAND
DJIBOUTI	MONACO	
DOMINICA	MONGOLIA	
DOMINICAN REPUBLIC	MONTENEGRO	UNITED REPUBLIC OF TANZANIA
ECUADOR	MOROCCO	
EGYPT	MOZAMBIQUE	UNITED STATES OF AMERICA
EL SALVADOR	MYANMAR	URUGUAY
ERITREA	NAMIBIA	UZBEKISTAN
ESTONIA	NEPAL	VANUATU
ETHIOPIA	NETHERLANDS	VENEZUELA, BOLIVARIAN REPUBLIC OF
FIJI	NEW ZEALAND	
FINLAND	NICARAGUA	VIET NAM
FRANCE	NIGER	YEMEN
GABON	NIGERIA	ZAMBIA
GEORGIA	NORWAY	ZIMBABWE

The Agency's Statute was approved on 23 October 1956 by the Conference on the Statute of the IAEA held at United Nations Headquarters, New York; it entered into force on 29 July 1957. The Headquarters of the Agency are situated in Vienna. Its principal objective is "to accelerate and enlarge the contribution of atomic energy to peace, health and prosperity throughout the world".

IAEA-TECDOC-1771

SPENT FUEL PERFORMANCE ASSESSMENT AND RESEARCH

FINAL REPORT OF A COORDINATED RESEARCH PROJECT ON SPENT FUEL PERFORMANCE ASSESSMENT AND RESEARCH (SPAR-III) 2009–2014

INTERNATIONAL ATOMIC ENERGY AGENCY
VIENNA, 2015

FOREWORD

At the beginning of 2014, there were 437 nuclear power reactors in operation and 72 reactors under construction. To date, around 370 500 t (HM) (tonnes of heavy metal) of spent fuel have been discharged from reactors, and approximately 253 700 t (HM) are stored at various storage facilities. Although wet storage at reactor sites still dominates, the amount of spent fuel being transferred to dry storage technologies has increased significantly since 2005. For example, around 28% of the total fuel inventory in the United States of America is now in dry storage.

Although the licensing for the construction of geological disposal facilities is under way in Finland, France and Sweden, the first facility is not expected to be available until 2025 and for most States with major nuclear programmes not for several decades afterwards. Spent fuel is currently accumulating at around 7000 t (HM) per year worldwide. The net result is that the duration of spent fuel storage has increased beyond what was originally foreseen. In order to demonstrate the safety of both spent fuel and the storage system, a good understanding of the processes that might cause deterioration is required.

To address this, the IAEA continued the Coordinated Research Project (CRP) on Spent Fuel Performance Assessment and Research (SPAR-III) in 2009 to evaluate fuel and materials performance under wet and dry storage and to assess the impact of interim storage on associated spent fuel management activities (such as handling and transport). This has been achieved through: evaluating surveillance and monitoring programmes of spent fuel and storage facilities; collecting and exchanging relevant experience of spent fuel storage and the impact on associated spent fuel management activities; facilitating the transfer of knowledge by documenting the technical basis for spent fuel storage; creating synergy among research projects of the participating Member States; and developing the capability to assess the impact of potential deterioration mechanisms on spent fuel and storage components.

This publication is based on results obtained in the participating Member States. A draft was prepared and discussed during the last research coordination meeting, held in Busan, Republic of Korea, 4–8 November 2013. This publication provides an overview of the technical issues related to spent fuel wet and dry storage and summarizes the objectives and major findings of the research carried out within the framework of the CRP.

EDITORIAL NOTE

CONTENTS

1. INTRODUCTION AND OBJECTIVES

Spent fuel storage is an interim step in the back end of the nuclear fuel cycle. The duration of this interim step is very much related to the back end of the fuel cycle policy that has been adopted by the Member State. For Member States opting for a once through fuel cycle policy, the reality is that there are no spent fuel disposal facilities currently available. The first geological disposal facility is expected to be operational by 2025, but it will be several decades before geologic repositories become available in all major nuclear countries. For those operating a fuel cycle policy involving reprocessing, storage of spent enrich uranium fuel (<5% ^{235}U) can be relatively short in duration. However, when the reprocessed plutonium and uranium are recycled, storage of spent mixed oxide (MOX) fuel will likely extend for several decades.

The nuclear power plant (NPP) operating environment has continued to move in the direction of ever increasing efficiencies, in particular through higher fuel burnups. Such developments have reduced the amount of spent nuclear fuel (SNF) being produced, but have put a greater burden on the SNF storage system; as a result, innovative approaches are necessary to meet this challenge, either through dry or wet storage. Higher burnup fuel results in greater decay heat, increased cladding corrosion and higher fission gas release leading to increased duty for the cladding (defects, stress, etc.). Higher fuel decay heat also impacts reprocessing operations and geological disposal. In the case of geological disposal, the fuel may have to be stored for long periods of time to ensure that thermal loading on the materials in the engineered and natural barriers systems will remain below thermal design limits. Under several expected scenarios, fuel cooled for 100 years or more may be required.

In terms of zirconium alloy clad fuels, higher fuel burnup leads to increased hydrogen pickup in fuel cladding. Due to the higher residual heat in these fuels, there is potential for the circumferentially aligned zirconium hydride platelets to re-orientate in the radial direction during dry storage (including accompanying operations, such as vacuum drying) and transportation (including re-wetting after transportation). Cladding mechanical properties changes induced by hydride reorientation could lead, especially in the lower temperature range, to a loss of ductility when the fuel rods are subjected to pinch loading forces. The investigation of hydrogen behaviour in spent zirconium alloy clad fuels and its impact on cladding mechanical properties are just two of the areas of research, which have been ongoing in Member States to improve the understanding of the processes that can impact long term spent fuel performance under dry storage conditions.

The International Atomic Energy Agency (IAEA) Spent Fuel Performance Assessment and Research (SPAR) Coordinated Research Project (CRP) is one vehicle where research and development to improve the understanding of both spent fuel and storage system behaviour over the long term is being discussed and reported by Member States.

This publication builds on a previous phase of the IAEA SPAR CRP identified as SPAR-II. In turns, the SPAR CRPs are a continuation of the previous BEFAST-I to III (BEhaviour of spent Fuel Assemblies in STorage) CRPs.

The overall objectives of the SPAR-III CRP were to develop a technical knowledge base on long term storage of power reactor spent fuel through evaluation of operating experience and research by participating Member States, and to extrapolate predictions of spent fuel behaviour over long periods of time. Specific research objectives included:

- Fuel and materials performance evaluation under wet and dry storage, and assessment of impact of interim storage on associated spent fuel management activities (like handling and transport);
- Surveillance and monitoring programmes of spent fuel storage facilities as one of the means to evaluate spent fuel performance during storage;
- Collection and exchange of relevant experience of spent fuel storage and the impact on associated spent fuel management activities;
- Facilitate transfer of knowledge by documenting technical basis for spent fuel storage;
- Creating a synergy among research projects of the participating Member States;
- Develop capability to assess the impact of potential deterioration mechanisms on spent fuel and storage components.

The third phase of the IAEA Spent Fuel Performance Assessment and Research (SPAR-III) CRP (2009–2014) involved the European Commission as well as 13 other organizations from 11 countries: Argentina, France, Germany, Hungary, Japan (2), Republic of Korea, Slovakia, Spain, Switzerland, United Kingdom (UK), and United States of America (USA, 2). Switzerland and the UK participated in the programme as active observers. Three research coordination meetings were held during the course of the SPAR-III CRP: the first in November 2010 in Tokyo, Japan; the second in May 2012 in Charlotte, USA; and the third in November 2013 in Busan, Republic of Korea.

The purpose of this document is to update the technical basis for the long term storage of power reactor spent fuel. This has been achieved through reporting the latest findings from participating Members States on:

- Information on fuel and materials performance evaluation under wet and dry storage;
- Information on monitoring programmes of spent fuel and storage systems;
- Information on spent fuel storage experience of the participating countries;
- Sub-chapters on areas of topical interest;
- A summary of CRP research activities.

This document with those previously published [1–2] provide the technical knowledge base for the long term storage of power reactor spent fuel; i.e. the overall objective for the CRPs. The specific objectives for this CRP, as out-lined above, were all met.

It is also brought to the attention of the reader that since the completion of SPAR-II CRP a new IAEA safety guide on the storage of spent nuclear fuel has been issued [3].

2. HISTORY OF THE BEFAST AND SPAR COORDINATED RESEARCH PROGRAMMES

The first phase of the BEFAST project (1981–1986) involved 12 organizations from 11 countries: Austria, Canada, Czechoslovakia (CSSR), Finland, Federal Republic of Germany (FRG), German Democratic Republic (GDR), Hungary, Japan, Sweden, USA, and USSR. A subsequent programme, 'BEFAST-II, Behaviour of Spent Fuel and Storage Facility Components during Long-term Storage' implemented during the years 1986–1991, involved organizations from 12 countries: (Argentina, Canada, FRG, Finland, GDR, Hungary, Italy, Republic of Korea, Japan, UK, USA, and USSR). BEFAST-III, implemented during the years 1991–1996 involved 15 organizations from 12 countries: (Canada, Finland, France, Germany, Hungary, Japan, Republic of Korea, Russian Federation, Slovakia, Spain, UK and USA). There was also an observer from Sweden.

During the three BEFAST Coordinated Research Projects (CRPs), the participating countries contributed their R&D results on fundamental questions of spent fuel storage. The reports from the BEFAST CRPs have been published as IAEA TECDOCs [4–6].

Towards the end of the BEFAST-III project, it became apparent that the R&D component of the project was decreasing steadily; more emphasis was being placed on the operation and implementation of storage technology. The storage technology (particularly dry storage) was undergoing a rapid evolution: new fuel and material design changes were coming on stream and target fuel burnup were steadily increasing. With the increased burnup came higher fission gas and fission product inventories, increased sheath (cladding) strains and increased cladding oxidation and hydriding. Because of all the new parameters that surfaced during the course of BEFAST-III, a subsequent project was proposed to address the effects of these new parameters on long-term storage and to determine their consequences on disposal.

The first phase of the IAEA Spent Fuel Performance Assessment and Research (SPAR) CRP (1997–2002) involved 11 organizations from 10 countries: Canada (2), France, Germany, Hungary, Japan, Republic of Korea, Russian Federation, Spain, Sweden, UK, and USA. Sweden participated in the project as an observer [1]. The second phase of the IAEA Spent Fuel Performance Assessment and Research (SPAR-II) CRP (2004–2008) involved the European Commission as well as 13 other organizations from 12 countries: Argentina, Canada, France, Germany, Hungary, Japan (2), Republic of Korea (only for a limited period), Slovakia, Spain, Sweden, UK, and USA. Sweden and the UK participated in the project as active observers [2].

The major topics for both wet and dry storage during all six CRPs are summarized in Table 1. It provides a record of the shift in emphasis between the various phases of the project between 1981 and 2014.

TABLE 1. RESEARCH SUBJECTS IN THE CRPs

Long-term behaviour	B-I	B-II	B-III	SPAR I	SPAR-II	SPAR-III	Surveillance	B-I	B-II	B-III	SPAR I	SPAR-II	SPAR-III	Facilities & Operation	B-I	B-II	B-III	SPAR I	SPAR-II	SPAR-III
Material aspect (cladding and components)	X	X	X	X	X	X	Monitoring; - Wet + Dry - Environment - Components - Fuel assemblies - Workers' dose rate		X	X	X	X	X	Capacity enhancement - High density racks - Re-racking - Double tiering - Doped coolant - Rod consolidation		X			X	
Degradation mechanisms and models	X	X	X	X	X	X	Fuel conditions - Operational - Fabrication - Technology - Defected fuel rods and assemblies	X	X	X	X	X	X	Changing modes Wet – dry		X	X	X	X	X
Validation - Experiment - Experience		X	X	X	X	X	Different reactor types	X	X	X	X	X	X	Handling of heavily damaged fuel		X	X	X	X	X
														System performance	X	X	X	X	X	

3. EXAMPLES OF NATIONAL SPENT FUEL MANAGEMENT STRATEGIES OF SPAR PARTICIPANTS

3.1. ARGENTINA

There are two operational NPPs in Argentina which supply about 8% of the total power generated in the country. The first one, Atucha 1 (CNA-1), a SIEMENS-KWU PHWR prototype, has been in operation since 1974. The other, Embalse (CNE), is a CANDU 600 pressure tube type Canadian reactor that started operations in 1984.

In Argentina, spent fuel is considered as a potential energy source. Spent fuel is either stored at reactor (AR) wet or away from reactor (AFR) dry storage pending the outcome of the National Radioactive Waste Management Programme (PNGRR); being delivered by the Comisión Nacional de Energía Atómica (CNEA). The NPP operators retain the responsibility for safe storage of spent fuel storage at the NPP site until it is transferred to the PNGRR after NPP shutdown.

At Atucha 1 NPP, spent fuel is stored in pools. The plant has two pool houses, the first was built with the plant (two pools) and a second house added in 1982 (four pools). At the present time, there are 9600 spent fuels in wet storage.

The end of life of Atucha 1 NPP is expected to be in 2019, but assuming the continuity of the present load factor (80%), the wet storage capacity will be exhausted in 2015. It is then proposed to provide additional storage capacity by the provision of a dry storage installation. At present, two proposals for the construction of an Atucha 1 dry storage installation exist: one proposed by the CNEA (responsible of the decommissioning of the plant), and the other by Nucleoeléctrica Argentina Sociedad Anónima (NA-SA); the utility owner of the plants. The conceptual design proposed by CNEA is adapted from the so called NUHOMS System (Nuteck Horizontal Modular Storage) that was developed and is presently used for both PWR and BWR type SF. The conceptual design proposed by NA-SA is based on the dry storage system implemented by Ontario Power Generation for their CANDU type SF.

Embalse NPP spent fuel is initially stored in an Atomic Energy of Canada Limited (AECL) designed concrete epoxy coated storage pool with a capacity for 44 688 fuel bundles (30% of the projected lifetime arisings). Additional storage capacity has been provided based on the AECL dry silo technology. The installation is modular and 184 silos have been built providing a total capacity for 99 360 fuel bundles.

The spent fuel is transferred to the dry silos after 6–8 years of cooling. Spent fuel is loaded to the storage baskets under water. Baskets holding 60 fuel bundles are transferred to a cell where they are dried and transported to a silo. After that, the basket is covered with a hood and welded hermetically. The silos are cylindrical metal container (tubes) imbedded in concrete that works as a biological shielding.

The programme for the construction of a geological repository is mostly linked to the decommissioning of the NPPs. It is considered that this repository should be in operation in the year 2050. At present geological studies for the repository location are being carried out, but the schedule is tentative and depends on economic, political and social issues.

3.2. FRANCE

France is a country in which reprocessing of spent nuclear fuel has been chosen for the back-end policy and has henceforth less need of interim storage systems. This has been confirmed in the national plan included in the new radioactive waste management law passed in June 2006. In order to reduce the radioactive waste stream and to recycle nuclear material, the reprocessing route for spent nuclear fuels in France is confirmed.

Spent fuel including MOX spent fuel from Électricité de France (EDF) NPPs is transported to La Hague reprocessing facility. There, spent fuel assemblies are unloaded from transport casks and stored in the La Hague pools for cooling before being reprocessed. The 6 pools of La Hague represent a capacity of 18 000 t(HM) of spent fuel, including 14 000 t(HM) for EDF.

3.3. GERMANY

In Germany, the approach of spent fuel management has changed completely; up to 1994 the Atomic Energy Act included the requirement of reusing the fissile material in the spent fuel. With the amendment of the Atomic Energy Act in 1994 the option of a direct disposal of spent fuel into a final repository became legally equal to the reprocessing scenario. Since 1 July 2005, delivery of spent fuel from power reactors for the purposes of reprocessing has been prohibited in accordance with an amendment to the Atomic Energy Act in 2002. Consequently, the direct disposal of existing spent fuel, and that to be generated in future, is now the only available option in Germany.

With regard to direct disposal, depending on the availability of a repository and the length of time required for heat generation to decay until disposal, it is projected that several decades of interim storage will be required to bridge the gap. The Federal Government's concept envisages that in future spent fuel is without exception to be placed in interim storage at the reactor sites where it is generated. Interim storage at the site means that spent fuel transportations will be avoided until its disposal in a repository. Decentralised interim storage facilities for spent fuel have been licensed under atomic law, constructed and commissioned at twelve sites with nuclear power plants. They are designed as dry storage facilities in which transport and storage casks loaded with spent fuel are emplaced. It was demonstrated and confirmed in the licensing procedure that the casks are suitable for at least 40 years of storage; the licenses limit the storage period correspondingly starting with the emplacement of the first cask. An extension of the storage period requires an authorisation.

3.4. HUNGARY

The Act CXVI on Atomic Energy (Act) adopted by the Parliament on December 10, 1996 expresses the national policy in the application of atomic energy. It regulates the various aspects of radioactive waste management. Among other items, this Act declares the priority of safety; defines the tasks of the national authorities; and prescribes the establishment of a central nuclear financial fund for financing the disposal of radioactive waste, the storage and disposal of spent fuel, and the decommissioning of nuclear facilities.

The work on research, development and demonstration for deep geological disposal of spent fuel and high level, or long lived radioactive waste has started.

The current situation in Hungary can be summarized as follows:

- 4 Units of Paks nuclear power plants in operation;
- Nuclear power supplies about 40% of the country's electricity production;
- Some spent fuel was shipped back to the Soviet Union (later Russia) between 1989 and 1998;
- A modular vault dry storage (MVDS) facility was commissioned, presently it has 20 vaults for 9308 FAs (approx. 1120 t(HM));
- Extension of the MVDS with a further 4 vaults starts this year;
- Preparation of arrangements plans, technical plans, and licensing documentation for an underground research laboratory for HLW disposal is in progress.

3.5. JAPAN

There were 54 commercial nuclear power units in Japan before the accident (March 11, 2011). After the accident at units 1–4 of the Fukushima Daiichi NPP, belonging to Tokyo Electric Power Company (TEPCO), the four units had been moved to the decommissioning stage in April 2012 and the activities along 'Roadmap towards Restoration from the Accident at Fukushima Daiichi Nuclear Power Station' are being carried out for early resolution to the accident. Additionally, units 5 and 6 were also moved to the decommissioning stage in January 2014. Thus, as of March 2014, there are 48 commercial nuclear power units (24 BWRs, 24 PWRs) and two BWRs are under construction. All the nuclear power plants are temporarily shut down whilst safety reviews are carried out to the new safety regulations.

Each site has spent fuel storage pools. The total amount of spent fuels stored at these sites was 14 340 t(HM) as of September 2013. The total controlled capacity, which excludes full core and reserve capacity, available for spent fuel storage at LWR NPP sites is about 20 640 t(HM).

3.6. REPUBLIC OF KOREA

In the Republic of Korea, there are 23 operational reactors and 5 under construction. All reactors are located at NPP sites of Kori, Ulchin, Wolsong and Yonggwang. There are 4 PHWRs and the remainder are PWR type.

The spent fuel management policy adopted back in 2004 was to store all fuel on the reactor site until 2016 and then to move it to interim storage. The Republic of Korea has since adopted consent based process for spent nuclear fuel management. The long term options to be decided by the process are whether to direct disposal, pyroprocess or adopt overseas recycling. In the interim a site or sites will be chosen for interim spent fuel storage.

3.7. SLOVAKIA

Slovakia has 4 operational and 2 shut down nuclear reactors of the WWER–440 type. Four units are installed in Jaslovské Bohunice (EBO 1–4, called NPP V1 and NPP V2) and two of them at Mochovce (SE-EMO 1-2). The reactor units at NPP V1 are shut down and all the spent fuel has been removed; EBO 1 was shut down on 31. 12. 2006 and EBO 2 on 31. 12. 2008.

The basic policy for spent fuel and radioactive waste management is derived from the Slovak Government resolutions numbers 930/1992, 190/1994, 5/2001 and 328/2008; which details the strategy for the back end of the fuel cycle. A closed fuel cycle in Slovakia is not deemed feasible at the present time as the WWER-400 reactors are not licensed to utilise MOX. Spent

fuel is therefore, short-term stored AR for 3–7 years before transfer to an independent spent fuel storage facility (ISFSF) at Jaslovské Bohunice site for long term storage; storage until 2047 is planned. Currently there is no ISFSF at Mochovce and fuel from units 1 and 2 is being transported to Jaslovské Bohunice. The intention is to provide a dry ISFSF at Mochovce site by 2017. The longer term goal is to construct a deep geological repository for spent fuel and highly active waste. This aside Slovak policy does not exclude an international or regional solution and looks to developments in spent fuel management.

3.8. SPAIN

There are 8 operating NPPs in six sites in Spain: Santa María de Garoña, Almaraz I and II, Ascó I and II, Cofrentes, Vandellós II and Trillo. Two other NPPs are currently undergoing decommissioning and dismantling; José Cabrera and Vandellós I. The spent fuel managed in Spain comes from the operation of these reactors, except from Vandellos I (a GCR whose fuel was sent for reprocessing). Most of spent fuel (~13 000 fuel assemblies) is kept in pools, all of which have been already reracked, so dry storage facilities have been implemented at some sites.

In December 2013, twenty three (23) dual purpose casks (483 fuel assemblies) are housed in the dry cask storage facility at the Trillo NPP site. Twelve (12) storage casks (377 fuel assemblies in total) are placed in the dry cask storage facility at the José Cabrera NPP site. Finally, two (2) storage casks (64 fuel assemblies) are placed in the dry cask storage facility at the Ascó NPP site.

The site for a centralized modular vault storage facility (ATC) was selected in December 2011 and is expected to be commissioned in 2017. The design life basis is a 100 years and a capacity of ~20 000 assemblies (~7000 t(U), i.e. 40 years of NPP operations); according to the Spanish General Radioactive Waste Plan. The Spanish SPAR-III research plans address high burnup fuel, burnup credit for transportation, hydrogen behaviour in fuel cladding and dry storage operational experience.

3.9. SWITZERLAND

In Switzerland, there are 5 operating NPPs on four sites: Beznau 1 and 2, Gösgen, Leibstadt and Mühleberg. Two sites operate PWR type reactors (either Westinghouse 2 loop or KWU 'Pre-Konvoi' 3 loop design) and the remainder operate BWR type reactors (either GE BWR 6 or 4 designs). Until 2006 spent nuclear fuel generated in Switzerland was sent for reprocessing (1139 t(HM)). Separated plutonium is recycled in the PWR reactors at up to 40% core loading. Nuclear generated power currently constitutes 36% of Swiss consumption.

AFR spent fuel storage facilities in Switzerland comprise the centralized dry store ZWILAG at Würenlingen, which accommodates both spent fuel and highly active waste, ZWIBEZ dry store located at the Beznau NPP site and the External Pool at Gösgen NPP. At the end of December 2013 around 580 PWR and 1890 BWR fuel assemblies were stored in dry storage casks and around 150 PWR fuel assemblies were stored in the external pool storage of NPP Gösgen.

In 2011, following the accident at Fukushima Daiichi NPP a decision was taken in Switzerland to phase out nuclear energy. The phase-out will be undertaken stepwise and the nuclear power will be in operation as long as they fulfil safety requirements. The Federal Council's energy strategy is to stabilize electricity consumption by 2015 and then to slightly reduce consumption. This will be achieved through saving electricity and energy efficiencies.

The deficit from removing nuclear power generation is to be made up through the expansion of hydropower and renewable energy, the potential provision of gas fired combined cycle power plants, and an expansion of electricity grids and connection to the European 'super grid'.

3.10. UNITED KINGDOM

In the UK, there are three basic types of nuclear power plant in operation; gas cooled reactor with natural uranium, magnesium non-oxidising clad fuel – 'MAGNOX Reactor', gas cooled reactor with enriched uranium oxide, stainless steel clad fuel – 'Advanced Gas Reactor (AGR)' and one Pressurised Water Reactor (PWR).

The Nuclear Decommissioning Authority (NDA) was established in April 2005, (under the Energy Act 2004) to take strategic responsibility for the UK's nuclear legacy). At the time the NDA was formed it was the Government's policy that decisions on spent fuel management strategy are a matter of commercial judgement of fuel owner (in effect, the NDA and EdF Energy Nuclear Generation Ltd.), subject to compliance with regulatory requirements [7]. However, subsequent developments of Government policy state that new nuclear power stations that might be built in the UK should proceed on the basis that spent fuel will not be reprocessed and any proposals for future spent fuel reprocessing would be subject to Government agreement and public consultation [8].

The decision on the back end policy adopted for spent fuel management is up to the fuel owners. The policies adopted prior to 2004 for individual fuel types were:

— MAGNOX (British Nuclear Group Sellafield Limited):
- Closed cycle (MAGNOX fuel is programmed to be reprocessed by end 2017);
— PWR (British Energy):
- Open cycle (Long term storage at reactor pending direct disposal (>2075));
— AGR (Managed by British Nuclear Group Sellafield Limited on behalf of British Energy):
- Closed cycle (Reprocess AGR fuel by end 2018);
- Open cycle (Non-reprocessed AGR fuel will be stored wet in existing facilities (Thorp Receipt and Storage) pending direct disposal (>2075).

Since April 2005, the responsibility for the management of spent nuclear fuel at Sellafield, MAGNOX Reactor Stations, and former UKAEA sites has transferred to the NDA. The NDA is also responsible for management of spent AGR fuel arisings. EDF Energy is responsible for management of spent PWR fuel arising from the Sizewell B NPP.

In July 2012, the NDA published a review of the strategy for spent MAGNOX fuel [9].The preferred strategy is to reprocess all spent MAGNOX fuel. However, there is some uncertainty associated with being able to deliver this strategy, primarily due to the age of the MAGNOX reprocessing facility (now 50 years old). Therefore, a contingency option of interim dry storage prior to geological disposal is also identified for further development for deployment should the reprocessing capability be lost irreparably.

In November 2011, the NDA published its 'Oxide Fuels Credible Options' paper [10].The preferred option for managing oxide fuels in the UK, for which the NDA has liability, was published in June 2012 [11].This is to:

- Complete the reprocessing contracts in THORP for overseas LWR fuel and a proportion of the AGR inventory;
- Place the remaining AGR fuel, including any future arisings into interim storage pending a decision to dispose to a GDF.

PWR fuel from the Sizewell B NPP, is currently stored wet at the reactor awaiting future geological disposal. As the capacity of the storage pond is expected to be reached in 2015, EDF Energy applied for planning permission to build a dry fuel store (DFS). The go ahead to build the DFS was given on September 2012 and work started on building the store January 2013. Fuel will be stored in Holtec ventilated storage casks housed inside a building. The facility will be run under a staged safety case, with the initial safety case covering the first 20 years of operation; the design life of the facility is 100 years.

The process for selecting a site for a Geological Disposal Facility (GDF) is being led by the UK Government, whose approach (as published in 2008 following a public consultation) is based on voluntarism and partnership, starting with local communities expressing an interest, with no commitment, in entering discussions about the siting process [12]. Three local authorities in Cumbria expressed a formal interest to host a GDF and in January 2013 voted on whether to participate in detailed studies on the suitability of the area to site such a facility. Despite two borough councils voting in favour of participation, the county council voted against participation and therefore the existing site selection process in Cumbria has ceased. The government remains committed to the current policy for site selection but, has launched a public consultation from the experiences to date.

3.11. UNITED STATES OF AMERICA

An application for a construction license at the Yucca Mountain site was submitted by the United States Department of Energy (DoE) to the United States Nuclear Regulatory Commission (NRC) on June 3, 2008. This application was subsequently withdrawn by DoE. At the direction of the United States Secretary of State, a Blue Ribbon Commission (BRC) was formed to recommend a path forward for the back end of the fuel cycle. The BRC recommendations were finalized in January 2012 [13]. In January 2013, DoE proposed an action plan to implement the BRC recommendations [14]. At its core, DoE's strategy endorses a waste management system containing a pilot interim storage facility by 2021; a larger, full scale interim storage facility by 2025; and a geologic repository by 2048. Work on these goals is only in the nascent stage as congressional changes in the Nuclear Waste Policy Act of 1982 and its 1987 Amendment would be required before centralized interim storage facilities could be approved. As a result of efforts by a group of petitioners who took action against the NRC, the District of Columbia Circuit Court of Appeals issued on August 13, 2013 a writ of mandamus that directed the NRC to resume work on the Yucca Mountain license application until all funds available to the NRC for that purpose are exhausted. After soliciting views on how best to use the limited agency funds, the Commission directed staff on November 18, 2013 to complete and release the 'Yucca Mountain Safety Evaluation Report (SER)'. Completion of the SER is presently scheduled for January 2015.

With the halt to the Yucca Mountain repository, efforts have turned to the technical issues that faced interim storage and transportation (EST) for periods beyond 100 years. In approximately the 2011 time frame, the NRC, DOE, and others issued their evaluations of the data gaps [15–17] that needed to be filled to technically support this extended time frame. Subsequently it was concluded that a few of these gaps were also relevant to the initial license duration of up to 20 years and first renewal of up to 40 years. The parties working to resolve

these gaps such as NRC, DOE, Utilities, cask vendors, and NEI meet regularly under the umbrella of the Electric Power Research Institute (EPRI) Extended Storage Collaboration Program (ESCP) to review progress in obtaining solutions to the gaps. R&D programmes have been mostly driven by regulatory issues centred on management of high burnup fuel, specifically on extension of dry storage licenses beyond their initial 20 year duration.

Results from some of these R&D programmes are already apparent. For example, behaviour of high burnup fuel in dry storage is no longer considered to be an unresolved regulatory issue; however, there is presently a lack of consensus about the behaviour of high burnup fuel during transportation and its impact on safety. A major issue affecting storage, and to a lesser degree transportation, is the corrosion of non-stress relieved welds present in austenitic steel canisters. Those canisters are susceptible to environmentally assisted stress corrosion cracking, in particular from chlorides.

Work on the behaviour of high burnup fuel rods has included:

- Development of models to predict zirconium hydrides precipitation and reorientation in heavily corroded, high fluence zircaloy cladding;
- Definition of failure criteria for claddings with both circumferential and radial hydrides under handling or transportation accident conditions;
- Characterization of the dynamic loading on the fuel rods as a result of vibration during transport and impact loading during accidents;
- Development of better temperature models to support thermal histories used for fuel assembly components degradation assessment.

Results obtained so far indicate that high burnup spent fuel rods with zircaloy cladding can retain high resistance to severe load challenges such as the dynamic forces resulting from cask drop accidents. Mechanical properties of advanced zirconium based claddings are being investigated for conformance within the acceptable performance envelope of zircaloy claddings.

Work on resolution of the canister corrosion is proceeding on two fronts. The NRC, and the DoE Nuclear Energy Universities Programmes (NEUP) are conducting studies to determine the conditions under which chloride induced stress corrosion cracking (CISCC) initiates, and the rate at which cracks might propagate. The DOE, EPRI, utilities, and cask vendors are developing monitoring systems, and using them to inspect canisters to determine what conditions actually exist in the field.

4.   WET STORAGE

Pool storage in the SPAR-III countries accounts for around 90 000 t(HM) of spent fuel up to January 1, 2014. The largest quantities of spent fuel in wet storage reside in the US (~49 000 t(HM)) and Japan (~14 000 t(HM)). Most of the spent fuel is in facilities located at reactor (AR) sites. The largest away from reactor (AFR) wet storage facilities are in Japan, Slovakia, and Switzerland or are associated with the reprocessing sites of La Hague (France), Rokkasho (Japan), and Sellafield (United Kingdom).

The experience in wet storing spent nuclear fuel now spans ~57 years. Wet storage continues to dominate as the primary method for storing spent nuclear fuel; >80% of all spent fuel is wet stored. The benefits provided by this technology are mainly associated with cooling efficiency and shielding. Water also facilitates safeguards, fuel inspections/examination exercises, and through pool water analysis enables us to establish ongoing fuel clad integrity.

Wet storage at NPPs was originally designed as a short term measure for initial heat decay before transport to a reprocessing facility. For a variety of reasons there has been a deviation from the original design which has resulted in spent fuel being left in AR storage for many decades. For this reason it is important to continue monitoring ongoing spent fuel and storage facility integrity. In the case of later reactors and current new builds these have been designed with lifetime capacities.

Despite the emergence of dry storage technologies, AFR wet storage facilities are still being planned or have been deployed in a number of Member States. The latest safety features being incorporated into these new pools are out-lined section 4.1.2. (8). The deciding factors [18] used in the choice of a wet interim spent fuel store over dry for the new build at Hinkley Point C (UK) were:

- Heat load;
- Importance of future flexibility;
- Specifics of European power reactor (EPR) fuel handling design;
- Fuel quantities;
- Disposal optimisation;
- Project risks of delivering the facility on time.

Reactors have been burning MOX-fuel since the early 1970s. MOX experience covers some 37 reactors in Europe, 4 in Japan and one in the USA. Spent MOX behaviour in wet storage is similar to UO_2 fuel apart from the higher end of life neutron radiation levels and associated decay heat. For these reasons significantly longer wet storage is required to achieve the comparable radiation and decay heat levels of UO_2 spent fuel prior to further processing (interim dry storage, reprocessing or direct disposal).

4.1.   SPENT FUEL STORAGE EXPERIENCE

4.1.1.   General performance

For primary barrier or containment purposes, cladding corrosion is the factor of most interest in wet storage. However, retention of fuel assembly structure integrity also becomes a most important factor when retrieval is taken into consideration.

For zirconium alloy clad fuel, data exist for continuous pool storage of greater than 50 years. These data indicate cladding corrosion to be extremely low (1 x 10^{-6} μm·yr^{-1}) and, therefore, corrosion is not viewed to be a time limiting factor for prolonged wet spent fuel storage; even under poor pool chemistry conditions.

For stainless steel clad fuels, continuous storage experience of 32 years (LWR) and 38 years (AGR) exists. Although the general cladding corrosion rates for these fuels are significantly higher than for zirconium based alloys (at ~0.1 μm·yr^{-1}), general corrosion is not a time limiting factor for the storage durations currently envisaged (up to 100 years). For AGR fuel, particular attention to pool water chemistry is required as parts of the fuel stringer become sensitised during reactor operation.

Magnesium alloy clad fuel is particularly susceptible to cladding corrosion under wet storage conditions. Although a protective magnesium hydroxide film is initially formed, the presence of any aggressive ions in the water promotes the dissolution of the protective oxide film and leaves the cladding open to pitting attack. For this reason, MAGNOX fuel is stored in dosed pool water and storage duration tends to be limited; normally <5 years.

In general, wet storage of spent fuel only appears to be limited by adverse pool chemistry conditions or deterioration of the fuel storage pool structure. Other factors that may influence fuel removal from NPP pools are removal of long stored fuel to maintain pool capacity, or complete closure of the pool on economic grounds at the time of reactor shutdown. In these cases, one of several options may be considered: interim dry storage, transportation to a centralised storage facility, reprocessing, or direct disposal.

4.1.2. Wet storage experience in the participating countries

The following paragraphs provide examples of the application of wet storage in the countries participating in the CRP.

4.1.2.1. Argentina

Atucha 1: The average discharge rate for natural uranium fuel assemblies is 1.4 a day. The use of slightly enriched uranium (SEU), which facilitates an increase in fuel burnup, has reduced the rate of discharge to 0.7 fuel assemblies a day. The arising spent fuels are stored in water filled pools.

The dimensions of the pools are 5 m × 5 m × 17 m. These pools have two levels. The deeper level or level one is the first to be filled. For the pools of the House 1, both levels of the pools are fully occupied. Spent fuel is vertically suspended from a hanger. The present hangers are a modification to the original design, changed in 1982, when the pools of House 2 came into operation. This improvement allowed pool storage capacity to be increased.

There are two types of hangers:

- Singles have 28 'combs' and from each comb six fuels are suspended, thus, a single hanger has capacity for 168 fuel assemblies;
- Doubles have 56 'combs' and 5 fuels can be hung from each comb. Each double, therefore can accommodate 280 fuel assemblies.

The total weight of each fuel assembly plus a filler body (of 4 m long) is of 400 kg. The hangers are moved using a bridge. The capacity of the bridge in House 1 is 60 tons, and 80 tons for the one in House 2.

The water of the pools is pure demineralized water. The water is regularly controlled in order to detect fission products, UO_2, etc. In addition the ambient air is monitored in order to detect escape of gaseous fission products. The temperature of the water varies from 25–30°C. As the nuclear fuel of the reactor is natural uranium or slightly enriched (0.85%) uranium, the critically coefficient is low ($k_{eff} \leq 0.6$), due to this neutron absorbers are not used in the water of the pools.

The pools are made of concrete covered by stainless steel (standard DIN 1.4541, equivalent to the AISI 321 stabilized by Ti). The hangers and combs are made of Austenitic stainless steel (standard DIN 1.4550 stabilized by Nb). From the existing knowledge concerning the metals involved, if the purity of the water is maintained under the normal limits for nuclear installations (conductivity <1 $\mu S \cdot cm^{-1}$, ion concentration <1 ppm) and deposits in the bottom of the pools are avoided, the durability of the spent fuels in the Atucha 1 wet storage will surpass the expected operating period of the plant, i.e. >2020.

4.1.2.2. *Eastern European Countries (Hungary, Slovakia)*

Hungary has AR pools at each reactor, while Slovakia has an AFR wet storage facility (capacity 1694 t(HM) – 14 112 FAs) beside the AR pools.

The behaviour of the Zr1Nb clad WWER fuel in storage has been good. Over ~40 years' experience of wet stored fuel exists, there have been no known fuel cladding failures as a result of wet storage; under normal operating conditions.

Corrosion studies have been conducted on Zr1Nb alloy cladding specimen being cut from WWER spent fuel assemblies of different burnup and cooling times. Results showed that burnup has a much more significant influence on the cladding plasticity than storage duration.

For WWER–440 fuel, the measured oxide film thickness is distributed uniformly along the total cladding; its average value was 0.01 mm. In the location of the spacer grids, a local increase in the oxide film thickness was observed, with an additional value of 0.005 mm.

4.1.2.3. *France*

Before reprocessing in France, spent fuels are stored in medium term buffer storages. At La Hague facility, the fuels are stored in the pools. The total surface of the pools is 5500 m² and the depth of water is 9 m. Spent fuels are stored in special baskets designed for handling. There are 2 types of baskets that can accommodate either 4 PWR fuel assemblies or 16 BWR fuel assemblies. The geometry and presence of neutron poison materials are used in order to guarantee sub-criticality.

The advantage of wet storage are: first, the evacuation of residual heat of spent fuels, as water is a good heat transfer medium and the second, the protection of operators and visitors from radioactive material: water provides dose rate attenuation and containment.

In the pools at La Hague, the water is cooled by heat exchangers connected to a close cooling loop. The heat exchangers are submerged in the pools. The heat is dissipated by external dry cooling towers. The radiochemical properties of the pool water are controlled continuously by

anion/cation ion-exchangers (cartridge type mixed bed exchangers, ionic 'Nymphea' concept).

Over the past 30 years there has been no indication of failure or degradation of the stored spent nuclear fuel. Storage performance continues to be good.

4.1.2.4. Germany

The spent fuel unloaded from the reactor core are first stored in cooling ponds within the reactor building, generally for a period of five years. These ponds allow the required decay of activity and heat generation until the fuel is placed into a dual purpose cask for dry interim storage, and provides the operator with sufficient flexibility to operate the plant. The remaining fuel assemblies after the shutdown of the plant at Obrigheim in May 2005 are currently stored in a wet storage facility outside the reactor building. It is planned to transfer the spent fuel in dual purpose casks to the dry interim storage at Neckarwestheim site. In Germany, 4065 t(HM) spent fuel is stored in cooling ponds (including Obrigheim) (reporting date 31.12.2012). Wet storage technology has been used for zircaloy clad fuel since decades. No limiting effects have ever been found. This also holds for high burnup fuel with new corrosion resistant structural materials.

4.1.2.5. Japan

The total amount of spent fuels stored at these sites was approximately 14 340 t(HM) as of September 2013. The total controlled capacity, which excludes full core and reserve capacity, available for spent fuel storage at LWR NPP sites is about 20 640 t(HM). Due to the amount of spent fuel in storage approaching the controlled capacity at a number of NPPs, and to meet future demands, re-racking (AR), expansion or modification to common-use for two or more reactors has been undertaken. Additional measures include the installation of some dry storage casks at two reactor sites and the building of a new centralized dry store.

As of September 2013, 3370 t(U) of spent fuels [19] had been transported to the water pool of the Rokkasho Reprocessing Plant and about 425 t(U) of them were used in the test runs [20].

The main specifications of this facility are as follows:

— Maximum storage capacity:	1500 t(U) for BWR spent fuel and 1500 t(U) for PWR spent fuel
— Number of pools:	3 (1: exclusive-use for BWR fuels, 1: exclusive-use for PWR fuels, 1: common-use for both BWR/PWR fuels)
— Maximum fuel enrichment before irradiation for receipt :	5.0 wt%
— Conditions of receiving spent fuel:	Residual enrichment less than 3.5 wt%
— Cooling time:	Over 1 year before receipt
— Burnup:	55 GW·d·t(U)$^{-1}$ maximum, 45 GW·d·t(U)$^{-1}$ average

4.1.2.6. Spain

Spent fuel has been wet stored in Spain since 1970. In view of the forthcoming saturation of the capacity of these pools, the original storage racks were progressively replaced with more compact units during the 1990's (re-racking). All wet fuel storage is AR, and storage experience has been good. There have been minor issues with top nozzle degradation in early manufactured PWR fuel and, in one BWR NPP, one fuel element fell off onto the pool rack in 2009 while being inspected (INES-1 event). Moreover, there were some issues concerning rack neutron absorber degradation. All fuel assemblies in storage have been moved at least once, when the AR pools were re-racked. As of December 2013, around 13000 assemblies of spent fuel were stored at the NPP pools.

4.1.2.7. Switzerland

Wet storage in Switzerland is mostly associated with the five AR pools at the four NPP sites. There is, however, an AFR at Gösgen NPP, the External Pool, with an original design capacity for 1008 spent fuel assemblies. The decision to build a pool was based on safety, technical and cost aspects in comparison with a dry storage facility. This decision was influenced by the mix of spent fuels being generated by the Gösgen NPP, i.e. HBU oxide and MOX fuel, which would need to be stored for a long period before they could be accommodated into dry storage casks or sent to reprocessing.

The Gösgen External Pool is the first AFR wet storage facility to be designed with a passive cooling capability in normal operation and in the case of accidents; a 1 MW heat removal capability. The facility was also designed against airplane crash, to with stand a seismic event to 0.25 g horizontal and 0.125 g vertical accelerations, and to be stand alone when the power plant shuts down. To minimize induced vibrations as a result of an airline crash damping units have been installed below the fuel pool.

This first of its kind facility was commissioned in 2008 with its half storage capacity. After few years of operational experience and testing, the heat removal system and the racks for the second half its total capacity are being constructed. The storage capacity could be increased to 1056 fuel assembly positions and a total heat removal capability to 1.25 MW. Other improvements have been the addition of HEPA filters on the air intake system and UV lamps in the pool to avoid biological contamination. As a result of the European Stress Tests Peer Review, temperature and water level indicators have been back fitted into the plant control room and emergency control room.

4.1.2.8. United Kingdom

The wet storage of fuel discharged from MAGNOX and AGR NPPs can be conveniently divided into two phases. The first covers short term storage at the reactor and the second covers the further interim storage away from reactor at Sellafield, prior to reprocessing. The only exception to the above is EDF Energy Sizewell B PWR reactor, where all spent fuel is currently wet stored at reactor.

The experience of wet storing commercial spent nuclear fuel on the Sellafield site spans over 50 years. There are four operational AFR storage pools at Sellafield: Fuel Handling Plant (MAGNOX/AGR), AGR Storage Pond (AGR), LWR Storage Pond (LWR/PIE), and Thorp Receipt & Storage (LWR/AGR). These pools store fuel from the first and second generation UK reactors, MAGNOX and AGR, and also irradiated fuel from LWR reactors, mostly from Sellafield Ltd. overseas customers.

The main differences between fuel storage at Sellafield and other facilities are:

- Fuel storage is based upon containerised systems (MAGNOX and AGR containers, Multi-element bottles for LWR and PIE material):
  - Isolation of the fuel from the bulk pool water;
  - The chemistry within the container can be different from the bulk pool water;
  - The spread of corrosion products / soluble activity to the storage facility is minimised;
- A variety of pool water chemistries are utilised, depending on the properties of the fuel being stored;
- Apart from a limited programme of fuel re-bottling, there are no individual fuel element handling operations, during storage;
- The pools are purged with demineralised water and, where applicable, dosed with sodium hydroxide as a corrosion inhibitor; resultant effluent is either treated by the Site Ion Exchange Plant, or filtered and sentenced prior to sea discharge.

4.1.2.9. *United States of America*

Spent fuel storage experience from the civilian reactor programme spans some 45 years. Apart from the General Electric AFR Morris facility in Illinois, all wet storage is AR. The current storage capacity is around 60 000 t(HM). As of January 2014, 49 000 t(HM) were stored in the pools of the reactors, and 670 t(HM) was in the GE Morris facility.

In general, the performance of wet storage systems has been excellent, with only occasional operational problems or incidents. In particular, top nozzle separations in older PWR Westinghouse assemblies occurred at the North Anna, Millstone, Farley, and Prairie Island sites. The degradation mechanism was identified as intergranular stress corrosion cracking of sensitised 304 stainless steel. Design and materials changes were implemented in later designs and procedural controls or hardware fixes have been implemented for managing spent fuel assemblies that may be susceptible to nozzle separation [21].

4.1.3. Research activities relating to wet storage

4.1.3.1. *France*

In the event that spent MOX fuel is interim stored in France, a study has been undertaken by the Commissariat à l'énergie atomique et aux énergies alternatives (CEA) to investigate the evolution of the fuel in wet storage for the fault scenario of a clad breach [22].

The release fractions were studied for an irradiated MOX fuel sample by leaching the fuel in pure aerated water; with and without external gamma radiation. Both leaching experiments were undertaken under static conditions and the test duration was 14 days. For the sample evaluated in the absence of gamma radiation, uranium and plutonium concentrations in solution steadily increased with time and no steady state conditions were reached. The sample leached in the presence of radiation, on the other hand, was found to reach steady state conditions quickly.

In the second set of experiments the evolution of the fuel surface was characterised by Raman spectroscopy. The characterization was primarily performed to compare the oxidation of the plutonium rich aggregates with the UO_2 matrix under conditions of radiolytic oxidation. The characterized sample was leached for 3 months in pure aerated water in the presence of

gamma radiation. Over the duration of the analysis only alteration of the UO_2 matrix was observed. In this case studtite $(UO_2)O_2(H_2O)_4$ was identified on the surface of the UO_2 grains.

The overall conclusion from this study is that in the event of a MOX fuel clad breach the behaviour will be no worse than that observed for standard UO_2 spent fuel.

Post Fukushima the Institut de Radioprotection et de Sûreté Nucléire (IRSN) have studied loss of coolant accident in spent fuel storage. Their analysis considered: Fuel behaviour at high temperature and dry conditions; Validation of emergency response plans; Microstructural changes in the cladding; Stress–strain curves; Oxidation phenomena/kinetics.

4.1.3.2. Slovakia

The storage capacity at Bohunice (SFIS) has been increased from the original design limit of 5040 fuel assemblies to 14 112 by the introduction of new compact racks in the pools. The racks structural materials are: 08Ch18N10T stainless steel and AISI 304 + B type borated stainless steel (ATABOR). A comprehensive monitoring programme was prepared for the SFIS in 1999, which uses two systems for corrosion monitoring of SFIS structural materials:

- Corrosion monitoring system based on the principle of surveillance samples:
  - All specimens are made from original or archive materials;
  - Specimens are placed into the original environment;
  - Specimens are loaded with stresses similar or higher to the operational ones;
- Monitoring system based on the acoustic emission (pool lining only):
  - In each pool 6 sensors are installed and measurements are periodically performed by a portable measurement system;
  - Acquired data are archived and evaluated by modern mathematic methods and the obtained results are compared with the previous ones;
  - As yet no significant findings have been detected.

No significant corrosion attack has been found; further information is given in Section 8.1.1. The structural material used is stable in given standard conditions and it would be possible to extend the life of SFIS; if necessary.

4.1.3.3. United Kingdom

As reported [2], studies were initiated to evaluate alternative AGR fuel corrosion inhibitors to sodium hydroxide dosed demineralised pool water to pH 11.4. Sodium nitrate was taken forward for active testing with high burnup AGR brace materials to confirm its suitability for storage deployment. This showed that 10 ppm nitrate could inhibit IGA corrosion in the presence of 2 ppm chloride. Nitrate dosing was subsequently evaluated using a series of controlled studies on a limited number of storage containers containing AGR fuel but isolated from the bulk pool water. This showed that nitrate could inhibit propagating corrosion in trace levels of chloride and prevented initiation of corrosion in up to 0.8 ppm chloride. However, fuel exposed to 2 ppm chloride in water dosed with 10 ppm nitrate resulted in corrosion. It was subsequently decided to abandon the implementation of nitrate dosing on the basis of a lack of operational experience, some uncertainties in the ability of nitrate to absolutely arrest corrosion during the lead container studies, and concerns over promotion of algal blooms.

Dosing with sodium hydroxide to pH 9 (rather than the standard pH 11.4) has been identified as an alternative water chemistry that is protective to sensitized AGR cladding in wet storage

and compatible with aluminium components currently stored in the pool. This offers a number of advantages including the extensive experience of using sodium hydroxide in storage ponds at Sellafield, re-alkalisation of the concrete structure of the pool and is likely to limit any potential for algal growth. Sodium hydroxide (pH 9) has also been evaluated by lead container studies. These have demonstrated this pool water chemistry to be capable of inhibiting corrosion of sensitised AGR fuel cladding in 1 ppm chloride for over 800 days. The study has been extended to include containers with chloride concentrations up to 2.5 ppm in order to demonstrate the operational envelope. Implementation of this chemistry is planned for 2014, dependent upon final materials compatibility testing.

In support of the deployment of alternative storage chemistry for AGR in the Thorp, receipt and storage facility compatibility studies have also been undertaken for fuels which will be stored alongside AGR fuels. Immersion tests have been undertaken on irradiated zircaloy-4 clad specimens at 50°C in a variety of potential storage chemistries. Polished and oxide layer intact specimens were immersed in sodium hydroxide (pH 11.4), sodium nitrate (up to 50 ppm) and demineralised water. Sodium hydroxide and sodium nitrate solutions were made up with demineralised water. The duration of the tests were up to 1 year. Samples were removed at selected time intervals based on the previous results and analysed by weight loss and metallographic (SEM).

The results of the study were:

- Corrosion rates were below the limit of detection. The default resolution limit of the SEM at 50nm was therefore taken as the worst case rate of corrosion for all chemistries; i.e., 50 nm/yr;
- No spallation of the original ZrO_2 layer or localised corrosion was observed;
- No effects on the adherence thickness or morphology of the oxide layer by any of the chemistries could be concluded.

Further research related to Interim Wet Storage of AGR fuel is ongoing and includes a range of activities to complete the technical underpinning required to support a transition of the Thorp Receipt and Storage pools from a reprocessing buffer store to an AGR fuel Interim Storage facility. The scope of work covers:

- Thermal modelling of pool system and storage containers;
- Extending corrosion performance basis to higher normal operating temperature and to include loss of cooling scenario;
- Extending corrosion understanding to evolved fuel designs;
- Relating 20+ years' experience to actual fuel condition;
- Study of effects of failed fuel on drying/disposability;
- Development of fuel corrosion sensors and inspection techniques.

Work is also ongoing to demonstrate the feasibility of wet storing MAGNOX fuel beyond the currently accepted durations as a potential contingency for failure of the MAGNOX reprocessing facility [9].

4.1.3.4.   United States of America

The potential for terrorist acts resulting in a rapid loss of water from the spent fuel and uncontrolled reaction of zirconium based alloy components with air (zirconium fires) became a renewed concern after the September 11, 2001 events. Strategies for mitigating the impact

of an extended loss of pool cooling were eventually introduced. Work was performed at Sandia National Laboratories by the NRC in order to get a better handle on the potential for zirconium ignition and propagation in racks containing BWR fuels [23]. At the completion of the BWR fuel project a second one, this time directed at the behaviour of PWR fuels, was undertaken at Sandia National Laboratories under the auspices of the OECD Nuclear Energy Agency. The PWR project was completed in 2013 [24].

In addition, the NRC staff studied spent fuel pool safety at a reference BWR plant that is similar to the Fukushima Daiichi plant and conducted a regulatory evaluation that extended the results of the safety study to all US nuclear plants. The results of the study indicate that there is about a one in 10 million year chance that a severe earthquake would cause a radioactive release from a spent fuel pool at the site studied. The regulatory evaluation confirmed that these results would apply to all U.S. plants [25].

4.2. POOL WATER CHEMISTRY

The role of water in spent pool storage is to:

- Facilitate heat removal from the spent fuel;
- Act as a biological shield;
- Maintain fuel cladding integrity;
- Facilitate spent fuel visual inspection.

To achieve these goals, water quality has to be optimised for the fuel being stored. Water chemistry must also consider criticality control and microbial control. Factors that may be affected include water chemistry, water quality control, and water temperature.

Operating experience gained since the 1950's shows:

- The ingress of aggressive ions such as chloride should be minimised;
- Where pool water quality has been maintained, spent fuel storage performance for all types of fuel has been excellent;
- Optimum pool water chemistry is linked to the fuel being stored;
- In the case of stored defected fuel, there has been no evidence of defect deterioration or propagation during prolonged storage. The only exceptions have been cases of canned defected fuel where adverse environments have been established.

Apart from some experience with water logged or filled canned fuel, for example RBMK, the general experience with defected fuel is that the defect does not deteriorate or propagate during prolonged storage.

4.2.1. Water chemistry

The objectives of controlling water pool chemistry are to:

- Minimize corrosion of metal surfaces (e.g., fuel cladding, stainless steel pool liners, storage modules and handling tools);
- Minimize the concentration of radionuclides in the water, and as a result reduce radiation fields and airborne contaminants in the pool area;
- Maintain clarity of the pool water for ease of in-pool fuel handling.

Chemical specifications have been developed to monitor the quality of the water chemistry in the pools. Specifications are also used for application of corrective action levels in the case of deviation in the water chemistry.

The storage of MAGNOX fuels requires particular attention in controlling pool water chemistry. Although magnesium alloy cladding dissolves in pure water by the following reaction:

$$Mg + 2H_2O \rightarrow Mg(OH)_2 + H_2,$$
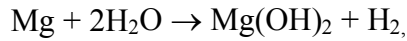
a passive/protective magnesium hydroxide film is formed. This protective film, however, is also susceptible to dissolution from acidic species dissolved in the water:

$$Mg(OH)_2 + 2H^+ \leftrightarrow Mg^{2+} + 2H_2O$$
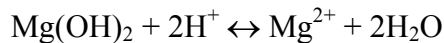
It is therefore important to minimise ions that would lead to cladding degradation; i.e., chloride, carbonate, and sulphate. To overcome these effects, MAGNOX fuel is stored in high purity caustic-dosed water to a minimum pH of 11.4. Away from reactors, these conditions are increased to pH 13.0 inside the storage containers. Fuel has been satisfactorily stored for up to 5 years at pH $\geq$11.4 by dosing with sodium hydroxide and keeping $[Cl^- + SO_4^{2-}] < 1$ mg·kg^{-1}.

Light water reactor fuels (PWR or BWR): apart from a very small amount of older stainless steel clad fuel (three NPPs), all LWR's use zircaloy cladding. Spent fuel is stored in open structures (such as racks or baskets used worldwide), or in sealed containers (such as the Multi Element Bottle used in UK). Water purity is controlled to suppress conditions that might lead to a corrosive environment for spent fuel cladding and structures.

The AR pools for PWR reactors are filled with borated water, while demineralised water is used for BWR reactors as well as for AFR wet storage installations serving both light water reactor types. Depending on the countries that operate LWRs, water chemistry for storage installations may be quite different. However, some general parameters can be defined; pH requirement is 4.5–5.5 and chloride and fluoride concentrations have to be limited to 0.1–0.15 ppm. In Japan, the pH requirement for BWR stations is 5.3–7.5; chloride and fluoride concentrations are limited to 0.5 ppm, while each operating value is generally maintained below 0.05 ppm.

For some storage pools that use Boraflex neutron poison material, the increasing concentration of silica may become a concern. The silica results from the degradation of the silicon rubber polymer and the release of crystalline silica present as filler material in the Boraflex.

Because pool water is evaporating due to decay heat, the boron concentration correspondingly increases in PWR facilities. As a result, measures are taken to bring the concentration back to the prescribed values.

WWER fuel with Zr1Nb alloy cladding is stored in borated water in the AR pools. Boric acid concentration is maintained within 12–16 g·kg^{-1}; concentrations of halides (Cl$^-$ and F$^-$) are kept below 0.1 μg·kg^{-1}; pH varies in the 4.3–6.5 range. AFR pools are filled with demineralised water. Halide concentrations are kept below 0.15 mg·kg^{-1}; pH values are within the 5.5–7.0 range.

4.2.2. Pool water activity

The main sources of pool water activity are from the leaching of activated corrosion products (commonly known as 'CRUD') adhered to the fuel, and from fuel or fission product species being released through cladding defects.

Water activity has to be maintained at a reasonably low level to limit dose to the operators and to minimise adsorption by in-pool structural components and ancillary equipment, as a means of facilitating final decommissioning activities.

4.3. SOURCES OF POOL WATER PARTICULATES

The main sources of suspended solids are from particulates associated with the flask if pool discharged, from crud dislodged from individual fuel assemblies, transfers to storage, movement of the fuel, or open fuel baskets in storage. Flask associated particulates include crud released from the fuel (thermal shock) when water is introduced to the flask internals, if shipped dry; dirt on the flask externals; and entrained particulates from the flask liner.

In the case of open storage bays, airborne particulates are also introduced.

4.3.1. Water treatment

Water treatment normally includes a mechanical treatment to remove the solid materials contained in the pool, in conjunction with a chemical treatment to extract both radioactive and non-radioactive chemical species dissolved in the pool water.

Mechanical treatment of the bulk pool water is generally performed by filters (pre-coated sand or mechanical), while chemical treatment is realised with ion exchangers (cationic and anionic resin types are used). In some cases, ion exchange is preceded by neutralisation. Generally only single bed organic ion exchange resins are regenerated when saturated. The resultant concentrate may include a boron recycling step, followed typically by evaporation and final encapsulation for disposal. Mixed bed filters and inorganic exchanger resins are also used. In these cases, there is no regeneration phase and the saturated beds are disposed of directly after encapsulation.

The build-up of particulates on the pool floor and walls is removed mechanically by in-pool cleaners. A variety of designs have been deployed from modified leisure pool cleaners, simple suction devices to purpose built two stage cleaners, coarse and fine (cyclone) filters.

In the case of ion exchange there are three types of systems in operation. These include: out of pool ion exchange columns, ion exchange floated on top of a pre-coated mechanical filter and in-pool water treatment units; examples of the latter include cartridge systems and the combined ion exchange/cooling Nymphea system (France).

Special attention is also required to avoid the growth of microbiological species that can reduce water clarity or even lead to microbial attack of storage materials. The main factors in limiting biological growth are to minimise the introduction of nutrients (especially phosphates), intensity of lighting in the storage area, and temperature.

Where bacterial growth does initiate, treatments have varied form the use of biocides to full scale mechanical cleaning and collection of the biogrowth. Operating pools at high pH also

prevents biological growth. Before using a biocide it is important to run materials compatibility checks.

4.3.2. Water temperature

Water temperature requirements may vary with the specific plant design and with the type of storage installation (AR or AFR). For AR pools, the temperature limits normally are about 45°C. For AFR storage installations, the spent fuel cooling time is greater and resultant pool water temperatures tend to be lower; <40°C in normal conditions.

Normal temperature limits are usually based on operating considerations, such as personnel occupation requirements and equipment operating limits, rather than fuel corrosion. Other considerations that make it preferable to operate pools at the lowest practicable temperature include lowering the release rate of radionuclides from defective fuels, minimising bacterial or microbial growth, and lowering the humidity level in the storage area.

In particular, the transfer of activity from the fuels to the storage water has been shown to double with each 7–10°C rise in temperature. It is, therefore, advantageous to keep pool water temperature as low as reasonably possible, thereby delaying release, and taking advantage of the decay of the activity while it is fixed to the fuel surface. The loading on the waste treatment systems becomes correspondingly lower [26].

Recently, modelling work has been under taken which adds support to a temperature dependent ^{137}Cs release rate. Caesium release rate was modelled in relation to temperature changes within the bulk pool water for a known inventory of leaking AGR fuel elements during the replacement of the pool cooling system.

This compares with previous data derived at CLAB; over the temperature range 28 to 36°C the activity level reached a new equilibrium 2.1 times higher, where the AGR activity release model predicts a 1.8 times increase in the ^{137}Cs release rate for the same temperature increase.

Alkali solutions, for example sodium or lithium hydroxide, are known to reduce activity release.

4.4. POOL COMPONENTS AND MATERIALS

The choice of pool components and materials is dependent upon the type of fuel being stored, cost, and to facilitate final pool decommissioning. The latter property has come to the fore as experience in both in-pool performance and final pool decommissioning has been gained. This has led in most cases to the almost exclusive usage of stainless steel for spent fuel storage structures, heat exchangers, piping and fuel handling equipment.

4.4.1. Pool lining

There are two main methods of treating the internals of the reinforced concrete pool structure to make it watertight, they are to line with welded sheets of stainless steel or to coat with a water resistant paint system.

All LWR AR storage pools are stainless steel lined, CANDU AR pools are stainless steel or epoxy lined, and MAGNOX pools use epoxy/paint lining. All AFR storage installations are stainless steel lined (France, Germany, Japan, Slovakia, Switzerland, USA), with the

exception of UK AFR storage pools where most are only lined at the wind/water line and the rest is painted.

To resolve the issue of epoxy/paint degradation in MAGNOX pools, alternative paint systems have been developed and deployed in the UK.

4.4.2. Storage racks

The designs/methods used for spent fuel pool storage can be fuel/facility type, and operator dependent. LWR AR fuel is typically stored in open top floor mounted borated stainless steel racks. In the case of AFR fuel interim storage, prior to reprocessing, the storage systems are designed to facilitate the bulk movement of fuel and as such tend to have a reduced capacity than can be achieved AR by the fixed high density rack systems. In the UK, the storage systems mainly comprise the basket used in transportation; i.e. the MAGNOX & AGR skips and the multi element bottle (LWR).

The materials of construction are primarily borated stainless steel, or stainless steel, in combination with a neutron absorbing material, metal matrix composites. One exception is the MAGNOX skip, where painted mild steel is used due to concerns with respect to the potential for electro-coupling between the fuel cladding and stainless steel. CANDU modules are also stainless steel, but not borated because of the lack of criticality concerns. The only other material that has found some use for structural components is aluminium; mainly for its corrosion resistance in deionised water; when passivated.

In Slovakia, the spent fuel is stored in compact storage canisters that contain 48 WWER fuel assemblies instead of the old baskets capable to hold 30 FA only. The neutron absorber in the canisters is made of boron alloyed stainless steel (ATABOR).

5. DRY STORAGE

5.1. INTRODUCTION

Around 40 years of favourable experience exists with the dry storage of spent power reactor fuel and about 50 years with the dry storage of research reactor fuel. Dry storage experience exists with fuel from a variety of reactor types (CANDU, HWR, PWR, BWR, WWER, MAGNOX and HTGR). Since its conception, dry storage of spent fuel has evolved into a wide variety of systems. Examples of these are concrete canisters (Argentina, Republic of Korea), metallic dual purpose casks (Germany, Japan, Spain, Switzerland, USA), steel lined concrete containers or casks and/or casks made of ductile cast iron (Germany, Japan, Spain, USA), and concrete vault like structures (France, Hungary, UK, USA) [27]. At the present time, almost all countries participating in SPAR-III (Argentina, France, Germany, Hungary, Japan, Republic of Korea, Spain, Switzerland, UK and the USA) are engaged in various dry storage technologies. Almost all participating countries are also actively pursuing a dry storage research and development programme. Based on the operating experience to date, the spent fuel examinations carried out so far, and the results of supporting research these indicate that fuel can be stored safely for many decades.

As regards licensing conditions for the dry storage facilities, different trends and licensing periods have been implemented throughout the SPAR countries as shown in the following Table 2.

TABLE 2. DRY STORAGE FACILITY LICENSING CONDITIONS IN VARIOUS MEMBER STATES

Member State	Initial licence period	Renewal period
Argentina	5 years[1]	5 years[1]
Germany	40 years	none
Hungary	10 years	10 years
Japan	Not limited	N/A
Spain	20 years	20 years
Switzerland	Not limited	N/A
United Kingdom	Not limited (covered under the reactor site licence)	N/A
USA	20 years	20 years[2]

---

[1] Part of the reactor license. The renewal period therefore, is the same as the reactor license.
[2] The first three Independent Spent Fuel Storage Installations (Surry, H.B. Robinson and Oconee) that applied for an extension to the original licensing periods received a 40 year renewal period. Rulemaking has changed the initial and renewal license periods to 40 years each.

Dry storage has become a mature technology and the quantities being placed into dry storage are increasing significantly. The inventory of spent fuel in dry storage in the above countries, up to 1 January 2014, was about 32 500 t(HM).

In the USA, as many of the spent fuel storage pools at or close to full capacity, dry storage is the major element in the utilities` spent fuel storage strategy. As of 1 January 2013, there are 56 dry storage facilities located at commercial reactor sites, with 18 000 t(HM) fuel in storage. Additionally about 2400 t(HM) is stored in casks at the Government sites.

In Germany, at present nine nuclear power reactors (7 PWR and 2 BWR) are in operation with a capacity of 12 696 MW(e) in total. Eight reactors with a total capacity of 8821 MW(e) were shut down on 6 August 2011 according to the 13th amendment of the Atomic Energy Act as a consequence of the events in Japan, which led to a reassessment of the risks associated with the use of nuclear energy. For seven of the eight reactors shut down in 2011 applications for decommissioning and dismantling have been made so far. These power plants are in a post operational phase until the grant of a decommissioning license has been obtained. For the remaining nine power plants in operation the operating licenses will expire between 2015 and 2022.

A helium storage environment is used in most dry storage systems. The exceptions are CANDU fuel, which is stored in dry air or helium, MAGNOX fuel, which is stored initially in carbon dioxide and then in air once the fuel has cooled (as is practiced in the core at shutdown reactors), and nitrogen which is used in the MVDS technologies deployed in Hungary and at Fort St. Vrain (USA).

Dry storage of spent LWR fuel in an inert atmosphere is licensed dependent on burnup and type of cask for temperatures up to 410°C in Germany, 400°C (and possibly higher than 400°C for low burnup fuel) in the USA and Spain [28–29]. Dry storage in nitrogen is licensed for a temperature of 410°C in Hungary for Zr1Nb clad fuel. In Germany no specific temperature for the licensing is required. The following two criteria should be met to exclude systematic fuel rod cladding failures during dry intermediate storage:

- The maximal tangential stress of the cladding shall not exceed a value of 120 MPa;
- The residual tangential strain of the cladding shall not exceed a value of 1% at the end of the intermediate dry storage period.

This leads in case of a fuel assembly with a burnup of 55 GW·d·t(HM)$^{-1}$ and a decay time of approx. Five years in the cooling pond to a temperature limitation of 360°C at the cladding surface.

Most of the fuel in dry storage is clad with a zirconium alloy (Zr2, Zr4, Zr2.5Nb and Zr1Nb); however, dry storage experience also exists for magnesium and aluminium clad fuels.

Average burnups of spent fuel presently in dry storage range from 4.5 to 33.5 GW d·t(HM)$^{-1}$, while the maximum burnups range from 7.5 to 55 GW d·t(HM)$^{-1}$. However, there is an almost universal tendency towards increasing the discharge burnup of the fuel elements. In Germany, for instance, average discharge burnups for PWR fuel assemblies have increased from 35 GW d·t(HM)$^{-1}$ in 1983 to 50 GW d·t(HM)$^{-1}$ in 1998, and a value of 65 GW d·t(HM)$^{-1}$ is achieved presently. In the USA and other SPAR countries, most of the spent fuel assemblies are being discharged with burnups in excess of 45 GW d·t(HM)$^{-1}$. Despite this, the majority

of dry storage systems are limited to a maximum fuel burnup between 45–65 GW d·t(HM)$^{-1}$; for LWR fuel.

5.2. DRY STORAGE STATUS AND EXPERIENCE

The amount of spent fuel in dry storage in SPAR CRP participating countries, up to 1st January 2014, is shown in Table 3.

5.2.1. Argentina

Argentina's dry storing spent fuel has been in concrete silos since 1993 at the Embalse NPP. To date 216 silos have been constructed and 191 were fully loaded as of the end May 2013. The deployed silo system is AECL designed and incorporates the standard features of 60 fuel bundles loaded into a welded basket, 9 baskets stacked in a re-enforced concrete vertical silo.

For the purpose of establishing the conditions inside the silos, the Autoridad Regulatoria Nuclear (ARN) requested that the silos were included in the Ageing Management Programme for Components and Systems of the Nuclear Power Plant Associated to Nuclear Safety.

TABLE 3. AMOUNT OF SPENT FUEL IN DRY STORAGE IN VARIOUS MEMBER STATES

Member States	t(HM) in dry storage (up to January 1, 2014)
Argentina	1949[3]
France	50
Germany	3482[4]
Hungary	922
Japan	340[5]
Republic of Korea	4500
Spain	360
Switzerland	450[6]
USA	20 400[7]

---

[3] As of June 2013.
[4] As of January 2013 the total amount of spent LWR fuel stored in the 12 decentralized on-site interim storage facilities and in the central facilities at Ahaus and Gorleben.
[5] JAPC and TEPCO facilities.
[6] In the central storages ZWIBEZ and ZWILAG, only fuel from NPPs.
[7] Government and commercial facilities as 1 January 2013.

The surveillance plan includes the monitoring of the condition of the silo, steel liner, and concrete structure. To supplement this ongoing monitoring programme, there is periodic measurement of aerosols, noble gas content and internal moisture of selected silos. Additionally there is external monitoring of the silos using TLD dosimeters; to establish if there are any changes in radiological conditions. To date no abnormalities have been observed.

A project is also at an advance stage for the emptying of the oldest fuel elements from the pools at Atucha I and to build a dry storage system; in order to achieve the projected end of life plan of 32 full power years for Atucha I. The project consists primarily of enlarging one of the two pool buildings at the station to enable spent fuel to be stored in vertical underground silos. Each silo will comprise of two storage units that containing 9 fuel elements each (18 fuel elements in each bin). This design allows for vertical storage of 2016 spent fuel elements (7 rows by 16 columns). The spent fuel elements will be transferred from the pool building to the dry storage building via a dedicated shield for lifting and transporting the spent fuel. To move the shield, the existing 60 ton capacity crane will be used. The operation time to emptying a complete pool will be approximately one year (1998 spent fuel elements). This conceptual design meets the basic principles of nuclear safety.

5.2.2. France

Dry storage has been developed in France at the CASCAD facility for spent fuel that does not require prompt reprocessing. As of 1 January 2014, approximately 50 t(HM) of heavy-water reactor fuel from the decommissioned EL4 Brennilis reactor had been stored in the vault at the CASCAD facility at Cadarache. The maximum capacity of the facility is about 100 t(HM). Spent fuel is canisterized at the reactor (within a dry cell). Canisters, vacuum dried and filled with helium, are transferred to the dry storage installation. Canisters are stored in storage wells ventilated by natural convection.

5.2.3. Germany

From June 30, 2005 the policy of spent fuel management was changed considerably as the re-use option of fissile material in spent fuel by means of reprocessing was abandoned by law. After that date any delivery of spent fuel to reprocessing plants abroad was prohibited. Therefore, direct disposal of spent fuel became the only option in practice in Germany today. The remaining and in future generated spent fuel in Germany has to be stored at on-site facilities until such time as a repository is commissioned. As a consequence, 12 dry decentralized on site interim storage facilities have been erected and taken into operation at the sites of the NPPs usually for a period of 40 years.

The Gorleben storage facility is the only licensed facility in Germany for the storage of vitrified high level radioactive waste (HAW) from the reprocessing of German spent fuel abroad. 108 casks with vitrified HAW waste transferred from France are already stored in the Gorleben interim storage facility.

The Ahaus facility is additionally licensed for the storage of transport and storage casks of the type CASTOR[®] THTR/AVR (Thorium High Temperature Reactor, Hamm-Uentrop) and MTR 2 (Material testing reactor).

As of 31.12.2012 the 12 decentralized on site interim storage facilities contain 3084 t(HM), the central interim storage facilities at Ahaus and Gorleben 92 t(HM) of LWR fuel assemblies filled in dual purpose casks. 583 t(HM) of WWER fuel assemblies from Rheinsberg and

Greifswald are stored in casks on the ZLN site. A total of 6675 t(HM) of spent fuel from the nuclear power plants have been shipped abroad, predominantly for reprocessing and only to a minor extent for permanent storage abroad. Up to now a total of approximately 1000 casks have been loaded and stored. Consequently, a great experience in loading, processing and dry storage of dual purpose casks, especially of the type CASTOR® V loaded with spent fuel of German nuclear power plants, has been gained. The accumulated time of cask operation is in the range of 12 000 years.

The leak tightness of each loaded cask during the intermediate storage period is verified by continuous pressure monitoring of the lid interspace. During the operating time from 1995 up to now no unallowable pressure drop in the inter lid space due to increased leakage rates of the lid sealing was detected. So far, all pressure drop notifications were caused by the auto supervision of the monitoring system.

Presently, a periodic safety reviewing is about to be applied to the interim storage facilities. In November 2010 the Nuclear Waste Management Commission (ESK) generated a draft of recommendations for the safety guidelines. Prior to their implementation, at first a two year review phase will have been finished, during which the performance of a periodic safety review for two selected interim storage facilities, Gorleben and Lingen, is being tested.

5.2.4. Hungary

A Modular Dry Vault Storage (MVDS) started operation at Paks to store spent WWER–440 fuel. The construction started in March 1995, the facility was commissioned in 1997 and the first vault containing 450 assemblies was fully loaded in 1997. Successive vaults have been filled since and further vaults have been added over the years; the facility is now licenced to build up to 33 vaults. The status at 1 January 2014, a total of 7748 assemblies were in the MVDS, which has 20 vaults constructed and further 5 vaults under construction.

5.2.5. Japan

Dry storage facilities were constructed at the Fukushima Daiichi Nuclear Power Station of Tokyo Electric Power Company (TEPCO) and the Tokai Daini Nuclear Power Station of Japan Atomic Power Company (JAPC).

The JAPC dry storage facility is a concrete building 54 m length × 26 m width × 21 m height, and has a capacity for 24 metal casks. The casks being used can hold 61 BWR fuel assemblies and are stored in a vertical position within the building. Operations commenced in 2001. As of November 2013, 160 t(HM) of spent fuel were stored in the building. The facility was not affected by the earthquake and resulting tsunami of 11th March 2011.

At the TEPCO site 80 t(HM), loaded into five large metal casks (capacity of 52 BWR fuel assemblies per cask) and four smaller metal casks (capacity of 37 BWR fuel assemblies per cask) were stored in a cask custody building (previously used as a buffer for transport casks to be sent overseas for reprocessing) before the earthquake on 11th March 2011.

During the tsunami a vast amount of seawater, sand and debris was deposited into the building which was located near to the sea. The nine casks after confirmation of the safety performance by the external appearance of the cask bodies were transported from the dry storage facility to the common pool at the site, and further inspections were carried out to confirm containment, sub-criticality and fuel integrity. After the investigation and

replacement of components such as metal lid gaskets, the casks have been moved to a new temporary cask custody area, located on higher ground, on the Fukushima Daiichi NPP site.

The new temporary cask custody area was approved by the Nuclear Regulation Authority of Japan (NRA) on 14 August 2013 under the 'Implementation Plans for the Fukushima Daiichi NPS designed as the Special Nuclear Power Facilities'. The plan was submitted by TEPCO on 7 December 2012. The new temporary cask custody area has a capacity for 50 casks. Casks are stored horizontally on a tied down support system on a concrete pad inside individual ventilated concrete box shielding. Transfer of spent fuels from the common pool to the temporary cask custody area commenced during 2013 to make space for spent fuels from the AR pools of units 1 to 4 to be received into the common pool. As of December 2013, 19 casks had been loaded using a combination of storage only and dual purpose casks of varying capacities and moved to the temporary cask storage facility. Future additions will be using DPC with a capacity for 69 BWR fuel assemblies.

Cask and fuel integrity inspections have been undertaken by both TEPCO and JAPC. TEPCO carried out the self-inspection on the cask at the Fukushima Daiichi site in 2000 and 2005 after five and ten years, and JAPC in 2009 after seven years of dry storage. The objectives of these inspections were to confirm the containment of the metal gasket and spent fuel integrity. As for the containment, visual inspection on the seal surface and gasket did not show abnormal condition on the cask at Tokai Daini site. The Fukushima Daiichi 2000 inspection, however, showed some colouring of part on the metal gasket surface used in the primary lid seal; this colouration had increased by the 2005 inspection. During the inspection in 2000, a white product on the surface was observed it was concluded that a reaction had taken place between the aluminium material of the gasket and residual water. In 2005, the white colouration changed resulted during immersion of the cask in the reactor pool for several days before opening the primary lid [30]. In the case of spent fuel integrity, no ^{85}Kr gas was detected by gas sampling of the cask cavity, and visual inspection of the fuel assembly surface did not show any abnormal condition.

5.2.6. Republic of Korea

All dry spent fuel storage facilities are located at the Wolsong NPP site and are associated with storing spent CANDU fuel from the four 600 MW(e) reactors. There are two dry storage system deployed. The first phase (1992—2010) comprises 300 AECL designed silo (concrete canister) systems which are identical to the ones operating at Pt. Lepreau station in Canada. The second phase (2010 onwards) comprises 7 MACSTOR/KN–400 which were designed specifically for Wolsong NPP due to limited available space and to increase the storage density over that provided by the concrete canisters. The new MACSTOR/KN–400 modules hold 400 fuel baskets in 4 rows of 10 storage cylinders providing a capacity for 24 000 bundles; i.e. 456 t(HM) of spent fuel. One module can store slightly more fuel than the entire annual spent fuel discharges at the Wolsong site.

5.2.7. Spain

Dual purpose (storage and transport) ENSA–DPT metal casks have been designed, licensed and manufactured to store spent fuel from the Trillo Nuclear Power Plant. Each cask, in a helium environment, can store 21 PWR fuel assemblies with a maximum burnup of 49 GW·d·t(HM)$^{-1}$, 4% initial enrichment and a minimum of 9 years cooling time. The initial cask licensed is for 20 years (storage mode) and 5 years (for transport). The first loading was in

2002. Currently, there are 23 ENSA–DPT casks in stored at the facility which has a total capacity for 80 casks.

At the Jose Cabrera NPP, steel-lined concrete storage casks (HI–STORM) have been designed, licensed and manufactured to store 377 fuel assemblies (26 of them classified as damaged) which are low burnup (<45 $GW \cdot d \cdot t(HM)^{-1}$) and low initial enrichment. The total inventory has been loaded into 12 HI–STORM modules.

Due to pool saturation, dry storage facilities have also been developed for the Ascó site and are in the process of being developed for the Santa María de Garoña site.

For Ascó I and Ascó II NPPs, the HI–STORM storage system been used. Currently, two HI–STORM modules holding 64 fuel assemblies each have been loaded. Although the storage license allows for fuel up to 55 $GW \cdot d \cdot t(HM)^{-1}$, 5% initial enrichment, with a minimum of 23 years cooling, in order to comply with the transport license, of the associated HI–STAR transport system, the storage containers have been loaded with low burnup fuel (<45 $GW \cdot d \cdot t(HM)^{-1}$).

At the Santa María de Garoña site, a metal dual purpose cask, the ENUN 52B, is being licensed which will be capable of holding 52 BWR low burnup fuel elements.

Spain is also developing a centralized storage facility (ATC). Site selection was completed in December 2011. The design is based on a modular vault storage system and it is expected to be commissioned in 2017. It targets a design life of 100 years and a capacity of ~20 000 assemblies (~7000 t(HM)). The basis is the total spent fuel inventory for 40 years of NPPs operation; as given in the Spanish General Radioactive Waste Plan.

5.2.8.   Switzerland

There are two operational dry storage facilities in Switzerland. The centralized store ZWILAG located at Würenlingen has been in operation since 2001 and was designed to accommodate 200 transport and storage casks i.e. TN97, TN52, TN24BH, TN81 and Castor. The facility also has access to an airplane crash resistant 'HotCell' to inspect or re-work casks if needed.

ZWIBEZ located at Beznau NPP started operations in 2008. As of December 2013 there are four transportation and storage casks TN24GB. High capacity storage cask type HI–STAR 180 is now being evaluated for future application. ZWIBEZ can accommodate up to 48 transport and storage casks.

5.2.9.   United Kingdom

The general experience with dry storage of MAGNOX fuel at Wylfa Power Station, since the 1970s, both in the short term CO_2 cooled stores and in the two longer term air filled stores, has been very good. As government policy is for all MAGNOX fuel to be reprocessed it is expected that the site will be defueled before 2020 [9].

At Sizewell B NPP the AR storage capacity is predicted to be full in 2015. To address the short-fall in storage capacity EDF Energy (now) have conducted an options study which recommended that dry storage in casks within a new building on the Sizewell B site was the consistently the most suitable solution for the circumstances facing the station [31].

Work on building the Sizewell B dry store commenced in January 2013 and it is expected to take 2 years to construct. Fuel will be stored in Holtec HI–STORM system using a double walled canister originally designed for use in the Ukraine.

5.2.10. United States of America

Most nuclear power plants in the USA were not originally designed with a pool storage capacity sufficient to accommodate the spent fuel generated over the operating life of the power plants. Utilities originally planned for spent fuel to remain in the spent fuel pool for a few years after discharge, and then to be sent to a reprocessing facility. Given that the reprocessing option was abandoned in 1977 and no other option for spent fuel disposition currently exists, utilities have expanded the storage capacity of their spent fuel pools by using high density storage racks. This has been a short term solution, however, given that most utilities have reached, or soon will reach, their spent fuel pool maximum storage capacity. Utilities have developed independent spent fuel storage installations (ISFSIs) as a means of expanding their on-site spent fuel storage capacity on an interim basis until a geologic repository is available to accept spent fuel for permanent storage. By the end of 2012, 60 independent dry spent fuel storage installations were operational. There was ~20 400 t(HM), or ~28 percent of the total spent fuel inventory of the country in dry storage at commercial and Government storage sites.

Dry storage beyond 20 years [32–34]–Virginia Electric Power Company (VEPCO) was the first licensee to apply for extending its Surry ISFSI license beyond twenty years. VEPCO, by then Dominion, submitted a license extension application in 2002. The initial approach was for VEPCO to request a 20 year license extension, but in a separate submittal, VEPCO requested consideration for an additional 20 years, i.e. for a licence extension of 40 years. The NRC issued, in February 2005, a favourable safety evaluation report granting a 40 year extension. The technical basis documenting (1) the absence of ageing mechanisms that would threaten the integrity of spent fuel in dry storage, and (2) the excellent performance of the storage system components was based on the results obtained in a joint NRC-EPRI-DOE project that consisted in re-opening a 15-year old CASTOR® V/21 dry storage system located at Idaho National Laboratory, and non-destructively and destructively examining its components and contents.

Later in 2005, Progress Energy, the H.B. Robinson ISFSI licensee, received a favourable safety evaluation report, also for a 40 year license extension. In May 2009, Duke Energy, the Oconee ISFSI licensee, was similarly granted a 40 year license extension. The combination of successful applications by the Surry, H.B. Robinson and Oconee ISFSIs is notable because they cover the range of dry storage technologies that have been implemented at the U.S. (and most worldwide) reactor sites.

Currently the NRC has received licence Renewal Amendments (LRAs) for the Calvert Cliffs and Prairie Island sites under site specific licenses, which are currently under consideration. The Prairie Island site uses TN40 and TN40HT directly loaded dual purpose casks. The LRA includes high burnup fuel. NRC also has a general LRA for the VSC-24 storage only cask that has a canister and is used at three different sites. These amendments are under current review.

The NRC has amended the 10 CFR Part 72 regulations concerning the initial and renewal license periods for Independent Spent Fuel Storage Installations (ISFSIs) and cask Certificate of Compliances. Now applicants can request 40 year initial and renewal terms if they can provide sufficient support that all safety regulations are met during the extended term.

Dry storage of spent fuel with burnup in excess of 45 GW·d·t(U)$^{-1}$ [35–36]–In November 2003, the NRC published Interim Staff Guidance 11 (ISG-11), Revision 3 "Cladding Considerations for the Transportation and Storage of Spent Fuel." This revision contained guidance and criteria applicable to all commercial spent fuel burnup levels and cladding materials, and enabled the placement in dry storage of all commercial fuel licensed by the NRC for power plant operations in a manner consistent with the regulations. This revision (1) clarified the meaning of some of the acceptance criteria, and (2) added criteria to allow higher temperature limits for low burnup fuels. However, it should be noted that contrary to the mention of "transportation" in the title of ISG-11, Revision 3 did not provide criteria for the transportation of high burnup (i.e., >45 GW·d·t(U)$^{-1}$ fuel).

A peak cladding temperature of 400°C is specified, unless it can be shown that cladding hoop stress are maintained below 90 MPa. For the latter, a higher peak cladding temperature may be calculated. This could be useful for spent fuel characterized by low to moderate burnups, benign fuel duty cycles, or both. There are also restrictions on thermally cycling the spent fuel when the temperature swings are greater than 65°C.

With publication of [35] the dry storage of high burnup fuel for 20 years is no longer considered a regulatory issue which merits further debated. The extended storage of high burnup fuel, however, is still a question being debated. In particular, there are unresolved issues with regard to the impact of dry storage on the transportability of the spent fuel after long periods of storage, in particular, with regard to the impact of potential changes in the distribution of hydrogen in the cladding as a result of the thermal transient that occurs as a result of the transfer of spent fuel from wet to dry storage and the subsequent slow cooling over many years (if not decades) of dry storage.

5.3. RESEARCH ACTIVITIES RELATED TO DRY STORAGE

Research activities relevant to dry storage have been carried out since the early 60s and have been reported in earlier BEFAST/SPAR projects [2–6] and elsewhere.

5.3.1. Argentina

See Section 5.2.

5.3.2. Germany

Dry storage was from the beginning a necessary element in the back end of the fuel cycle strategy of Germany. Therefore, an extended R&D programme was previously performed to define the conditions for safe storage of spent fuel under dry conditions and to develop performance prediction codes, which were validated in a demonstration programme using original spent fuel and representative storage casks.

The ongoing trend to increase the target burnup will be reflected by an increasing number of high burnup FAs which have to be transported after their long-term intermediate storage to their final destination. High burnup spent fuel assemblies are exposed to mechanic stress challenges especially in case of a hypothetical transportation accident. Potential effects of high burnup and the impact of cladding corrosion associated with increasing operational time in the reactor on the fuel rod resistance to failure have to be taken into account because a release of spent fuel into the cask is regarded as the most serious consequence in compliance with the criticality safety requirements. Thus the amount of fuel released from fuel rod

samples within a wide burnup range which were broken under distinct experimental conditions, needs to be evaluated.

Likewise the barriers of a DPC are of fundamental relevance since they have to ensure that the containment retains sufficient integrity under all conceivable circumstances (hazardous incidents, accidents, ageing, impact, etc.), which can occur during the entire operational lifetime of the cask. In order to protect the environment and humans, the release of activity has to be limited to the lowest, achievable value and must respect the legally required limits with a sufficient safety margin. Therefore, ongoing investigations are focussed on the cask closure system. Special attention is paid to metal gaskets and bolts.

5.3.3. Japan

R&D for dry cask storage has been carried out mainly by the Central Research Institute of Electric Power Industry (CRIEPI) [37–39]. The first R&D programme, undertaken between 1987 and 1991, dealt with metal cask storage technology and its results provided reference data for the licensing of dry cask storage technology in Japan.

CRIEPI also carried out from 1992 to 1996 an advanced research programme on spent fuel storage technology. Major activities of this programme dealt with the evaluation and related tests on dry storage methods suitable for a high burnup spent fuel and MOX fuel in terms of safety and economy. The activities also included various designs and development projects for advanced dry storage technologies, such as concrete cask with improved safety and economy.

A further R&D programme for interim storage was started in 1997 to 1999. This programme dealt with verification tests related to concrete modular storage technology such as horizontal concrete silos and concrete casks and also dealt with integrity of spent fuel during dry storage. A demonstration programme for concrete casks was carried out from 2000 to 2003. Major activities of this programme dealt with determining concrete cask performance including the fabrication of full-size concrete cask, heat removal test, and seismic test. The programme also dealt with pellet oxidation examination and the development of a non-destructive monitoring technique for spent fuel. Metal cask tests were added to the programme in 2004 which continued until 2008. In this programme, drop test, airplane crash test and long-term sealability test of lid structure were carried out. The potential for stress corrosion cracking (SCC) of storage canisters, (including SCC initiation critical condition, mitigation method, salt measurement system) was evaluated between 2004 to 2013. Other studies have included: the detection method of helium gas leak from canister, and evaluation of influence of the vibration on sealing performance of the ageing gasket (started 2006 and 2012).

The Japan Nuclear Energy Safety Organization (JNES) has a mission to support the regulatory body by researching the data of technical standard and regulation. Investigating spent fuel integrity during long term dry storage is one of them.

JNES had concerns of high burnup fuels from a view point of:

- Increase of hydrogen concentrations in cladding;
- Increase of hydrides precipitated radially;
- Fuel integrity or ductility effect on potential criticality under accident condition during storage and transportation.

Therefore JNES had been planning and performing tests in order to evaluate fuel integrity in interim dry storage [40–42]. By 2003, thermal creep testing and irradiation hardening recovery testing had been performed using irradiated cladding tubes, and the creep equation for boiling water reactor (BWR 50 GW·d·t(U)$^{-1}$ type) and pressurized water reactor (PWR 48 GW·d·t(U)$^{-1}$ type) fuel cladding had been established. Between 2004–2008, JNES performed tests using irradiated cladding tubes, in which the effects of hydride reorientation were investigated for fuel burnups up to 55 GW·d·t(U)$^{-1}$; on type BWR and PWR fuel cladding.

Since 2009 JNES has been performing dynamic load impact tests. The objectives of these studies were to acquire the following behaviour data by dynamic load impact tests on high burnup spent fuel rods of BWR and PWR to enable regulatory guidance of spent fuel storage and transportation to be improved:

- The limit of load and strain for high burnup fuel in the cask drop accident;
- The amount of deformation of high burnup fuel rods under dynamic load impact;
- The amount of fuel pellet material released from fuel rods under dynamic load impact.

Zircaloy-2 (BWR) and MDA™[8] (PWR) claddings and segmented rods of around 55 GW·d·t(U)$^{-1}$ irradiated fuel were used for the tests. Elemental mechanical test of cladding, axial dynamic load impact test, and lateral dynamic load impact test on BWR and PWR fuel rod were carried out.

In Japan, interim storage of spent fuels in dual purpose dry metal casks is planned for up to 50 years prior to reprocessing. Spent fuel after confirming their integrity will be loaded and transported to a centralized dry storage facility. Storage over the long term, maintaining fuel integrity, is based on research achievements in Japan and overseas. To reduce the risk of radiation exposure to workers and from waste materials the interim storage facility has no hot cell. Ongoing spent fuel integrity will be confirmed indirectly by monitoring the casks during storage and transported after the storage without opening the cask lid. Currently, spent fuel storage in dry metal casks is a proven method mainly in Europe and the United States based on numerous tests including demonstration tests. The Nuclear Safety Commission of Japan (NSC now NRA) requires that the utilities accumulate knowledge and experience on the integrity of spent fuel and casks during dry storage; the basis being ongoing spent fuel dry storage in Japan. To fulfil this requirement for PWR fuel, the utilities (The Japan Atomic Power Company, The Kansai Electric Power Company and Kyusyu Electric Power Company) planned a long term storage test in a domestic research facility to confirm ongoing fuel integrity in a similar environment to actual casks [43]. In this test, a compact test container (Fig. 1) will be installed in the research facility and to store two different spent PWR fuel assembly types (43 GW·d·t(U)$^{-1}$ and 55 GW·d·t(U)$^{-1}$) loaded. The container internal gas will be analyzed every 5 years for a maximum 60 years. The current plan is to start the demonstration test programme in 2014.

---

[8] MDA is a trade mark of the cladding developed by Mitsubishi Heavy Industries Ltd. MDA is zirconium alloy containing Nb.
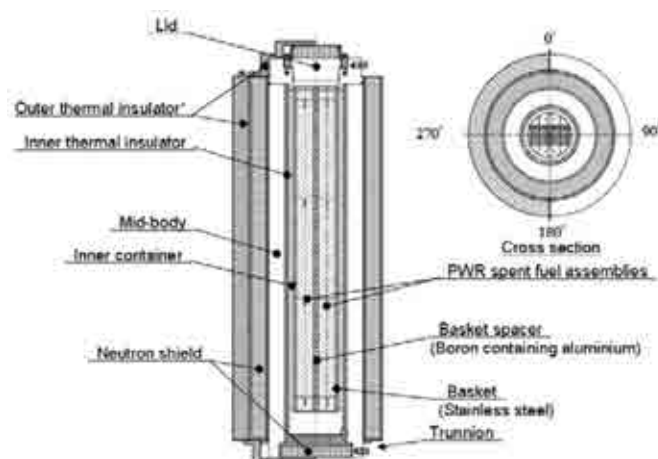
FIG. 1. Test container profile.

*Note: Outer thermal insulator installed at loading only 48 GW·d·t(U)$^{-1}$ fuel assembly will be removed when 55 GW·d·t(U)$^{-1}$ fuel assembly is added in future.

5.3.4. Republic of Korea

A phased R&D programme (initiated in 2009) is underway in the Republic of Korea to underpin the dry storage of PWR fuel and in support of the development of its own dry storage system.

Studies to date have included: fuel clad creep, hydride reorientation and the design/manufacture of a demonstration test to be carried out in a storage pool. The studies on spent fuel properties are provided in Chapter 6.

5.3.5. Spain

Several R&D programmes were developed in Spain related to spent fuel performance. One of them was performed on six high burnup (> 50 GW·d·t(U)$^{-1}$) fuel rods that had been dry stored in air for more than 25 years, at temperatures not in excess of 175°C, and demonstrated that the fuel cladding did not suffered any degradation under these conditions.

Another was focused on isotopic measurements of PWR and BWR fuel. PWR sampling was chosen with these objectives: high burnup and high enrichment samples for isotopes representative of shielding, gas production, reactivity, residual heating and burnup determination. A different approach was followed concerning BWR samples. Although the BWR samples burnup were lower, the aim was to highlight the void effect and the different neutron spectra of a BWR compared to a PWR. Results have been included in the NEA database (SFCOMPO).

Concerning mechanical testing of irradiated materials, five high burnup PWR ZIRLO™ samples were creep tested and characterized to investigate the behaviour of advanced cladding materials under dry storage conditions. The results have been consistent with the expected behaviour from reference CWSR material, zircaloy-4. The higher hoop stress and temperature, the greater creep deformation. The samples kept significant ductility during tests. Metallographic tests performed afterwards showed significant hydride reorientation (due to

cooling after test procedure). However, no specimen failure was observed during cool-down. Hardness measurements showed partial recovery in some of them.

Another set of five BWR zircaloy-2 samples were creep tested and characterized. Creep tests showed lower creep rates for RX material than those obtained for ZIRLO™, consistent with published data. Special procedures for cooling were implemented to reorient hydrides in the cladding. The radial fraction increased with the stress and some degree of reorientation was observed even at 70 MPa hoop stress, consistent with published data. Axial tensile tests show the effect of the irradiation damage annealing on mechanical properties.

The previous tests were also checked against unirradiated material: ZIRLO™ rods were chosen to obtain the mechanical properties at ambient temperatures and at other temperatures representative of in-pile or storage conditions. A model was developed for its mechanical behaviour. A hydrogen charging method was developed to show the effect of hydrides. A method of hydride reorientation was developed to obtain the influence of reoriented hydrides on the cladding mechanical behaviour. Mechanical tests included axial tensile, ring tensile and ring compression tests.

5.3.6. Switzerland

Research activities in Switzerland have focused on demonstrating fuel cladding integrity, i.e. understanding thermal creep properties, hydride related issues and clad oxidation, and have been performed by the Paul Scherrer Institute mostly on behalf of the Swiss nuclear industry.

The methods utilised and the results of these studies are provided in Chapter 6.

5.3.7. United Kingdom

See Section 5.4.

5.3.8. United States of America

Storage and Transportation of spent fuel with a fuel burnup greater than 45 GW·d·t(U)$^{-1}$ [44–51].

While issues related to dry storage have largely been resolved, transportation issues have not, at least for spent fuel with discharge burnups greater than 45 GW·d·t(U)$^{-1}$. A research programme sponsored by industry was launched in late 2002 following two NRC industry meetings held on September 6, 2002 and October 23, 2002. The aim of the research programme was to assess the performance of high burnup spent fuel cladding under normal and accident conditions of transportation, as prescribed by 10 CFR 71, considering the physical characteristics and mechanical properties of cladding at the end of dry storage.

The results of analytical studies sponsored by EPRI during the past several years indicate that damage to high burnup spent fuel under prescribed regulatory conditions of dry storage and transportation will not impair its operational management. Dry storage effects on cladding physical and material conditions, including creep related deformations, have the potential to impact fuel rod performance during transportation. Specifically, cladding resistance to failure under the dynamic loading of transportation accidents depends on fuel cladding gap size and radial hydride formation, both of which could (to a limited extent) occur during long term dry storage. The results of the hypothetical accident analysis indicate that cladding failure would be bi-modal taking the form of 1) a state of failure initiation at the cladding inside diameter

(ID) remaining as part wall damage (with less than a 2% probability of occurrence) and 2) a through wall failure with a probability of 1×10^{-5}. The response analysis under normal conditions of transport shows a large margin against fuel rod failures. The grids and guide tubes, which form the structural elements of the fuel assembly, are predicted to remain structurally competent. As a result, the geometric form of the spent fuel assemblies is not expected to be substantially altered.

An NRC/EPRI/DoE sponsored experimental programme is being conducted at Argonne National Laboratory. The programmes' initial goals were to understand the fundamentals of hydride reorientation and determine if there was a lower stress limit under which the process did not occur. Due to experimental problems the goal changed to determine the effect of hydride reorientation on cladding behaviour if reorientation did occur. The major conclusion from this programme is: if hydride reorientation occurs, it will result in a shift of the ductile−brittle temperature to a higher value. The amount of shift will depend on the stress, material, processing, condition, and quantity of hydrogen available. Details and results from this programme are given in Section 6 of this report.

DoE/NRC/EPRI/industry all have major projects to address one or more of the issues related to the question if chloride induced stress corrosion cracking is a major issue of concern for dry storage canisters: what conditions are required for it to occur; are those conditions available at the storage sites; how do we determine if these conditions exist (inspection methods); and what are the consequences of the degradation.

5.4. MAGNOX FUEL DRY STORAGE CANISTER CHEMICAL MODELLING WORK

5.4.1. Introduction

The first generation of commercial nuclear power plants (NPP) in the United Kingdom utilised the gas cooled MAGNOX reactor type, which have been operational since 1956. Out of the 11 MAGNOX NPPs constructed, seven have been shut down and de-fuelled, three have been shut down and are undergoing de-fuelling operations, and one station (Wylfa) remains operational.

Spent fuel arisings from the MAGNOX NPPs are wet stored at station ponds (with the exception of Wylfa, where fuel is discharged into one of three carbon dioxide cooled silos) prior to transport to the Fuel Handling Plant at Sellafield. At Sellafield, fuel elements are transferred for decanning prior to reprocessing. The reprocessing facilities for MAGNOX fuel have been operational since 1964 and acute or chronic failure of the facility is a credible risk. Contingency options for managing MAGNOX fuel in the event of reprocessing failure have been considered. Work has been performed to develop a process to retrieve and dry wetted MAGNOX fuel for interim storage in sealed canisters as a contingency option.

Uncertainty over the practical drying capability and resulting water carryover, together with the choice of a sealed storage canister mean that there is a risk of canister pressurisation. To assess this risk, modelling of the chemistry of the canister has been performed to estimate the likely canister pressurisation and composition over a range of storage conditions and scenarios.

5.4.2. Background

5.4.2.1.   MAGNOX fuel description

The features of a typical MAGNOX fuel element are shown in Fig. 2. It should be noted that the exact design of the MAGNOX fuel elements evolved as new reactors were constructed and knowledge of the heat transfer behaviour advanced.

MAGNOX fuel elements consist of a cast metallic uranium bar encased in MAGNOX (<u>mag</u>nesium <u>non-oxi</u>dising) cladding. Most MAGNOX fuel element cladding is manufactured from MAGNOX Al80, an alloy which was developed to resist the oxidising effects of the carbon dioxide reactor coolant. MAGNOX Al80 is primarily composed of magnesium, with 0.8 %w/w aluminium.

Although the majority of MAGNOX fuel manufactured was of natural enrichment, some of the reactors were loaded with low enriched uranium fuel in the latter stages of reactor operation.

5.4.3.   MAGNOX fuel drying project

The MAGNOX fuel drying project is intended to provide a contingency response to the potential failure of MAGNOX reprocessing at Sellafield by enabling wetted spent MAGNOX fuel stocks to be rapidly removed from the Fuel Handling Plant and NPP ponds, dried, sealed in high integrity canisters and placed in dry interim storage for up to 150 years.

The project is based on the experience of the United States Department of Energy (US DoE) process used at the Hanford site. This was used to retrieve and place in storage bulk quantities of N reactor zircaloy-2 clad (with a small quantity of aluminium clad) metallic uranium fuel stored in the K East and K West basins. A cold vacuum drying process was used to remove the majority of water from the fuel, and the dried fuel was sealed into high integrity canisters for an interim storage period planned to be approximately 40 years.
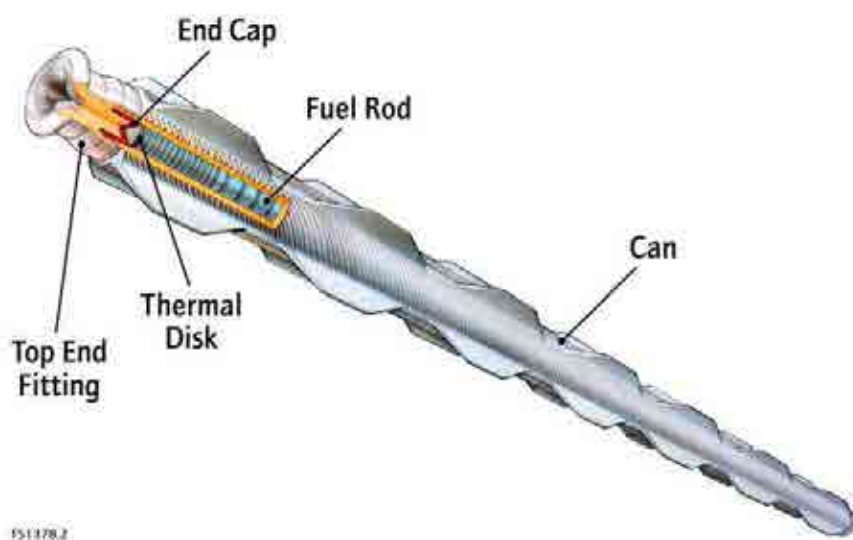

FIG. 2. Features of a typical MAGNOX fuel element.

It is estimated that the maximum quantity of spent MAGNOX fuel that may require treatment is of the same order of magnitude as the Hanford project, and is composed predominantly of intact fuel with some degraded fuel.

The outline process for MAGNOX fuel drying and packaging is summarized in Fig. 3. This involves retrieval of individual MAGNOX fuel elements from a skip held in a transport flask, which are loaded into a drying basket in a regular array. The drying basket is then held to allow excess water to drain before being transferred to the fuel drying rig (Fig. 4) where the basket is lowered into the storage canister and the drying lid sealed onto the top of the canister body. The drying process consists of four stages:

- System purge–tests the seal between the drying lid and canister body, and purges the canister with argon;
- Heating/drying–heats the fuel to drive evaporation in order to remove the bulk free water;
- Vacuum drying–removes residual water through evaporation promoted by reduced pressure;
- Cycle validation and venting– proves that adequate drying has been achieved.

After drying, the canister lid is welded onto the canister body and the seal non-destructively tested. The canister (Fig. 5) is inerted with high purity argon and a seal plate welded into position above the gas port. Finally, the canister is monitored for external contamination and decontaminated, if required, prior to transferral to the interim storage facility.
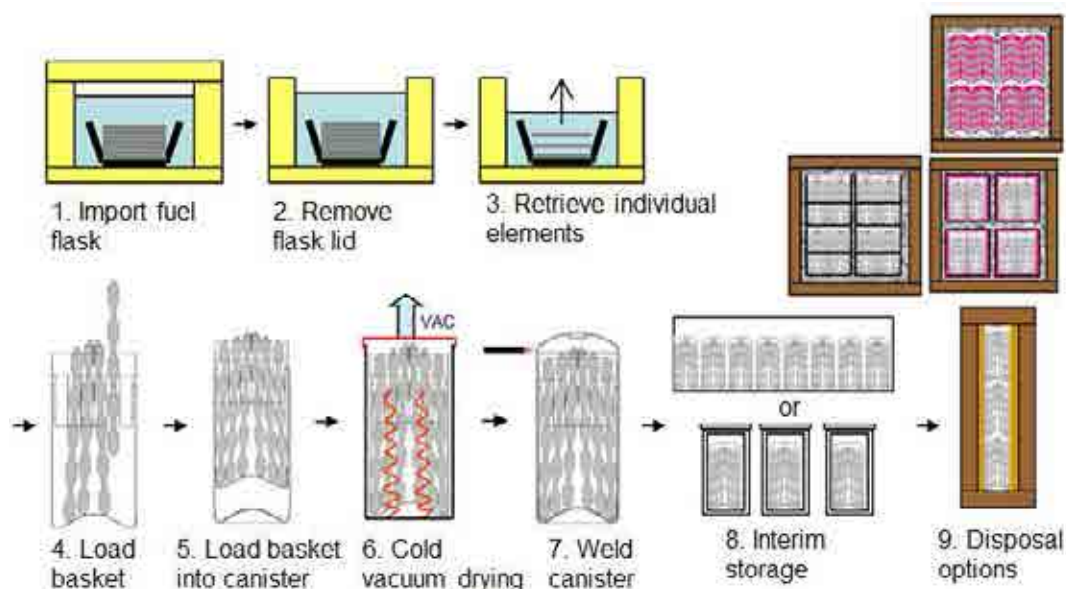

FIG. 3. Outline scheme for MAGNOX fuel drying and packaging process.
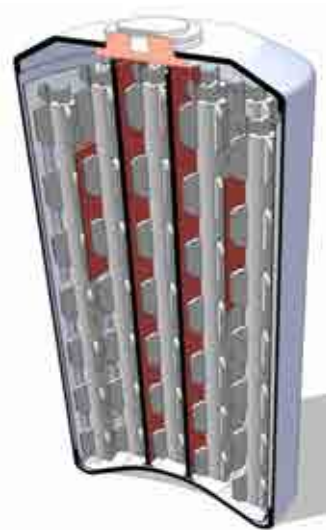
FIG. 4. Fuel drying test rig.

FIG. 5. Schematic of the sealed, loaded canister.

5.4.4. Canister chemistry modelling

5.4.4.1. Purpose

Previous estimates of canister pressure and gas composition that have been undertaken early in the project development were based on simple and highly conservative assumptions. The latest modelling work performed was intended to provide a less conservative, but still bounding, assessment for worst case and typical scenarios in order to support the canister design process and safety case development.

This has been done by development of a dynamic model of the storage canister chemistry, which has been run in the gPROMS process modelling tool (capable of solving mixed sets of differential and algebraic equations). A sub-component to cover radiolysis reactions has been developed using a kinetic model written using the FACSIMILE modelling tool/language. The overall model provides information on the sensitivity of the canister pressure and chemistry to water carryover, temperature, corrosion reactions, radiolysis and initial gas composition.

5.4.4.2. Principal Reactions

The principal reactions known to affect storage of MAGNOX fuel where reviewed and the best available rate data was collated to input into the model. The reactions included are:

MAGNOX corrosion:

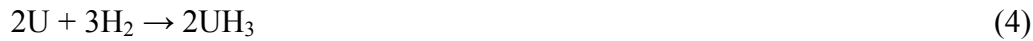$$Mg + 2H_2O \rightarrow Mg(OH)_2 + H_2 \tag{1}$$

Uranium reactions:

$$U + [(2 + x)/2]O_2 \rightarrow UO_{2+x} \tag{2}$$

Where
 $0.006 < x < 0.1$

$$U + (2 + x)H_2O \rightarrow UO_{2+x} + (2 + x)H_2 \tag{3}$$

Where
$0.13 < x < 0.20$

$$2U + 3H_2 \rightarrow 2UH_3 \tag{4}$$

Uranium hydride reactions:

$$2UH_3 + 2H_2O \rightarrow UO_2 + \frac{7}{2}H_2 \tag{5}$$

$$2UH_3 + 2O_2 \rightarrow UO_2 + \frac{3}{2}H_2 \tag{6}$$

Radiolysis of water:

$$H_2O + \gamma \rightarrow \rightarrow H_2, O_2 \tag{7}$$
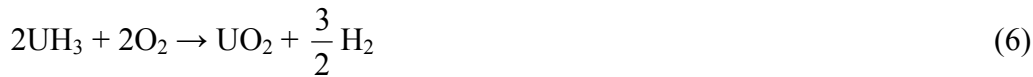
5.4.4.3.   Assumptions

The canister model describes a system for which no actual active storage data exists, so a number of simplifying assumptions have been made. It should also be noted, for this reason, it has not been possible to validate the model against experimental data.

The general assumptions are summarized below:

- Temperature–The model was run at three temperatures (55°C, 75°C, 100°C), assumed to remain constant over the storage period. The range selected reflects anticipated conditions, but not all conceivable fault conditions. The model also excludes heat transfer effects;
- Initial gas composition–The canister is initially purged with argon (99.9% Ar). The fault condition of the canister not being inerted is also included, in which case the initial atmosphere is composed of air;
- Spatial effects–The canister is assumed to contain 26 identical fuel elements, each in an identical environment, with 1/26 of the total water carried over and will react in the same way.
- Corrosion reactions–All corrosion is assumed to be general/uniform, and all of the material reacts until it becomes depleted. Localised corrosion mechanisms are neglected. All the corrosion reactions are modelled as first order;
- The ideal gas laws are obeyed.

Three classifications of fuel condition were included in the matrix of scenarios modelled:

- Intact fuel–Fuel whose cladding integrity has not been degraded during irradiation, storage, transport or handling. It is assumed that no prior oxidation of the MAGNOX surface has occurred. The model accounts for changes in the surface area as material corrodes;
- Degraded fuel–For the purpose of the model, the limiting case for degraded fuel is a bare uranium bar. It is assumed that all uranium bars have a diametral swelling of 10%

as a result of irradiation effects. For degraded fuel it is assumed that the surface area remains constant with time;

- Debris–Fuel debris is modelled as a MAGNOX fuel element that has been broken into pieces of dimensions $6 \times 50 \times 20$ mm, but stacked vertically to approximate the shape of the original fuel element. The model accounts for changes in the surface area as material corrodes.

The residual water (or water carryover) remaining after fuel drying has been modelled for two scenarios: the design case of 28 $g(H_2O) \cdot element^{-1}$; and the maximum case of 100 $g(H_2O) \cdot element^{-1}$ for safety assessment purposes in case of total failure of drying process. The distribution of this water between the liquid and gas phases has been evaluated by assuming that the canister gas is saturated with respect to water. The geometry of the water carryover could either be modelled as a uniform mist of droplets or as a single volume collected in the base of the canister. Following sensitivity studies, the difference in results between the two options was seen to be minimal and therefore the water was modelled as a single slab for simplicity.

Radiolysis of water has been modelled on the basis of the dose rate taken from LWR fuel of similar irradiation and cooling as the bounding MAGNOX fuel inventory. The radiation was taken to be entirely gamma and no correction was made for the dose rate to decrease with time. The intensity of the radiation transmitted through absorbing materials in the canister was calculated using the Beer-Lambert law. Dose to the gas phase was disregarded. It was also assumed that once released into the gas phase hydrogen and oxygen do not recombine.

5.4.5. Results–pressure

Both the maximum canister pressure and the variation of pressure over time are important properties of the system to understand and predict. The design intent of the canister is to withstand a nominal pressure of 3 MPa and a maximum pressure of 10 MPa.

The canister pressure is seen to be controlled by a number of factors. For illustration, the variation of pressure with time for a representative selection of cases is shown in Fig. 6. The maximum pressure and time for the pressure to stabilise are shown for a selection of cases from design basis to worst case scenarios in Table 4.

The maximum pressure in the canister is predicted to be low and none of the cases modelled exceed either of the canister pressure limits; the highest pressure predicted is 1.31 MPa. The variation of pressure in the canister is initially dominated by the amount of water available to react until the water becomes depleted, at which point the pressure is predicted to stabilise. For all cases, the time taken for the pressure to stabilise is of the order of tens of days.
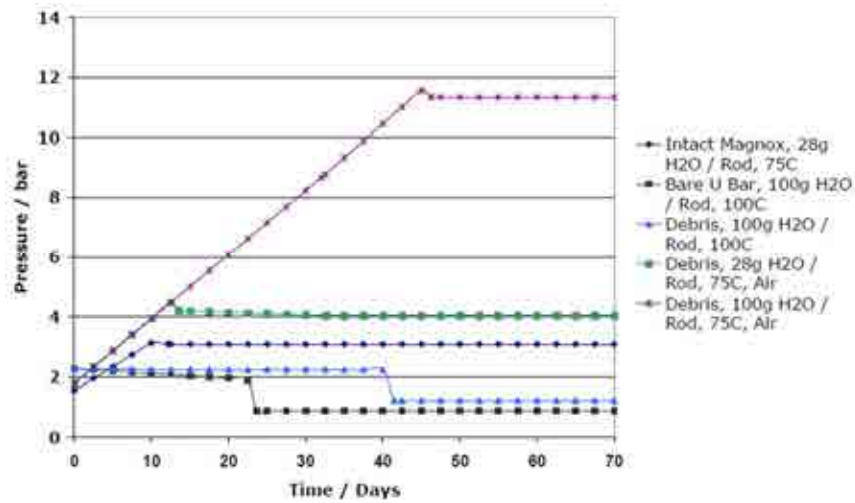
FIG. 6. The variation of canister pressure with time for a selection of cases (1 bar = 0.1 MPa).

TABLE 4. SUMMARY OF MAXIMUM CANISTER PRESSURE AND TIME FOR PRESSURE TO STABILISE FOR SELECTED CASES

Surface area	Conditions	Maximum pressure (MPa)		% Difference in pressure	Time for pressure to stabilize (days)	
		Without radiolysis	With radiolysis		Without radiolysis	With radiolysis
Intact MAGNOX (No defects)	28 g H_2O/ element, 75°C	0.3111	0.3114	0.097	12.2	12.0
	100 g H_2O/ element, 75°C	0.7717	0.7719	0.024	42.0	42.0
Bare U rods	28 g H_2O/rod, 75°C	0.1551	0.1554	0.196	16.50	16.55
	100 g H_2O/rod, 100°C	0.2259	0.2305	2.04	24.0	23.6
Debris	28 g H_2O/rod, 75°C	0.1551	0.1554	0.196	22.9	30.2
	100 g H_2O/rod, 100°C	0.2259	0.2261	0.078	9.1	28.5
	28 g H_2O/rod, 75°C, Air Present	-	0.448	-	-	32.7
	100 g H_2O/rod, 100°C, Air Present	-	1.31	-	-	11.0

The variables affecting canister pressure are described subsequently in more detail:

a) Water carryover: the amount of water carryover effects both the maximum pressure and the time for the pressure to stabilise, as shown in Fig. 7. When there is more water present to react with MAGNOX cladding (1) and or uranium (3), more hydrogen will be formed. In addition, it will take longer for the water to become depleted allowing the pressure to stabilise. However, this is only relevant for cases where hydrogen can build up in the canister, in effect when the reaction of hydrogen with uranium (4) is suppressed either if there is no exposed uranium or by the presence of oxygen;

b) Uranium hydrogen reaction: the reaction between uranium and hydrogen (4) effectively limits the canister pressure by rapidly consuming hydrogen formed by corrosion reactions (Fig. 8); this reaction only occurs if there is exposed uranium and if the oxygen concentration is less than 8 ppm. Modelling of radiolysis predicts that it will not generate sufficient oxygen to suppress the reaction;

c) Temperature: although increasing temperature does not exert as significant effect as water carryover, it affects the maximum pressure according to the Ideal Gas law and also affects the time for the pressure to stabilise by increasing the corrosion rates, thereby depleting water at a greater rate. This is illustrated in Fig. 9;

d) Radiolysis: the quantities of gases generated by radiolysis of water (7) are predicted to be small compared to the gas generated by the corrosion reactions. In addition, the quantity of oxygen predicted to be generated by radiolysis is predicted to be insufficient to inhibit the consumption of hydrogen by reaction with uranium (4). The effect of radiolysis on maximum pressure is predicted to be less than 4 % in all cases;

e) Volatile fission products: some volatile fission products, primarily ^{129}I and ^{85}Kr, could be released from the fuel as a result of corrosion. However, they are not predicted to be released in high enough quantity to greatly affect the maximum canister pressure;
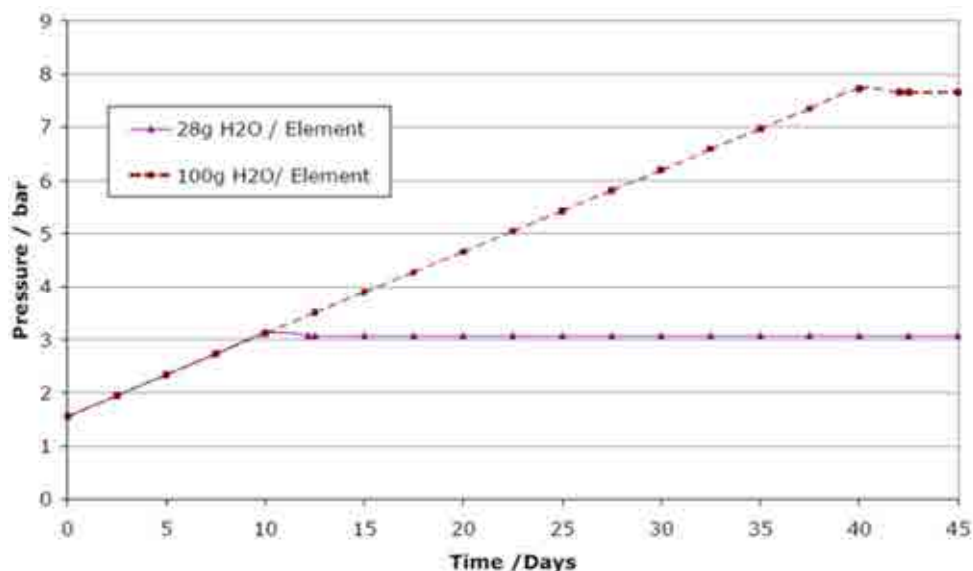

FIG. 7. The effect of water carryover on the canister pressure for intact fuel at 75°C (1 bar = 0.1 MPa).
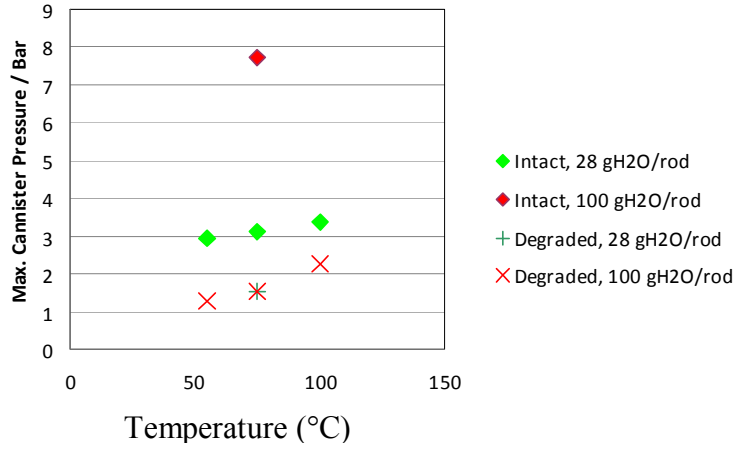
FIG. 8. The effect of the U/H$_2$ reaction on maximum canister pressure. The reaction does not occur with intact fuel, but does with degraded fuel, where there is exposed uranium (1 bar = 0.1 MPa).

f) Hydrogen migration: the small atomic radius of hydrogen compared to metallic atoms means that there is potential for hydrogen to diffuse through the canister wall. This was assessed using Fick's First Law. It is predicted that this mechanism will have a negligible effect on the pressure over the storage duration (0.01 MPa decrease over 150 years);

g) Air in the canister: in the event that the canister is not inerted and is initially filled with air rather than argon, the maximum canister pressure is predicted to be much greater than the corresponding case where the canister is inerted (Fig. 10). This is because the oxygen content in air initially suppresses the uranium–hydrogen reaction (4). The presence of air in the canister also results in higher partial pressures of hydrogen and oxygen from radiolysis because the initial radiolysis products can react with the dissolved oxygen, which alters the distribution of intermediate species and hence the overall yield of gaseous products. The pressure stabilises and or decreases once the oxygen becomes depleted and the hydrogen may then be consumed by reaction with uranium.
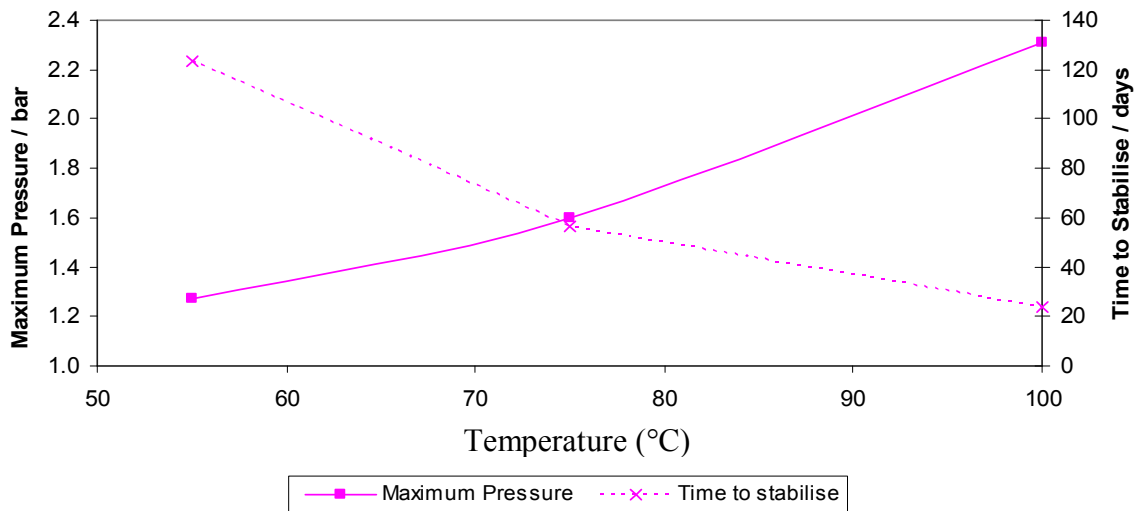

FIG. 9. The effect of temperature on the maximum canister pressure and the time for the pressure to stabilise for degraded fuel with water carryover of 100 g(H$_2$O)·rod^{-1} (1 bar = 0.1 MPa).
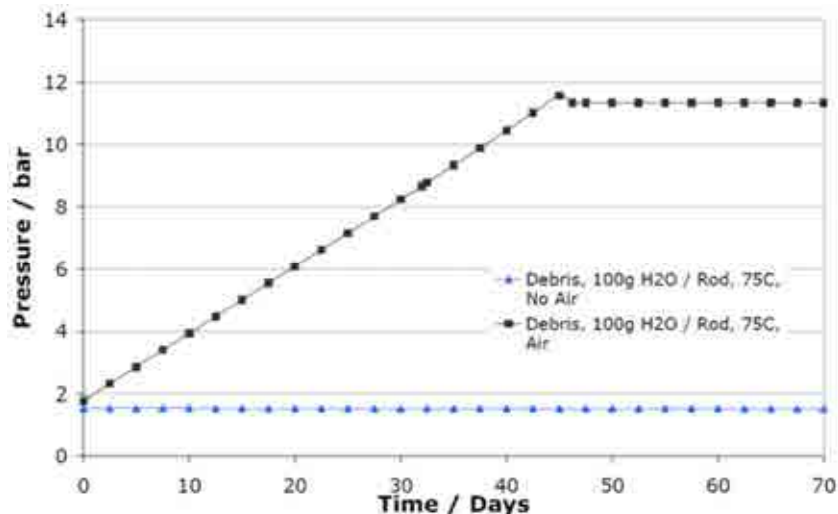
FIG. 10. Effect of canister being filled with air in comparison to argon for fuel debris with 100 g(H_2O)·rod^{-1} at 75°C (1 bar = 0.1 MPa)..

5.4.6. Results–formation of uranium hydride

While the reaction between uranium and hydrogen (4) has the effect of limiting canister pressure, it results in the formation of uranium hydride, UH_3, which is potentially pyrophoric. This will not be an issue during the storage period when the canister is inerted, but could represent a hazard in the event of air ingress.

Thermodynamic modelling calculations show that at 75°C uranium hydride is stable over a large range of compositions of uranium, hydrogen and water. When there is a high mole fraction of water and or hydrogen present, uranium hydride, however, will not form. In effect, this means that uranium hydride will form in the canister, although possibly only once the water becomes depleted by reactions (1) & (3). The maximum theoretical amount of UH_3 formed in the canister was predicted to be 23.2 kg, in the case of a water carryover of 100 g(H_2O)/rod.

5.4.7. Results–canister gas composition and flammability risk

The canister gas composition, particularly with respect to hydrogen and oxygen, was assessed to determine the risk of flammable mixtures being formed that could ignite generating high pressure and temperature with the potential for structural failure of the canister and release of radioactivity. Potential sources of hydrogen are the corrosion reactions and radiolysis, and potential sources of oxygen are radiolysis and if the canister is filled with air rather than argon.

Flammability will not be an issue where there is exposed uranium because it will rapidly react with hydrogen (4), unless the uranium surface has been passivated by reaction with oxygen (2) or high water content inhibits the reaction. Furthermore, flammability is not an issue for the storage of intact fuel because the oxygen generated by radiolysis is insufficient.

However, in the fault scenario that the canister has not been inerted and is filled with air there is the risk of flammable gas mixtures being formed at least transiently (Fig. 11). The hydrogen content will increase as a result of the corrosion reactions (3) & (6). Meanwhile, the

oxygen content in air means that hydrogen removal by reaction with uranium is suppressed so that an oxygen/hydrogen mixture will exist in sufficient proportions to be flammable. The flammable mixture does not persist for more than 15–20 days, as oxygen is predicted to become depleted by the corrosion reactions (2) and (6).

5.4.8. Formation of corrosive substances

The potential for the formation of corrosive substances was assessed in the context of the risk of corrosion of the canister walls, the fuel basket and the fuel materials. The canister is proposed to be fabricated from duplex stainless steel, which has high corrosion resistance in comparison to other stainless steels.

It is postulated that carbonic acid could arise from radiolysis of carbonaceous deposits or by dissolution of carbon dioxide. Scoping calculations performed suggest that formation of carbonic acid will be minimal.

There is potential for nitric acid formation by the radiolysis of nitrogen that may be present from residual air in the canister. Simple modelling of nitrogen radiolysis predicts that nitric acid formation is negligible if the container is inerted. If the canister is initially filled with air, higher concentrations of nitric acid may form, less than 3 M, which could cause some corrosion of the canister.

5.4.9.   Potential further developments of the canister model

The predictions of the modelling work are intended to be conservative as the model has not been validated against actual storage data. There are potential developments that could be made to the model to reduce the pessimisms in the modelling assumptions and uncertainty in the results could be addressed by the following developments:

- A heat transfer correlation to assess whether there is potential for runaway reactions from localised high temperatures;
- Spatial discretisation to address the assumption that corrosion reactions occur uniformly, and predict where corrosion products will form and hence more accurately estimate the quantities of corrosion products;
- Assess localised corrosion mechanisms to predict whether localised hydrogen generation is significant;
- Investigate thermodynamic (long term) reactions, e.g. the reaction between magnesium and hydrogen;
- Studying the behaviour of solid hydrated components, the effect of dose rate and refining the assumed water carryover in relation to modelling radiolysis reactions.
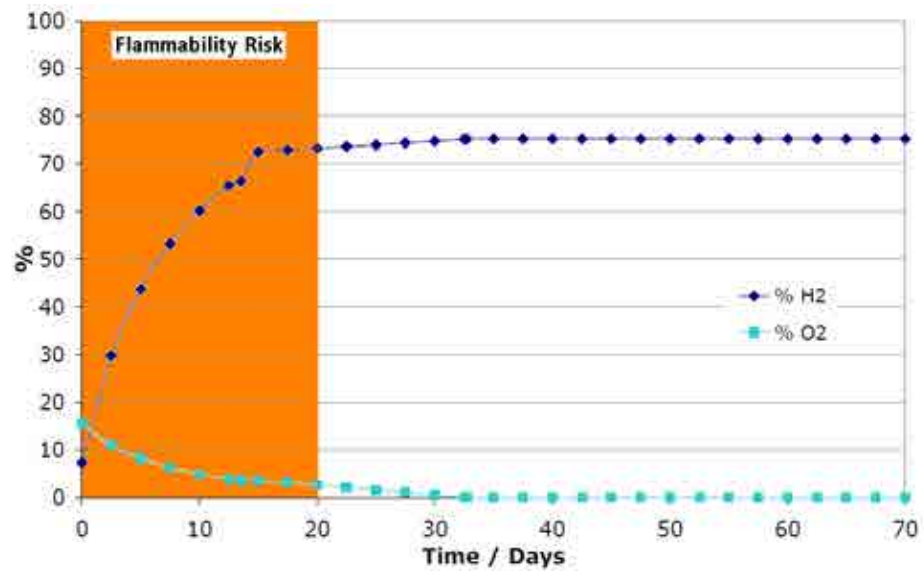
FIG. 11. Hydrogen and oxygen composition for fuel debris with 28 g $H_2O \cdot rod^{-1}$ at 75°C.

6.   HYDRIDE REORIENTATION IN ZIRCALOY CLAD FUELS

6.1.   WHAT IS HYDRIDE REORIENTATION AND WHY IS IT IMPORTANT?

6.1.1.   Brief description

Hydride reorientation can occur as a result of the following sequence of events. During reactor operation, part of the elemental hydrogen created by oxidation of the cladding by water is absorbed by the zirconium based alloy, and once the solubility limit of hydrogen in the cladding material matrix is reached, hydrogen precipitates in the form of hydride platelets predominantly aligned in the circumferential and axial directions. Additional circumferential axial (or simply 'circumferential') hydrides precipitate during reactor shutdown due to the decrease of the hydrogen solubility limit with temperature.

Following wet storage in pools at prevailing temperatures of ~30–40°C, spent fuel is moved to dry storage or transported to a centralized storage or reprocessing facility. Dry storage and/or transport operations may cause significant increases in cladding temperature: peak cladding temperatures of up to 400°C (dry storage) or up to 420°C (transport) are generally considered. The temperature increase from pool conditions to dry storage/transport conditions results in hydride dissolution and in a corresponding increase of the hydrogen in solid solution in the zirconium alloy matrix up to the hydrogen solubility limit. The temperature increase also leads to an increase in the rod internal pressure. Subsequent cooling during dry storage or re-wetting after transportation causes hydrogen in solid solution in the cladding materials to re-precipitate, but possibly aligned in the radial and axial directions (or simply 'radial') due to the influence of the tensile hoop stress in the cladding; caused by the internal rod pressure that is no longer compensated by external means such as the coolant pressure in the reactor.

6.1.2.   Hydrogen content in claddings discharged from light water reactors

Hydrogen can exist in three forms in irradiated zirconium based alloys: (1) as soluble hydrogen; (2) as hydrides; (3) as hydrogen trapped by complex irradiation produced defects.

Hydrogen solubility in zirconium based alloy matrices has been extensively investigated.

The solubility of hydrogen in zirconium alloys can be different depending on whether the solubility limit is reached by heating from a low temperature, i.e., by reaching the temperature at which all hydrides initially present in the alloy are dissolved (terminal solid solubility for dissolution (TSSD)), or by cooling from a high temperature, i.e., by reaching a temperature at which precipitation of hydrides is first observed (terminal solid solubility for precipitation (TSSP)). At a given temperature, the solubility given by the TSSP curve can be significantly higher than the solubility given by the TSSD curve. The differences between TSSP and TSSD are often referred to as "hysteresis."

The 'trapped' hydrogen cannot be classified as either 'soluble hydrogen' or 'hydrides' at any particular temperature and it can be released to the matrix only when trapping defects are eliminated by thermal annealing. Trapped hydrogen does not participate in the hydrogen-in-solid-solution/hydride-precipitate equilibrium derived from the terminal solubility curves; except when the temperature is high enough to result in the release of hydrogen from the irradiation defects.

Understanding of phenomena associated with 'hysteresis' as well as the potential impact of stress on the terminal solubility of hydrogen in zirconium based alloys are the topics addressed in Section 6.4.2.

At a burnup of 50 GW·d·t(U)$^{-1}$, the hydrogen content in PWR claddings may range from ~600 ppm for zircaloy-4 to less than 100 ppm for M5$^®$ (Fig. 12). PWR claddings with hydrogen contents in excess of ~300 ppm are characterized by an outer hydride rich layer referred to as the hydride rim (Fig. 13). For BWRs, hydrogen contents are typically in the 100–300 ppm range (Fig. 14). BWR fuels with an inner liner are characterized by a hydride rich layer in the liner.

Hydrides typically precipitate in the form of small platelets that align themselves in directions dictated by the alloy microstructure (texture, grain shape, etc.) and its state of stress resulting from the superposition of local internal stresses and applied external stresses. Cold-worked and stress-released annealed claddings (zircaloy-4 and ZIRLO™) are characterized by elongated grains that minimize the formation of radial hydrides, while materials that have been partially recrystallized (optimized ZIRLO™) or fully recrystallized (M5$^®$) are characterized by more 'rounded' grains that are expected to be slightly more susceptible to alignment of hydride platelets in the radial direction. BWR claddings (zircaloy-2) are fully recrystallized; in addition, late beta quench treatments in the fabrication process can introduce significant texture variations, which can result in more random platelet alignments.

Under pool storage conditions following reactor discharge, hydrides are primarily oriented in the circumferential direction. Circumferential hydrides, in combination with hardening due to irradiation effects, decrease cladding ductility in response to axial and hoop loads, but high burnup cladding often retains enough residual ductility at temperatures as low as 20°C [52].
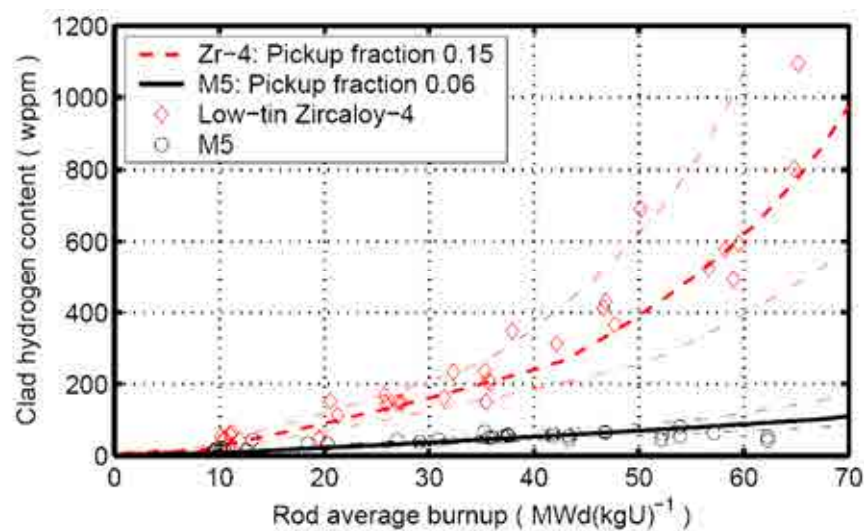

FIG. 12. Hydrogen pickup versus burnup for zircaloy-4 and M5$^®$; from [53].
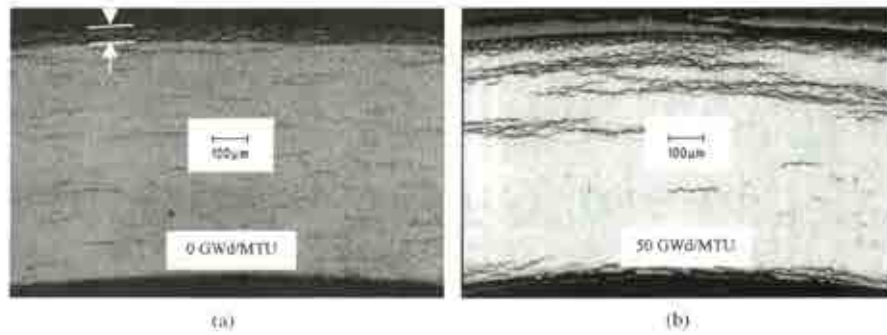
FIG. 13. Hydride rim: unirradiated (a); irradiated (b) (50 GW·d·t(U)$^{-1}$) zircaloy-4 cladding); from [54].
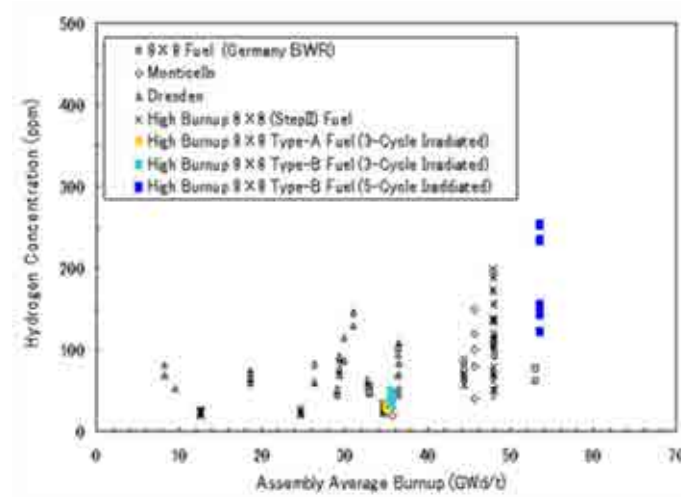

FIG. 14. Hydrogen pick up versus burnup for zircaloy-2.

6.2. WHY IS HYDRIDE REORIENTATION RELEVANT TO SPENT NUCLEAR FUEL STORAGE AND TRANSPORTATION?

Ensuring cladding integrity in spent fuel is central to establishing regulatory acceptance criteria for licensing transportation and dry storage systems. It is well known that hydride orientation has a significant influence on cladding materials properties [55]. The presence of radially oriented hydrides may significantly weaken the cladding's mechanical integrity especially when challenged in the pinching mode at temperatures below the material's ductile to brittle transition temperature (DBTT); leading to operational and regulatory concerns over handling and transportation conditions. It is therefore, important to establish mechanical properties and failure limits of irradiated cladding specimens that have been subjected to thermo-mechanical treatments similar to those experienced in industrial applications.

6.3. TESTING FOR HYDRIDE REORIENTATION AND EFFECTS

Test methods have been developed to subject cladding samples to reorientation conditions and to determine the effects of the hydride reorientation. These two operations may or may not be able to be conducted in the same experimental setup depending on the chosen approach. Once hydride reorientation occurs, a method to quantify the extent of the reorientation must be agreed upon so that results from various researchers' can be compared. Past work on zirconium alloys has shown that many experimental parameters influence hydride reorientation. The most important parameters include:

1) Material type (composition and initial microstructure) [56];
2) Hydrogen content and distribution [57–58];
3) Fluence [54], [59];
4) Temperature;
5) Applied stress [58];
6) Cooling Rate [60];
7) Extent of temperature history, such as cycling and annealing [57, 61].

In laboratory settings, some of these parameters can reliably replicate actual field conditions (such as numbers 1, 2, 3, 4, and 7) by using cladding specimens from irradiated fuel elements, while others can only be approximated (such numbers 5 and 6). True cladding stresses, at present, cannot be accurately estimated due to the potential impacts of creep and fuel cladding bonding, while cooling rates during dry storage can be orders of magnitude lower compared to those typically implemented in laboratory experiments. Potential artefacts introduced in laboratory testing, such as empty cladding tube vs. fuelled cladding tube testing, must eventually be assessed in confirmatory programmes consisting in examining the contents of prototypical dry storage systems; such as those conducted and planned in Japan and in the USA (see remainder of this report for descriptions of these tests).

6.3.1. Hydride reorientation test methods

The study of hydride reorientation may require as many as three different experimental apparatus depending on whether non-irradiated or irradiated samples are being used, and whether the apparatus is capable of conducting studies to both make the hydrides reorient and assess the effects of the reorientation. If the samples are non-irradiated as fabricated, they must be infused with hydrogen, preferably with the same morphology as established in reactor. Hydride reorientation requires an apparatus that brings the sample to temperature and then applies either a constant or decreasing stress as the sample is cooled at a known rate. To study the effects of hydride reorientation, the apparatus must be able to deliver to the sample a known stress impulse similar to that experienced by the cladding during storage and either normal or accident transport conditions. Test methods used by the participating laboratories are described below. Similar types of apparatus are used worldwide to study the hydride reorientation phenomena.

6.3.1.1. Non-irradiated hydriding procedures

1) Argentina

In-situ Synchrotron X ray Diffraction (SXRD) experiments were designed to study the effect of stress on the temperature of terminal solid solubility (TTSS) associated with hydride dissolution and precipitation, and the effect of crystallographic texture on hydride

reorientation. Studies were also aimed at characterizing the state of stress of the hydride phase and its dependence on hydride morphology, given that in delayed hydride cracking (DHC), the fracture of the hydride phase at the crack tip is dependent on both applied external stress and hydride internal stress.

Hydride reorientation in fuel cladding materials takes place under conditions set by the presence of hydrogen in the matrix, temperature changes and the effect of the hoop stress applied by internal gas pressure and/or fuel swelling. Due to the characteristics of the cladding, it is difficult to reproduce this stress state under controlled experimental conditions for in-situ SXRD experiments. In an initial attempt to overcome this difficulty, the material chosen for these investigations was a Zr-2.5Nb alloy extracted from the wall of a non-irradiated CANDU type pressure tube containing hydrogen added by cathodic charging. The tube wall thickness allowed the preparation of flat bone shaped specimens for uniaxial tensile tests where the applied stress direction coincides with the tube hoop direction. Specimens′ dimensions and the experimental setup are shown in Fig. 15. X ray diffraction experiments were conducted at the beam line 1-ID of the Advanced Photon Source at Argonne National Laboratory (ANL). The tensile probes were fastened in a loading frame, and heating and cooling cycles were performed using a lamp furnace in air under applied stress. Fig. 15(b) shows the applied temperature and stress programmes. Each temperature cycle consisted in heating the sample up to 400°C, holding this temperature for approximately 5 min, followed by a subsequent cooling down to 90°C. Applied heating and cooling rates were 20°C·min^{-1}. For the hydrogen concentration range of the samples, all pre-existing hydrides were completely dissolved at the higher temperature limit. Stress was applied in increasing steps. The maximum applied stress, 225 MPa, was high enough to produce a partial reorientation of hydrides. Figure 15(c) shows the distribution of hydrides in the hoop radial plane of the specimen before (left) and after (right) the complete thermo-mechanical treatment. Before testing, the sample contained almost exclusively circumferential (hoop) hydrides, i.e., platelet hydrides with the plate normal along the tube radial direction. After the tests, a considerable fraction of radial hydrides had formed (plate normal along the tube hoop direction), yet a fraction of circumferential hydrides could still be observed.

2) Spain

Non-irradiated specimens of ZIRLO™ cladding with 9.5 mm outer diameter and 0.57 mm wall thickness were obtained by cutting the cladding into 10 mm length samples. This dimension was chosen to ensure a plane strain state during the ring compression tests (RCT). Samples with hydrogen contents of 150, 500 and 1200 ppm were prepared by means of cathodic charging in KOH. The hydrogen in these samples formed δ-hydrides homogeneously distributed along the hoop direction of the samples [62–63].

3) United States of America

As fabricated (AF) cladding samples were pre-hydrided by gaseous charging to hydrogen content values in the range of 100 to 1000 ppm. This was accomplished by heating cladding segments to 350–400°C in a flowing or static H_2–He gas with H_2 contents of 4%, 30%, or 100%. In most cases, the cladding segments were heated to 400°C, in a static 30% H_2 gas mixture for five thermal cycles prior to annealing at 400°C for 24–36 hours in high purity Ar. Hydrogen concentration gradients in the axial and circumferential directions were minimized by pickling of surfaces with ≈1% HF solution, wrapping samples in high purity Al foil, and subjecting only the outer surface to pickling, Al foil, and hydrogen flow.
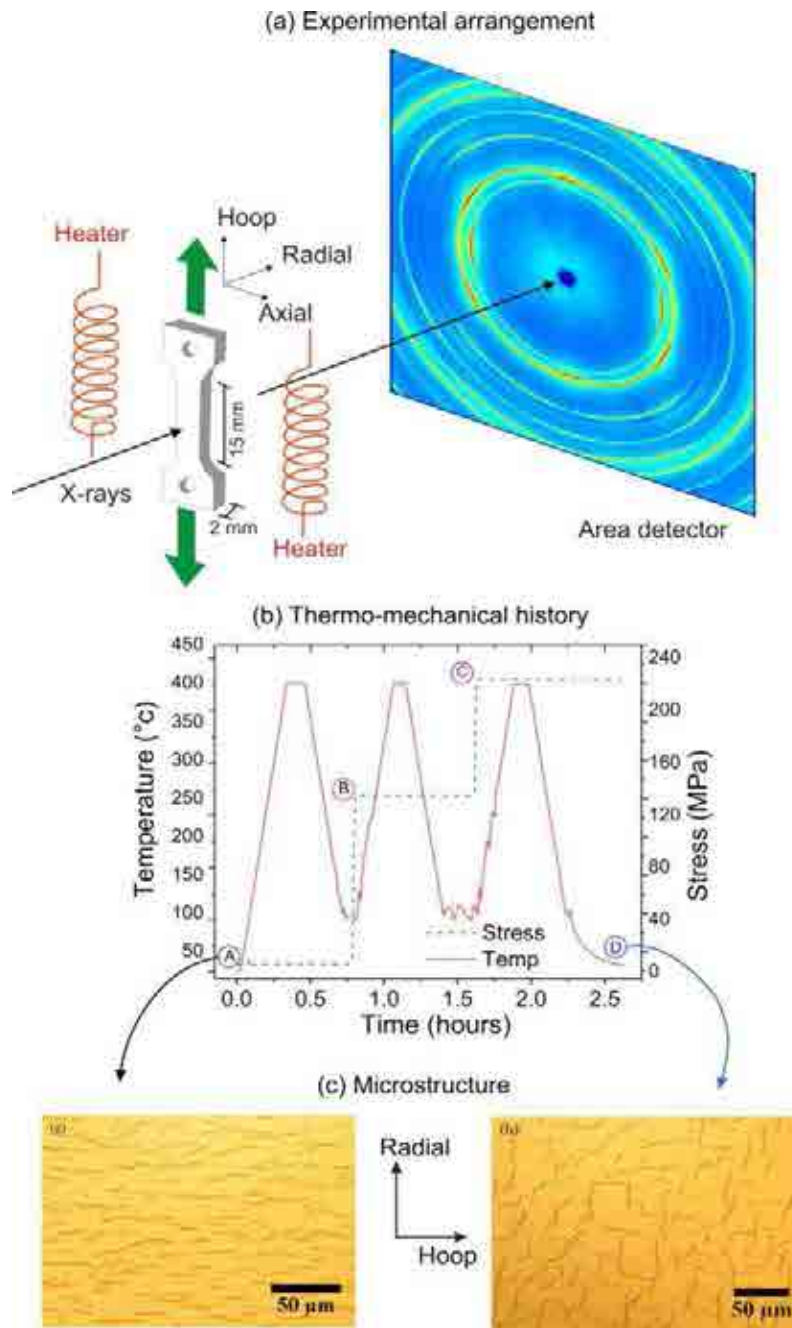
FIG. 15. a) Schematic view of the in-situ hydride reorientation experiments performed at the beam line 1-ID of the Advanced Photon Source at Argonne National Laboratory; b) Applied temperature and stress programs; c) Microstructure of the samples before (left) and after (right) the experiment. Hydrides (seen with the darker contrast) partially reoriented during treatment.

6.3.1.2. Hydride reorientation test in Japan

A hydride reorientation treatment (HRT) has been performed using the test apparatus (Fig. 16(a)). The biaxial stress in the cladding tube specimen was applied by an inner pressure of argon gas. The specimen temperature was held for 30 (for PWR cladding) or 60 (for BWR cladding) minutes at the HRT solution temperature in the furnace to dissolve the hydrogen. The temperature was then decreased to around room temperature to precipitate the hydrogen. The hoop stress in the cladding was held constant, as shown in Fig. 16(b).

6.3.1.3. Tube testing in the Republic of Korea reorientation

For tube testing, the top end of the tube is sealed with a high pressure fitting and the bottom end is connected to an argon or helium noble gas supply line to establish an internal gas pressure to simulate the hoop stress seen during storage (Fig. 17). Because hydride reorientation testing requires the temperature to be slowly decreased with time, it is necessary to control the gas pressure according to the ideal gas law in order to keep constant hoop stress inside the cladding tube. The stress is expressed by the thin walled approximation. This method has a number of advantages and disadvantages compared to the ring testing method. There is no azimuthally variation of the stress, so the testing is closer to real spent fuel storage conditions and it is easier to analyse the test results. Moreover, it is possible to evaluate the changes of mechanical properties by performing tensile and compression tests using multiple samples from the same tube length after hydride reorientation.
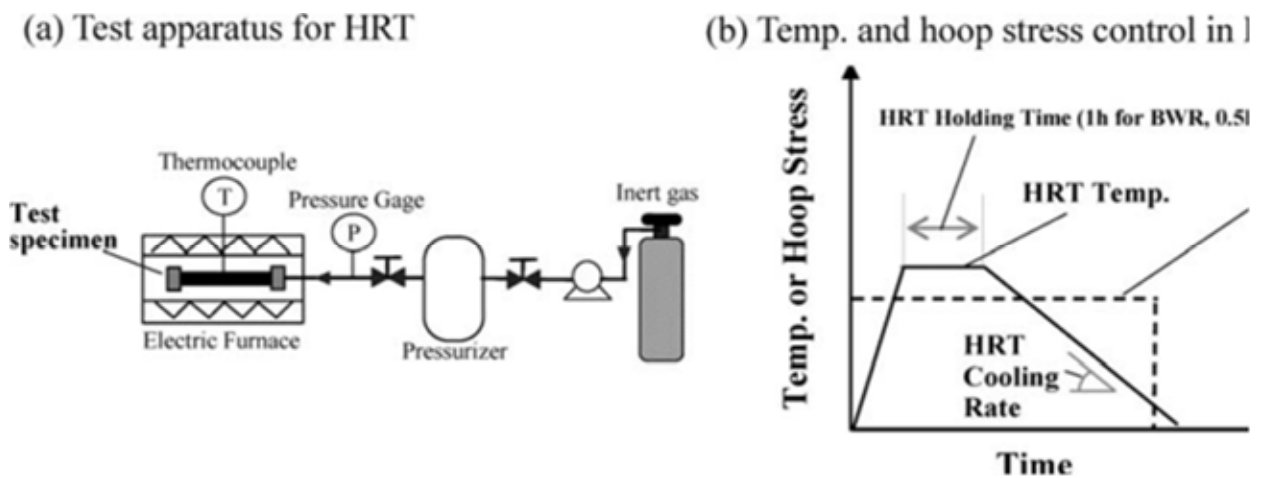

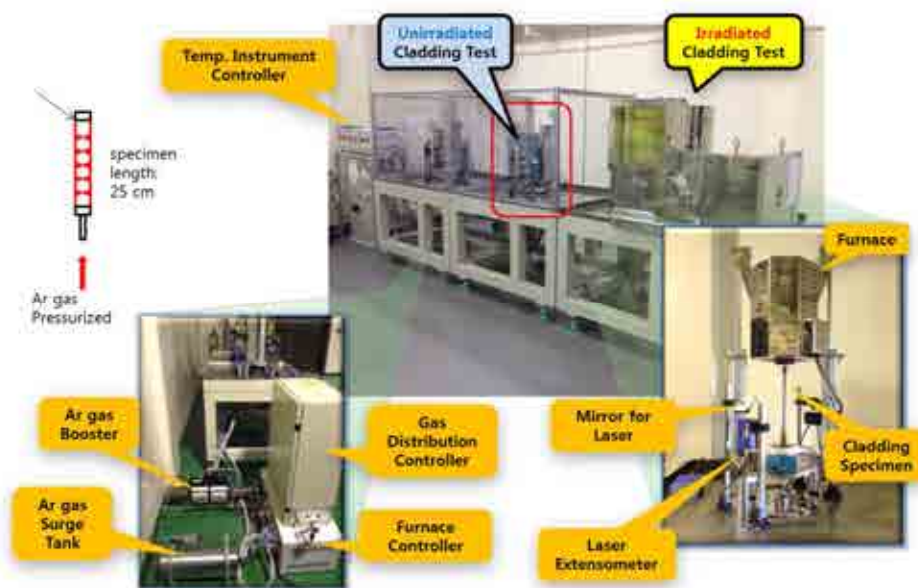FIG. 16. Japanese method for hydride reorientation test [64].

FIG. 17. Korean tube test for hydride reorientation.

There are some disadvantages to this method because the testing tube specimen is longer:

- More tubing is necessary, which may be a problem if the available irradiated cladding for testing is limited;
- Uniform temperature distribution control over the length of the tube may be difficult;
- The furnace system must be large enough to accommodate a long specimen (high radiation requires significant shielding);
- There is safety issues in case of an accident because of the high temperatures and high pressures used.

6.3.1.4.   Ring testing in the Republic of Korea

For ring testing, the hoop stress is applied to the cladding inner wall by the movement of an inner mandrel on short ring type specimens. The mandrel is expanded in a controlled manner to establish the stress either two half cylinder or a three piece mandrel, with a central dog bone (Fig. 18), are used.

The ring sample may be notched to enhance the uniformity of the hoop stress and strain, but it also induces a stress concentration at the notched area. This notched specimen effect is higher in the plastic region than in the elastic region, which means this effect is negligible at the lower stress conditions where hydride reorientation testing is usually performed. The ring test without a notch is therefore, preferable because it is simpler to prepare; especially for irradiated specimens.

There are advantages to this method compared to the tube test described above:

- Relatively easy control of a uniform temperature on short ring specimen;
- Easy testing system installation compared to tube testing;
- Smaller cladding samples, so a lot of various testing results can be obtained for a given tube length;
- Allows correlation of the degree of reorientation with the stress gradients across the sample wall, which reduces the number of samples that need to be tested;
- Low radiation therefore, simpler shielding requirements;
- Relatively easy handling of specimens.

The disadvantages of the ring test method are:

- Finite element modelling (FEM) analysis is necessary to understand the stress gradient across the ring wall. Accurate FEM input material properties at various temperature and stresses are needed to make the FEM analysis results more reliable. This could be considered an advantage of this method by some as one can measure reorientation at many different stress levels in one sample (Fig. 19);
- Acquiring materials data that might change with hydride reorientation is very difficult for an irradiated cladding specimen;
- Variable results and low reliability of ring test results compared with tube testing;
- Because hydride reorientation occurs locally at most high stress gradient region, it is difficult to get additional material properties data using tensile or compression testing.

6.3.1.5.   Hydride reorientation testing in Spain

Non-irradiated samples with 150, 500 and 1200 ppm of hydrogen were subjected to a thermo-

mechanical treatment to produce the reorientation of the hydrides [63]. First, the samples were heated at 400°C, and this temperature was maintained during two hours. During the last 30 minutes, a hoop stress was applied to the samples by using a universal testing machine. The samples were then slowly cooled down (1.2 K·min^{-1}) until 20°C was reached, while the hoop stress was kept constant.

The hoop stress was applied by means of two semi-cylindrical beams which are in contact with the inner surface of the sample (Fig. 20). The experimental device (beams and sample) were placed inside an oven. The applied load was measured with a load cell (5 kN at full scale). A graphite polish was used to lubricate the contact surface between the sample and the loading beams.

A 3D finite element (FE) model was developed with ABAQUS V. 6.7–5 to simulate the thermo-mechanical treatment and calculate the applied loads; in order to obtain the target hoop stresses. Only one fourth of the sample was employed due to geometry and loading symmetries. A detail of the mesh employed is shown in Fig. 21. It is a structured mesh formed by quadratic elements (parallelepipeds with 20 nodes). The different thermal properties of the beams and the sample were considered.

The calculated hoop stress is quite homogeneous through the sample thickness in almost all the sample; except at the contact zone between both beams (Fig. 21). The loads associated to different hoop stress (60, 90, 120, 140 MPa) were calculated using the FE model for all the process steps. Consequently, the applied load was decreased during cooling down to keep constant the hoop stress.

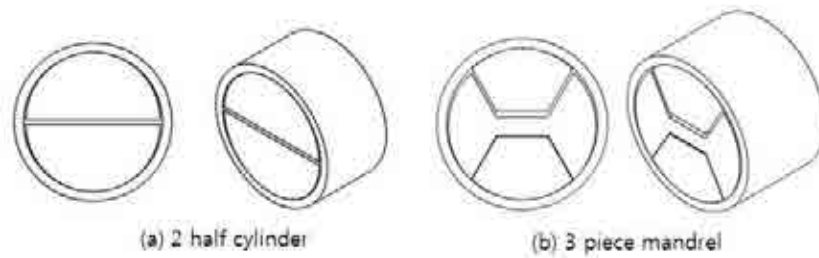(a) 2 half cylinder   (b) 3 piece mandrel
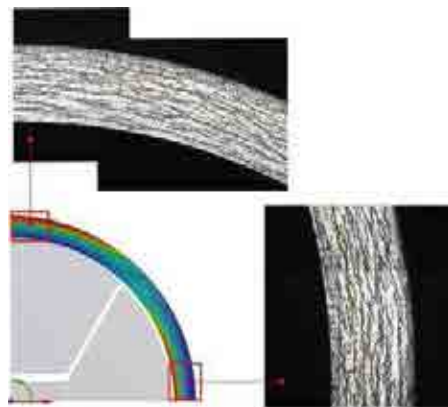
FIG. 18. Tensile movement mandrels.

FIG. 19. Hydride morphologies of ring test at 400°C with applied load of 127 N [65].

Irradiated test material was obtained from a 17 × 17 (9.5 mm outer diameter and 0.57 mm wall thickness) fuel rod using standard ZIRLO™ clad in cold work stress relieved annealed condition (CWSR). This fuel rod was irradiated in the Vandellós II NPP. Due to the more demanding irradiation conditions used in this programme, the achieved oxide thickness on some of the test specimens was ~120 μm and consequently the hydrogen absorbed in the cladding was ~800 ppm (cladding average); these properties can be considered as bounding for the fuel to be stored in the future. Six tests under constant internal pressure have been conducted using the ZIRLO™ rod material. In order to study hydride reorientation, the cool down of the specimens after the creep tests was specified to be < 2°C per minute; with a corresponding pressure decrease rate representative of the gas content and void volume of a high burnup rod. This procedure was maintained until a temperature below 150°C was reached; i.e. when the hydrogen remaining in solid solution can be considered negligible Fig. 22.

In a similar manner, the BWR tested material came from a General Electric GE-14 (10 mm outer diameter) fuel rod fabricated from standard zircaloy-2 clad (with liner) in recrystallized condition (RX) [63]. This fuel rod was irradiated for 5 cycles in Forsmark-3 NPP up to a rod average burnup of 41.3 GW·d·t(U)$^{-1}$. Some of the samples were subjected to a cool down procedure similar to the one described for PWR fuel, in order to study hydride reorientation.

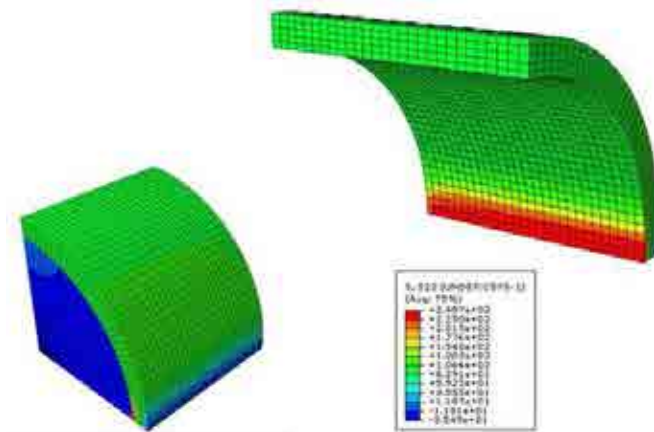FIG. 20. Experimental device employed in Spain..

FIG. 21. Calculated hoop stress in the cross section of the sample during the reorientation process (90 MPa; 400°C).
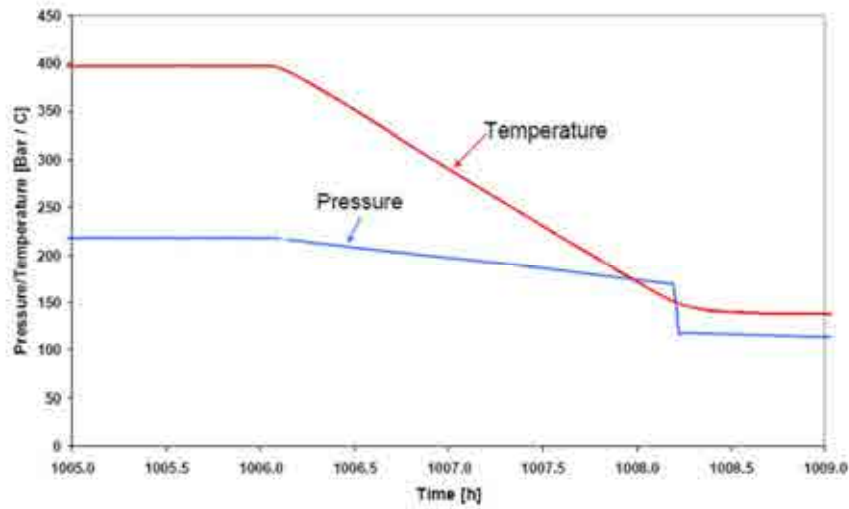
FIG. 22. Test cycle for hydride reorientation tests in Spain.

The reorientation process was carried out by keeping constant the hoop stress in the samples. During cooling down, the applied load was decreased in a linear fashion. The calculated load values at the beginning (400°C) and at the end (20°C) of the process are given in Table 5. These values were calculated using the FE model described above.

6.3.1.6.   Cladding tube deformation testing (CTDT) in Switzerland

To study cladding material properties and degradation mechanisms like hydride reorientation a kind of ring tensile test called 'cladding tube deformation test' (CTDT) was adopted at Paul Scherrer Institute (PSI) in Switzerland. As of 2012, hydride reorientation tests were conducted on zircaloy-2 cladding samples that were either non-irradiated [66], or irradiated [67] in a BWR. Other tests for crack resistance characterization of non-irradiated [68] zircaloy-4 and irradiated [69] zircaloy-2 have also been carried out to investigate the influence of hydrides on the axial crack propagation. The irradiated zircaloy-2 material came from a higher power density BWR after seven irradiation cycles and had been fully characterized [70].

TABLE 5. HOOP STRESS AND APPLIED LOAD VALUES FOR THE REORIENTATION PROCESS

Hoop stress (MPa)	Load applied at 400°C (kN)	Load applied at 20°C (kN)
60	0.796	0.610
90	1.222	0.924
120	1.682	1.222
140	1.934	1.430

Experimental setup

The CTDT experimental setup consists of a universal testing machine with a furnace that is able to apply thermo-mechanical loading on a specimen of 12 cm length. The cladding is loaded by two halve cylinder mandrels inserted into the cladding which results in a three dimensional stress field across the wall Fig. 23. The stress field needs to be calculated by finite element method.

The advantages of the CTDT setup are:

- Universal testing equipment reduces costly special purpose apparatus;
- Precise control of load and temperature;
- Specimen size makes it possible to test irradiated samples;
- Simple specimen preparation precludes any induced residual stress.

The disadvantages of the CTDT set-up are:

- As a non-standard technique, CTDT produces test specific results;
- Resultant stress fields differ from the real one in an internally pressurized tube and have to be examined numerically;
- The interaction between the cylinder halves and cladding influences the mechanical response.
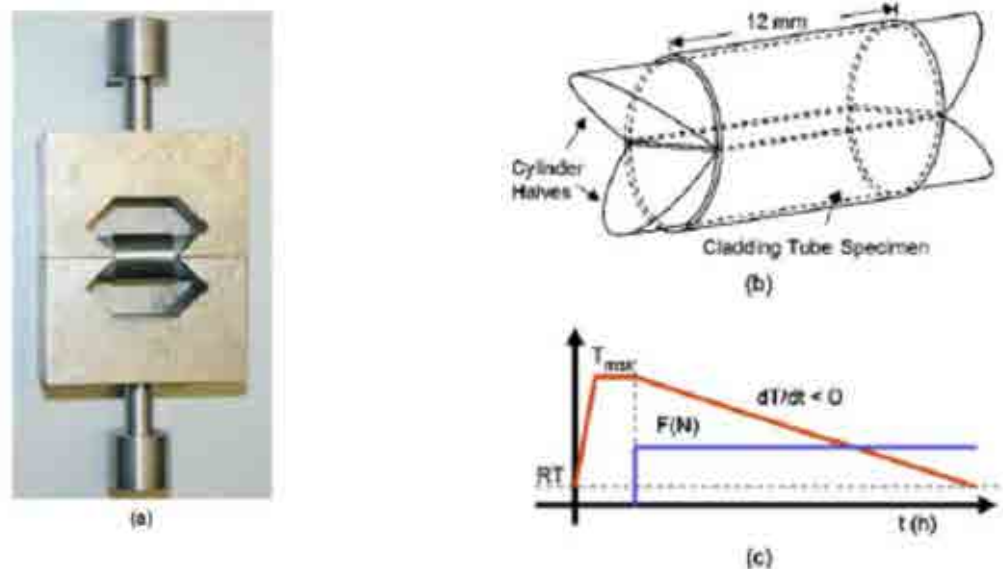

FIG. 23. (a) Cladding tube deformation test setup; (b) Specimen loading mechanism; (c) Loading cycle used in the test. Where RT is room temperature, T_{max} is maximum temperature of the cycle, dT/dt is the cooling rate, and F (N) is the applied force in CTDT.

Testing materials and procedures

The hydride reorientation was tested on zircaloy-2 fully recrystallized cladding provided by Westinghouse.

In case of non-irradiated material [66], the intention was to develop and validate the method and to investigate the influence of hydrogen content on the hydride reorientation. Nine specimens with hydrogen contents between 250 and 750 ppm were prepared. The inner liner was removed so that the initial hydride distribution was quite homogenous having on average only 5% radial hydrides. Eight of the nine tests were conducted at a temperature of 400°C and only one at 350°C.

Six irradiated [67] samples were extracted from two fuel rods (3 samples each) having a burnup ~66 $GW \cdot d \cdot t(U)^{-1}$. The hydrogen content in the relevant metallic bulk cladding was measured between 215 and 318 ppm. The hydrides in the heavily hydrided inner liner were not taken into account. The hydrides were initially distributed in the outer part of the cladding having initial fraction of radial hydrides around 10%. Three tests with two samples from each rod were conducted:

- High temperature (390–350°C) and one loading cycle;
- High temperature (390–420°C) and three loading cycles;
- Medium Temperature (330–350°C) and one loading cycle.

The test procedure was the same for non-irradiated and irradiated samples: Heat up to maximum test temperature; Hold at the temperature for 30 min; Apply load of 290 N; and Cool down at constant rate (Fig. 23(c)). In the case of loading cycles, the same procedure was applied repeatedly.

Validation

In order to validate the CTDT, pressurization tube tests were conducted on non-irradiated specimens [66]. The zircaloy-2 cladding specimens were hydrided to 250 ppm. In contrast to CTDT, the inner liner was kept; this was found to influence the hydrogen content in the bulk cladding. In two tests at 400°C the hoop stress varied between 55 and 170 MPa. Overall, similar results for local stress and hydride reorientation were obtained for pressurization tube tests and CTDT which supports validated of the CTDT technique.

6.3.1.7.   Tube testing under decreasing stress in United States of America

High burnup and pre-hydrided non-irradiated segments were fabricated into sealed and pressurized (with argon) rodlets. Bottom and top end fixtures fabricated from Zircadyne 702 were welded to each cladding segment. A zirconia pellet (25 mm long) was inserted into the rodlet to reduce the stored energy. The top end fixture contained a small hole to allow for pressurization of the rodlet. Room temperature (RT) pressures were selected to achieve target values of pressure and cladding hoop stress at 400°C.

The samples were heated to 400°C, held at 400°C for a pre-set time, cooled at 5°C·h^{-1} to 200°C, and cooled at a faster rate from 200°C to room temperature. Figure 23 shows the temperature history for a drying–storage simulation experiment; conducted with a 1 hour hold time and 1 cycle cooling. Some tests were conducted with slow and/or fast temperature cycling (from 400°C to 300°C to 400°C) prior to cooling to 200°C at 5°C·h^{-1}. In these experiments, simulated drying–storage is referred to as radial hydride treatment (RHT). Finite

element analysis (FEA) was performed to predict the thermal, elastic, and creep response of pressurized 17 × 17 and 15 × 15 cladding rodlets subjected to the reference simulated drying–storage temperature history shown in Fig. 24.

6.3.2. Test methods for effect of hydride reorientation on cladding mechanical properties including pros and cons

A number of mechanical test methods may be used to study the influence of radial hydrides on cladding embrittlement: ring compression test (RCT); uniaxial (hoop) ring stretch test; expansion due to compression test; and pressurized tube test. All four test techniques induce tensile hoop stresses. Except for the RCT, the other three test methods induce relatively uniform tensile hoop stresses across the cladding wall, which results in a more severe loading condition that may lead to lower DBTT values. For the RCT, stresses transition from tensile to compressive across the wall and non-uniform bending moments in the hoop direction result in peak stress regions at and around four orientations (i.e., 12, 3, 6, and 9 o'clock). The RCT better simulates pinch type loading.

6.3.2.1.   Ring compression test in Japan

The mechanical property change due to radial hydride reorientation was evaluated using ring compression tests at room temperature. The ring compression test method is shown schematically in Fig. 25. Ring specimens 8 mm in length were prepared from the cladding tube after the RHT. Ring specimens were compressed in the radial direction on the flat plane with a crosshead speed of about 2 mm·min^{-1} at room temperature. The test was also performed on as irradiated specimens as the reference.

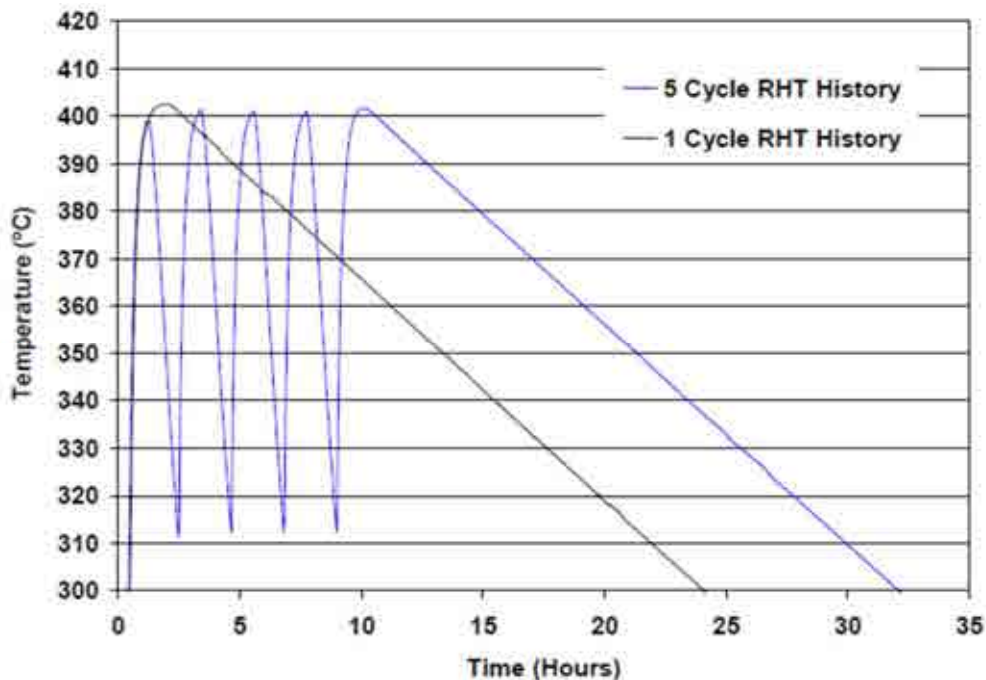*FIG. 24. Rodlet temperature history simulating one heating cycle and five heating cycles (final cooling rate of 5°C·h^{-1} to 200˚C; furnace power was turned off at 200˚C to achieve faster cooling to room temperature).*

6.3.2.2. Ring compression test in Spain

Ring compression tests (RCTs) have been carried out with samples which have been subjected to the reorientation treatment. The reorientation hoop stress values employed were 60, 90, 120 and 140 MPa and the hydrogen contents of the samples were 150, 500 and 1200 ppm.

The RCTs were performed using a universal fatigue testing machine (Instron 1275) at three temperatures: 20, 135 and 300°C. To this end, a furnace (Instron 3119) was attached to the testing machine. The load was measured using 5 kN load cell. A compression load was applied by means of two steel plates (plane and parallel).

6.3.2.3. Mechanical testing in Switzerland

To date, no mechanical tests have been conducted to assess the impact of hydrogen reorientation tests. However, axial crack propagation tests on non-irradiated and irradiated cladding tubes were run to investigate fracture mechanics properties. Although the irradiated cladding failed in a much brittle way, the scanning electron microscopy method did not reveal any adverse influence of hydrides on crack propagation. The cladding had not been subjected to hydride reorientation and the initial crack flaw and crack opening were in axial direction, i.e., parallel to cladding rotational axis.

6.3.2.4. Ring compression test in the United States of America

RCTs were conducted in two mechanical test systems: a table top Instron screw type machine for non-irradiated samples and an Instron servohydraulic mechanical test system enclosed in a glove box for irradiated samples. Figure 26(a) shows a schematic of the RCT sample, loading, and displacement. The tests were run in the displacement controlled mode. The crosshead displacement rate was pre-set at 5 mm·s^{-1} and the displacement (δ) is measured as a function of time. The response load (P) was measured by a load cell located in the static support component (6 o'clock position). Figure 26(b) shows a cladding ring resting on the support plate of the Instron with a small space between the loading plate and the top (12 o'clock) of the ring outer diameter. A clamshell radiant heating furnace provided the heat for elevated temperature tests with high burnup cladding. Three thermocouples (TCs) contacted the ring at the 3, 6, and 9 o'clock positions for elevated temperature tests. For RCTs with non-irradiated cladding, oven heating and a single TC at the 6 o'clock position were used. For both heating systems, the TC at the 6 o'clock position was used to control the furnace or oven power, as well as to secure the sample by means of TC spring loading.
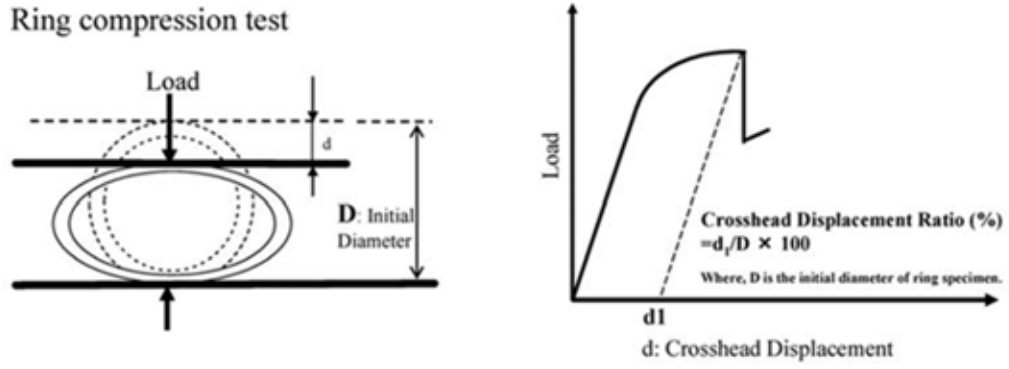
FIG. 25. Test methods of ring compression test [64].

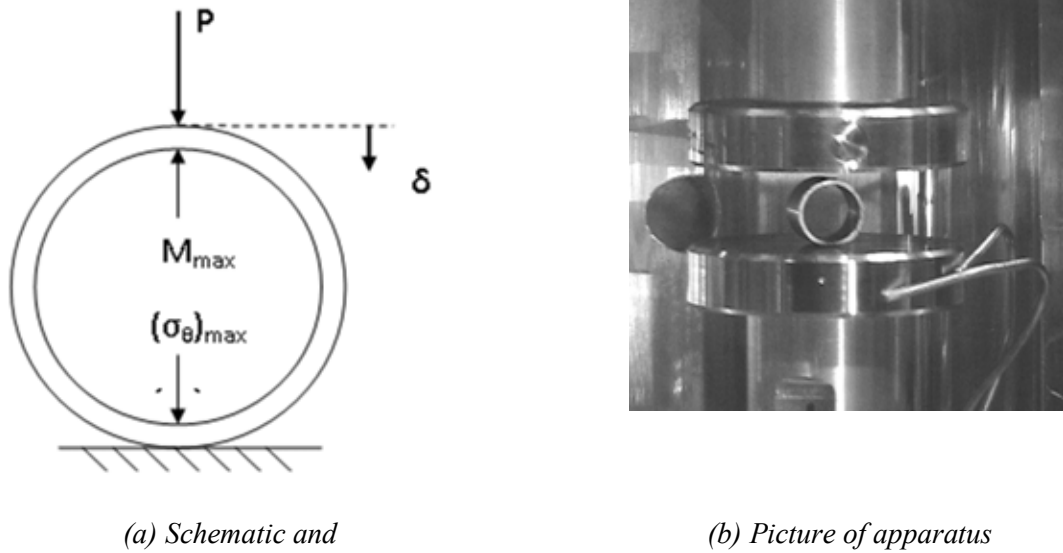*(a) Schematic and*   *(b) Picture of apparatus*

FIG. 26. Ring compression test. The top plate (above the ring) is attached to the movable loading rod. The bottom plate (below the ring) is attached to the static support rod, which contains a load cell to measure P. Tests are conducted in a displacement (δ) controlled mode.

The ring stiffness decreases with increasing displacement as the ring cross sectional shape progresses from circular to oval with some flattening under the loading plate and above the support plate. As this occurs, the load progresses from a concentrated line load to a distributed load at the contact points. These geometric changes, along with residual stresses during unloading due to localized plastic deformation, lead to an unloading slope that is less than the loading slope that is usually used to determine offset displacement. In the studies, the ring is treated as a spring. The permanent displacement, which is determined after removal of the load, is considered to be the more accurate measure of the plastic deformation of the spring. Strain is determined from the RCT results by normalizing offset and permanent displacements to the pre-test outer diameter of the ring sample. Figure 27 shows benchmark load displacement results for a non-irradiated as fabricated 17×17 cladding ring with 9.48 mm (D_o), wall thickness 0.63 mm (h_m), and 7.7 mm length (L). Test conditions were the same as those used for the high burnup cladding at RT: 5 mm·s^{-1} loading displacement rate; 1.7 mm total loading displacement; 5 mm·s^{-1} unloading displacement rate. Because $L \cdot h_m^{-1}$ is >10,

wide beam theory (i.e., plane–strain constraint in the axial direction) was used to determine the K_c value given in Fig. 27. Normalizing the displacements to D_o gave a 12.6% offset strain and 11.1% permanent strain. Although permanent strain gives a more accurate measure of plastic strain for rings that do not fail, it cannot be determined accurately for rings that crack prior to 1.7 mm total displacement. Based on assessments of error measurements and data trends, cladding with either ≥1% permanent strain or ≥2% offset strain prior to the first crack extending through >50% of the wall is classified as ductile. Cladding that cracks through >50% of the wall prior to achieving 2% offset strain is classified as brittle in the current work.

6.3.3. Hydride reorientation quantification

An issue in comparing testing results from various researchers was that a variety of measures of the hydride reorientation were used, and insufficient raw data were provided to relate the variety of quantification techniques. Some of the quantification methods currently in use are described below.

6.3.3.1. Radial hydride fraction (RHF) method in Japan

The morphology of the hydrides, including the orientation, was evaluated by image analysis from metallography after the HRT (Fig. 28). The hydride morphology of as irradiated (no RHT) cladding was also evaluated as the reference. The degree of radial hydride orientation was evaluated using *Fn(40)* and *Fl(45)*; defined (8) and (9). Here, hydrides in the metallographic sections, except those in the zirconium liner or at the interface between the zirconium liner and zircaloy-2 matrix area, were analyzed for both *Fn(40)* and *Fl(45)*. Hydrides with less than 16 μm in length were excluded for *Fn(40)*. *Fn(40)* is the conventionally used definition, and *Fl(45)* is a second indicator of the amount of radial hydride:

$$Fn(40) = \frac{\text{(Sum of the number of hydrides in radial direction ±40°)}}{\text{(Sum of the number of all hydrides)}} \tag{8}$$

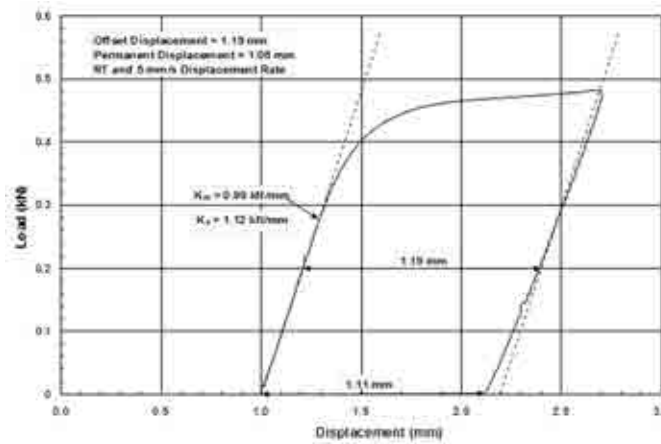$$Fl(45) = \frac{\text{(Sum of the number of hydrides in radial direction ±45°)}}{\text{(Sum of the number of all hydrides)}} \tag{9}$$

FIG. 27. Results of RCT benchmark using the Instron 8511 to compress an as-fabricated 17 × 17 cladding ring at RT and 5 mm·s^{-1} loading and unloading displacement rates.

6.3.3.2. Hydride reorientation quantification and characterization in Spain

The variation of the hydride reorientation fraction F_n as a function of the hoop stress is shown for the three concentrations tested: 150, 500 and 1200 ppm In Fig. 29. F_n was calculated using expression (10) as given in [71]:

$$F_n = \frac{P_{L\perp}}{P_{L\perp} + P_{LII}} \tag{10}$$

Where $P_{L\perp}$ is the number of intersections of the radial hydrides with equispaced horizontal lines and P_{LII} is the number of intersections of the circumferential hydrides with equispaced vertical lines.

Hydride morphology and distribution were studied by metallography. Samples were cold mounted with epoxy resin and then polished with a 1 micron alumina suspension. The last finishing step involved polishing with a mixture of colloidal silica (0.05 micron), H_2O_2 (30% vol.) and HF (40% wt.) in the proportion (50 vol.: 10 vol.: 1 vol.). After polishing, samples were etched for 90 seconds with a solution of HNO_3 (69% wt.), lactic acid (95% wt.) and HF (40% wt.) in the proportion (48.5 wt.: 48.5wt: 3 wt.). This way, the hydride structure was revealed.

6.3.3.3. Hydride reorientation quantification and characterization in Switzerland

In case of non-irradiated samples, the section images taken by optical microscope were digitalized and semi-automatically analyzed to avoid repetitions. After finding the dominant hydride axis, all amounts of hydrides within an angle of ±30° around the circumferential direction were defined to be circumferential and the ones around the radial direction within the same angle range to be radial oriented hydrides. Hydrides smaller than 15 μm and with the length to width ratio less than 2.5 were not accounted for.

The irradiated samples were evaluated in a similar manner, but with the help of a more sophisticated procedure so that radial and azimuthal distributions of the hydride frequency and length could be found. Circumferential hydrides were defined to lie within ±45° around the circumferential direction.
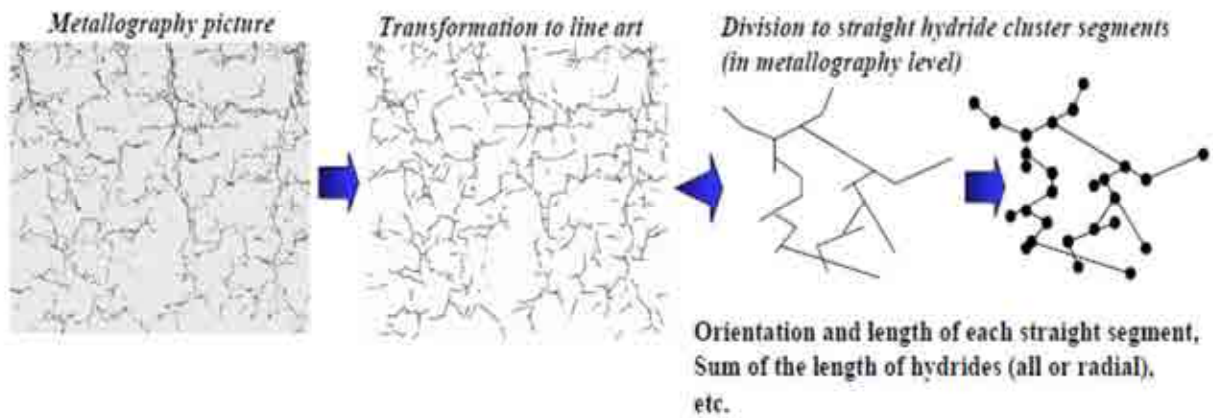

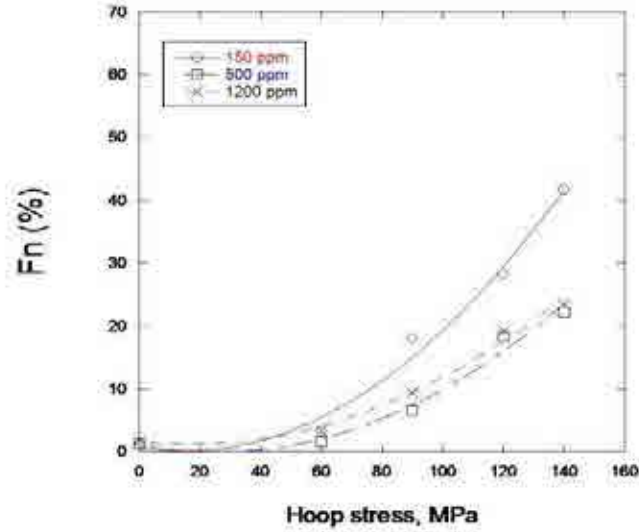FIG. 28. Image analysis of hydrides [64].

FIG. 29. Hydride reorientation fraction, F_n, as a function of the hoop stress for the three concentrations tested: 150, 500 and 1200 ppm of hydrogen.

Collected data like the size, position, and orientation were linked with the local principal stress calculated by FE method to find the hydride reorientation stress threshold. Reorientation was indicated as soon as the local fraction of radial hydrides rose above the initial level.

6.3.3.4. United States of America radial hydride continuity factor (RHCF)

The hydride continuity coefficient (HCC) has been used by Canadian researchers to characterize the extent of radial hydride formation in Zr-2.5%Nb pressure tubes [72–73]. It is determined by projecting the radial hydrides within a 0.11 mm circumferential band onto the radius across the metal wall. The net length of these projected hydrides is normalized to the metal wall thickness to determine HCC. Neither RHF nor HCC is an adequate metric for predicting crack growth under RCT loading. For example, rings with short discontinuous radial hydrides and rings with long continuous hydrides might have RHF and HCC values of 100%, but the latter would be more prone to significant cracking during RCT loading. A new metric was developed, the radial hydride continuity factor (RHCF), to better correlate hydride orientation and morphology with crack initiation and growth.

Figure 30.(a). shows the hydride morphology following RHT at 190 MPa and one of three long cracks that formed during 1.6 mm displacement for a ring containing 630 ± 110 ppm. The crack, imaged in Fig. 30(a), initiated at the cladding outer surface, propagated along radial hydrides at three locations, and propagated along circumferential hydrides at two intermediate locations. Circumferential hydrides connecting the radial hydrides were within a 150 μm band. The RHCF is assessed to be 100% within this 150 μm band. Fig. 30(b) shows a section of a ring, with 190 ± 10 ppm hydrogen, which has been subjected to RHT at 190 MPa. The 12 o'clock (as determined by a clock face with a 12 o'clock being up) crack extended through about 90% of the wall, and the 6 o'clock crack extended through 100% of the wall. The RHCF is clearly 100% for this image.

The RHCF is assessed as being a better metric than RHF or HCC for correlating hydride morphology and orientation with extent of cracking during RCT loading. It represents the length of continuous radial–circumferential hydrides across the cladding wall (normalized to the wall thickness) within a circumferential band of 0.15 mm. RHCF, however, does not distinguish radial–circumferential hydrides emanating from the inner cladding surface from those located near the cladding mid-wall or those located near the cladding outer wall. In the RCT, the hoop tensile stress is highest at the cladding inner surfaces below the applied load and above the support plate. Continuous radial–circumferential hydrides emanating from this inner surface would induce crack initiation and propagation with very small or no plastic deformation. Continuous radial–circumferential hydrides emanating from the outer surface just under the hydride rim would participate in unstable crack growth initiated in the rim. Continuous radial–circumferential hydrides located near the cladding mid-wall would be subjected to very low hoop stress levels during RCT loading.

6.4. RESULTS OF STUDIES
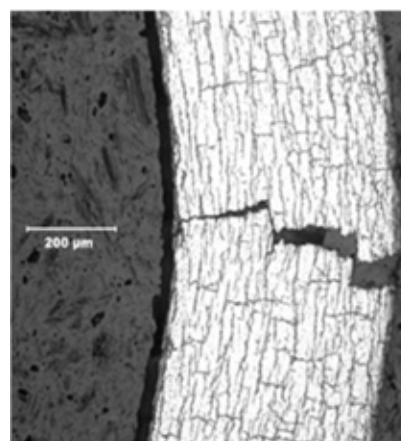
6.4.1. Effects of temperature

It has been established that only hydride that is dissolved by raising cladding temperatures by transferring spent fuel from a wet environment to a dry environment, and then re-precipitated during subsequent cooling can potentially reorient. Therefore, the cladding temperature determines how much hydrogen goes back in solid solution in the zirconium based alloy matrix.

For illustration purpose, the solubility curves (TSSD and TSSP) established for non-irradiated alpha annealed zircaloy-4 are shown in Fig. 31.

Heating from pool temperature to 400°C results in up to ~210 ppm of hydrogen going into solution in the alloy matrix, assuming that the alloy originally contains at least that amount of hydrides. While heating to 300°C only dissolves up to ~77 ppm.
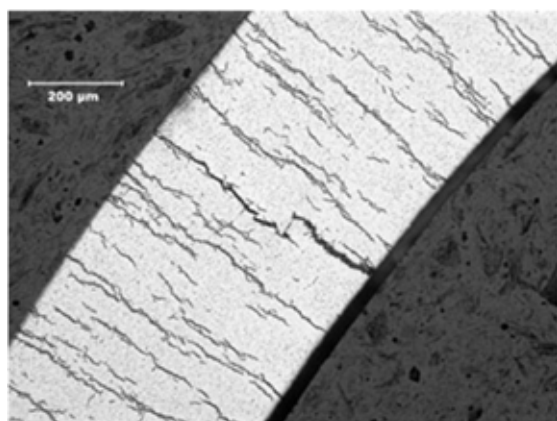
(a) 630±110 ppm hydrogen.   *(b) 180±10 ppm hydrogen.*

FIG. 30. Through-wall crack paths for pre-hydrided (PH) and RHT ZIRLO™. RHCF is 100% for both images.

Upon cooling from 400°C, hydride re-precipitation of hydrides is initiated at ~335°C, based on the curves shown in Fig. 31. This is the expected behaviour when the material contains hydrogen at or near the solubility limit of 210 ppm. If it is assumed that the alloy contains 500 ppm of hydrogen, then at 400°C the expectation is ~210 ppm of hydrogen will be in solution and the balance (~290 ppm) of hydrogen will remain as hydrides. Upon cooling Colas and Motta [74] found, using in-situ XRD, for non-irradiated cold worked stress relieved annealed zircaloy-4 cladding that hydride re-precipitation occurred with no or little hysteresis. Under these conditions, they also observed that the threshold hoop stress for hydride reorientation is between 150 and 200 MPa; which is substantially higher than the threshold stress observed for samples with no hydride present at 400°C.

6.4.1.1.   Results from France

Results obtained in several investigations pursued in France are shown in the Fig. 32. These results are qualitatively in agreement with those obtained at PSI (Switzerland).

6.4.1.2.   Results from Spain

It can be observed in Fig. 29, that for the same hoop stress value, the parameter F_n is higher for 150 ppm than for 500 and 1200 ppm. The evolution of F_n with the hoop stress, however, is similar for 500 and 1200 ppm.

Some representative micrographs of the reorientated samples are shown in Fig. 33; for hoop stresses of 120 and 140 MPa and hydrogen concentrations of 500 and 1200 ppm.

6.4.1.3.   Results from Switzerland

Non-irradiated:

- Since the majority of the samples were tested at 400°C and only one sample at 350°C, the hydride reorientation dependency on temperature was not investigated;
- Testing of non-irradiated samples showed that the hydride reorientation stress threshold rises with hydrogen concentration reaching a plateau at some level. At the hydrogen concentrations of 250 ppm and 550 ppm, the stress threshold was found to be 72 and 120 MPa, respectively.

Irradiated:

- At high temperatures around 420°C, either after one or three loading cycles, significant hydride reorientation at the outer part of cladding with higher initial hydride concentration was observed. The stress threshold for reorientation at this temperature level was found to be ~50 MPa;
- On the other hand, at medium temperatures around 350°C, different results were obtained. Whereas in one rod the radial hydride fraction almost doubled, in the other rod nearly no reorientation was observed. The reproducibility of the test at this temperature level failed. It is believed that at higher temperatures most of the hydrogen is in solid solution and has the potential to precipitate, depending on the stress, in one direction. At lower temperatures less hydrogen is dissolved and thus less able to precipitate somewhere else.
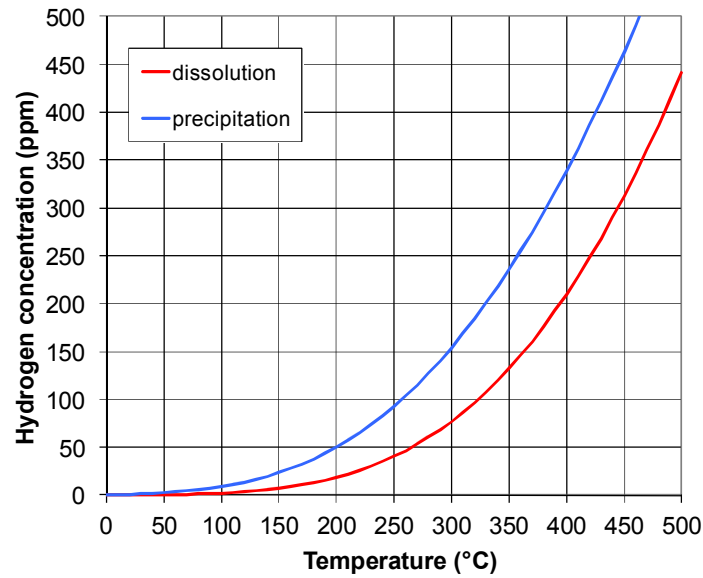
FIG. 31. Solubility curves for alpha annealed zircaloy-4 (adapted from [75]).
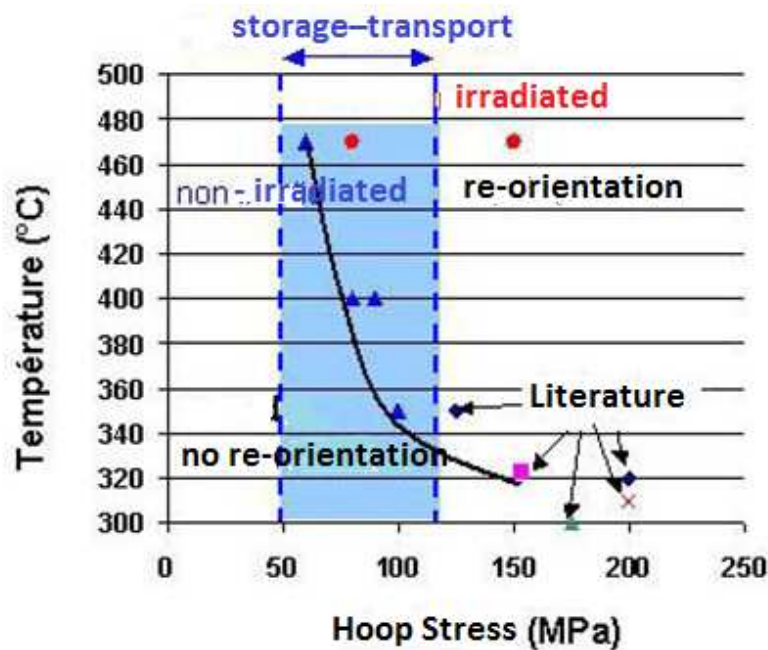
FIG. 32. Hydride reorientation domains vs. stress/ temperature [76].

6.4.2. Effects of initial stress

The stress on the cladding is determined by a number of factors that can be highly uncertain. It is clear that as a rod begins to cool either after drying or due to natural radioactive decay that the stress will decrease as governed by the ideal gas law. Much of the work to study hydride reorientation, both past and current, was done under constant stress. As shown by Fig. 32, both the stress and temperature affect the degree of reorientation, but the curves may shift depending on the measure of reorientation used; since the temperature affects the amount of

hydrogen that goes into solution (if the measure is a ratio to the total hydrides, one would expect the ratio to increase at higher temperatures because more hydrogen in solid solution is available for reorientation).

The end of life (EOL) rod internal pressure (RIP) is the primary protagonist for evolutionary changes during long term dry storage that affect cladding resistance to failure when spent fuel assemblies are subjected to normal and accident conditions of transport. At the maximum temperature attained either during vacuum drying or dry storage, EOL rod internal pressures (EOL RIP) determine the maximum stress state in the fuel rod cladding, which in turn sets the initial conditions for potential time dependent changes in the hydrides structure in the cladding as the latter undergoes slow cooling in the inert environment of the storage cask. In addition, EOL RIP values must be modified for the temperature and void volume distribution in the fuel rod that exists during vacuum drying or dry storage. Finally, there is uncertainty with regard to the role interaction layers that exist between cladding and fuel when dealing with spent high burnup fuel. During the very slow cooling process, cladding stress will be slowly reduced. Cladding stress may be further reduced due to cladding creep, which causes the fuel rod void volume to increase; assuming that fuel cladding bonding is not sufficiently strong to impede thermal creep. On the other hand, fuel cladding bonding may be sufficiently strong such that cladding and fuel structurally form a composite material; in such a situation, cladding stresses are likely to be significantly lower than estimated when a gap between fuel and cladding is assumed to exist. After some period of time, local cladding temperatures reach levels where the hydrogen in solid solution begins to re-precipitate upon further cooling, which is the time at which the value of cladding stresses is most relevant.

6.4.2.1. Stress effect on reorientation

The Spanish PWR test shutdown procedure was quite successful to precipitate the hydrogen in solid solution in the radial direction for irradiated fuel. All the samples taken from the different tests showed radial hydrides (for example Fig. 34). Significant radial hydrides precipitated, but no failure was observed during the cool-down process.

For the BWR fuel, the radial hydrides seemed to increase with hoop stress during shutdown and some degree of reorientation was observed even at 70 MPa hoop stress. Based on published data, the situation is different for CWSR material where the reorientation has been observed for higher stress values. Additionally, load at cracking for RCT usually increases as *Fn* factor decreases but, a more detailed analysis should be performed as some influence of previous deformation, due to the creep-tests, was clearly observed in one of the tests performed. The influence of annealing should also be assessed.

In Fig. 35, the Japanese plotted *Fn(40)* and *Fl(45)* versus RHT hoop stress for BWR Zircaloy-2 claddings with zirconium liner. For 300°C RHT specimens, a slight increase in *Fn(40)* and *Fl(45)* was observed at RHT hoop stresses of 40 and 70 MPa, and a certain degree of hydride reorientation occurred at RHT hoop stress of 100 MPa; both factors appear to be increasing linearly with stress at 300°C, and even at 100 MPa the degree of reorientation is less than 40%. In 400°C RHT specimens, both *Fn(40)* and *Fl(45)* increased with the hoop stress within the tested hoop stress range.
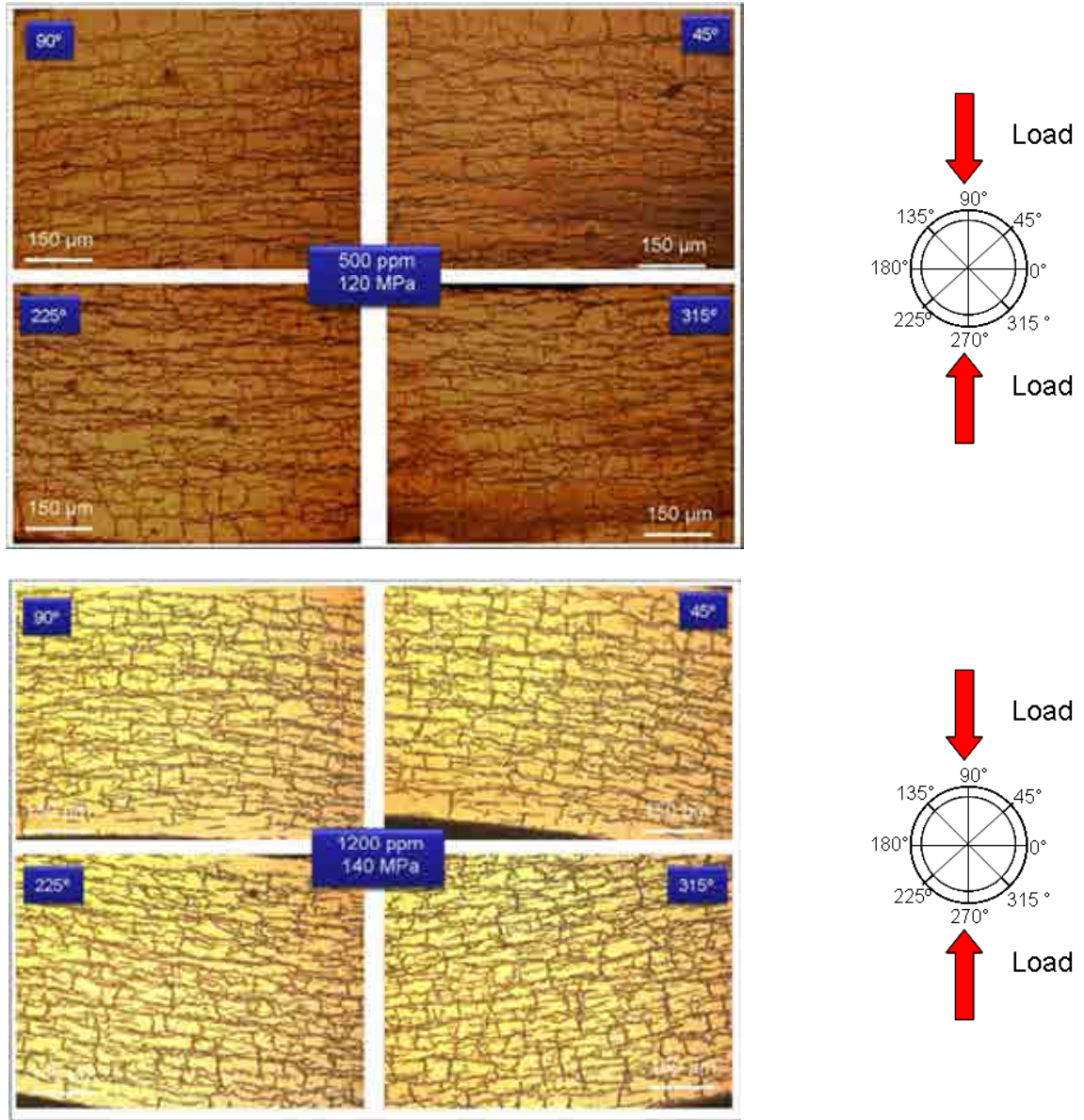
FIG. 33. Micrographs of reorientated samples (hoop stresses 120, 140 MPa and hydrogen concentrations of 500, 1200 ppm) – Spanish results.

Fne has been calculated using the data given in Fig. 35(a) and by using equation (11) shown in Fig. 36. *Fne* is the normalized *Fn* by considering the dissolved hydrogen amount at each RHT.

$$Fne(40) = \frac{C_{H\_t} \cdot Fn(40) - (C_{H\_t} - C_{H\_d}) \cdot Fn(40)_0}{C_{H\_d}} \tag{11}$$

Where

C_{H_t} is total hydrogen content of the specimen;

C_{H_d} is dissolved hydrogen content at HRT temperature;

If C_{H_t} is more than C_{H_d}, C_{H_d} is equal to TSSD of the cladding;

If C_{H_t} is less than C_{H_d}, C_{H_d} is equal to C_{H_t} and Fne(40) is equal to Fn(40);

Fn(40)_0 is equal to Fn(40) of the irradiated specimen
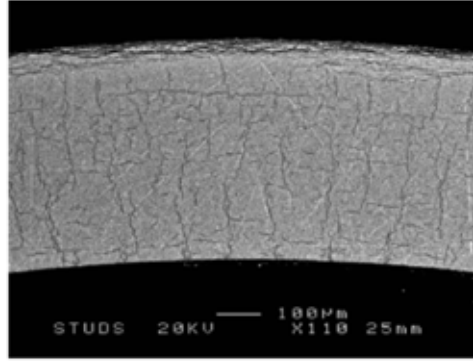
FIG. 34. Spanish PWR test sample showing hydrides precipitated in the radial direction.
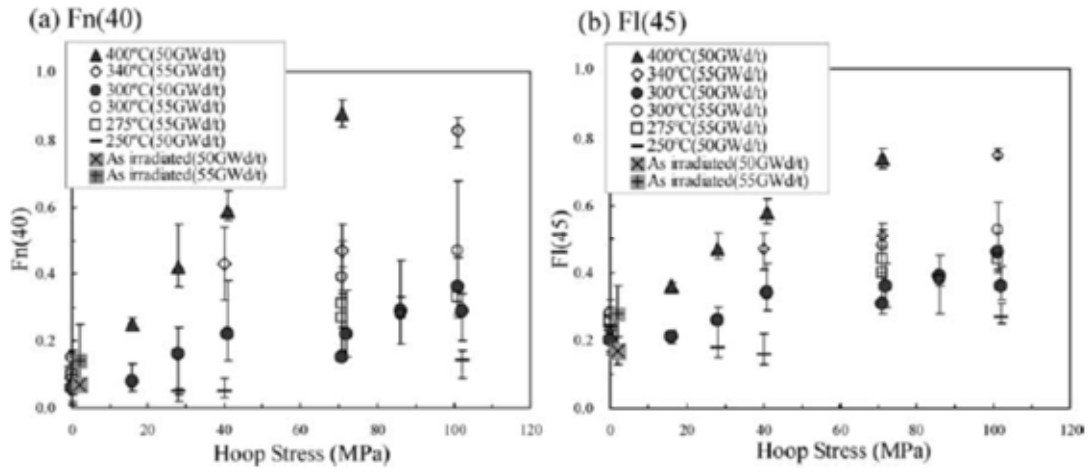
FIG. 35. Correlation between the degree of reorientation, Fn(40) and Fl(45), and the RHT conditions for irradiated BWR zircaloy-2 cladding with zirconium liner (cooling rate: 30°C·h^{-1}) [64].

FIG. 36. Correlation between the degree of reorientation, Fn(40) and Fl(45), and the HRT conditions for irradiated BWR zircaloy-2 cladding with Zr liner (cooling rate: 30°C·h^{-1}) [64].

The results of hydride reorientation tests for irradiated PWR 48 GW·d·t(U^{-1}) type zircaloy-4 cladding were evaluated in the same way as for BWR cladding, and the results are shown in Fig. 37. The radial hydride ratio increased for the specimens after a 115 MPa, 300°C, 30°C·h^{-1} HRT compared to the as-irradiated specimens, as shown in Fig. 37.

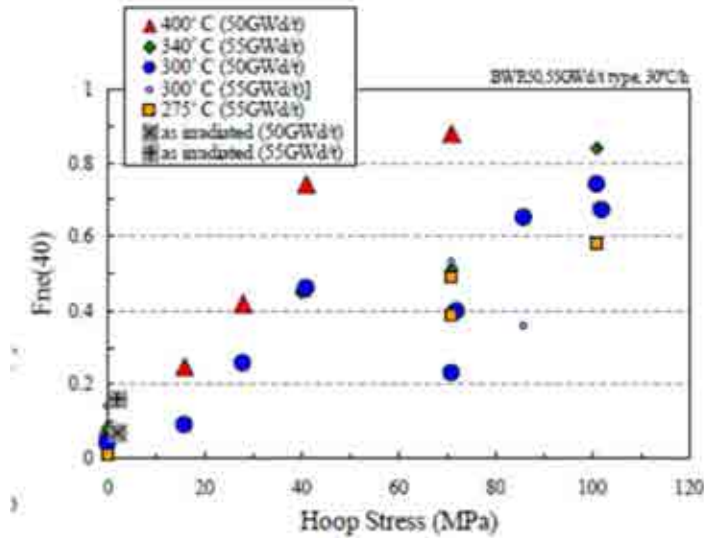Using the pressurized tube method with a decreasing stress, Argonne National Laboratory (ANL) evaluated the effects of the initial stress at maximum temperature on the degree of hydride reorientation using the radial hydride continuity factor as a measure of the reorientation [77]. As can be seen in Table 6, the higher the initial applied stress, the higher the reorientation.

Information from all the investigators points to a higher degree of hydride reorientation with a higher applied stress on the cladding. Unlike past studies, on mostly non-irradiated material and supported by ANL studies on non-irradiated material (over the stress range used in the study), there does not appear to be an intrinsic applied stress below which no reorientation is observed (no stress threshold for reorientation). The degree of reorientation is clearly dependent on the definition of reorientation that is used.

6.4.2.2.   *Effects of RHT stress on cladding ductility*

Figure 38 summarizes the results for BWR zircaloy-2 cladding with a zirconium liner. The crosshead displacement ratio did not show hoop stress dependence for the 300 and 250°C RHT specimens; although some degree of reorientation was observed in the 300°C, 70–100 MPa range RHT specimens. On the other hand, the crosshead displacement ratio and ductility increased for the 400°C, 0 MPa RHT (heat treatment only with no stress) specimens compared to as-irradiated specimens, and it decreased with an increase of the hoop stress in RHT (or with the amount of radial hydride).
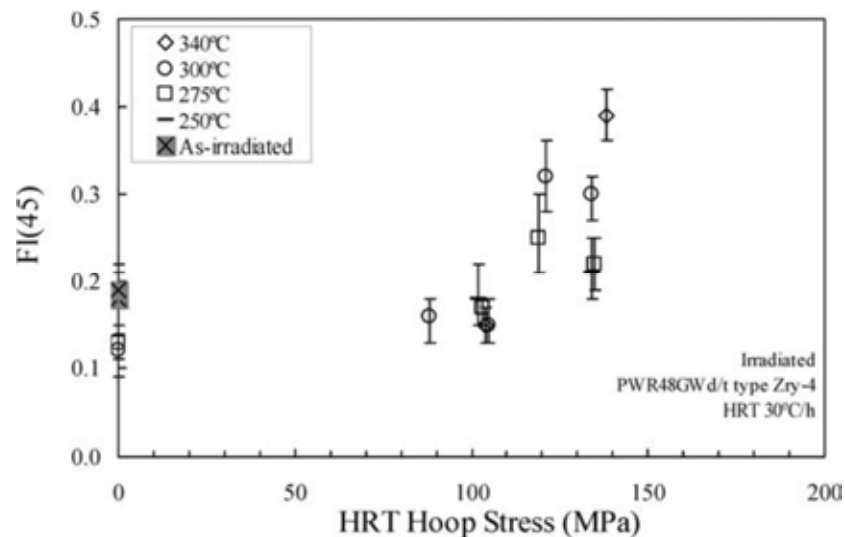

FIG. 37. Correlation between the degree of reorientation and the RHT conditions for irradiated PWR zircaloy-4 cladding [64].

TABLE 6. RHT CONDITIONS AND POST RHT CHARACTERIZATION RESULTS FOR 70 GW·d·t(HM)$^{-1}$ ZIRLO™ AND FOR 67 GW·d·t(HM)$^{-1}$ ZIRCALOY-4

Material	σ_θ at 400°C MPa	C_H ppm	RHC %	RHCF data points
ZIRLO™	140	650±190	65±17	16
	110	425±63	27±10	8
	110	350±80	33±14	33
zircaloy-4	110	520±90	9±5	11
	140	615±82	16±4	12

The results of the ring compression test for 48 GW·d·t(HM)$^{-1}$ type zircaloy-4 cladding are summarized in Fig. 39. The crosshead displacement ratio was almost the same level for the 250°C and 275°C, 100 MPa RHT specimens when compared to as irradiated specimens. The specimens after a 340°C, 100 MPa RHT and 300°C, 100 MPa RHT showed a lower crosshead displacement ratio compared to as irradiated specimens; although *Fl(45)* did not show an increase after these RHT conditions. It is proposed that the morphology change including the orientation, length, and the amount of hydride may have affected the ductility.

ANL/NRC used the offset displacement measured in a ring compression test to determine the degree of ductility after hydride reorientation tests. The reference describes how offset strain lower than 2% represents brittle behaviour [77]. The results of those tests are shown in Table 7.

In addition to the reorientation studies on irradiated material, Racine studied the tensile circumferential behaviour at ambient temperature of some pre-hydrided SRA zircaloy-4 [78]:

- Without hydrogen (NH);
- With 200 ppm hydrogen in the form of[9]:
  - Circumferential hydrides (C) with 3 % radial hydrides[10] (200 C);
  - Radial hydrides with 65 % radial hydrides platelets (200 R);
- With 500 ppm hydrogen in the form of:
  - Circumferential hydrides with less than 10 % radial hydride platelets (500 C);
  - Circumferential and radial hydrides with less than 10 % radial hydride platelets (500 M);
  - Circumferential and radial hydrides with 13 % radial hydride (500 R).

The objective of the tests was to evaluate the influence of hydride orientation. The data was used to justify cladding resistance for an applied pinch load through a maximum allowable

---

[9] C = circumferential, R = radial, and M = mixed hydrides
[10] Radial hydrides: oriented at 90° of circumferential direction (+/- 45°). Radial hydride fraction is defined as the sum of the length of all radial platelets divided by the sum of all platelets.

displacement ratio. The different tested materials showed differences in strain at rupture (see Fig. 40).

Figure 41 [78] shows strain at rupture measured on various materials of Fig. 40, versus hydrogen content in cladding tube.

Three rupture modes are observed by Racine:

- Ductile for NH and 200 C cases;
- Brittle for 200 R case with ~ 65 % radial hydrides; rupture is totally brittle without plasticity, therefore rupture occurs in the linear part of the strain force curve (Fig. 39);
- Brittle after beginning of plasticity for other cases.

Clearly, the more radial hydrides the lower the strain to failure for the material.
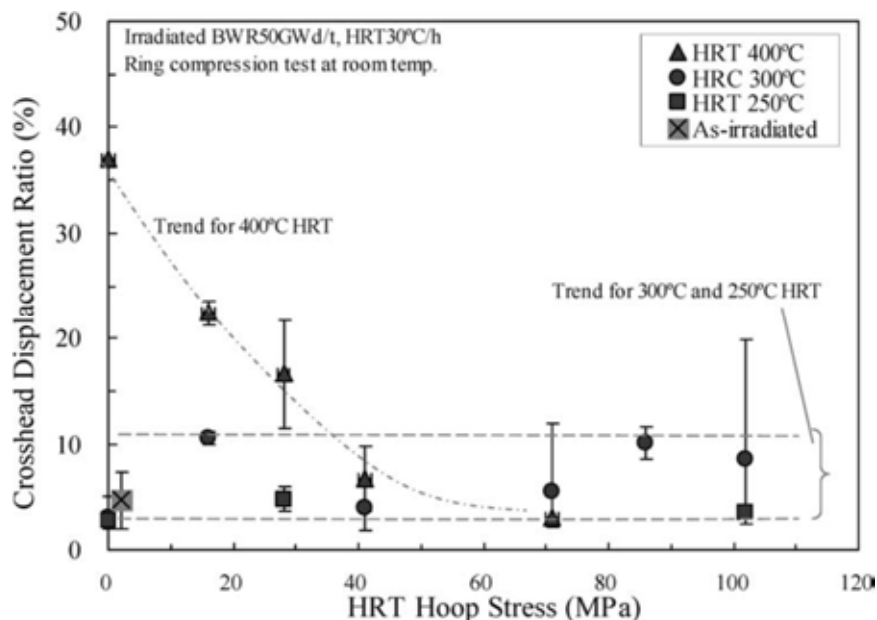

FIG. 38. Correlation between the ductility of the specimens and HRT conditions for irradiated BWR zircaloy-2 cladding with a zirconium liner [64].

TABLE 7. SUMMARY OF RING COMPRESSION TESTING (RCT) RESULTS FOR RHT RODLETS SUBJECTED TO SIMULATED DRYING–STORAGE TEMPERATURE HISTORIES WITH A MAXIMUM TEMPERATURE OF 400°C, HOOP STRESSES OF 110 MPA OR 140 MPA, AND COOLING AT 5 °C·h^{-1} WITH DECREASING HOOP STRESS

Material	HRT σθ at 400°C (MPa)	C_H ppm	RHCF %	RCT (°C)	Corrected offset strain (%)[11]
ZIRLO™	140	650 ± 190	65 ± 17	150	0.0
				150	1.4
				195	4.5
ZIRLO™	110	425 ± 63	27 ± 10	30	0.6
				150	>9.5
				150	8.6
				150	>9.0
ZIRLO™	110	350 ± 80	33 ± 13	30	0.3
				90	0.4
				120	1.7
				150	>10.2
zircaloy-4	110	520 ± 90	9 ± 5	24	2.8
				90	5.0
				120	6.7
				150	>9.2
zircaloy-4	140	615 ± 82	16 ± 4	30	1.2
				90	3.3
				150	5.8

[11] The '>' sign means that the ring survived a 1.7 mm displacement with no cracking, or <50% wall crack.
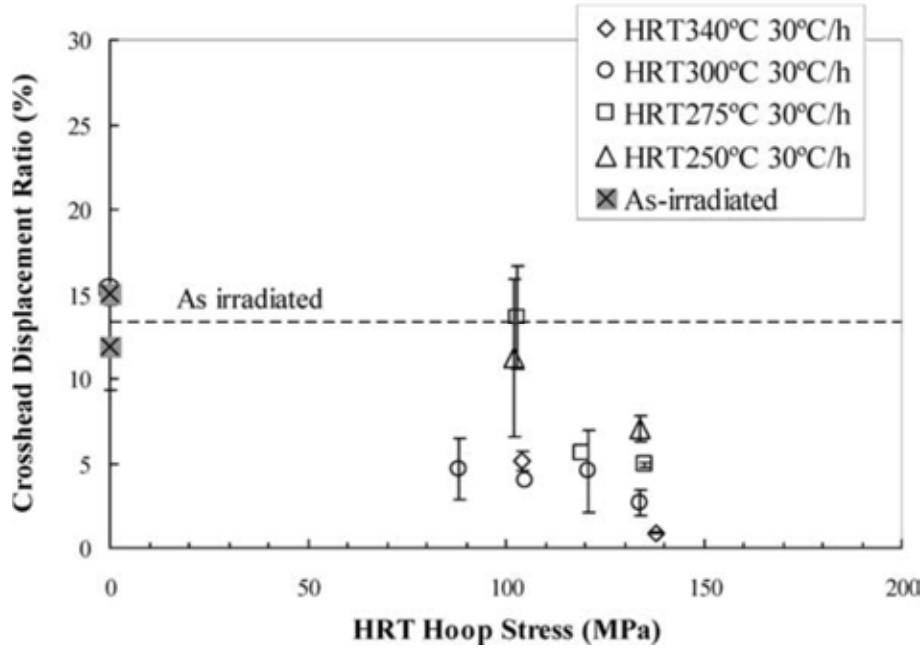
FIG. 39. Correlation between the ductility of the specimens and the HRT conditions for irradiated PWR 48 GW·d·(t(HM)⁻¹) type zircaloy-4 cladding [64].
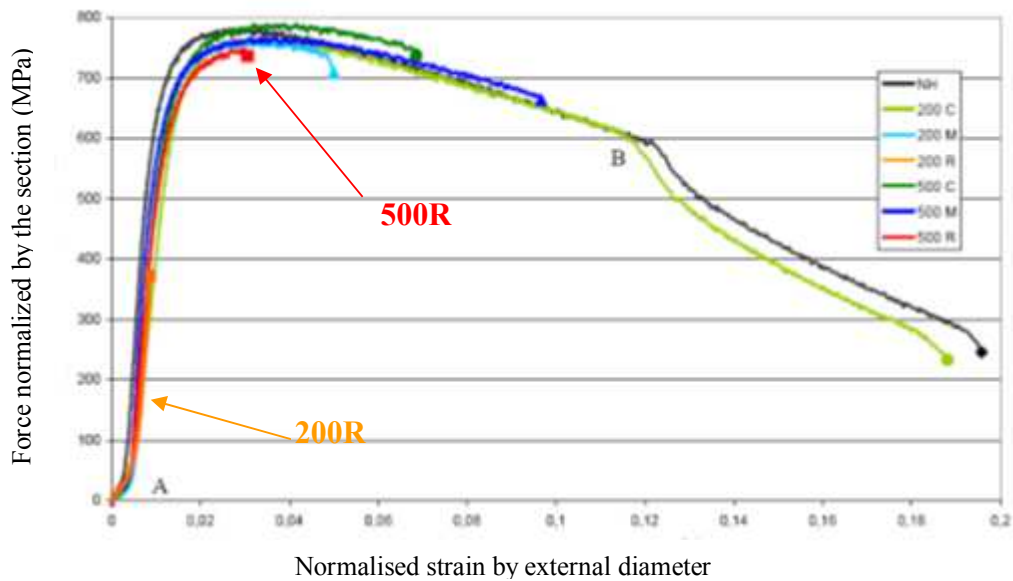
FIG. 40. Force normalized by the section vs. normalised strain by external diameter [78].

All the studies both on pre-hydrided non-irradiated cladding and high burnup irradiated cladding showed the same trend; the higher the applied stress during drying or storage, the more likely the cladding will become brittle and potentially fracture.

FIG. 41. Strain at rupture (normalized strain by external diameter) vs. effective radial hydrogen content (ppm) of each specimen [78].

The Spanish used ring compression tests to measure load–displacement curves with reorientation load, compression test temperature and hydrogen content as variables. The RCTs were carried out at 300°C using samples with hydrogen contents of 500 and 1200 ppm; the results are shown in Fig. 42. As can be seen in Fig. 42, at 300°C, the reorientation stress has little impact on the load–displacement; even at 120 or 140 MPa.
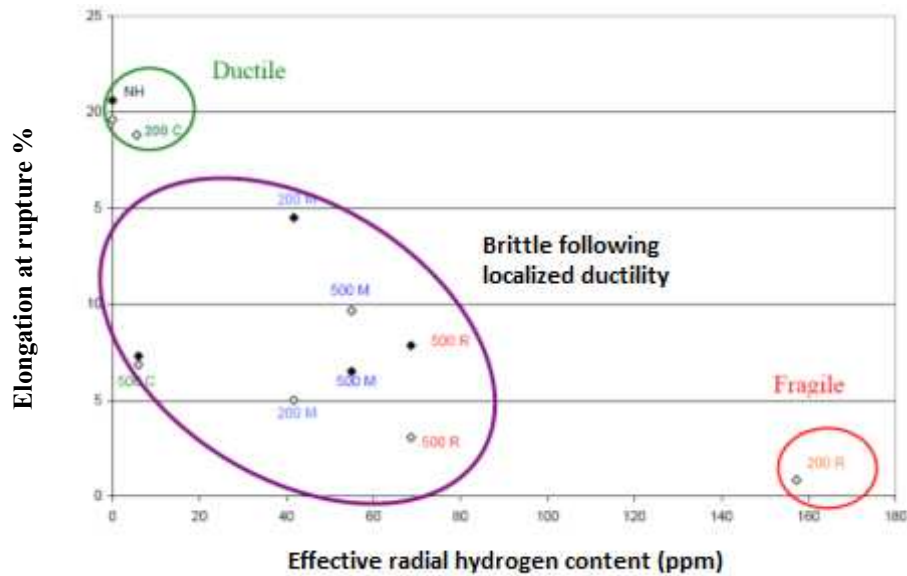
The Figs. 43–44 show the ring compression tests performed at 135 and 20°C in samples subjected to the reorientation treatment. For 500 and 1200 ppm of hydrogen, the behaviour of the samples with radial hydrides is very similar to the ones with circumferential hydrides (reorientation stress=0 MPa) when the ring compression tests are performed at 135°C. For the samples with 150 ppm of hydrogen, however, brittle failure is sometimes observed; especially at 20°C for reorientation stresses larger than 90 MPa. When there are radial hydrides in the samples, unloads are usually seen in the experimental load–displacement curves.

6.4.3. Effects of material type and condition

The results of RCTs conducted at ANL indicate a significant difference in the extent of radial hydride formation (RHCF) and DBTT for high burnup ZIRLO™ rodlets tested compared to high burnup zircaloy-4 rodlets tested following simulated drying storage; for the same temperature and stress histories [77]. Several factors were considered in evaluating these results:

- Pre-test radial distribution of hydrides;
- Texture;
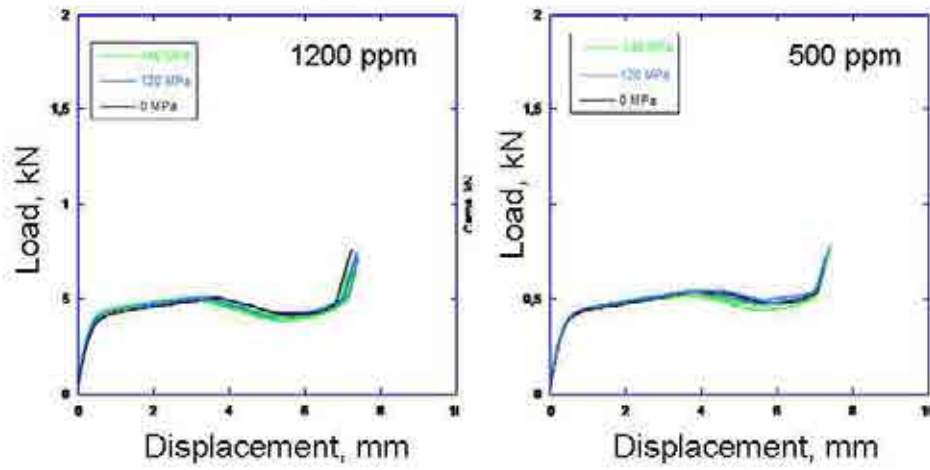- Residual stresses;
- Alloy composition.

80

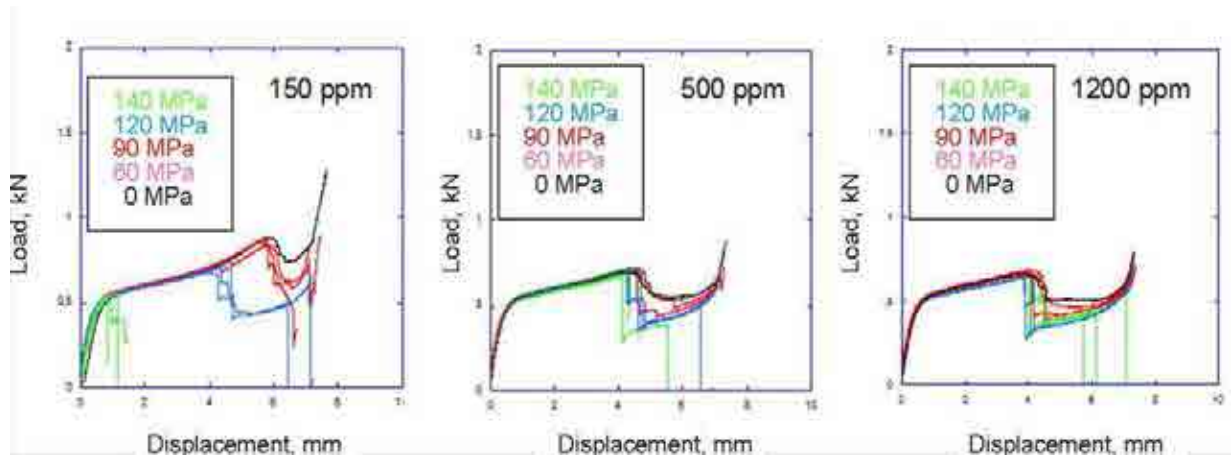*FIG. 42. Load–displacement curves of RCTs carried out at 300°C.*

FIG. 43. Load–displacement curves of RCTs carried out at 135°C.
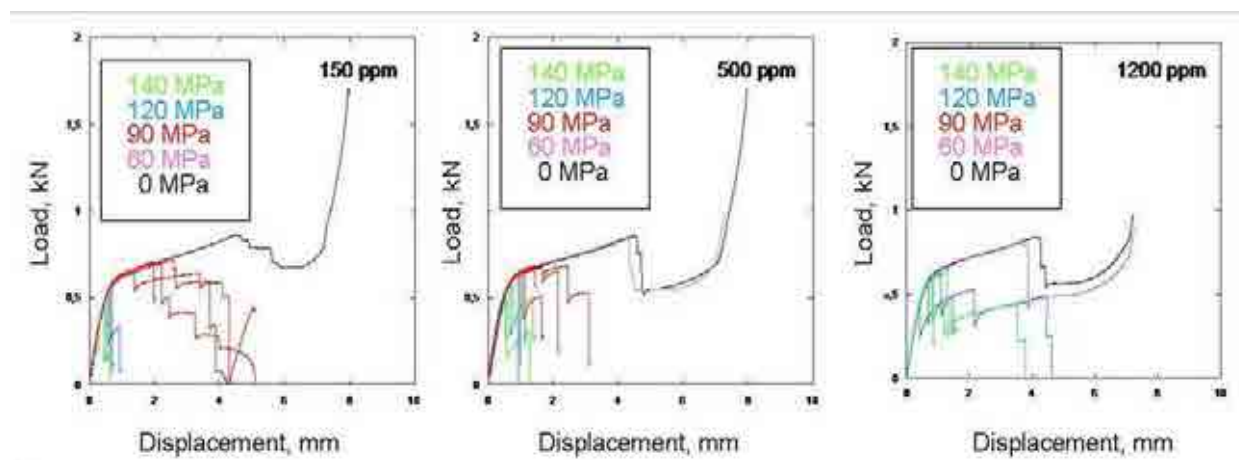

FIG. 44. Load–displacement curves of RCTs carried out at 20°C.

81

Based on metallographic examination of sibling pre-test samples, the hydride rim was denser and more localized for high burnup ZIRLO™ cladding as compared to high burnup zircaloy-4 cladding. Significantly, the average hydrogen content below the hydride rim appeared to be higher for zircaloy-4 than for ZIRLO™. Based on optical microscopy images, it was estimated that the average hydrogen content in the inner two thirds of the zircaloy-4 segments was >200 ppm, while the average hydrogen content in the inner two thirds of ZIRLO™ segments was <150 ppm. Differences in pre-test hydrogen content can have a significant effect on RHCF [77]. The absence of pre- and post-RHT hydrides at the zircaloy-4 inner surface suggests that the primary difference between results for high burnup ZIRLO™ and zircaloy-4 was not due to differences in the pre-test radial distribution of hydrides. The results suggest that high burnup ZIRLO™ is more susceptible than high burnup zircaloy-4 to radial hydride precipitation at the inner surface of the cladding during reactor shut down; as well as during simulated drying storage conditions.

Texture has been shown to have a significant impact on the susceptibility of cladding materials to radial hydride precipitation during cooling under tensile hoop stress. Aomi et al. [64] observed that high burnup recrystallized annealed (RXA) zircaloy-2 formed radial hydrides at a lower stress than high burnup CWSRA zircaloy-4. The ZIRLO™ and zircaloy-4 used in the ANL test programme are both CWSRA materials. Zircaloy-4 fabrication details were provided to ANL for this cladding manufactured in 1977 and used to fabricate the H. B. Robinson (HBR) fuel rods. No such details, however, were provided for the ZIRLO™ cladding used to fabricate the North Anna rods; for which irradiation was initiated in 1987. It is possible that there were texture differences between these two cladding materials that may have contributed to differences in results.

Residual tensile hoop stresses from fabrication and irradiation can enhance radial hydride precipitation. Following stress free hydrogen pre-charging of AF RXA zircaloy-2 with a zirconium liner on the zircaloy-2 inner surface, ANL observed precipitated radial hydrides emanating from the cladding outer surface in local regions around the circumference. These radial hydrides were relatively long (≤30% of the Zircaloy-2 thickness). The results suggest that additional processing steps were used following cladding liner co-extrusion and recrystallization. If local residual stresses were present in AF zircaloy-2, they would have partially relaxed during irradiation due to creep. Aomi et al. did not observe the presence of these radial hydrides in as-irradiated zircaloy-2 cladding. Although residual stresses can enhance radial hydride precipitation, no information is available to suggest that residual tensile hoop stresses are higher at the cladding inner surface for either AF or high burnup ZIRLO™ as compared to those for AF or high burnup zircaloy-4. However, during irradiation and reactor shut down, non-uniform pellet–cladding mechanical interaction (PCMI) can result in post irradiation residual stresses. The radial hydrides observed within the inner third of the as-irradiated ZIRLO™ cladding [77] may have been caused by a higher and more non-uniform PCMI than experienced by the high burnup zircaloy-4 [77] used in this study.

In terms of alloy composition, ZIRLO™ differs from HBR zircaloy-4 in Sn content (about 1 wt% vs. 1.4 wt%) and Nb content (about 1 wt.% vs. 0 wt.%). Other Nb bearing zirconium alloys used as cladding are RXA M5® (zirconium: 1%Nb). The data is not publically available for the behaviour of M5® under simulated drying–storage conditions. However, even if such data were available, high susceptibility to radial hydride formation would likely be the result of the RXA texture and low hydrogen content (≈100 ppm or less) rather than the

presence of Nb. Although still possible, it is unlikely [77] that the presence of Nb in ZIRLO™ is the sole cause of the higher susceptibility to radial hydride precipitation observed in high burnup ZIRLO™.

In Japan, zircaloy-2 from BWR and zircaloy-4 from the PWR spent fuels are the main cladding tube test materials. In addition, MDA™[12] and ZIRLO™ claddings prepared from PWR spent fuel were also tested. As shown in Fig. 45, at a burnup of 55 GW·d·t(HM)$^{-1}$ the *Fl(45)* for ZIRLO™ cladding was relatively large when compared to other PWR cladding materials tested in this study. MDA™ cladding on the other hand showed the same level of *Fl(45)* as 48 GW·d·t(HM)$^{-1}$ zircaloy-4 clad.

This experiment also revealed the different reorientation behaviour between cladding materials. As indicated in the literature [79], the difference in reorientation behaviour between zircaloy-2 (RXA) and PWR cladding materials (SRA) is attributed to the effect of heat treatment; which affects material properties such as grain structure including grain size, grain boundary orientation, internal stress/strain, and so on. As for the difference in reorientation behaviour among PWR cladding materials (SRA), it is proposed that the factor which caused the large reorientation for ZIRLO™ cladding was not the texture represented by the Fr value, because the Fr for ZIRLO™ cladding was the same as that for 48 GW·d·t(HM)$^{-1}$ zircaloy-4. The effect of the alloying element seemed not to be the dominant factor because for example, the zircaloy-4 and MDA™ showed relatively similar behaviour, although ZIRLO™ showed a different behaviour. The annealing temperature in the tube production process for ZIRLO™ cladding, however, is lower than that for zircaloy-4 cladding [80]. Hence, properties which are affected by annealing temperature, grain size for example [81], might be possible factors.

6.4.4. Effects of irradiation

6.4.4.1. *Comparison between non-irradiated hydrogen charged cladding specimens and high fluence cladding tube samples*

The uniform distribution of circumferential hydrides across the cladding wall in ZIRLO™ charged with 530 ppm hydrogen is significantly different from the radial distribution of hydrides in high burnup cladding. This begs the question whether non-irradiated hydrogen charged samples are a good surrogate for irradiated samples when studying the potential for hydride reorientation and the effects of that orientation.

Results of RCTs for pre-hydrided and RHT non-irradiated cladding samples were initially evaluated on a pass–fail basis at ANL in the sense that the success criterion was survival of 1.7 mm RCT displacement with wall cracks that penetrated into ≤ 50% of the wall thickness. Figure 46 shows results of the pass–fail RCTs conducted at 150°C. Pass–fail embrittlement was observed as the hydrogen content dropped below a critical level: 275±25 ppm for 150 MPa hoop stress at 400°C; 200±20 ppm for 135 MPa hoop stress at 400°C; and <100 ppm for 120 MPa hoop stress at 400°C.

---

[12] MDA is a trade mark of the cladding developed by Mitsubishi Heavy Industries Ltd. MDA is zirconium alloy containing Nb.
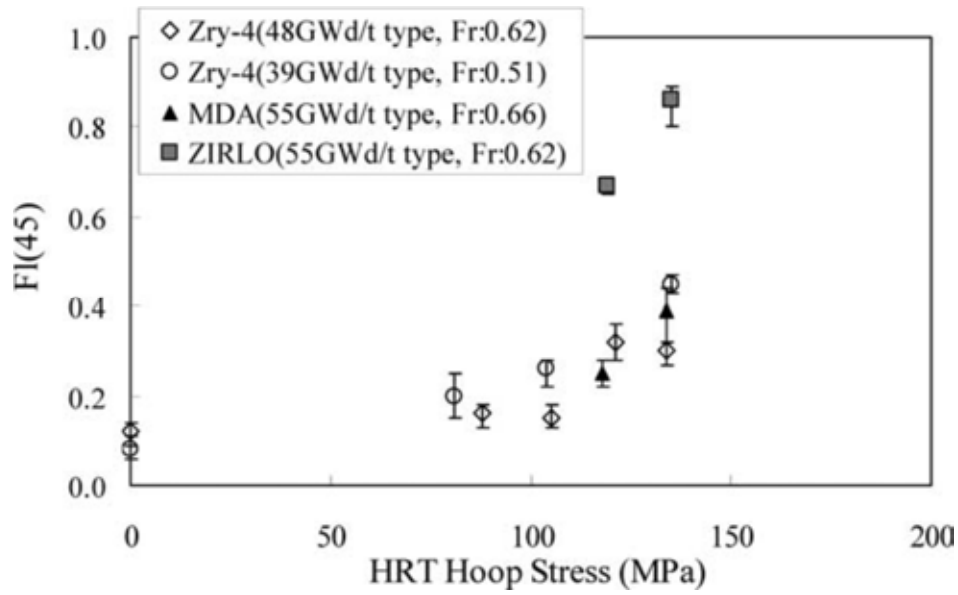
FIG. 45. Comparison of reorientation behaviour among irradiated PWR cladding materials (RHT 300°C, 30°C·h⁻¹) [64].
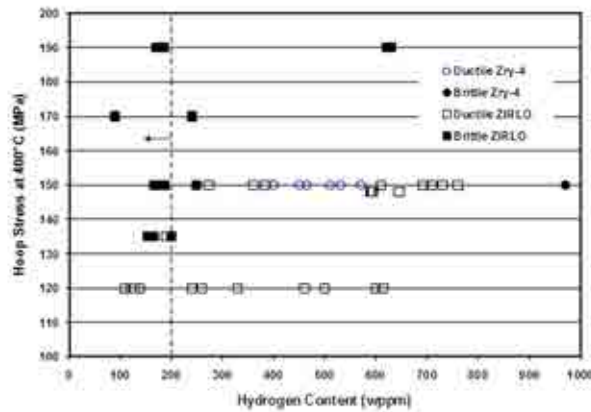
FIG. 46. RCT data at 150°C for pre-hydrided zircaloy-4 and ZIRLO™ following RHT. Where open symbols represent rings that survived 1.7 mm displacement with ≤50% wall cracks. Solid symbols represent samples with cracks >50% of the wall thickness.

RCT on rings of pre-hydrided rodlets with hydrogen contents (350–650 ppm), representative of high burnup cladding material, were tested with 150 MPa hoop stress at 400°C. The rings exhibited high ductility (>10% offset) at 150°C where all, but one of the rings survived the RCT with no indication of cracking. The high ductility matrix samples, with uniform distributions of hydrogen across the radius, however, proved to be very poor surrogates for high burnup cladding. The high burnup ZIRLO™ rodlet (650 ppm hydrogen) subjected to the same thermal cycle at slightly lower stress (140 MPa at 400°C) behaved in a highly brittle manner at 150°C RCT temperature. The primary difference between the test materials was the pre-test radial distribution of hydrogen; uniform for pre-hydrided cladding and highly non-uniform for high burnup cladding.

Figure 47 shows metallographic sections of BWR zircaloy-2 cladding samples before and after RHT in Japan. Comparing Fig. 47(b) and Fig. 47(g) with Fig. 47(a), shows a small degree of hydride reorientation to the radial direction after RHT at a hoop stress of 70 MPa,

temperature of 300°C, and cooling rate of 30°C·h⁻¹. In Fig. 47(b) and Fig. 47(g), hydride reorientation was observed more clearly in the zircaloy-2 inner side area near the zirconium liner, although little reorientation seemed to occur in the area near the outer side. On the other hand, a large degree of hydride reorientation to the radial direction was observed for specimens after RHT at 70 MPa and 400°C (Fig. 47(c)). At 400°C all the hydrogen was estimated to have dissolved for most of the specimens. The hydrogen content of non-irradiated cladding specimens (Fig. 47(d) and Fig. 47(f)) was so low that the hydrogen dissolved completely at each RHT temperature. The reorientation for irradiated cladding seems somewhat larger than that for non-irradiated cladding; comparison of Fig. 47(c) and Fig. 47(f).

In addition, through comparing the results of reorientation studies on non-irradiated versus irradiated samples, the Japanese evaluated the effect of burnup on reorientation. A comparison of *Fl(45)* after a 300°C, 30°C·h⁻¹ RHT was carried out for each of the claddings shown in Figs 47 and 48. The 39 GW·d·t(HM)⁻¹ zircaloy-4 cladding showed a relatively high value compared to 48 GWd·t(HM)⁻¹ zircaloy-4 cladding. This is consistent with the fact that the Kearns factor *Fr* for the 48 GW·d·t(HM)⁻¹ cladding is larger than that for 39 GW·d·t(HM)⁻¹ cladding.

Although it appears that pre-hydrided non-irradiated cladding may not be a good surrogate for high burnup cladding, the experience gained from conducting tests with pre-hydrided cladding has proved to be useful in determining a metric to define the extent of radial hydride formation, in visualizing the discontinuity of cracks along the axial direction (indicative of discontinuity of radial hydride platelets), and in determining the effects of low hydrogen content on radial hydride precipitation and radial hydride induced embrittlement. Pre-hydrided non-irradiated samples may prove more useful when the morphology of the hydrides can be made more like that of irradiated cladding with the same hydrogen content. A similar assessment was offered by the Swiss participant who concluded: 'Since the irradiated material came from power reactor service with considerable oxide layer that influenced the hydrogen/initial hydride distribution, it is questionable how to attribute only irradiation effect on reorientation'.

6.4.4.2.   *Effects of irradiation defects on hydride terminal solid solubility*

Hydrides typically show a significant hysteresis between precipitation and dissolution characterized by the temperature gap between the two solvii. This means that during cooling from solution temperature hydrides start to precipitate at a certain temperature, TTSSP (temperature of terminal solid solubility in precipitation), and during heating hydride dissolution ends at a quite different temperature, TTSSD (temperature of terminal solid solubility in dissolution). McMinn et al. [82] observed a hysteresis temperature gap of 46°C in zircaloy-2 and zircaloy-4 for dilute hydrogen contents (≤80 ppm). Kammenzind et al. [75] studied the same phenomenon for higher hydrogen contents (<500 ppm) in zircaloy-4. Based on interpolation of their data, the measured hysteresis temperature gap was 65°C for 210 ppm hydrogen dissolved at 400°C. The materials tested in both of these studies were in the stress free condition. For stress free zirconium alloys, the hysteresis gap is about 55±10°C between dissolution and initiation of precipitation of circumferential hydrides. However, it is not clear that the same results would be obtained with cladding subjected to a tensile hoop stress during cooling from 400°C. The hysteresis gap may be dependent on the level of tensile stress and may be <55°C for high enough stresses.

Before HRT   HRT 300℃, 70MPa, 30℃/h   HRT 400℃, 70MPa, 30℃/h

Irradiated Cladding (50GWd/t type)

(a)   (b)   (c)

(b') longitudinal cross section

Unirradiated Cladding (50GWd/t type)

(d)   (e)   (f)

300℃, 70MPa, 30℃/h   300℃, 70MPa, 3℃/h   300℃, 70MPa, 0.6℃/h

Irradiated Cladding (50GWd/t type)

(g)   (h)   (i)

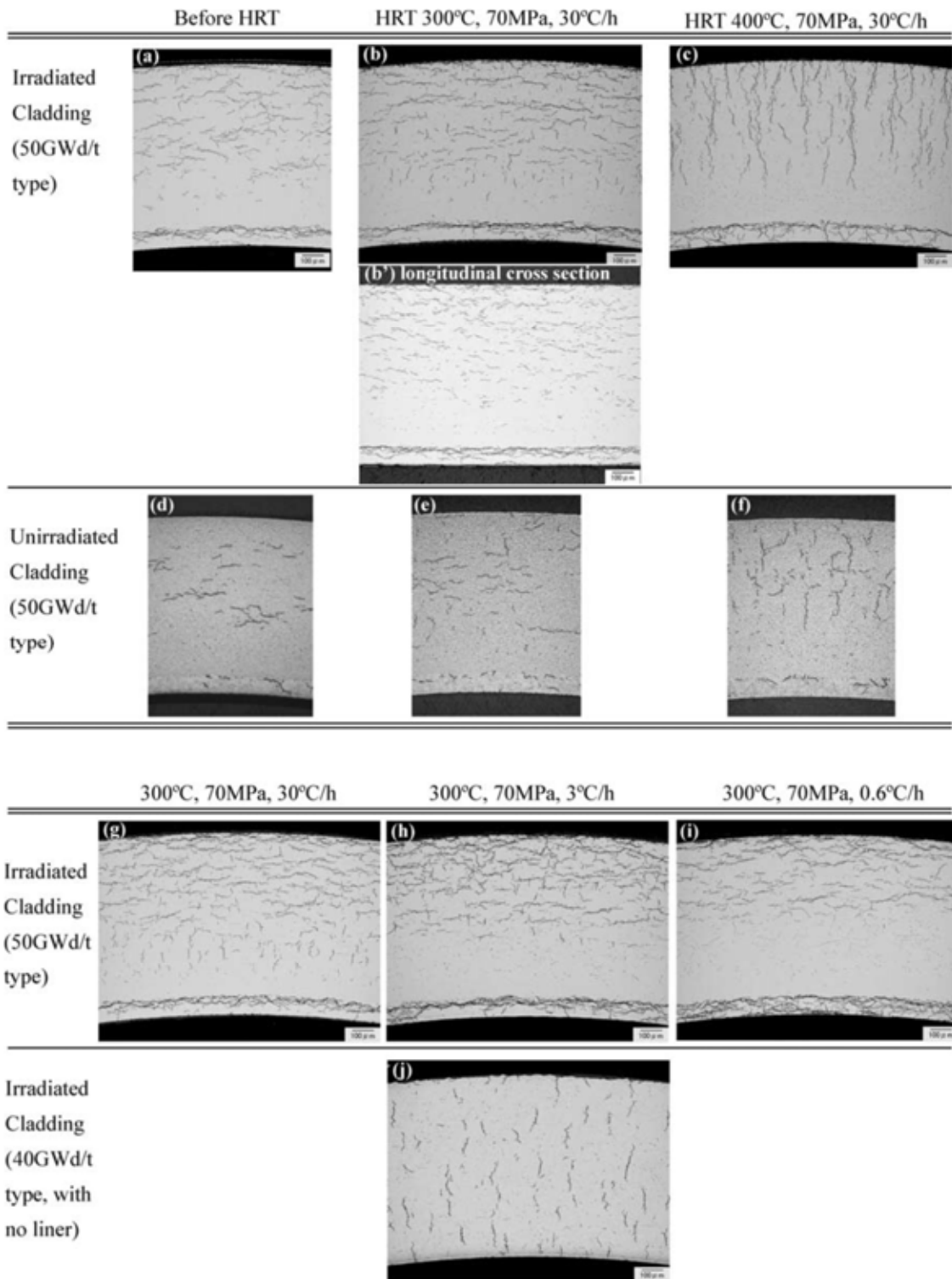Irradiated Cladding (40GWd/t type, with no liner)

(j)

FIG. 47. Metallographic sections of BWR zircaloy-2 cladding specimens in hydride reorientation tests[13] (radial cross section except for (b)) [64].

[13] Unirradiated cladding (50 GW·d·t(HM)$^{-1}$) means non-irradiated cladding from sister material of 50 GW·d·t(HM)$^{-1}$ irradiated cladding.
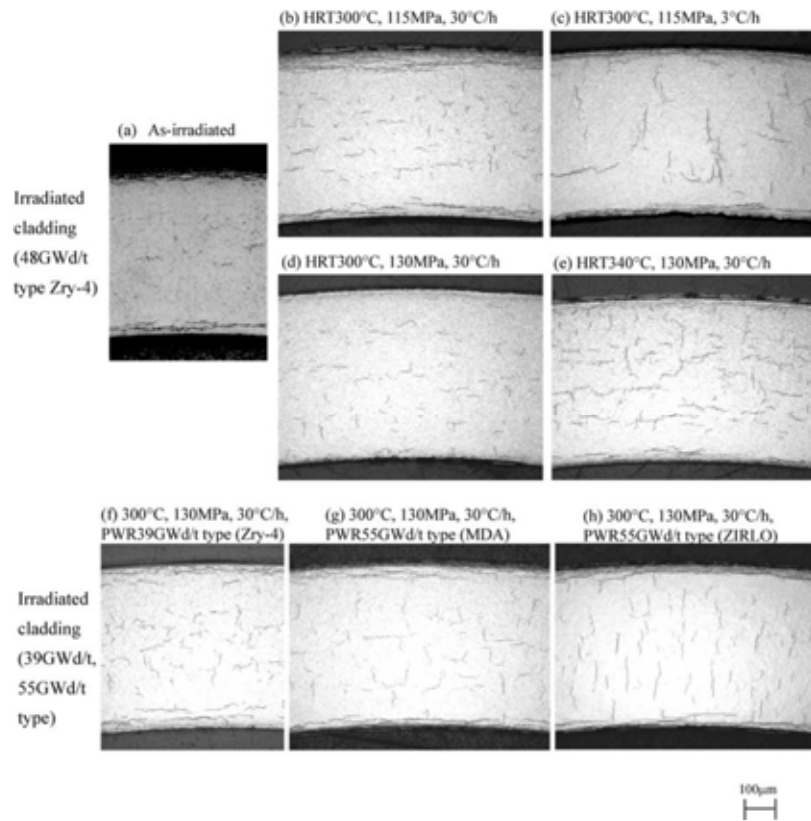
FIG. 48. Metallography pf PWR cladding specimens before and after RHT [64].

While hydride dissolution is very fast during increasing temperatures, precipitation of hydrides is more difficult and results in supersaturated hydrogen content prior to initiation of precipitation. As zirconium hydrides have lower density than zirconium metal, precipitation causes a local volume increase of 17% [83] that is associated to the great strain misfit between the hydrides and the matrix and has to be accommodated by the cladding metal. For precipitation of isolated hydrides, the hydride thickness grows under increasing compressive stress, while the metal experiences increasing tensile stress. It is thus of great interest to evaluate the effect of stresses and matrix strain on the solubility of hydrogen in zirconium alloys. There is still controversy about the effect of stress on the terminal solid solubility of H, and its role on the process of hydrogen redistribution. This controversy is reflected in a number of publications, with [84] stating that the effect of stress on hydrogen solubility in zirconium is negligible and that hydrogen concentration in solution around the crack is higher than in the bulk; whilst [85] proposes an exactly opposite scenario.

These uncertainties have a direct impact on the accuracy of models used for hydride reorientation prediction. According to Kearns [86–88], dissolution of hydrides and hydrogen diffusion during the heating phase are very rapid in non-irradiated zirconium, zircaloy-2, and zircaloy-4. These results apply to cladding without a hydride rim. The terminal solubility in these alloys was determined to be 207 ppm at 400°C. High tensile hoop stresses favour the precipitation of radial hydrides. During slow cooling (e.g., 5°C·h^{-1}) under tensile hoop stress, hydrogen would have ample time to diffuse in the radial, circumferential, and axial directions. However, the diffusion path may be limited by the spacing of precipitated hydrides.

Regardless of the magnitude of the hysteresis gap, the stress level in high burnup cladding rodlets at the initiation of precipitation would decrease by <10% for a hysteresis temperature gap of <65°C.

Comisión Nacional de Energía Atómica (CNEA), Argentina, is engaged in a research project to experimentally investigate these effects. The investigated material was from zircaloy-4 cooling channels removed from the Atucha I heavy water reactor (HWR) after 14 years in service with fluence between 1×10^{20} and 6.6×10^{21} n·cm^{-2}, and 60–260 ppm H. The microstructure was fully recrystallized with a grain size of (20±6) μm .Some samples were annealed at different temperature/times with the aim to recover the radiation damage. For reference purposes, a hydrided non-irradiated zircaloy-4 sheet and powder were also prepared. The microstructure of the zircaloy-4 sheet was similar to those of the irradiated material, with fully recrystallized grains of 15–20 μm. Hydrogen was incorporated into the non-irradiated zirconium matrix by cathodic charging. H diffusion inside the material was obtained after thermal annealing for 3 h at 550°C. X ray diffraction diagrams were obtained at a powder diffraction line of the Brazilian synchrotron.

Transmission electron microscopy (TEM) was used with the aim to determine the dislocation density in the irradiated matrix. A high density of dislocation loops were observed in samples in the as received irradiated condition. Figure 49 shows irradiation defects, which were identified as <a> dislocation loops (~10 nm) and <c> dislocation loops (100–180 nm), respectively, similar to the observations previously made by Adamson in zircaloy-4 [89].

Also, Figs 49(c–f) show a high density of very small hydrides precipitated parallel to, and flanked by, <c> dislocation loops. These hydrides show the typical orientation relation with the α-Zr matrix, i.e., $(\bar{1}1\bar{1})_\delta//(0002)_\alpha$ and $[110]_\delta//[11\bar{2}0]_\alpha$. Since <c> dislocation loops are vacancy loops, the local absence of matrix atoms and the consequent local expansion favours hydride nucleation in these sites, the orientation of which is close to the habit plane $(10\bar{1}7)_\alpha$ of the δ-hydrides in zircaloy-4. These observations give additional support to the hypothesis of hydrogen-defect interactions [87; 90–92]. Although a direct verification of this hypothesis is not yet possible (hydrogen atoms could not be detected), it is possible to establish a chain of events which, based on this hypothesis, determine the macroscopic consequences observed in the bulk; an apparent hydrogen solubility increase in the irradiated zirconium alloy matrix.

As was already pointed out, the as received material is characterized by a high density of radiation induced dislocation loops. Assuming that the <c> dislocation loops plays a role as hydride nucleation sites, as can be qualitatively observed in Fig. 49, a hydride size distribution biased to small sizes should exist. Such a difference should affect TTSSd determinations when this parameter is determined by a dynamic technique like differential scanning calorimetry (DSC). Since hydride dissolution is controlled by diffusion, the time required to dissolve a large hydride is longer than the one to dissolve the same mass distributed in many small hydrides [93].

The hydride size distribution was determined from optical and TEM field images. The histograms are shown in Fig. 50. In the present analysis, 1 μm was taken as the border between the optical and TEM fields. The analysis of optical fields shows that the size distribution is biased to small sizes. The maximum length frequency (2700 particles) is observed at 2.75 μm and 25% of the detected hydrides are shorter than 5 μm. Only 10.5% are longer than 20 μm. This distribution is not typical of non-irradiated materials.
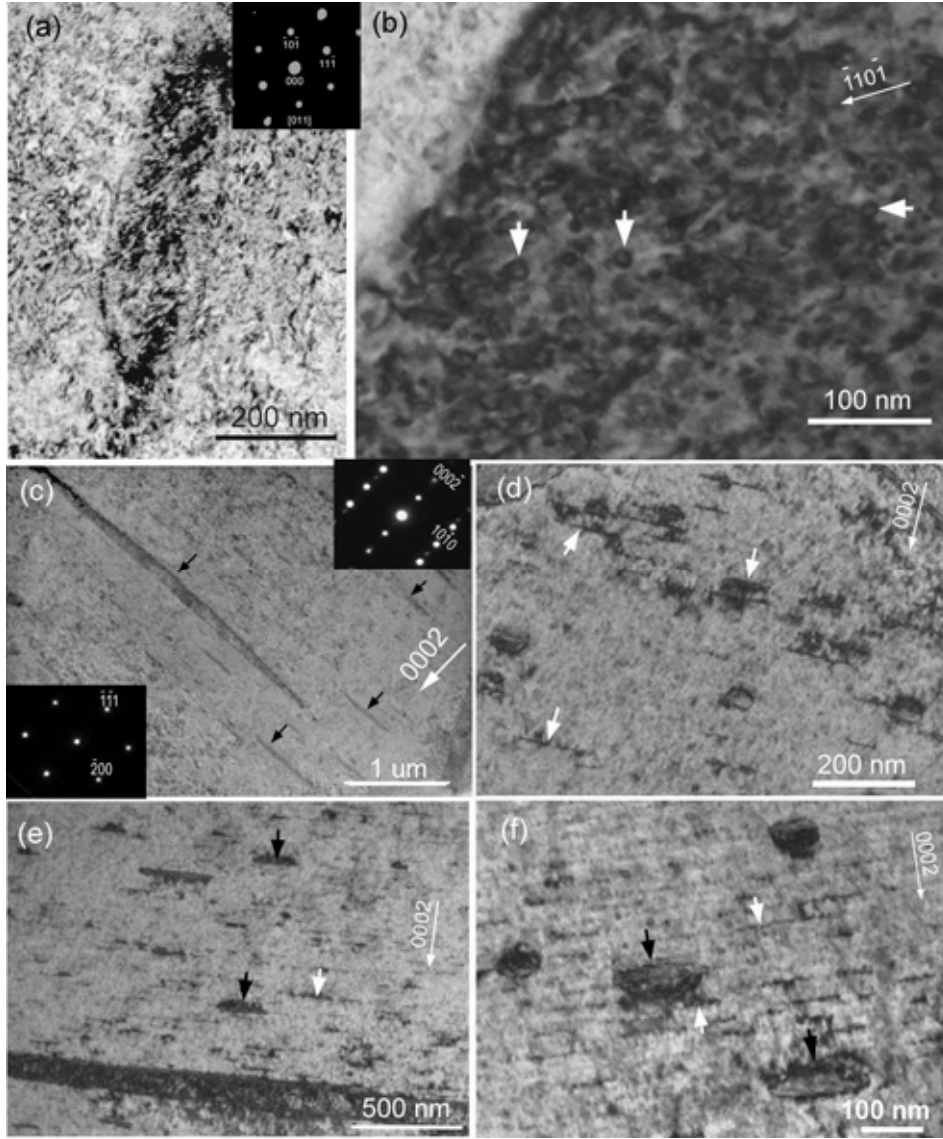
FIG. 49. TEM images of <a> and <c> loops and hydrides observed in samples (~10²²
neutrons/cm²) [91]. (a) A hydride affected by irradiation damage and <a> dislocation loops are
observed in bright field. The indexed diffraction diagram indicates cubic structure (δ-hydride). (b)
<a> dislocation loops observed close to the α-Zr/hydride interface (white arrows). Zone axis =
[12Ī3]. (c) Hydrides parallel to the basal planes (black arrows). The SAD (selected area
diffraction) patterns of the α-Zr matrix and that of the large δ-hydride observed show the typical
crystallographic relationship. Zone axis_α= [11Ī0], zone axis_δ =[011]. (d) <c> dislocation loops
microstructure (white arrows) with sizes varying between 100 and 180 nm. (e) and (f) Hydrides
are observed (black arrows) and <c> dislocation loops (white arrows) are parallel to them. Zone
axis = [11Ī0].

Although the maximum frequency is at 25 nm in the TEM fields, the size distribution is more homogeneous than the size distribution in the optical range. In TEM range, 30% of the observed hydrides are shorter than 100 nm.

If we consider now the intervals [10, 1000] nm and [1, 100] μm, which correspond to the TEM and optical ranges, respectively, the challenge is finding a way to integrate the data from two hydride populations that coexist, but cannot be observed simultaneously. A simple

parameter to quantify the relative weight of these two populations is density. First, density is defined as the ratio of the sum of hydride lengths (particle size) divided by total scanned area. The sum of the lengths of the detected hydrides in the optical range is 152.9 mm, so that, in this range hydride density is ρ_{optic} = 152.9 mm/6.1 mm^2 = 25.1 mm^{-1}. In the same range, the sum of the lengths shorter than 5 μm is 37.9 mm. Then their density is $\rho_{<5\ \mu m}$ = 6.2 mm^{-1}. On the other hand, the sum of the hydride lengths of the TEM range is 43.9 μm. Thus, hydride density is ρ_{TEM} = 43.9 μm/126 μm^2 = 0.35 μm/μm^2 ≡ 348.9 mm^{-1} and the ratio between both densities is ρ_{TEM}/ρ_{optic} ~13, which indicates a large preponderance of sub microscopic hydrides. However, it is possibly an overestimate. Length as a parameter to characterize hydride size is unsatisfactory when dimensions are close to the extremes of the interval. A hydride length at the top of the optical range can be 1 μm in width, while the sub microscopic hydrides at the bottom of the TEM range are of a few nanometres in width. This problem could be solved by redefining density as the ratio between the area occupied by hydrides and the scanned area. This area in the optical range is 0.360 mm^2. The density will be then ρ_{optic} [area] = 0.360 mm^2/6.1 mm^2 = 0.059. In TEM range the area occupied by hydrides is 0.986 μm^2. Thus, ρ_{TEM} [area] = 0.986 μm^2/126 μm^2 = 0.078. Then, the ratio between both ranges becomes ρ_{TEM}/ρ_{optic} ~ 0.13. Sub microscopic hydride density is 13% of the hydride density observed in the optical field. Possibly this is an underestimate, since in the optical field the etchant used to reveal hydrides affects much more hydride width than hydride length, and this does not occur in TEM samples. Yet, this last value is more reasonable than the value derived from measuring hydride length.

Summarizing the results of the statistical analysis, it can be stated that a non-negligible amount of submicroscopic hydrides, higher than 13%, not visible in the optical range exists. Considering that in the optical range 25% of hydrides are shorter than 5 μm, a wide hydride size distribution exists, extending over four orders of magnitude, from 10 nm to 100 μm, biased to sizes shorter than 5 μm.

Finally, hydride lengths observed by TEM in samples annealed 24 h at 600°C are generally longer than 1 μm and shorter hydrides were not observed as is also the case in non-irradiated material. Thus, such differences in size distributions could be responsible for the hydrogen solubility increase in irradiated zircaloy-4.
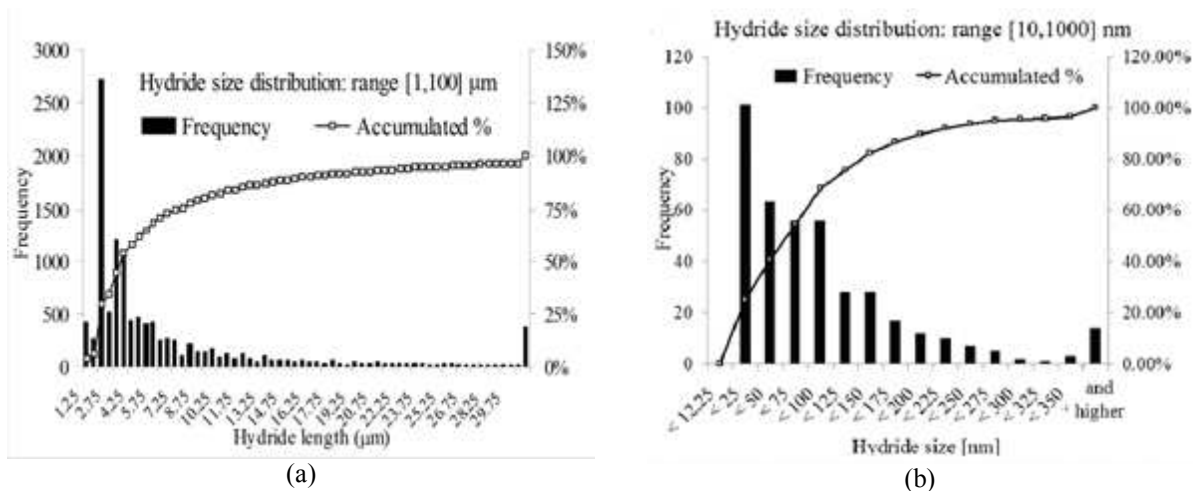

FIG. 50(a). Optical range: the histogram indicates a high concentration of hydrides smaller than 5 μm (maximum frequency at 2.75 μm); (b) TEM range: the histogram shows a hydride size distribution biased to small sizes. The maximum frequency is observed at 20-30 nm [90].

6.4.5. Effects of cooling rate

The fast cooling rates (e.g., 25°C·h^{-1} to 600°C·h^{-1} reported [64; 94–97]) used to test pre-hydrided and irradiated cladding tend to result in shorter radial hydrides and higher DBTT values because the path length for hydrogen diffusion is limited.

Figure 51 shows the effect of cooling rate on *Fn (40)*, *Fl (45)*, and the sum of the length of hydrides per area; which reflects the total hydride amount in the zircaloy-2 cladding. As shown in Fig. 47(h) and Fig. 47(i)., the amount of hydride in the inner zircaloy-2 area near the zirconium liner decreased and the amount of hydride in the zirconium liner increased with decreasing cooling rate. The effect of cooling rate on hydride morphology described above was confirmed quantitatively in Fig. 51. This influence of cooling rate on the zirconium lined cladding is easily understood as the result of larger hydrogen migration in the lower cooling rate samples from the zircaloy-2 matrix to the zirconium liner due to the terminal solid solubility precipitation (TSSP) difference between zirconium and zircaloy-2 [95]. Zircaloy-2 cladding with no zirconium liner showed a relatively large degree of hydride reorientation as observed in Fig. 47(j), which was different from the behaviour exhibited by the zirconium lined cladding.

The effect of cooling rate on ductility is shown in Fig. 52. The crosshead displacement ratio increased with a decrease of cooling rate for the zirconium liner cladding. It is consistent with the decrease the amount of radial hydride at low cooling rate as shown in Fig. 51. The crosshead displacement ratio after a 300°C, 70 MPa, 3°C·h^{-1} RHT for cladding with no zirconium liner indicates a low ductility (cross head displacement ratio of 0.3–0.4 %) among the BWR specimens in the ring compression test, although the hydrogen content of the no liner specimens was the lowest (40 ppm H) among the materials tested. It is deduced that this result was due to both the large ratio of radial hydride and the crack growth initiating from the inner surface, which is different from the case for zirconium lined cladding.

The effect of cooling rate on hydride morphology is shown in Fig. 53 *Fl (45)* in 3°C·h^{-1} cooled specimens seemed to be larger than that in 30°C·h^{-1} cooled specimens; while it was almost the same in 0.6°C·h^{-1} cooled specimens (Fig. 53(a)). Radial hydride length increased when the rate of cooling was decreased from 30°C·h^{-1} to 3°C·h^{-1}; the effect was less noticeable for a decrease from 3°C·h^{-1} to 0.6°C·h^{-1}.

The effect of RHT cooling rate on ductility in ring compression deformation is shown in Fig. 54. The crosshead displacement ratio in 0.6°C·h^{-1} cooled specimens are similar to those cooled at 3°C·h^{-1}; in comparison there was a decrease between 3°C·h^{-1} cooled specimens with those cooled at 30°C·h^{-1}. As shown in Fig. 53, an increase in both the degree of reorientation (*Fl(45)*) and the length of hydride was observed in 3°C·h^{-1} cooled specimens compared to those cooled at 30°C·h^{-1}, whilst those cooled at 0.6°C·h^{-1} gave similar results to 3°C·h^{-1} cooled specimens. It is deduced that the effect of cooling rate on ductility is in agreement with the change in hydride morphology as illustrated in Fig. 53.

Based on the Japanese data, it appears that there is a distinct difference between the effect of cooling rate on BWR zircaloy-2 and PWR zircaloy-4 cladding. As the cooling rate drops in zircaloy-2, there is less reorientation and shorter hydrides, but within the scatter of the data there is no effect on ductility at hydride reorientation treatment at 300°C and 70 MPa. This might be expected since most of the hydrogen has migrated to the pure zirconium liner and very little is available for reorientation. This tendency was also evident in the testing performed at PSI (Switzerland). In testing the same non-irradiated and irradiated material

zircaloy-2 recrystallized cladding, provided by Westinghouse, was studies. In the case of the non-irradiated tests the inner liner wasn't removed, contrary to the approach taken in the CTDT testing of the irradiated material. The inner liner having a different solid solution curve appeared to influence the contiguous cladding bulk material and act as hydrogen sink.

On the other hand for PWR zircaloy-4 cladding undergoing hydride reorientation at 115 MPa stress, there is no difference with cooling rate in the number of hydrides that reorient but, those that do reorient are much longer due to the longer diffusion time. The data also showed that the ductility nominally decreases with the longer hydrides and lower cooling rate. More data may be necessary to confirm if this difference in materials behaviour with cooling rate is universal.
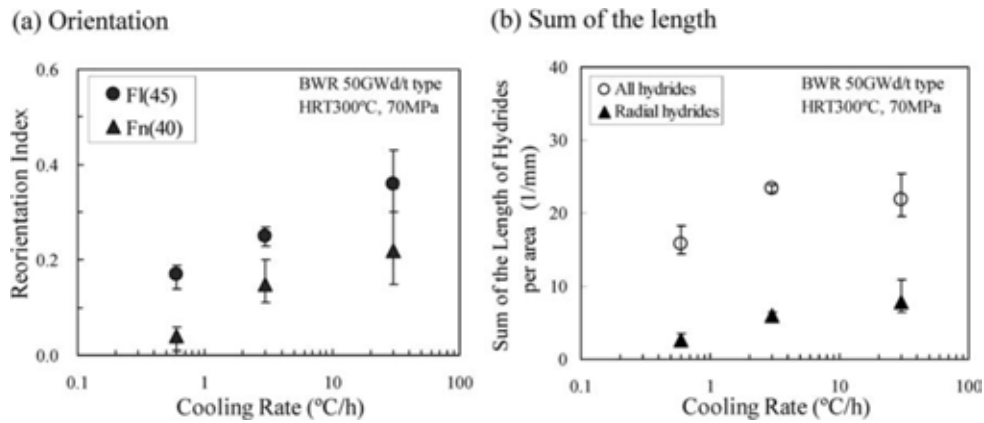
FIG. 51. Effects of HRT cooling rate on hydride morphology for irradiated BWR zircaloy-2 cladding with zirconium liner. ["Sum of the length of hydrides per area (1/mm)"="Sum of the length of hydrides those are measured in the observed area (mm)"/"The area where the measured hydrides are observed (1/mm^2)." "All hydrides" marks represent the value for all hydrides regardless of the orientation. "Radial hydrides" marks represent the value for the hydrides in radial direction ±45° [64].

FIG. 52. Effects of RHT cooling rate on ductility in ring compression deformation for irradiated BWR zircaloy-2 cladding with zirconium liner (50 GW·d·t(HM)$^{-1}$) [64].

92

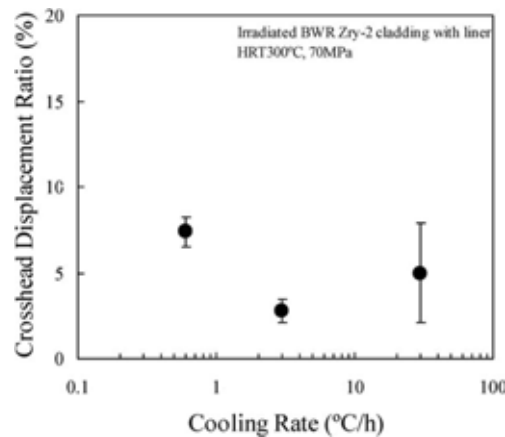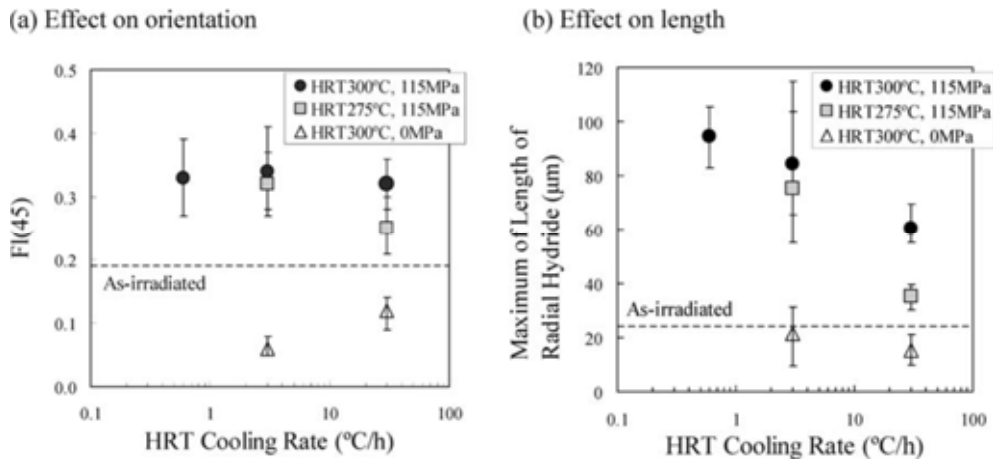*FIG. 53. Effects of RHT cooling on hydride morphology for irradiated PWR 48 GW·d·t(HM)$^{-1}$ zircaloy-4 cladding (the definition of vertical axis in (b) is "the maximum value among the length of hydride in radial direction ±45°) [64].*

6.4.6. Effects of cycling

Hydride precipitation takes place mainly at grains of two ideal orientations: (i) grains (hoop grains) corresponding to crystallites having their c-axis along the tube hoop direction (the main texture component of the material) and (ii) grains (tilted grains) which have the c-axis pointing along an intermediate direction in the hoop-radial plane of the tube. Work performed in Argentina yielded the following results:

- On cooling from solid solution, hydride precipitation is more likely and occurs at a higher temperature (~5°C) in tilted grains than in hoop grains.
- On heating from room temperature, dissolution of hydrides precipitated in hoop grains occurs at lower temperatures (~15°C) than those precipitated in tilted grains.
- Application of a tensile load along the hoop direction during thermal cycling changes precipitation (5°C before) and dissolution (15°C after) temperatures, which reduces the hysteresis in both grain families.
- The measured shift in precipitation temperature suggests that precipitation of δ hydride involves a martensitic transformation, where the volume change associated to the phase transformation is accommodated normal to the habit plane.
- The change in precipitation temperatures is accompanied by a large increase in the number of hydrides precipitated in hoop grains. This redistribution of hydrides occurs on cooling, due to the observed changes in precipitation temperatures.
- Application of a load while H is in solution in the α-Zr matrix does not result in significant redistribution between different grain orientations.

The connection between applied stress and change in precipitation temperature can be used to improve models describing H redistribution during thermal cycling of zirconium based alloys.

The effect of three loading cycles compared to one was investigated on irradiated samples at 420°C by PSI (Switzerland). The results showed that increasing the number of cycles promotes hydride re-orientation. It was found that the hydride reorientation takes place homogeneously and as soon as the principal stress becomes positive.

Some tests at ANL have been conducted with slow and fast temperature cycling (up to 5 cycles) from 400°C to 300°C to 400°C prior to cooling to 200°C. No significant effects due to thermal cycling were observed under these conditions.

6.5. IMPACT OF HYDRIDE REORIENTATION ON DRY STORAGE AND TRANSPORTATION

Most of the assessments associated with hydride reorientation have focused on hypothetical transportation accident conditions. There are no direct regulatory, IAEA prescribed performance criteria for spent fuel integrity during accident conditions; transportation safety criteria are driven by potential radioactive releases, radiological exposure, and criticality considerations. The assumed state to the cladding is an input into those safety assessments.

A major analytical effort for the failure evaluation of spent fuel under normal and hypothetical accident conditions was performed as part of a source term study by Sandia National Laboratory in the late eighties/early nineties for low to intermediate burnup fuel (~35 GW·d·t(HM)$^{-1}$) [97]. The failure criteria adopted for determining failure frequency were based on cladding peak strain, in which the initiation of fracture implied total through wall failure. Failure mode dependent failure probabilities were calculated for PWR fuel for the three failure modes depicted in Fig. 55; i.e. 2×10^{-4} for pinhole failure Mode-I, 5×10^{-5} for rod breakage Mode-II, and 2×10^{-5} for longitudinal slit Mode-III.

These failure probabilities are roughly within one order of magnitude, and failure in any of these three modes can be regarded as equally likely for intermediate burnup fuel. This may not, however, be the case for high burnup spent fuel because of the role of radial hydrides; which uniquely affect 'Mode-III'. The latter requires that pinch loading be imposed on fuel rods at a low enough temperature (below DBTT) in order to engage the radial hydrides present in the cladding, which are responsible for a substantial decrease in ductility or fracture toughness, as characterized by some RHCF value or other figure of merits. Pinch loading is typically associated with drop accidents with the spent fuel assembly or package in a horizontal configuration.
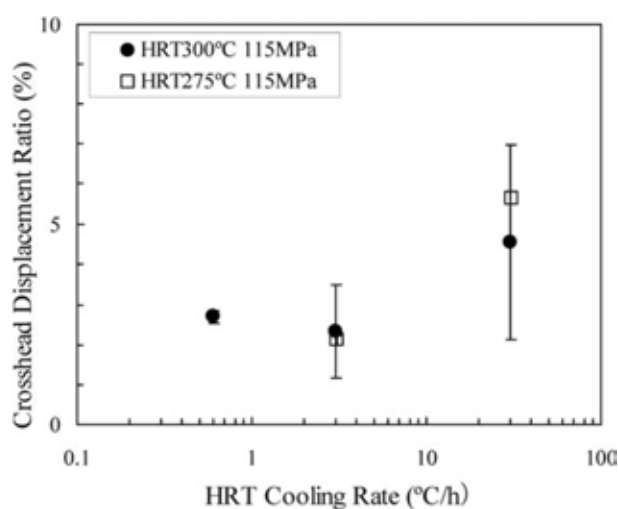

FIG. 54. Effects of RHT cooling rate on ring compression deformation for irradiated PWR zircaloy-4 cladding [64].

94

Grid locations are the most susceptible locations. It should also be noted that cladding diametral deformations, under pinching load conditions, are limited, typically to <0.5% for high burnup fuel, before UO_2 fuel assumes a major fraction of the pinching load.

The basis for the structural modelling and failure analysis methodology developed in an EPRI programme focused on high burnup spent fuel properties, which considered the effects of long-term dry storage, was developed from [97]. Cladding mechanical properties were largely based on data obtained on reorientation specific to zircaloy-4. The results from these detailed structural assessments [45–48] are described in a series of reports and publications reported in previous SPAR programmes. The structural assessments were used as input into related safety driven assessments such as spent fuel criticality evaluations (burnup credit and fuel reconfiguration) and probabilistic safety assessments of storage and transportation operations. As more data becomes available, models are being updated to support and predict the outcome of the nascent US DOE's confirmatory high burnup demonstration programme.

6.5.1. Ductile to brittle transition temperature

6.5.1.1. PWR cladding

The DBTT values for high burnup zircaloy-4 following simulated drying–storage at 110 MPa and 140 MPa were <20°C and about 55°C, respectively. Most radial hydrides that precipitated in zircaloy-4 were relatively short and close to the cladding mid wall where the RCT hoop bending stresses were very low. They participated in crack propagation, but not in crack initiation.
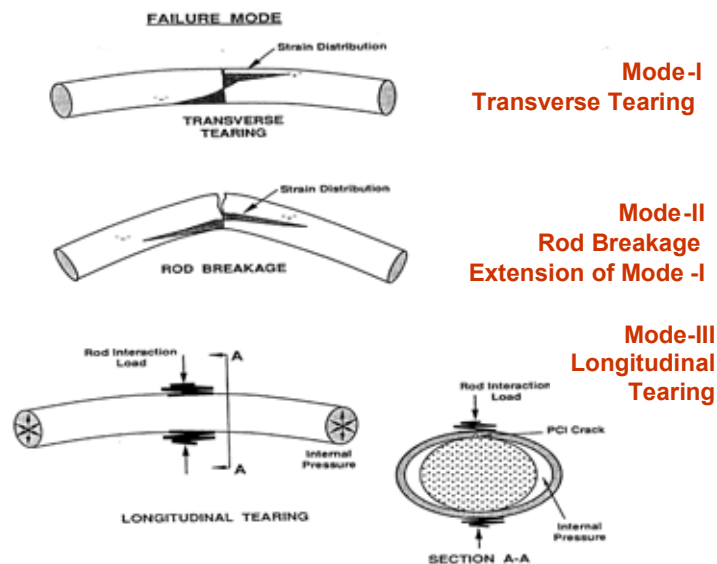

FIG. 55. Possible failure modes under cask drop in horizontal orientation [97].

For high burnup ZIRLO™, radial hydrides were found to be relatively long and to extend from the inner cladding surface, which is subjected to the maximum RCT hoop bending stress under the applied load and above the support plate. The DBTT is a function of the cladding material, stress at maximum drying–storage temperature, and pre-drying radial distribution of hydrogen. The hold time at maximum temperature did not appear to influence the DBTT. The higher DBTT and extent of degradation in mechanical properties associated with this higher DBTT are affected by the radial hydride fraction and radial hydride continuity factor (RHCF), total hydride amount, maximum annealing temperature and stress, and cladding composition and morphology as shown in Fig. 56.

Aomi et al. [64] did testing at room temperature (RT) and slow displacement rate (2 mm·min^{-1}) for high burnup zircaloy-4. Their RHT differed from the ANL study in that pressure and stress were held constant during cooling. Most of Aomi's data was generated for the faster cooling rate of 30°C·h^{-1}. For high burnup zircaloy-4 tested by Aomi et al., the hydrogen contents appear to be low relative to the samples used in the ANL study and the maximum annealing temperature was lower (250–340°C vs. 400°C). The only zircaloy-4 data point that indicated brittle behaviour (<2% offset strain) was for the sample annealed at 340°C and about 140 MPa hoop stress prior to cooling. The result is consistent with the ANL RT data point for high burnup zircaloy-4 subjected to a 400°C anneal with a 140 MPa hoop stress prior to cooling. The Aomi et al. data points for zircaloy-4 subjected to a 340°C anneal with about 100 MPa indicated ductile behaviour at RT. Again, this result is consistent with the ANL data point for zircaloy-4 subjected to an RHT at 400°C and having 110 MPa hoop stress prior to cooling. For other data in [64], RHT conditions (250–300°C) were too low to allow for a one to one comparison.

The ring compression tests were carried out on ~80 specimens of cladding. Test results for each material were plotted in figures, for example Fig. 38. RHT conditions (RHT temperature and hoop stress) for threshold of ductility degradation have been derived from the figures. The summary of RHT thresholds for PWR clad materials is shown in Table 8. The results show that the threshold is cladding material dependent; ZIRLO™ and MDA™ claddings have lower thresholds than zircaloy-4 cladding.

For the ANL data Fig. 56, the DBTT is defined as the temperature where there is an offset of 2%, which is essentially equivalent to the value of the lower shelf. It appears the temperatures shown in Table 8, derived from the Japanese studies; correspond to the value of the upper shelf. While the results of the USA and Japanese studies may be consistent, it can cannot be determined if they are the same in the absence of more detailed information.

6.5.1.2. BWR Cladding

Aomi et al. [64] did testing at RT and a slow displacement rate (2 mm·min^{-1}) for high burnup zircaloy-2. Their RHT differed from the ANL study in that pressure and stress were held constant during cooling. Most of Aomi's data was generated at a faster cooling rate of 30°C·h^{-1}. RXA zircaloy-2 with a zirconium liner showed a high susceptibility to radial hydride formation for relatively low stress (70 MPa) and cooling from 400°C. Based on published metallographic images, the hydrogen content in the cladding outside the liner appears to be quite low (<100 ppm). For other data in [64], RHT conditions (250–300°C) were too low to allow a one to one comparison.
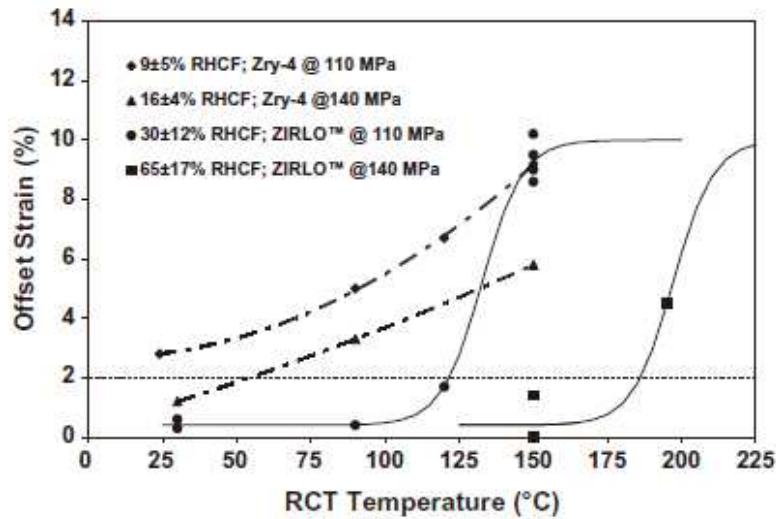
FIG.56. Offset strain (measure of ductility) as a function of RCT temperature for high burnup ZIRLO™ and zircaloy-4 cladding [95].

The ring compression tests were carried out on ~ 80 specimens of cladding. Test results for each material were plotted in figures like Fig. 38. The figures have been reviewed, and RHT conditions (RHT temperature and hoop stress) for threshold of ductility degradation were derived. The RHT thresholds for BWR clad are summarized in Table 9. The threshold is dependent on whether a liner is present. BWR zircaloy-2 cladding without liner has a particularly low threshold (200 ºC, 70 MPa).

TABLE 8. SUMMARY OF PWR CLAD RHT THRESHOLDS OF NO DUCTILITY DEGRADATION AFFECTED BY HYDRIDE REORIENTATION [98]

Cladding type		Threshold of no ductility degradation that would be due to hydride reorientation	
		Temperature (°C)	Hoop stress (MPa)
PWR (SR)	39 GW·d·t(HM)⁻¹ zircaloy-4	$\leqq 275$	$\leqq 100$
	48 GW·d·t(HM)⁻¹ zircaloy-4	$\leqq 275$	$\leqq 100$
	55 GW·d·t(HM)⁻¹ MDA®	$\leqq 250$	$\leqq 90$
	55 GW·d·t(HM)⁻¹ ZIRLO™	$\leqq 250$	$\leqq 90$

TABLE 9. SUMMARY OF BWR CLAD RHT THRESHOLDS OF NO DUCTILITY DEGRADATION AFFECTED BY HYDRIDE REORIENTATION [98]

| Cladding type | Burnup | Threshold of no ductility degradation that would be due to hydride reorientation | |
		Temperature (°C)	Hoop stress (MPa)
BWR zircaloy-2 (RX)	40 GW·d·t(HM)$^{-1}$ no liner	$\leqq 200$	$\leqq 70$
	50 GW·d·t(HM)$^{-1}$ with liner	$\leqq 300$	$\leqq 70$
	55 GW·d·t(HM)$^{-1}$ with liner	$\leqq 300$	$\leqq 70$

7.   IMPACT OF SPENT FUEL

7.1.   DEFINITION

The impact of spent fuel corresponds to the situation in which the fuel is submitted to severe loading; i.e. forces and/or accelerations associated with incidents or accidents.

To support post storage transport licensing, a key issue is the behaviour of spent fuel under transport package accident conditions. The reference regulatory documents generally consider three conditions where impacts could occur:

- The transport before storage, which can be normal or accident conditions as defined in [99];
- The dry storage, especially severe conditions such as cask tip over (as for an earthquake) or accident during handling;
- The transport after dry storage, in normal or accident conditions as defined in [99], but with additional consideration of potential degradation of used fuel; especially if longterm storage is assumed.

7.2.   BASIC ASPECT OF SAFETY

Transport/storage cask package design safety analysis aims to demonstrate that a loaded cask will comply with the relevant passive safety functions to meet the following protection goals:

- Safe enclosure of the radioactive substances;
- Safe removal of the decay heat;
- Prevention of criticality;
- Protection against radiation exposure.

Apart from the component features of the transport and storage casks, compliance with these protection goals is also established by understanding the behaviour of the loaded fuel assemblies for each design relevant operating scenario.

The prerequisite for the fulfilment of the safety requirements is that the protection for human beings and the environment is guaranteed for all operations, during and after storage, and under both routine and normal or accident conditions. It is, therefore important to know the behaviour of used fuel and its geometry under both normal and extreme mechanical and thermal accident conditions. The information is used for criticality safety analysis and to define the source terms for containment, thermal and shielding analysis.

Under normal conditions of storage, routine or normal transportation the stresses imparted to the spent fuel assemblies (FA) are relatively low. Structural changes to the FA geometry and their array due to mechanical and thermal stresses do not occur. Since a systematic failure of the fuel cladding can be excluded, then no release of fissile containing material can be assumed.

In the event of an accident the damage scenarios to be investigated are typically fuel reconfiguration, disruption of the FA, the possible rupture of fuel rods and the dispersion of radioactive material. According to [99] criticality safety (multiplication factor $k_{eff} < 1$) has to be proven. For dry casks this includes the hypothetical case of the cask cavity becoming

flooded with water (optimal moderation is assumed); the exception is where water exclusion can be demonstrated by multiple highly effective barriers.

To demonstrate cask robustness under transport accident conditions a series of drop, heat and water immersion tests are carried out. The high mechanical and thermal stresses resulting from these tests are also used in the evaluation of the impact on the FAs. Bounding test conditions are selected and combined in such a way that maximum damage will be caused for safety analysis. In undertaking this analysis the initial condition of the fuel rods is taken into consideration; i.e. whether the fuel rods are deformed and the amount of clad thinning. In addition to the nuclear characteristics, the temperature dependant, dynamic strength and failure properties of the FA are established.

The potential for a critical mass of fuel to accumulate in the cask cavity mainly depends on the amount of fuel released and the free space available in the cask cavity. The amount fuel released under an accident scenario is a function of: the cladding, internal pressure, clad failure mode, and crack position. In terms of failure mode, the amount of fuel released may be higher in the case of a complete shear fracture compared to cracks due to buckling stresses, bending or twisting of the cladding tube. Similarly, the crack position also determines whether fuel is released; for example if the break is within a fuel free section.

As described in this chapter, experimental studies on irradiated cladding tubes where a shear fracture has been selectively induced have been used as the basis for establishing the bounding amount of fuel released per fracture. Using this information and the number of possible rod fractures in the cask then the worst case amount of fuel released to the cask cavity can be established.

The residual mechanical strength of irradiated cladding material is a function of the clad physical properties at the beginning of storage, the storage conditions and the cladding material. For example, the behaviour of zircaloy clad FAs are highly influenced by in reactor corrosion, hydrogen uptake, hydride distribution and hydride reorientation.

The loads experienced by a FA in an accident mainly depend on the overall transport system, storage cask and FAs. Simulating these conditions to predict FA behaviour is very complex due to the many variables which would need to be modelled, and makes interpretation of the results difficult. Fuel rod behaviour therefore, is studied using simplified models in order to quantify the number of potential fractures. The behaviour of a single fuel rod under quasi-static load conditions is determined analytically with regard to the failure load (without plastic deformation) due to bending, buckling and shearing in the simplest case. This failure load of the fuel rod is converted to a deceleration limit in consideration of dynamic influences and compared to the deceleration limit of the overall dry transport and storage system. If the maximal deceleration limit of the overall system is smaller than that of the fuel rod, it is assumed that the fuel rods remain intact.

In addition to the amount of fuel released or not, the resultant deformation of the fuel rods and FA structure are also required for criticality analysis. Since the FAs are designed to be under moderated, a broadening of the fuel rod bundles, for example, leads to an increase in FA reactivity. The plastic deformation of the FA array as a result of an accident depends on the drop orientation and can lead to a shift in the originally regular lattice spacing. Due to the large number of fuel rods in a FA, many arrays with irregular lattice spacing (broadening as well as narrowing) are possible.

The extent of FA geometry alteration due to an impact also depends on the design of the fuel skeleton or structural elements; for example the shock absorbing capability of the head and end pieces and spacer stability. If the spacer is deformed during a horizontal impact, the distance between the fuel rods will become smaller, but the regular fuel rod bundle will be maintained. The length of the fuel rod section between two intact spacers determines the potential free bending of a fuel rod.

7.3. INVESTIGATION METHODS, TESTING AND/OR ANALYSIS

Only a limited number of studies on evaluating spent fuel behaviour under impact conditions have been carried out; due to the requirements for working with irradiated fuel and the complex nature of the studies. Nevertheless technical data has been recently acquired in some Member States. The investigations and experimental results reported here are from France and UK, Germany, Japan and Spain. The results presented confirm the basic safety aspects presented in section 7.2., are relevant to the situations being studied, provide consistent information on the impact resistance of spent fuel and allow for realistic assumptions for safety analysis to be established.

7.3.1. France and UK investigations [100–101]

In France and UK, a methodology was developed to evaluate the nature and the extent of FA damage during cask package accident drops as required by [99].

Mechanical studies on fresh and irradiated fuel rod samples and the development of models has been undertaken to provide data on the behaviour of irradiated fuel under impact conditions. As a result the main mechanical properties for a drop have been identified and quantified. The data has been used to develop a fuel integrity methodology which provides guidelines for studying the effects of a lateral or axial drop on a cask package loaded with fresh or irradiated PWR and BWR FAs. Several conservative mechanical evaluations based on direct calculations or dimensionless comparisons with appropriate reference tests enable FA damage to be determined; which gradually increases with acceleration. First, elastic models distinguish the null or slight damage cases; then, plastic models identify cases with extreme FA damage that lead to unacceptable criticality hypotheses; finally, other plastic models quantify the extent of fuel rod deformations in moderate FA damage cases. Fuel integrity methodology application to a given case leads to the following output, for use in criticality safety analysis:

- Existence or not of fuel rods rupture, number of rods ruptured, location of rupture;
- Amount of fuel material released, extent of fuel rod array deformation, and sliding.

Data was acquired from 9 m drop tests on casks loaded with FAs or on fuel rods; for example Figs 57 and 58. The casks were loaded with depleted UO_2 PWR and BWR FAs.

The tests provided information related to fuel pin deformation modes, grid and nozzle yielding, fuel pin array deformation and sliding, and the maximum allowable loads for un-irradiated cladding.

In addition, some elementary tests on fuel rods (lateral bending, axial compression) were also carried out on fresh PWR and BWR fuel rods to determine the maximum load which can be supported by un-irradiated fuel claddings; Figs 59 and 60. Some of these tests were dynamic and others were quasi-static. In the case of an axial 9 m cask drop test containing fresh LWR

fuel rods, the rods only showed minor lateral deformations, without any cladding crack or rupture; for decelerations up to about 800 g.

In the case of dynamic bending of fresh BWR fuel rods, the cladding deformation mode and the associated maximum angle of deformation angle of 15° without rupture have been determined for a 9 m cask drop test.

To evaluate the effects of irradiation, tests on fuel rods with burnups between 40–50 GWd·t(U)$^{-1}$ were performed as shown in Figs 61 and 62.

The results from lateral bending tests on PWR and BWR rodlets, (3 point bending tests Fig. 61) and quasi static inter grid bending tests of LWR irradiated fuel rod samples allowed the deformation mode, the associated elongation and deflection at rupture (about 35 mm at 25°C and 60 mm at 500°C), and the subsequent fuel material release (2.60 g per rupture at most) to be determined.

Quasi-static bending tests on BWR irradiated fuel rod ends allowed the deformation mode, the associated angle and deflection at rupture (about 10 mm measured on a 22 mm span and for a deformation angle ranging from 25 to 30°), and the subsequent fuel material release (7.65 g per rupture at most) to be determined.

Crushing tests of empty irradiated BWR fuel pin claddings (Fig. 62) demonstrated that for a longitudinal loading, empty claddings of irradiated fuel rods have a significant strength before crushing and rupture.

FIG. 57. Fresh PWR FA after 9m drop test.

FIG. 58. Fresh BWR FA after 9m drop test.

FIG. 59. Dynamic bending of the end of a BWR fuel rod.

FIG. 60. Inter-grid bending test on a fresh PWR fuel rod; quasi static test.

The test programme and preliminary damage analysis, has enabled most of the mechanisms that can lead to fuel rod and FA damage/fuel rod rupture to be established and the maximum loads (i.e. maximum loads before or at rupture) sustained by fuel rods to be determined for transport accident scenarios. The work has helped to build up a damage analysis catalogue which describes the resulting damage in terms of drop direction (i.e. axial or lateral) and sometimes FA type.

The mechanisms which lead to fuel rod damage and deformations are:

- For a lateral drop:
  o Inter-grid bending and transversal shearing at grids level;
  o longitudinal compression and shearing on cladding;
  o Transversal shearing at rods ends in BWR FA when the nozzle is not supported by lodgement walls;
- For a axial drop:
  o Euler buckling in the bottom inter-grid region mainly in PWR FA;
  o Pure axial compression and impacts of fuel rod ends on the nozzle.

Concurrent bending of rods ends and nozzle plate in BWR FA.

For the lateral drop (Fig. 63), the slight packing down of end grids and collapse of central grids leads to limited rupture risks (moderate g-load), whereas complete packing down of fuel pin array in the FA central part leads to uncontrollable rupture risks (high g-load).

For an axial drop (Fig. 64), moderate g-loads leads to general bending or elastic buckling of the fuel rods. At higher loads local plastic buckling, unacceptable deformations and rupture of the fuel rods results.

FIG. 61. Rupture after bending tests of used fuel rod.

FIG. 62. Crushing of empty claddings from irradiated BWR fuel rods.
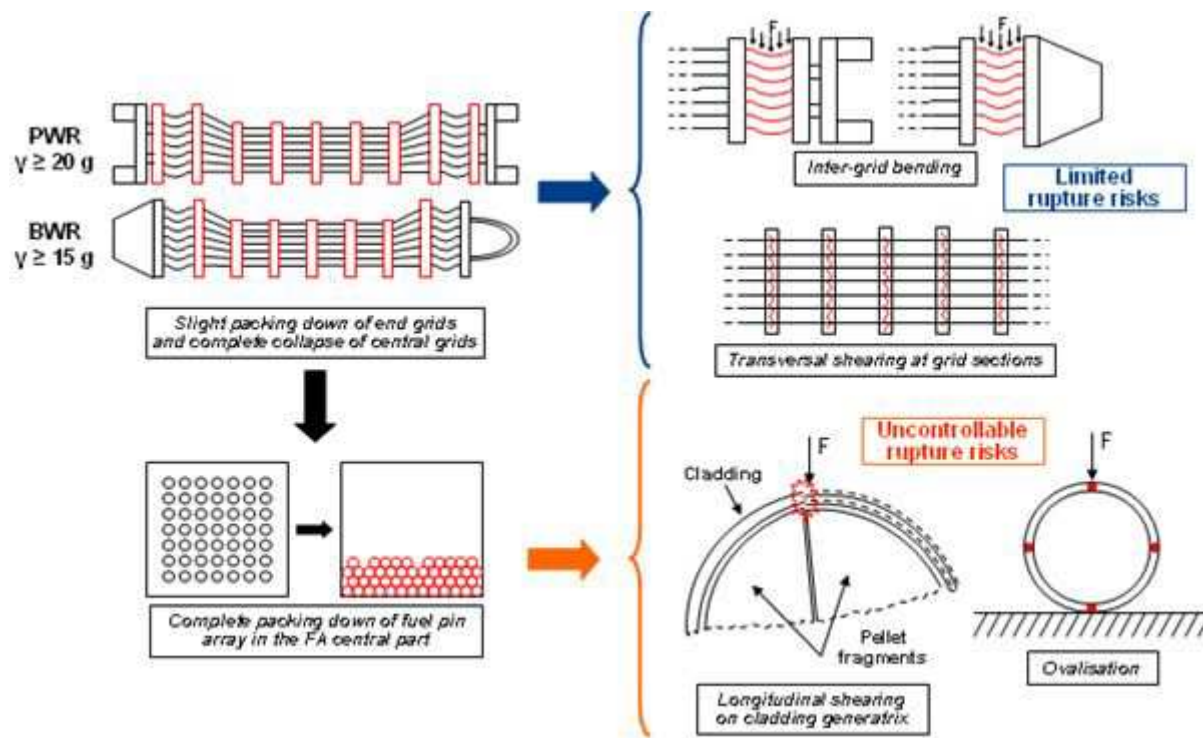
FIG. 63. Cladding rupture risks evaluation in lateral drop.
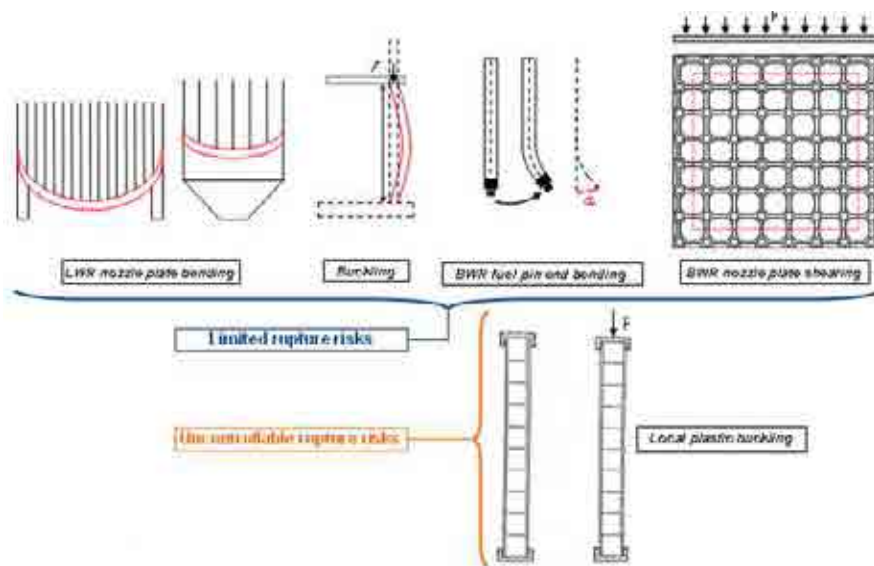

FIG. 64. Cladding rupture risks evaluation in axial drop.

The rupture locations for a lateral and axial drop are given in Fig. 65. The amount of fuel released is based on an analysis of the results, standardisation of the results and adding a degree of conservativism. The amount of fuel released per rupture is estimated: 1 or 3.5pellets per section of broken fuel pin.
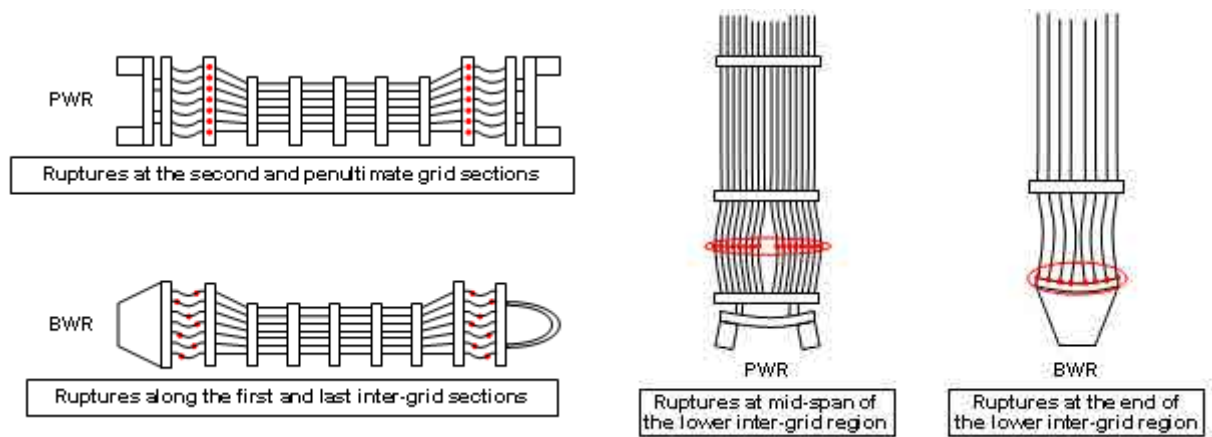
FIG. 65. Rupture locations in relation to drop direction; lateral and axial drop.

Array deformation for a lateral drop is a function of grids collapse pattern. As grids collapse in the central part of the FA (Fig. 66) there is a reduction in FA fissile cross section and generally a reduction in reactivity in the case of LWR FAs. The conservative approach is to retain the initial fissile cross section as the base data set for criticality analysis.

Fuel array deformation as a result of an axial drop is dependent on fuel rod deformation. For PWR fuel rods Euler buckling occurs which leads to an expansion of the PWR fuel array. In comparison, BWR fuel rod ends bend and the BWR fuel array contracts at the bottom inter-grid region. For BWR FAs, similarly to the lateral drop, the conservative approach is to apply the initial non-deformed geometry in the bottom inter grid, while an expansion could be introduced in the next inter grid because of the continuity of deformation. For PWR FAs, as the extent of longitudinal Euler buckling cannot be easily determined, the pessimistic approach is to consider a uniform expansion of the array in the deformed bottom inter grid (Fig. 67).

7.3.1.1. Potential for rod sliding

For a lateral drop, there is no load to induce either fuel rods sliding through the grids or nozzle deformation; in consequence, no array displacement is considered so that the active zone of fuel rods (active zone: with fissile content) remains in its initial position.
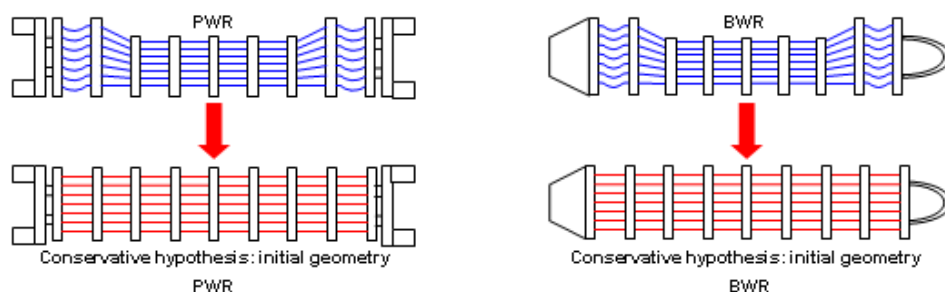
FIG. 66. Array deformation in lateral drop.

For an axial drop, except for extremely low g-loads, PWR fuel rods move uniformly to close the gap between their ends and the bottom nozzle plate. There is no such gap in BWR FA as BWR fuel rods are fixed to nozzles (Fig. 68). Then, depending on the design of the nozzle for both type of FA, LWR fuel rods displacement consists of: uniform sliding in case where the nozzle has easily crushed parts (shell, tripods, etc.) and differential sliding induced by the bending of the nozzle plate, submitted to the loading of FA top part in axial drop. As a result of array displacement, the final position of the active zone is deduced.

Finally, with the amount of fuel potentially released, the hypotheses of array deformation and sliding that are the results of fuel integrity methodology application, realistic and conservative hypotheses are used as input for safety analysis of transport packages.

FIG. 67. Array deformation in axial drop.

FIG. 68. Assumptions used for fuel array displacement for an axial drop.

7.3.2. Germany – Fuel rod fracture behaviour studies [102–103]

The studies were carried out at the European Commission's Joint Research Centre Institute of Transuranium Elements (JRC-ITU). The aim the studies was to assess spent fuel rod fracturing behaviour under transversa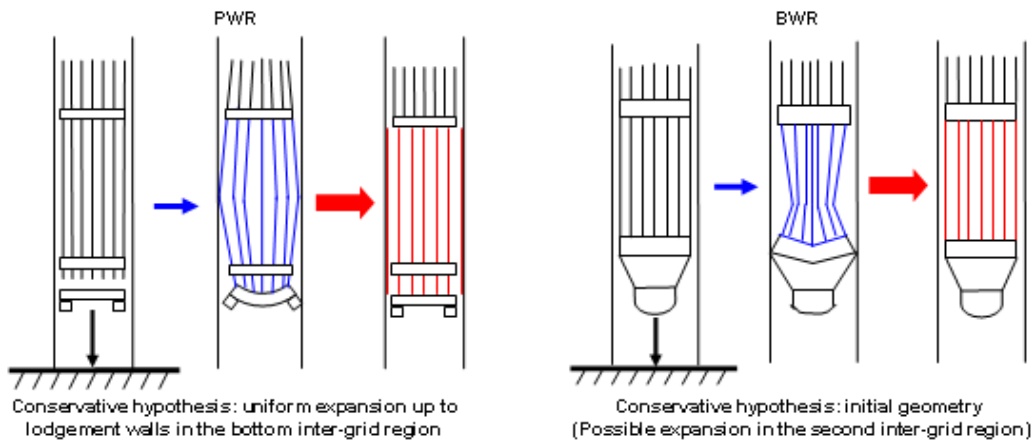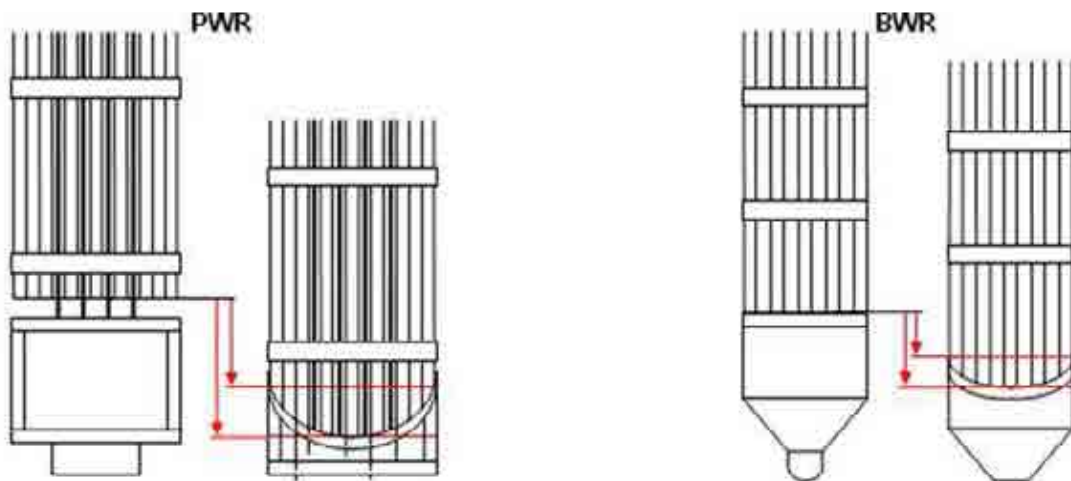l impact load conditions and the amount of fuel material released in the event of rod fracture. In addition, the relation between fuel burnup and the amount of fuel release was also studied. A device for rupturing fuel rods under transient impact load was developed and a campaign of in hot cell impact tests on irradiated fuel rod segments was performed.

7.3.2.1. Experimental setup

Figure 69 shows the apparatus used for the impact tests. The procedure consisted of releasing a free falling hammer through a vertical guiding column. The hammer was released from the top end of the column and impacted the sample laterally. The height of the column and the mass of the hammer determined the load on the sample. For the campaign, a 5.5 kg hammer was used. The impact velocity of the hammer was ~4.6 m·s^{-1}. To determine the amount of fuel released during the impact, the fuel rodlets were weighed before and after each test. The mass difference after the breakage corresponded to the amount of fuel released.

The tests were performed on PWR and BWR UO$_2$ fuel rods with fuel burnups between 19–74 GW·d·t(HM)$^{-1}$. Table 10 summarizes the main features of the fuel rods used in the experiments.
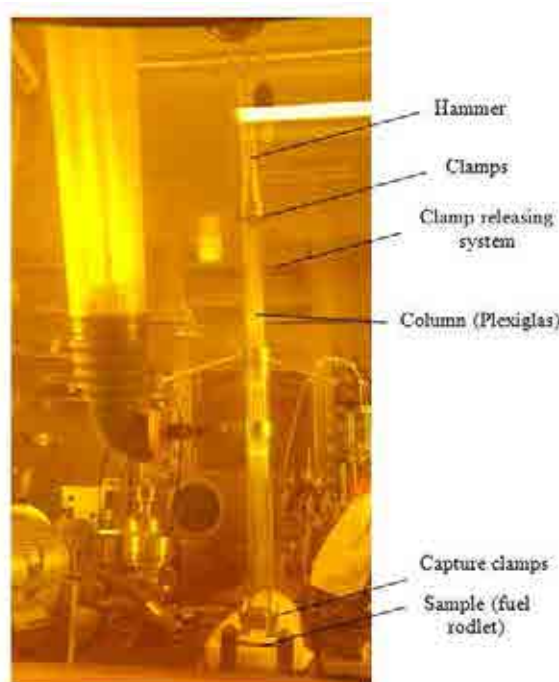
FIG. 69. The test apparatus installed in hot cell The apparent curvature of the plexiglas column in the picture is an optical effect due to the thick hot cell window.

TABLE 10. CHARACTERISTICS OF THE FUEL ROD SAMPLES SELECTED FOR THE IMPACT TESTS

Fuel Type	Burnup GW·d·t(HM)$^{-1}$	Cladding type	Outer diameter mm	Cladding thickness mm	Average clad. outer corrosion thickness μm	Cladding hydrogen concentration ppm
PWR	19.0	duplex Zry-4	10.75	0.725	<50	<200
	42.6					
	73.6					
BWR	53.0	Zry-2	10.05	0.605	<50	<100

Figure 70 shows some photographs, captured by high speed camera, before and during the impact on a 74 GW·d·t(HM)$^{-1}$ PWR rodlet, and Fig. 71 shows the resulting fracture surfaces.
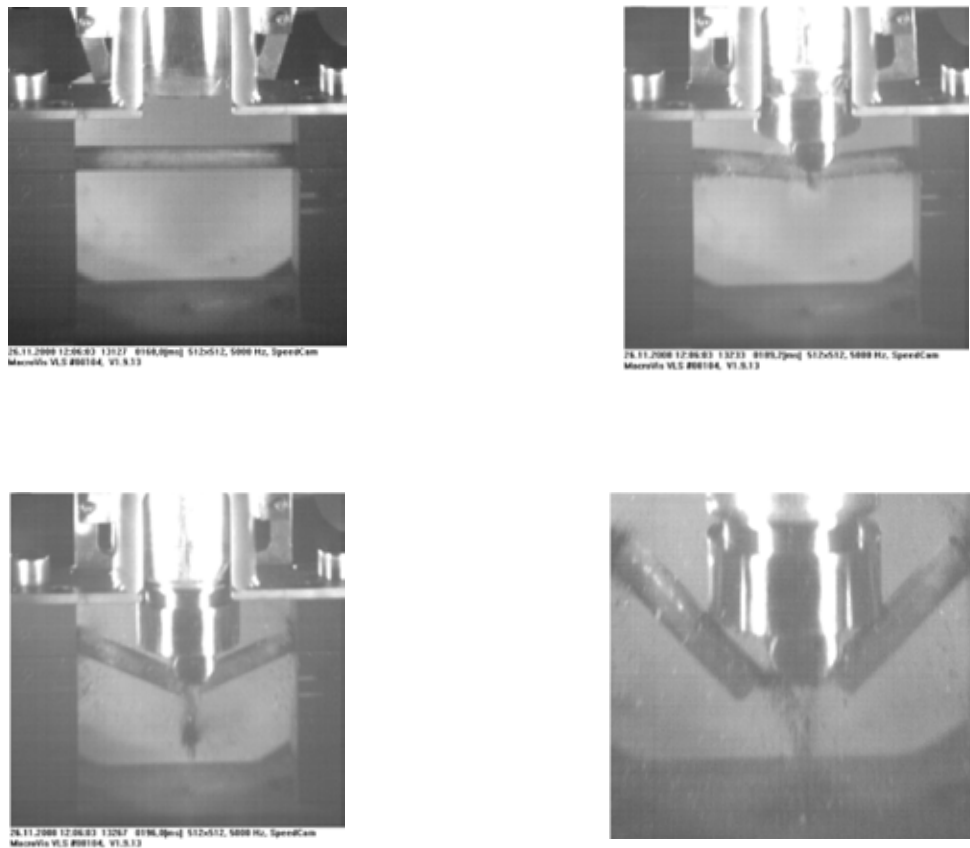
FIG. 70. Impact tests: High speed camera photographs showing the impact fracture of a ~74 GW·d·t(HM)$^{-1}$ PWR fuel rodlet.
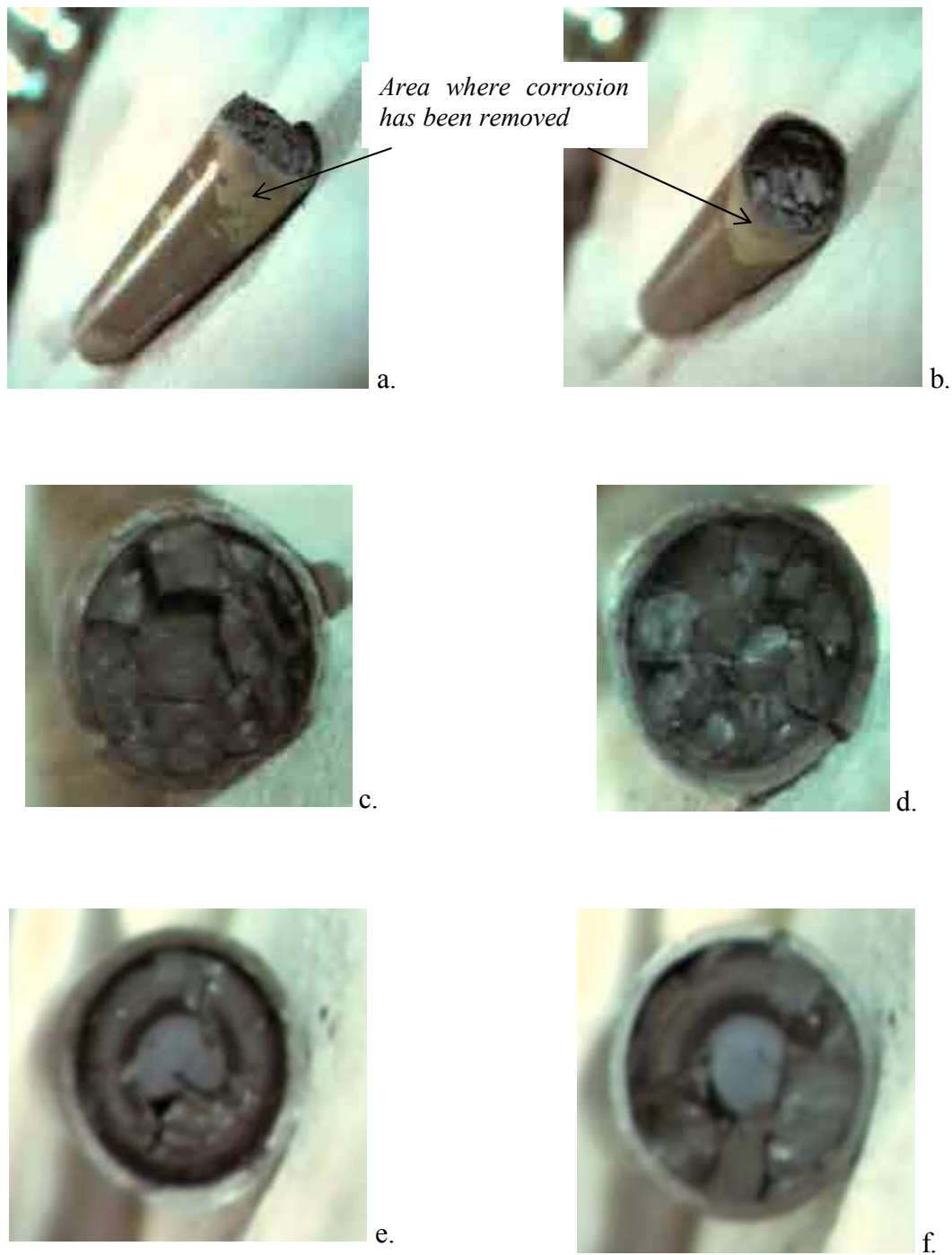
FIG. 71. (a, b): Fragments of the 74 GW·d·t(HM)$^{-1}$ PWR fuel rodlet after the impact test; corresponding fracture surfaces are shown; the arrow indicates the region where the outer corrosion layer was removed from the cladding during the early stages of the impact; (c, d): Corresponding fracture surfaces for the 43 GW·d·t(HM)$^{-1}$ PWR sample; (e, f): Corresponding fracture surfaces for the 19 GW·d·t(HM)$^{-1}$ PWR sample showing that the fracture occurred at a pellet–pellet interface.

Figure 72 shows the fuel particles collected after the impact test on the lowest burnup rodlet (19 GW·d·t(HM)$^{-1}$). Table 11 reports the amount of fuel particles collected after each test. Similarities were observed for all rodlets tested; in particular, the amount of fuel released per fracture is comparable for all the samples. In all the tests the released fuel collected at the bottom of the device corresponded to < 2g per fracture. No 'flow out' of fuel pellets associated with the presence of an open gap between fuel pellet and cladding was observed in the case of the lowest burnup fuel rod sample.

7.3.2.2. Bending tests

Fuel rod bending studies were carried out at Studsvik AB nuclear laboratories. Two high burnup fuel rod segments available at Studsvik from Ringhals-2 and -3 NPP were chosen for the tests. The basis of the test was to mechanically bend a fuel rod until it broke and to collect the fuel particles released for visual inspection and weighing. For this purpose one end of the approx. 1 m long fuel rod segment was inserted into a hole drilled in an aluminium block and screwed tightly. The major part of the fuel rod segment was inserted into a steel tube used as a handle when bending the fuel segment by means of a manipulator in the hot cell. The length of the fuel segment that was not covered by the steel tube was approx. 10 cm. Both, the aluminium block and the uncovered part of the fuel rod segment were surrounded by a transparent plastic bag in order to collect the fuel particles released by rod breakage. The test equipment and setup is shown in Fig. 73.

7.3.2.3. Results of the bending test

The burnup at the bending area of the two fuel rod segments was 65 GW·d·t(HM)$^{-1}$ and 68 GW·d·t(HM)$^{-1}$ respectively. One fuel rod segment broke after a bending of about 45 degrees, the other after about 30° of bending. The fracture position was much closer to the block than to the free end of the fuel rod segment. The images taken from the fracture surfaces are shown in Figs. 74 and 75.

FIG. 72. Fuel fragments released during the test on a 19 GW·d·t(HM)$^{-1}$ PWR fuel sample.

TABLE 11. MASS OF FUEL RELEASED DURING THE IMPACT TESTS

Fuel type	Burnup (GW·d·t(HM)$^{-1}$)	Number of fracture positions	Amount of fuel released (g)
PWR	19.0	3[14]	3.9
	42.6	3	4.8
BWR	73.6	3	5.6
	53.0	3	4.7

The fuel particles collected after breaking the fuel rod segment are shown in Fig. 76. The test setup was limited to the collection of fuel particles whose sizes were sufficient to catch them; thus very fine fuel powder particles were ignored. Hence the amount of particles released is de facto higher than the amount of particles collected in these experiments. This approach, though unable to give a complete particle size distribution, was useful to estimate the approximate amount of fuel particles released.

When the burnup range 20–75 GW·d·t(HM)$^{-1}$ of the samples and the results from the bending and hammer impact tests are taken into consideration it can be concluded that there is no relationship between the amount of fuel released as a result of rod breakage and the degree of burnup. Moreover, the experimental approach, rod bending or hammer impact, has no significant effect on the amount of fuel released.

In spite of the binding between cladding and pellet observed in high burnup rod tests, the fuel released was of the same order of magnitude as that released during medium and low burnup rod tests. This may be due to deformation at the fracture point of the cladding impeding a gliding of pellets out of the cladding tube even if the pellets are not bonded to the internal surface of cladding tubes. As a result, the fuel release does not change significantly. Besides that, the cracks in the fuel matrix are not rectilinear so that the fuel fragments get stuck. Hence, those cracks let only a small fuel release happen because of their non-straight path in the fuel matrix.

FIG. 73. Rod bending test equipment/setup at Studsvik before and during the fuel rod segment bending.

---

[14] No full severing of the sample.
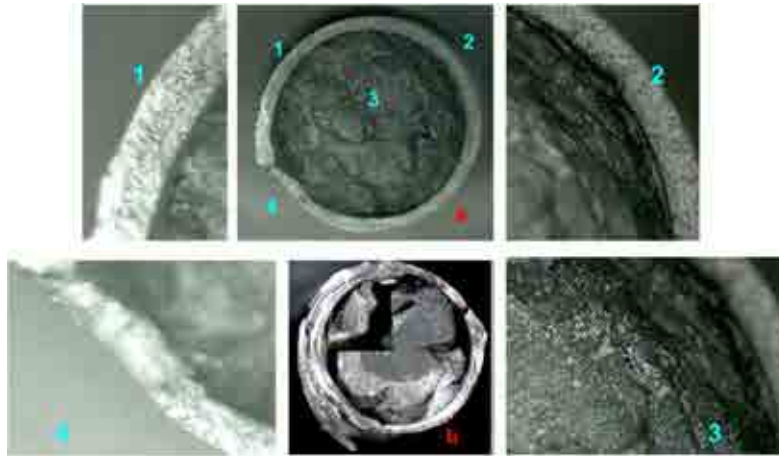
FIG. 74. Images taken from the fracture surface of the first fuel rod segment. a) Fracture surface of the rod end fixed in the aluminium block and b) Fracture surface of the long, free end.
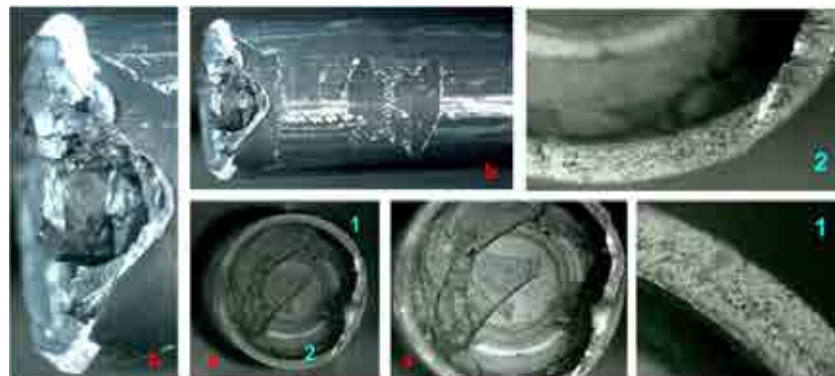
FIG. 75. Images taken from the fracture surface of the second fuel rod segment. a) Fracture surface of the rod end fixed in the aluminium block and b) Fracture surface of the long, free end.

16 mm

FIG. 76. Example of particles collected from a fuel rod impact test.

7.3.3. Japanese studies [104–106]

7.3.3.1. Objectives, impact test equipment and test matrix

The objective of the tests was to establish the behaviour of high burnup BWR and PWR fuel rods as a result of an impact.

Dynamic impact tests were carried out on high burnup spent fuel rods irradiated in commercial BWR and PWR reactors in Japan. Axial and lateral loading of fuel rods were studied (Fig. 77) to establish fuel rod failure loads, failure strain and the amount of fuel material released on impact.

Zircaloy-2 and MDA™ claddings and segmented rods from fuel irradiated up to 55 $GW \cdot d \cdot t(HM)^{-1}$ were used in the tests. Elemental mechanical testing of the cladding consisted of tensile and ring compression tests. Dynamic load impact tests on fuel rod were carried out at two modes: axial drop and lateral drop. Hydride reoriented claddings were also tested in ring compression tests and lateral load tests. The full test matrix is given in Table 12.

Elemental mechanical tests consisted of tensile and ring compression tests. Axial tensile yield strength, failure strain, ring compressive strength, and failure fattening ratio were acquired. Maximum strain rate for the tests was 10^2 per second. The tests were carried out at room temperature as a conservative condition from a viewpoint of cladding brittleness.

The sample dimensions are illustrated in Fig. 78.

FIG. 77. Loading modes: axial and lateral.

FIG. 78. Sample dimensions used in Japanese studies; dimensions in mm.

TABLE 12. JAPANESE TEST MATRIX FOR DYNAMIC IMPACT TESTING OF IRRADIATED FUEL RODS AND CLADDING

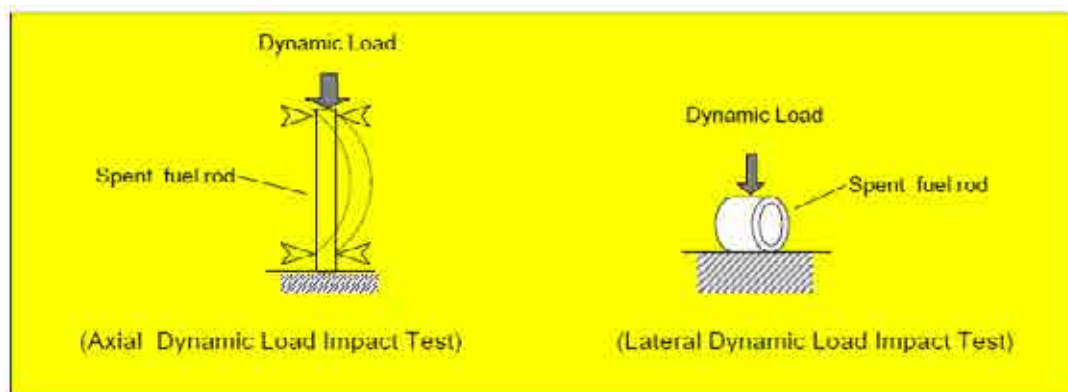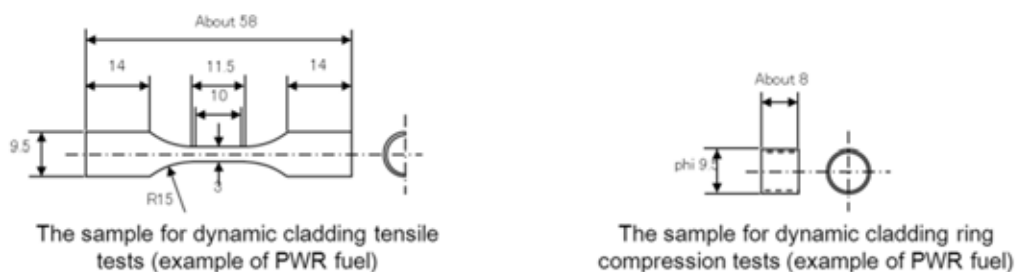| Fuel type/burnup			BWR 55 GW·d·t(HM)$^{-1}$	PWR 55 GW·d·t(HM)$^{-1}$
Cladding type			Zircaloy-2[1]	MDA™
Elemental mechanical test of cladding	Dynamic tensile test (up to $10^2\,\text{s}^{-1}$)		6	12
Dynamic impact test of fuel rod	Dynamic ring compression test (up to 4000 mm·s^{-1})	As irradiated	4	3
		Hydride reoriented	4	6
Dynamic load impact test of fuel rod	Axial load		5	5
	Lateral load	As irradiated	5	6
		Hydride reoriented	1[15]	2[16]

7.3.3.2. *Results of dynamic tensile tests on BWR and PWR fuel claddings*

The results of dynamic tensile tests on BWR and PWR fuel claddings have been plotted in terms of ultimate tensile strength vs. strain rate and total elongation vs. strain rate; as shown in Fig. 79. With an increase in strain rate, ultimate tensile strength increased and total elongation decreased. Whilst the mechanical characteristics of un-irradiated zircaloy-2 and MDA™ are different, the behaviour of the irradiated materials leads to similar results.

7.3.3.3. *Results of dynamic ring compression test on BWR & PWR fuel claddings*

The results from dynamic ring compression tests on BWR and PWR fuel claddings presented as crosshead displacement ratio vs. compression speed are shown in Fig. 80. The majority of the results are on hydride reorientation treated material. In all cases the ductility decreases as compression speed (up to 100 mm·s^{-1}) is increased.

The hydride reorientation treatment was 300°C for material with an initial 70 MPa hoop stress. The cool down rate was 30°C·h^{-1}. At a given compression speed, the hydride reorientation treatment (300°C; 70 MPa; 30°C·h^{-1} cool down rate) applied to BWR cladding specimens had no effect on the value of the crosshead displacement ratio, i.e., on the ductility index of BWR cladding. However, for PWR cladding, the effect of the hydride reorientation treatment on the crosshead displacement ratio (i.e., on the cladding ductility index) can be clearly seen.

7.3.3.4. *Dynamic load impact test equipment*

The equipment for the impact load testing of BWR fuel rods was designed to be dual purpose for axial and lateral impacts as shown in Figs. 81 and 82. To retain the fuel in the cut rods, the ends of the fuel rodlet were fitted with Swageloks™ as shown in Fig. 83.

---

[15] Zirconium liner
[16] Dummy pellets loaded (Forsterite composition: 2 Mg)
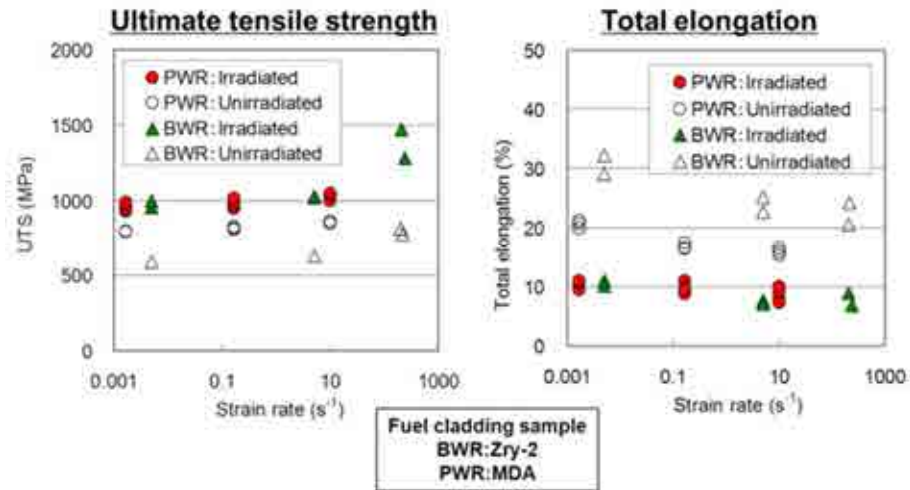
FIG. 79. Results of tensile tests.
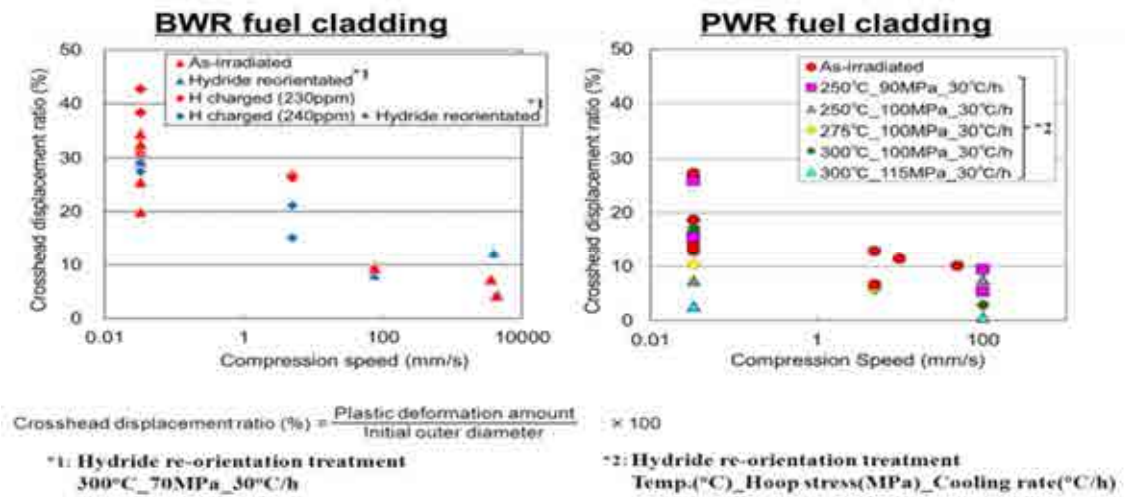
FIG. 80. Results of dynamic ring compression tests.

FIG. 81. Impact load testing equipment for BWR fuel rodlets; axial setup.
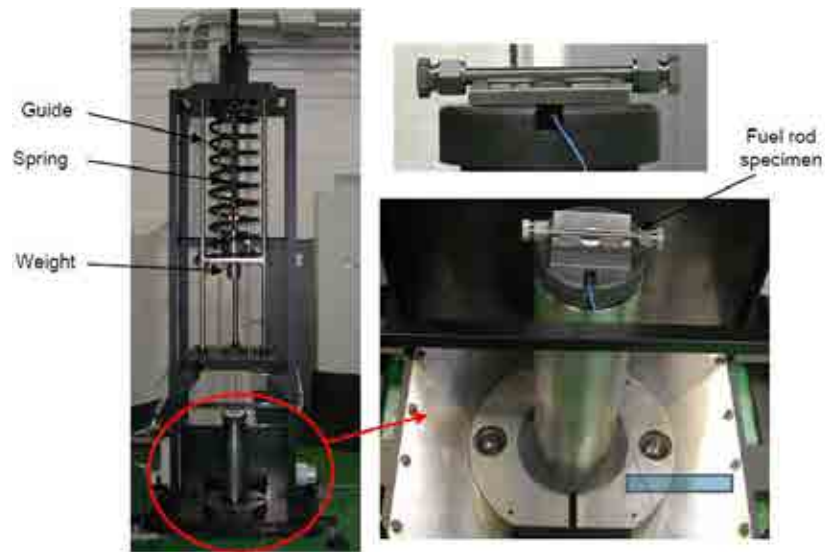
FIG. 82. Impact load testing equipment for BWR fuel rodlets; lateral setup.

a.

b.
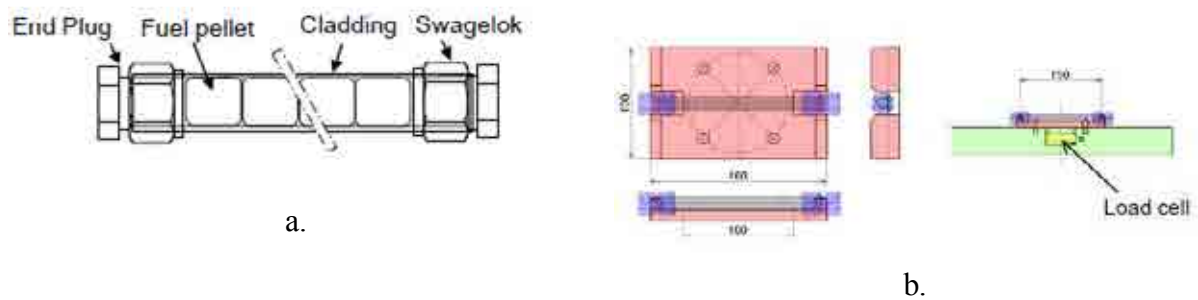
FIG. 83. Specimen setup (a.) and holding device for lateral load impact tests (b.); dimensions in mm.

A schematic of the equipment used for the dynamic load impact testing of PWR fuel rodlets is shown in Fig. 84 and the experimental setups for axial and lateral impact tests in Figs 85 and 86.
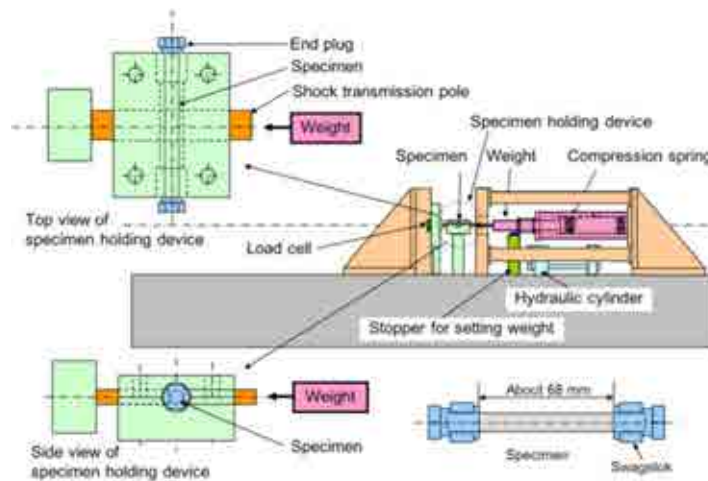
FIG. 84. Schematic of the testing equipment used for impact testing of PWR rodlets.
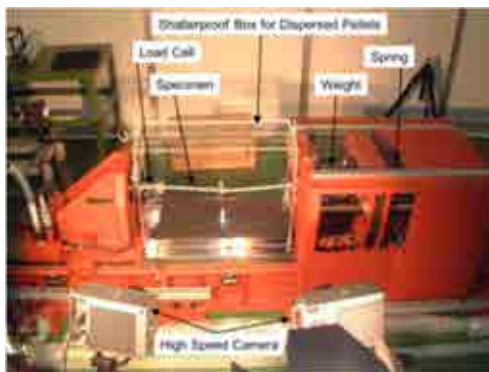
FIG. 85. Impact load testing equipment for PWR fuel rodlets; axial setup.

FIG. 86. Impact load testing equipment for PWR fuel rodlets; lateral setup.

7.3.3.5.   *Measuring methodology*

The collision load was measured using a load cell. Pictures of fuel rodlet deformation were taken by two high speed cameras. Weight and particle size measurements were carried out on the fuel particles collected after impact.

The fuel rods selected for impact testing are listed in Table 13.

7.3.3.6.   *Axial impact tests on BWR fuel rods*

The weight of BWR rods used in the axial impact tests was 3.5 kg. Collision speed was varied between 3.7–12 m·s^{-1}. Tests were performed on rodlets cut from the fuel stack and upper plenum region.

Cladding rupture and release of fuel material only occurred in the 12 m·s^{-1} test (Fig. 87). The rupture was 152 mm from the upper end and rupture length was around 40 mm equivalent to a spiral round. It occurred at 0.1–0.2 ms after load impact. Shearing rupture and spiral crack

propagation occurred without buckling. Bowing without clad fracture occurred in the 9 m·s⁻¹ case and the test on the upper plenum rodlet.

Analysis of load versus time curves (Fig. 88) shows similar load history profiles except for the upper plenum case. The peak loads in the region of 0 to 0.2 ms are proportional to the impact speed.

7.3.3.7. *Lateral impact tests on BWR fuel rods*

Test specimens were prepared from hard bonding[17] material, loose bonding material, and hydride reorientation treated material. Rodlet weights were between 0.6–2.6 kg. Collision speed was either 4 or 8 m·s⁻¹. Ruptures were observed in three cases (see Figs 89 and 90) with fuel material only being released in the case of the impact at 8 m·s⁻¹.

In Fig. 90 plots of the load on the lower end plug vs. elapsed time are presented. The plots show two peaks where rod rupture occurred and only one where there was no rupture. The slope of the first peak for the hydride reoriented material (with dummy pellet) was steeper than other material tested at a collision speed of 4 m·s⁻¹.

TABLE 13. FUEL ROD DATA FOR FUEL TESTED

Fuel Type	BWR	PWR
NPP	Fukushima Daini – unit 1	Ohi unit 4
Fuel assembly identifier/burnup	2F1Z2[18], 53 GW·d·t(HM)⁻¹	M04F74[19], 52 GW·d·t(HM)⁻¹
Fuel rod number/burnup	A5, 56 GW·d·t(HM)⁻¹ E1, 56 GW·d·t(HM)⁻¹	H11, 52 GW·d·t(HM)⁻¹
Cladding type	Zircaloy-2 (with zirconium liner)	MDA™
Pellet type	Current	Current

---

[17] Bonding refers to the pellet to clad interface.
[18] 5 cycle irradiated fuel
[19] 4 cycle irradiated fuel
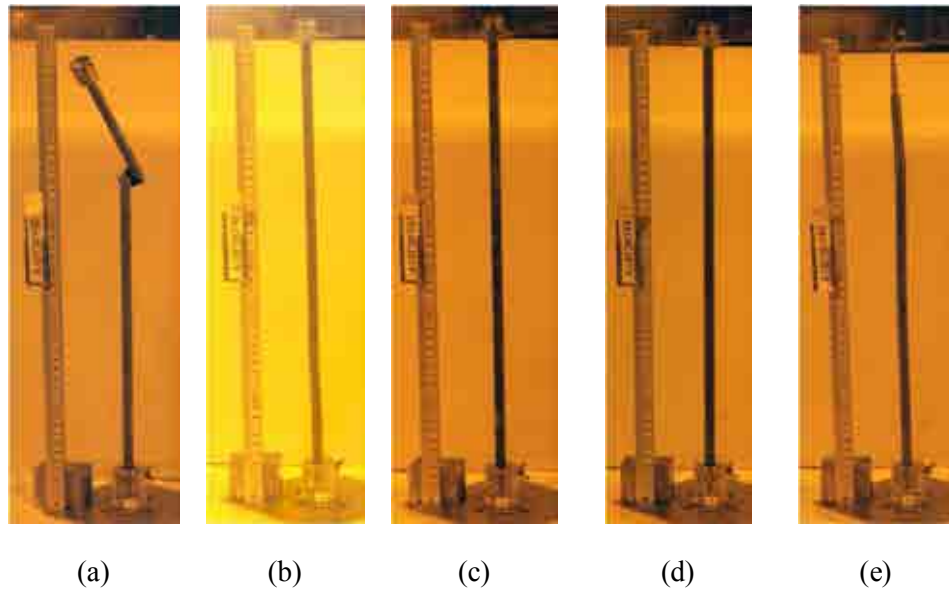
	(a)	(b)	(c)	(d)	(e)
Weight mass	3,5 kg				
Collision Speed	12 m·s⁻¹	9 m·s⁻¹	6 m·s⁻¹	3.7 m·s⁻¹	6 m·s⁻¹
Specimen Type	Fuel section (hard bonding material)				Upper plenum
Pellet Dispersion	Yes	No	No	No	No
Deformation	Spiral breakage	Bowing at lower part	None	None	Jack knifing at plenum part

FIG. 87. Impact test results on BWR rods – axial direction.
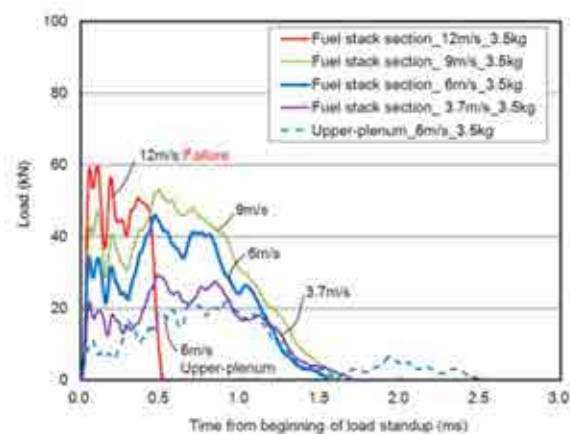
FIG. 88. Load versus time curves for impact test results on BWR rods – axial direction.

BWR fuel rod Post test	Weight mass	Impact speed	Proof load kN·mm^{-2}	Hydride re-oriented	Results
	2.60 kg	8.0 m/s	0.96	No	Failure Pellet dispersion
	2.60 kg	4.0 m/s	0.71	No	Failure
	0.63 kg	4.1 m/s	0.77	Yes	No-failure

FIG. 89. Impact test results on BWR rods – lateral direction (Hydride re-orientation treatment 300°C, 70MPa, 30°C·h^{-1}).
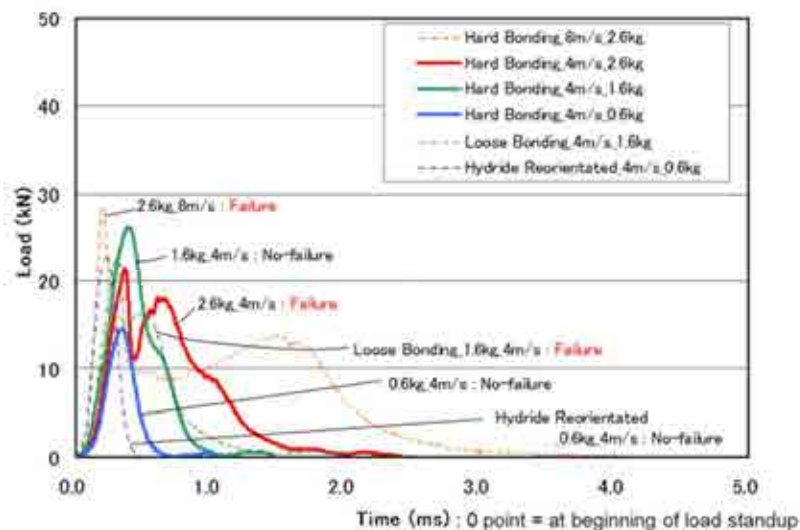
FIG. 90. Load versus time curves for impact test results on BWR rods – lateral direction.

If the results from ring compression and impact tests on BWR fuel, 'with' and 'without' pellets, are compared, it can be concluded that the strength of fuel rods with pellets are one order higher than those without pellets; for impact tests in the lateral direction.

7.3.3.8. Lateral impact tests on PWR fuel rods

A summary of the impact tests on PWR rods in the lateral direction are given in Fig. 91. Where the rod did not fail this believed to be due to the support effect of dummy pellets which have a higher strength than UO$_2$ pellets. A threshold of failure load was not determined as this is dependent upon pellet/cladding interaction. Failure strength 'with' pellets was found to be one order of magnitude higher than 'without' pellets. Influence of hydride slightly reoriented was not observed.

7.3.3.9. *Fuel material released as a result of testing-amount and particle size distribution*

The fuel material release as a result of axial and lateral impact testing on BWR and PWR rods is shown in Fig. 92.

Where BWR fuel rods ruptured, the amount of fuel material released, axial impact testing, was equivalent to approximately two pellets and about 60 % of the material was very fine powder. In case of lateral impact testing, the amount was equivalent to approximately three pellets and about 40 % was very fine powder.

For the PWR cases, the amount of fuel material released was less; around 1.4 g.

7.3.4. Spanish studies

The aim of this study was to investigate fuel cladding response under impact conditions. To this end, a comparison between results obtained in both dynamic (i.e. drop weight tests) and static ring compression tests (RCT) was made [107].

7.3.4.1. *Experimental*

The material employed was un-irradiated ZIRLO™ cladding in stress relieved condition [108]. The cladding dimensions were 9.5 mm outer diameter with a 0.57 mm wall thickness. The samples were cut into rings 10 mm length.

Samples with 150, 250 and 500 ppm of hydrogen were prepared. After the hydriding process, the samples were subjected to a heat treatment. The resulting hydride distribution was homogeneous through the cross section, with hydrides oriented along the hoop direction of the samples [109].

PWR fuel rod Post test	Weight mass	Impact speed	Proof load kN·mm^{-2}	Hydride re-oriented	Results
	3 kg	12.9 m/s	1.5	No	Failure Pellet dispersion
	3 kg	11.0 m/s	1.1	No	Failure Pellet dispersion
	3 kg	10.9 m/s	1.4	Yes	No-failure

FIG. 91. *Impact test results on PWR rods – lateral direction (Hydride re-orientation treatment 300°C, 70MPa, 30°C·h^{-1}).*
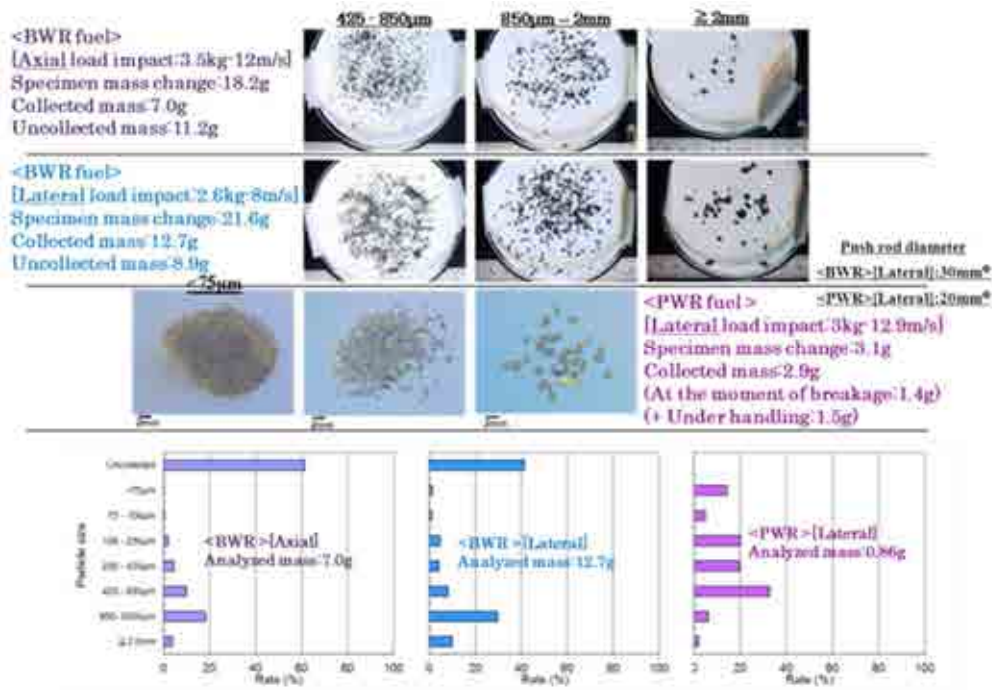
FIG. 92. Dispersed pellets amount and particle size distribution; PWR and BWR rod dynamic tests. [20]

The impact experiments were performed in a drop tower test machine which provides a motorized latch block that suspends a crosshead. Upon computer command, the crosshead is released from the latch block into free fall guided by two twin columns. The velocity of the crosshead was measured using an infrared sensor fixed to the drop tower that sensed the passage of a flag mounted to the crosshead. In the context of this work, the applied impact velocity was 3 m·s⁻¹.

Samples in as-received condition (0 ppm of hydrogen) and with 150, 250 and 500 ppm of hydrogen were tested at 25, 135 and 300°C. For tests at temperature (135 and 300°C), a resistance furnace was placed between the guide columns, above the T-grooved baseplate to heat the samples (Fig. 93).

Quasi static RCTs were performed with a universal testing machine (Instron). The applied load was measured using a load cell of up to 5 kN capacity. Compression load was applied by means of two steel plates (plane and parallel). Tests were carried out by applying a constant displacement rate to the plates. Tests were carried out at three displacement rates: 0.5, 100 and 1000 mm·min⁻¹, and at 25, 135 and 300°C.

Cross sections of the resulting fracture surfaces were subjected to qualitative fractographic examination using a field emission scanning microscope.

7.3.4.2.   Load versus displacement curves - static and dynamic RCT tests

The shape of the drop weight tests (3 ms⁻¹) curves were similar to the ones produced from static testing (Fig. 94).

---

[20] *Where Uncollected = (Specimen mass before test) – ((Specimen mass after test) + (Collected mass))*

The slope of the RCT curves, after the initial displacement, increases with an increase in strain rate. This means that the cladding stiffness, Young's modulus, is increased. There was no significant difference between samples with and without hydrogen. Only a variation in the maximum load reached, and the displacement value at this point, can be observed.

In quasi static loading conditions, a typical ductile fracture surface aspect was developed, with large micro voids oriented in the direction of crack growth. Test temperature does not seem to influence the fracture mechanism. Similar results were obtained for both, hydrided and as received samples.

An interesting observation is the fracture behaviour under dynamic loading. It can be seen that temperature plays an important role in fracture micro mechanisms. For example, dynamic loading provokes the occurrence of brittle fracture features in hydrided cladding at low temperatures (room temperature and 135°C).

Table 14 summarizes the observations for different test conditions on hydrided specimens.
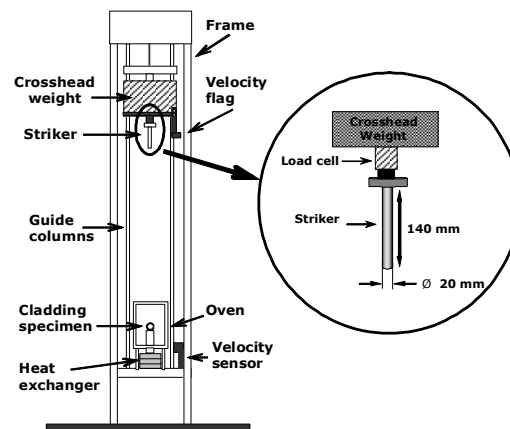
FIG. 93. Experimental device employed for the dynamic Ring compression tests (RCTs).
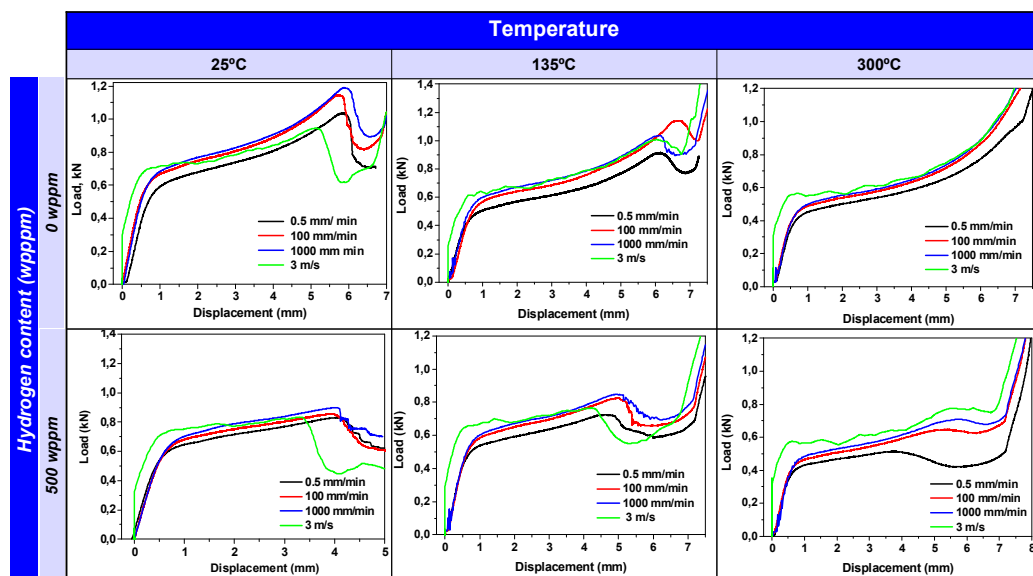
FIG. 94. Load versus displacement curves - static and dynamic RCT tests.

TABLE 14. CHARACTERISTICS OF FRACTURE SURFACE OF HYDRIDED SPECIMENS (500 PPM) TESTED UNDER QUASI-STATIC AND DYNAMIC LOADING

	Temperature		
	25°C	135°C	300°C
Quasi-static tests (conventional RCTs)	Ductile	Ductile	Ductile
Dynamic tests (drop weight conditions)	Brittle	Brittle + ductile	Ductile

In the fracture surface of specimens tested at room temperature, there is a predominance of brittle areas (Figs. 95 and 96). Ductile fracture also occurs, but is limited to ZIRLO™ matrix (Fig. 97).

At 135°C, dimples and brittle areas coexist in the fracture surface. Nevertheless, the proportion of dimples is greater than at room temperature (Fig. 98). At 300°C, fracture is totally ductile (Fig. 99). From these results, it could be inferred that temperature has a beneficial effect on cladding resistance.
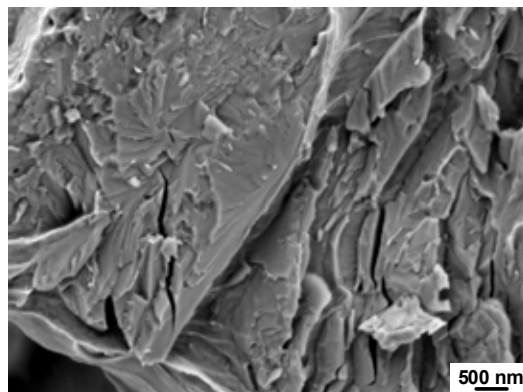
FIG. 95. Brittle area found in the fracture surface of a 500 ppm hydride tested at room temperature under dynamic loading.
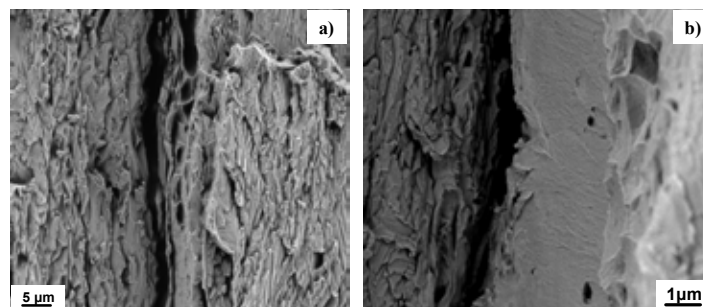
FIG. 96. a) Brittle zone in a 500 ppm hydride specimens tested at room temperature in the drop weight tower; b) Magnification of fracture surface of a hydride platelet.
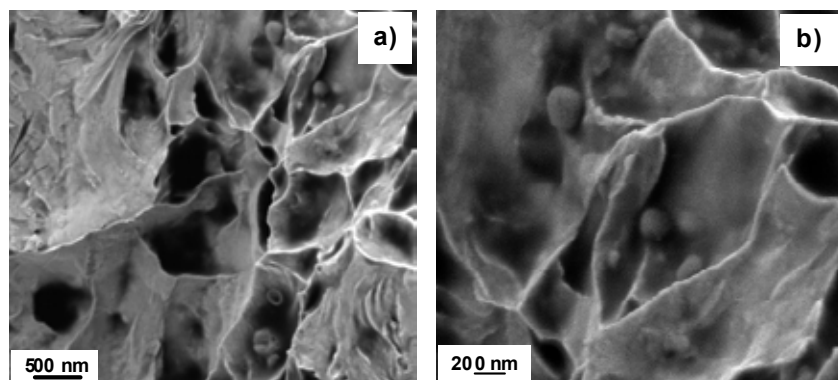
FIG. 97. a) Micro voids coalescence in a ductile fracture of ZIRLO matrix; b) Magnification of them.
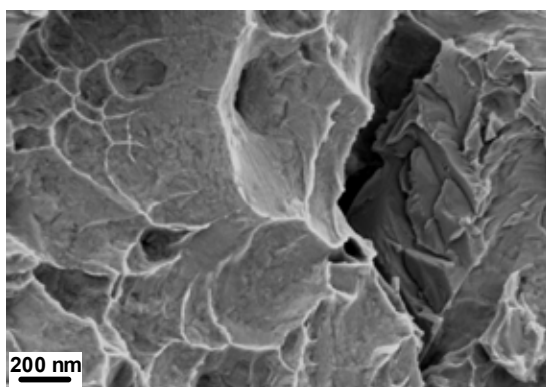
FIG.98. Coexistence of ductile and brittle areas in the fracture surface of a 500 ppm hydride specimen tested in a drop weight tower at 135°C.
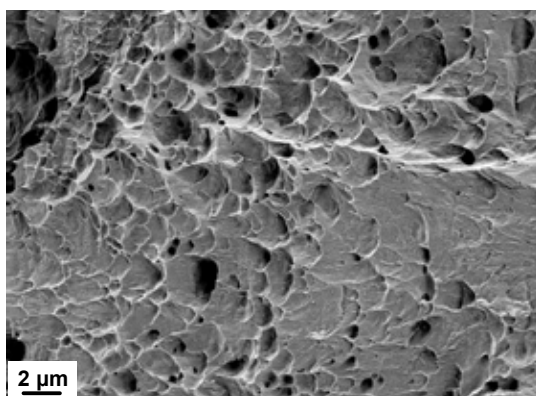
FIG. 99. Dimples oriented in the crack direction in the fracture surface of a 500 ppm hydride specimen tested in a drop weight tower at 300°C.

7.3.4.3. Conclusions

Cladding stiffness and strength increased at increasing displacement rates. This fact is in good agreement with the generally accepted assumption that during an accident the higher load application rate would lead to better cladding strength.

The effect of temperature and hydrogen concentration on load versus displacement curves is similar in both the dynamic and quasi static ring compression tests.

Increasing temperature has a beneficial effect under dynamic loading. At room temperature, impact provokes the occurrence of brittle fracture features, not expected in a ductile material. Increasing temperature leads to a progressive recovery in clad ductility. This fact is more noticeable at 300°C.

8. STORAGE FACILITY COMPONENT DEGRADATION IN WET AND DRY STORAGE

8.1. WET STORAGE

8.1.1. Stainless steel

8.1.1.1. Slovakia long term corrosion monitoring programme

Detailed in SPAR II [2] Vűje has been undertaking a materials surveillance programme on behalf of Jaslovské Bohunice spent fuel interim storage facility (SFIS) since 2005. The materials being monitored are neutron absorber materials used in spent fuel storage baskets, type ANSI 304 stainless steel alloyed with a minimum of 1.1% boron (ATABOR), and the pool liner fabricated from ANSI 321 stainless steel.

The methodology used in the surveillance programme is:

- All test specimens are made from original or archive materials;
- Specimens are placed in the operating environment;
- Specimens are loaded with stresses similar or higher than in the operating environment.

The long term performance of these materials is being established through immersion of corrosion coupons in the storage pool and in-situ monitoring (pool liner only). Corrosion coupons comprise:

- Standard corrosion coupons;
- U-bend;
- Circular bead welded;
- Crevice bent beam (CBB);
- Special types, for example hexagonal welded joints.

Corrosion coupons have been examined on a periodic basis up to 8 years. The weight loss measurements from coupons which have been immersed for 6 and 8 years are summarized in Tables 15 and 16. From the data collected to date the long term thinning of either metal is expected to be <1 $\mu m \cdot y^{-1}$.

Inspection of CBB coupon surfaces by stereomicroscopy has not revealed any corrosion damage (Fig. 100). On the surface of the coupons prepared from the ATABOR steel several micro cracks have been found in the base metal. X ray microanalysis has shown that these cracks are located at areas of high chromium content (Fig. 101).

In the case of circular bead welded coupons, after cleaning, some deposits and rests of slag and several surface micro cracks were observed (Fig. 102). The cracks were found to be corrosion free and are the result of initial sample preparation due to the brittle nature of the Cr–B bonds. There has been no evidence to support crack propagation.

No corrosion or cracks have been found to date on any of the other corrosion coupons.

TABLE 15. WEIGHT LOSS RESULTS FROM ATABOR STEEL COUPONS IMMERSED FOR UP TO 8 YEARS

sample ID	sample position	steel 1.4541 - tube # 6			
		weight before	weight after	difference	weight loss
		[g]	[g]	[g]	[g.m^{-2} /year]
6 - 1	water level fluctuation	129.8586	129.8575	-0.0011	0.0232
6 - 2		117.7891	117.7879	-0.0012	0.0253
6 - 3		118.6235	118.6216	-0.0019	0.0400
6 - 4	under water	123.2360	123.2338	-0.0022	0.0463
6 - 5		124.4851	124.4835	-0.0016	0.0337
6 - 6		115.2342	115.2316	-0.0026	0.0547

TABLE 16. WEIGHT LOSS RESULTS FROM ATABOR STEEL COUPONS IMMERSED FOR UP TO 8 YEARS

sample ID	sample position	ATABOR - tubes: Z 12, Z013, Z015, Z016			
		weight before	weight after	difference	weight loss
		[g]	[g]	[g]	[g.m^{-2} / year]
Z12 - 1	under water	68.0326	68.0289	-0.0037	0.0671
Z12 - 2		69.4370	69.4343	-0.0027	0.0490
Z12 - 3		70.8696	70.8655	-0.0041	0.0743
Z013 - 3		46.9488	46.9465	-0.0023	0.0844
Z015 - 3		58.1117	58.1088	-0.0029	0.0884
Z016 - 3		57.5883	57.5859	-0.0024	0.0732

To supplement corrosion coupon monitoring the integrity of the pool liner is periodically monitored in-situ using the technique of acoustic emission. There are six sensors installed in each pool and measurements are recorded using a portable data collection system.

The technique involves listening to the natural energy waves released when a material undergoes plastic deformation. In the case of a metal pool liner this results from changes in load, pressure or temperature. It is a qualitative technique for establishing damage within a structure and is used for monitoring the development of active defects. Defects are detected as the stress levels (and corresponding energy levels released) in front of the crack tip are several times higher than the surrounding metal.

To date there has been no significant defects detected.
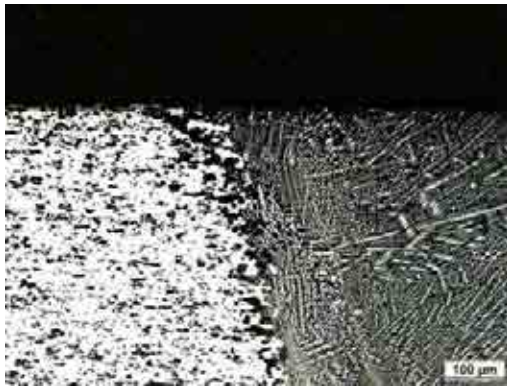
Cross section of weld joint.

Cross section of base metal.

FIG. 100. Inspection of CBB specimen surfaces by stereomicroscopy.
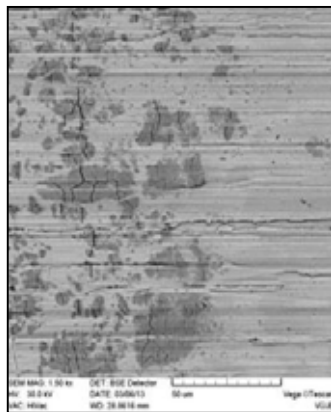
Scanning electron micrograph showing areas of chromium borides.
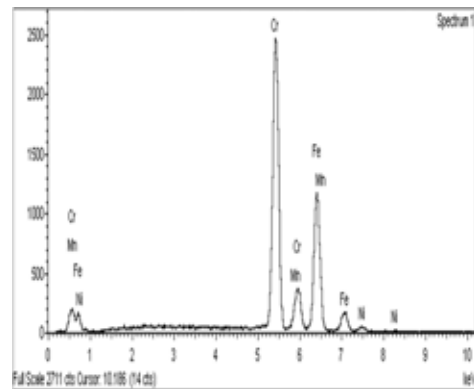
X ray spectra showing high chromium (chromium borides).

FIG. 101. Analysis of CBB ABATOR specimens at crack sites.
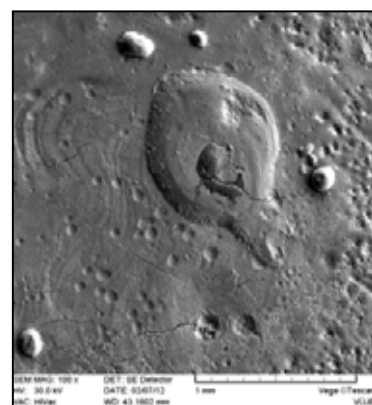
FIG. 102. Micro cracks on the surface of a circular bead welded specimens of pool lining sheets.

8.2. DRY STORAGE

8.2.1. Stainless steel–stress corrosion cracking (SCC)

Since 1997, the Central Research Institute of Electrical Power Industry (CRIEPI) in Japan has been conducting research programmes into the interim storage of spent fuel in casks. Most of these studies have focused on the ventilated concrete cask technology. As these casks are likely to be sited at marine locations CRIEPI identified [1] the potential for the inner stainless steel canister to be vulnerable to stress corrosion cracking (SCC) as the temperature of the canister drops and the surface becomes entrained with salt. CRIEPI initiated research into this area during SPAR II and has continued their investigations during SPAR III.

In the USA there are around 68 independent spent fuel storage installations (ISFSI) in operation with the majority using either a ventilated concrete cask or silo storage system. Both of these storage systems use an inner welded canister for storing the spent fuel. Many of these canisters have been fabricated from austenitic stainless steel with non-stress relieved welds. As some of these systems are located at a marine site the U.S. NRC has requested further information on SCC as a priority and is currently funding research in this area.

8.2.1.1. Japanese welded canister studies [110]

Stress corrosion cracking (SCC) occurs when the residual stress in the welds of a welded stainless steel canister are exposed to a salt laden air environment; as shown in Fig. 103. A methodology has been proposed for ageing management of welded canisters based on an anticipated storage period of over 50 years. The methodology is based on two scenarios (Fig. 104). In scenario I, the initiation of SCC is prevented by restricting the concentration of salt (chloride) adhering to the canister surface. In scenario II, where SCC has initiated, the crack growth depth (CGD) is monitored to ensure it remains below an allowable value.

In support of scenario I, SCC initiation and salt deposition tests have been carried out on stainless steel (UNS S30403 or 304L). Based upon the test results shown in Fig. 105, the minimum concentration of salt to initiate SCC has been found to be 0.8 $g \cdot m^{-2}$ as Cl. The criteria used for SCC initiation was when a surface crack length exceeded 100 μm.
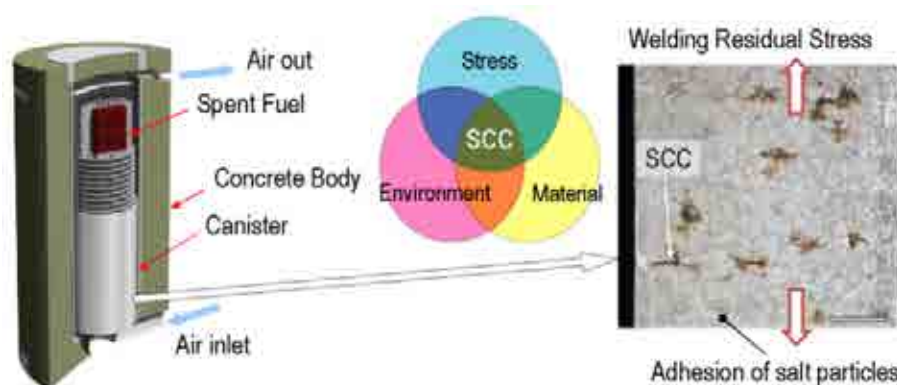
FIG. 103. Chloride induced SCC of stainless steel canister in concrete cask storage [110].
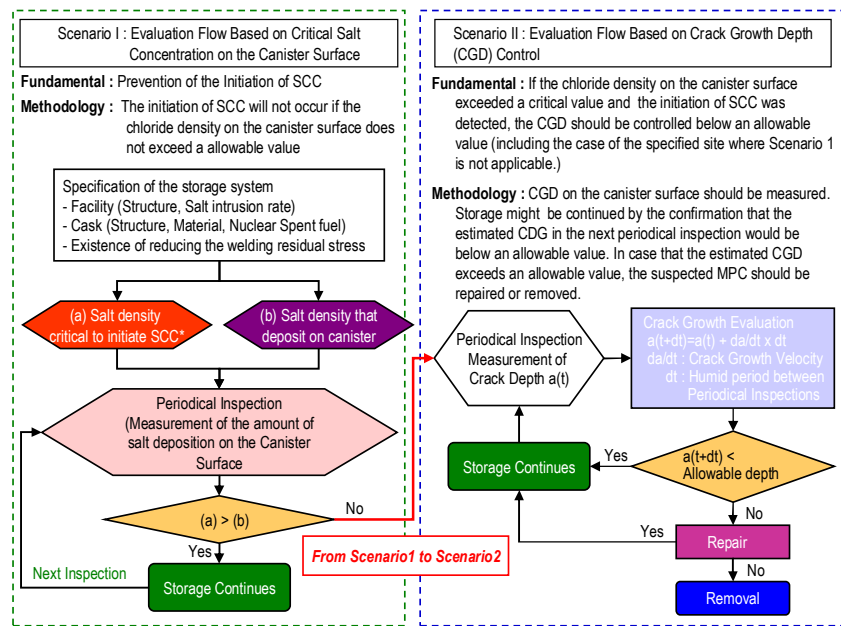
FIG. 104. Proposed ageing management methodology for welded canisters.
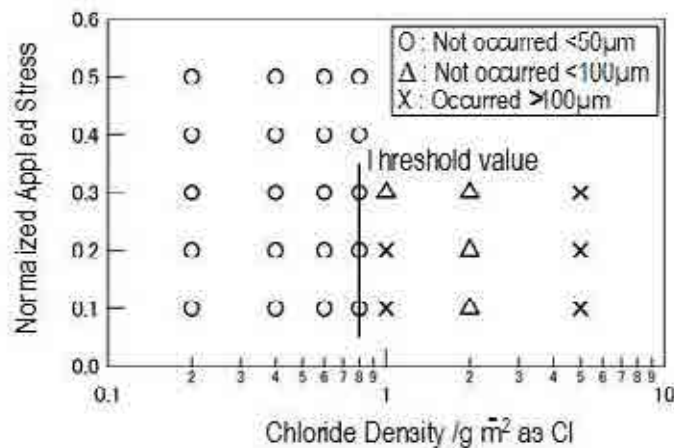
FIG. 105. SCC initiation test results–specimen B for 5000 hr, hardness 247 Hv.

To evaluate the potential for SCC initiation, it is important to estimate the salt accumulation transported by salt laden cooling air on the canister surface. The cooling air flows along the canister surface in the concrete cask and the airborne salt particles may collide with the surface due to diffusion and turbulence effects. To measure the deposition rate CRIEPI have performed laboratory and field tests. From these tests the rate of salt deposition on the canister surface as a function of time has been estimated.

The tests undertaken in support of scenario II include: Measurement of crack growth rates; Modelling of relatively humidity with time for the canister environment; estimating crack propagation; Methods for stress relieving cold worked canister material.

The crack growth rate (CGR) under various conditions has been measured using a four point bend test specimen made from 304L stainless steel (304L SS). Figure 106 shows the results for a test specimen placed under conditions of constant temperature and relative humidity

(RH); i.e. 80°C and 35% RH. The measured CGR shows that the crack initially propagated fast, whereupon the propagation rate declined. Assuming an initial crack size as a result of the initial fast crack propagation, the remaining canister wall can be evaluated with slow propagation rate data. An example of the calculated RH on the canister surface with time is shown in Fig. 107. According to this calculation, the accumulated time period where the RH exceeds 15% (threshold for SCC to occur) would be approximately 15,000 hours (i.e. <2 years) during a 60 year storage period. Using a CGR of 1×10^{-11} m·s^{-1}, the estimated crack propagation value during this period is only 0.5 mm.

The process of welding canisters can generate high tensile residual stresses at the surface and near surface of cold worked canister material. A cost effective method for relieving high tensile stress involves inducing compressive stress into the critical regions of the welded canister. Surface treatment techniques such as shot peening (SP), laser shot peening (LSP) and low plasticity burnishing (LPB) are currently being used in the nuclear industry to mitigate or impede SCC by inducing compressive stresses into the surface material [111].

To investigate the ability to produce a deep layer of stable compression to prevent SCC and to characterize the treated surface, tests using 304L SS circular plates with several kinds of surface treatments have been performed. The circular plates were nominally 100 mm diameter × 13 mm depth (Fig. 108). A 7 pass tungsten inert gas (TIG) weld and 1 pass laser beam weld (LC) with wash pass were used. Surface treatments were applied to half of the LC and TIG welded test plates. X ray diffraction was carried out to measure the levels of residual stress on a total of six welded plates which had been subjected to SP, LSP and LPB surface treatments. Figure 109 shows a welded test coupon with half the plate treated with LPB.
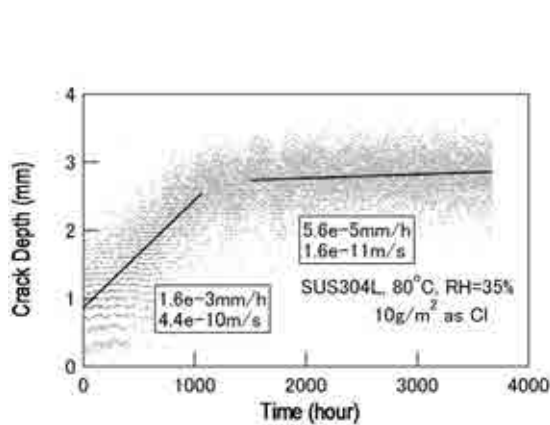
FIG. 106. Crack growth test results.
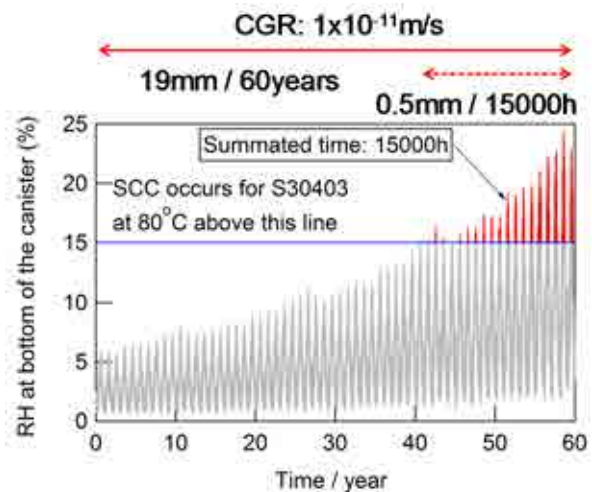
FIG. 107. Relative humidity change at the canister bottom with time.
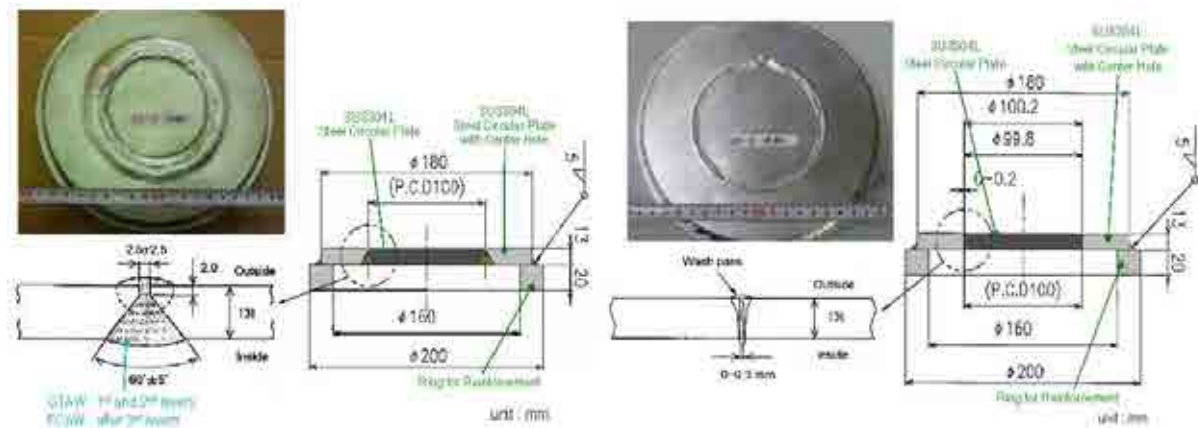
FIG. 108. Dimensions of the 304L SS (UNS S30403) circular test plates.

FIG. 109. Welded test plate treated with LPB.

Figure 110 shows the residual radial stress vs. distance from the centre of the plate at a depth of 0.51 mm and the residual stress distributions obtained adjacent to the weld. It is noted that residual compressive stress is observed (Fig. 110a) at the surface for the as machined, LPB and SP treated test plates, whilst the LSP treated plate resulted in high tensile residual stress. At a depth of 0.51 mm (Fig. 110b), the as machined TIG and LC welded plates show a residual stress with a peak tension exceeding +300 MPa; in and adjacent to the weld. The LPB, SP and LSP treated plates (Fig. 110b) are in compression; with LPB treated plates showing the highest compression for each weld type.

Fig. 111 shows the results from corrosion testing of a LC welded plate which has be LPB treated. The accelerated corrosion test involved contacting the plate with a salt concentration of 4 g·m^2 (as Cl$^-$); i.e. >5 times the threshold for initiation of SCC in 304L SS (UNS S30403). The test conditions were set at constant temperature of 80°C and 35% RH for over 1000 hours. Even in the severest environmental condition, SCC initiation was not observed on the treated plate section (Fig. 111). This seems to indicate that a well-qualified surface treatment could relieve the residual stress imparted into the surface as a result of cold working.
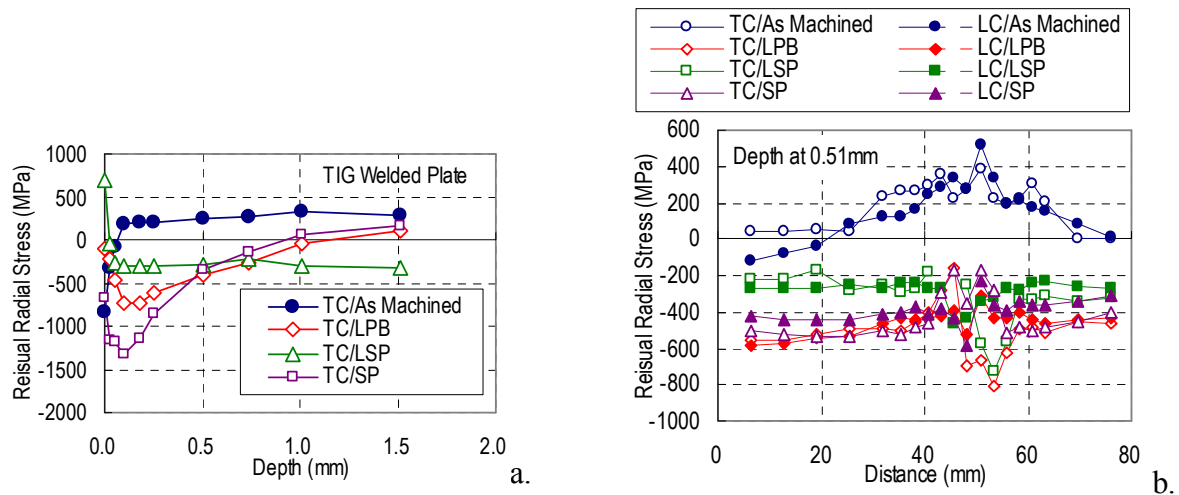
FIG. 110. Measured residual radial stress distributions in the test coupon.

Untreated - SCC initiated.

LPB treated-only surface corrosion.
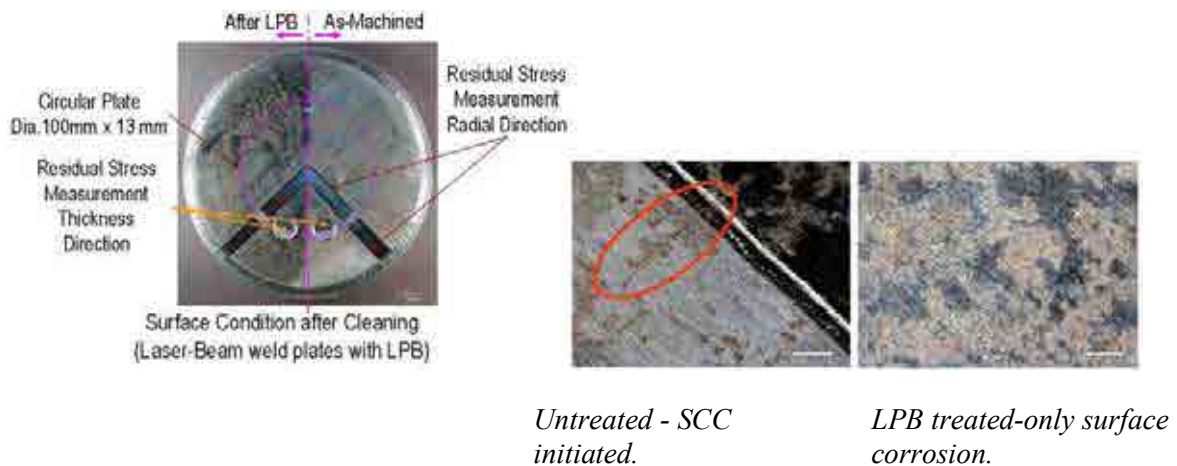
FIG. 111. Results of corrosion testing a laser beam welded plate low plasticity burnishing treated.

8.2.1.2.   Studies in the USA in support of U.S. NRC request for further information

A scoping study investigating the susceptibility of welded and unwelded 304, 304L and 316L austenitic stainless steel to atmospheric stress corrosion cracking has been conducted by the Southwest Research Institute [112]. The study evaluated the performance of these materials in simulated sea salt solution and salt fog; the later studies were considered to be more realistic of the conditions likely to be experience at some storage sites.

The studies using salt fog are summarized. Testing was carried out on single and double U-bend specimens at three temperatures (43°C, 85°C and 120°C) for 32 weeks. Only SCC was observed on the 43°C specimens. Transgranular and intergranular cracking was observed in 304 and 304L specimens after 4 weeks of exposure. Cracking of 316L specimens was not observed until 32 weeks. The crack growth, for all alloys, increased with exposure. Cracks were concentrated on the arch of the U bends; where pits and general corrosion were also

noticed. Corrosion of the double U bend specimens was limited to the specimen edges. The results and discussion of the observations are detail in [112].

A recently completed follow up study sought to better define the conditions where SCC could occur and examine the effects of atmospheric deposit chemistry on the SCC susceptibility of stainless steels used in welded canisters [113]. Deliquescence relative humidity (RH) testing showed that the deliquescence to sea salt occurred at RH values between the deliquescence RH values of pure $CaCl_2$ and $MgCl_2$. $CaCl_2$ has a calculated deliquescence RH close to 20% over the 27–80°C temperature range considered in the study, while $MgCl_2$ is in the range of about 30–35%. Even though NaCl is the main constituent of sea salt, the RH for deliquescence of simulated sea salt is much lower than the RH for deliquescence of NaCl.

Under plausible natural atmospheric conditions with a maximum absolute humidity of 30 $g \cdot m^{-3}$, SCC initiation was observed on Type 304 U bend specimens at temperatures ranging from 35–60°C when the RH during exposure was above the measured RH for deliquescence of simulated sea salt. SCC initiation was observed on specimens deposited with as little as 0.1 $g \cdot m^{-2}$ of simulated sea salt which was originally believed to be below the threshold salt concentration for SCC. The extent of cracking increased with increasing salt surface concentration. Because no testing was conducted at salt concentrations below 0.1 $g \cdot m^{-2}$, the threshold surface salt concentration for SCC was not determined. Furnace sensitized material was more susceptible to SCC. The heat affected zones of welded U bend specimens showed SCC susceptibility and had a microstructure similar to the as received material.

SCC was also observed on Type 304L C ring specimens that were strained to 0.4 or 1.5%, with deposited surface salt concentrations of with 1 or 10 $g \cdot m^{-2}$ at temperatures of 35–52°C. No tests at higher or lower temperatures were conducted. At the strain of 0.4%, the stress on the C ring specimen is approximately equal to the material yield stress.

No SCC was observed on Type 304 U bend specimens with deposits of NH_4NO_3, NH_4HSO_4, and fly ash which would be expected from agricultural, commercial, and industrial activities. SCC was observed on Type 304 U bend specimens that were exposed to mixtures of NH_4NO_3 and NaCl with NO_3^-:Cl^- mole ratios of 3.0 and 6.0, but less than 10 $g \cdot m^{-2}$ of NaCl indicating that NO_3^- is not an effective inhibitor for chloride SCC.

In addition to the studies on SSC of stainless steels the U.S. NRC has also initiated studies into the residual stress in welds and industry inspections at ISFSIs. Some preliminary observations from the analysis of canister lid closure welds are shown in Fig. 112. Initial findings suggest that high tensile stresses remain welding after welding in the hoop direction. Potential cracks which develop near the lid closure would, therefore, tend to orientate radially or axially.

In June 2012, two NUHOMS canisters at Calvert Cliffs ISFSI were visually inspected, had surface samples taken (by wet and dry methods) and the temperature at accessible points taken. Using the applied techniques the salt concentrations were found to be very low $mg \cdot m^{-2}$ region, no cracks were observed by visual inspection and the temperature data collected has been used in thermal modelling work being undertaken by Pacific Northwest National Laboratory (PNNL) as part of the Department of Energy (DoE) used fuel disposition campaign.
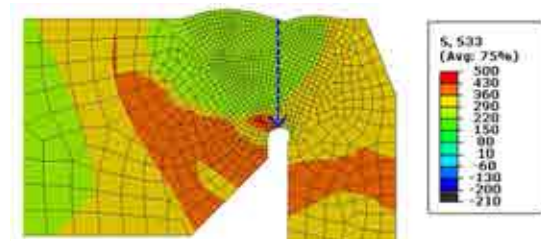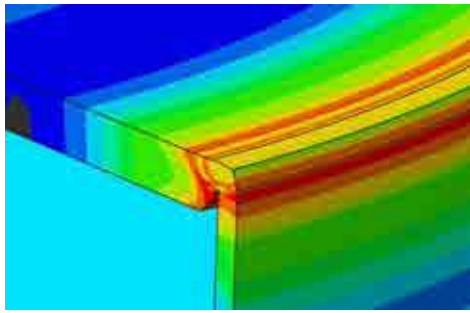
Hoop stress distribution (MPa)
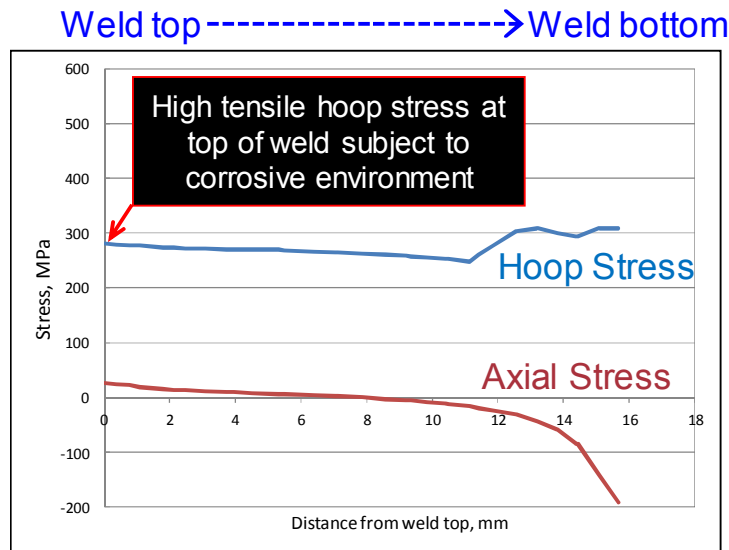
FIG. 112. Analysis of residual stress in canister lid closure welds; preliminary observations.

8.2.1.3. Welded canister surface analysis using laser induced breakdown spectroscopy [114–116]

In order to detect whether the environmental conditions, i.e. the presence of chloride, to induce SCC on non-stress relieved welded canisters are present, the technique of laser induced breakdown spectroscopy (LIBS) has been investigated by CRIEPI. The advantages of this technique are that it is non-contact and therefore would facilitate in-situ analysis without taking samples this enables canisters at high temperature to be analysed and potentially could reduce dose uptake to operators.

LIBS, in the collinear double pulse configuration, was performed on stainless steel (type 304L, 316L) samples that had been sprayed with synthetic seawater. The experimental setup is shown in Fig. 113. Nd:YAG laser pulses were focused onto the samples and the emission of the ablated plasma was detected by a spectrometer and an intensified CCD camera. The energy of both laser pulses was set as 30 mJ. The spectrum peak of chlorine at 837.5 nm was used to estimate the relationship between emission intensity and chlorine concentration. The experimental results are shown in Fig. 114. The chlorine emission intensity normalized by oxygen emission intensity increased monotonically versus chlorine concentration in the range 0.05 to 0.4 $g \cdot m^{-2}$ (mostly up to 1.0 $g \cdot m^{-2}$). These results show that the quantitative analysis of chlorine concentrations on canisters using LIBS is feasible.

136

8.2.2. Shielding materials

8.2.2.1. Reinforced concrete-Japanese studies

In order to operate spent fuel concrete storage modules in Japan an evaluation of the potential damage from salt ingress to the reinforced concrete structures is required; as the modules will be located in the vicinity of the coast and the concrete can reach relatively high temperatures due to the decay heat of the spent fuel. CRIEPI has proposed a verification method based upon initiation of corrosion to the reinforcing steel as the limiting factor [117].

To establish if a threshold concentration of chloride ion, which would initiate corrosion, can be reached, an immersion method has been used. The results have been used to establish the rate of chloride ion penetration for different concrete mixtures (under different conditions), and have been used as the basis to propose the verification method. A separate corrosion test was carried out to determine the threshold concentration of chloride.
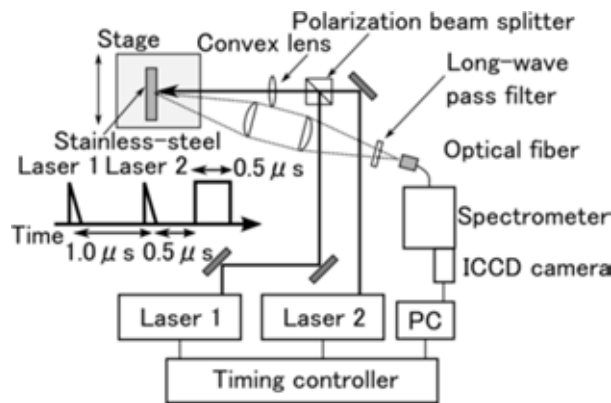
FIG. 113. Schematic of experimental setup [114].
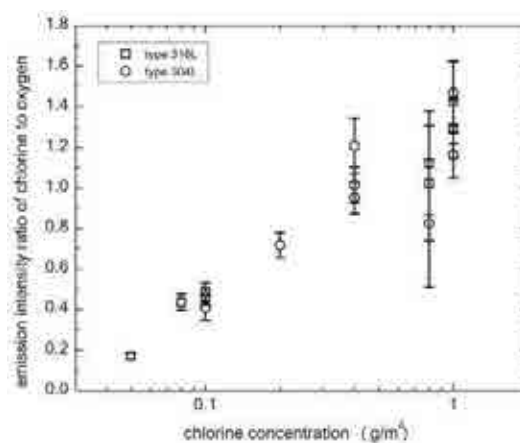
FIG. 114. Chlorine concentration dependence with chlorine emission intensity divided by oxygen emission intensity.

Immersion test

Cylindrical concrete specimens 150 mm in diameter and 100 mm in high were used in the immersion tests; as shown in Fig. 115. To only allow penetration by the chloride solution at the ends, the other surfaces were covered with waterproof tape. Three water–cement ratio mixes (W/C = 40, 50, and 60%) were used; as given in Table 17.

The cement type was Ordinary Portland Cement. Fineness modulus of sand and gravel aggregate was 2.76, and 6.62%, respectively. Percentage of water absorption of them was 1.56 and 0.76%, respectively. The concrete specimens were cured in the solution that was saturated with calcium hydroxide at 20°C for 4 weeks. The concrete specimens were immersed in 10% sodium chloride solution kept at constant temperature. Tests were performed at five different temperatures; 25, 45, 65, 80, and 90°C. Figure 116 shows the immersion testing equipment. Six different test durations were used which required six specimens with the same mix proportion and the same temperature. The heat to fixed temperature was set at 10°C·h^{-1}. The analysis was carried out on a sample taken from the central region (45 mm in diameter) of each specimen; as shown in Fig. 115.
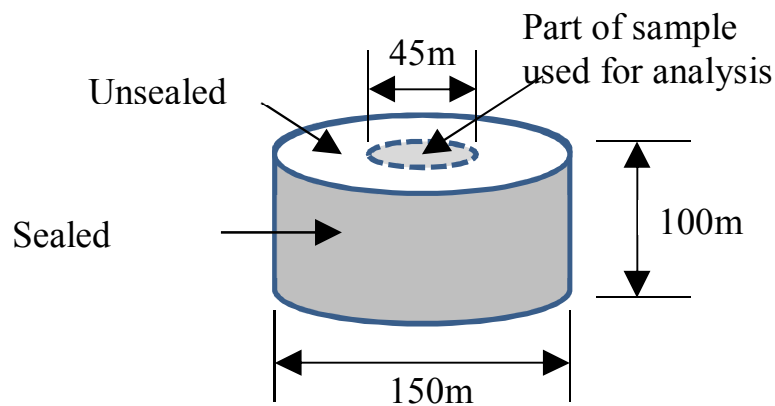
FIG. 115. Immersion test specimen [119].
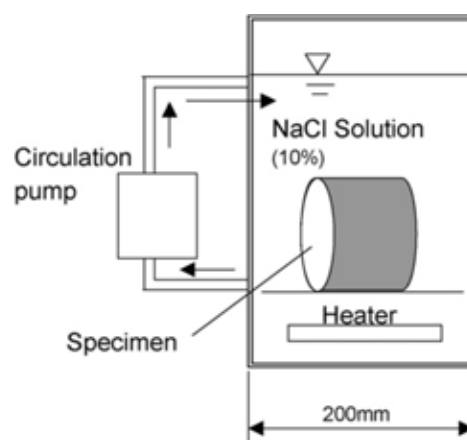
FIG. 116. Equipment for immersion testing under high temperature [117].

TABLE 17. CONCRETE SPECIMEN CHARACTERISTICS

	G_max (mm)	Slump (mm)	Air (%)	W/C (%)	s/a (%)	Unit weight (kg/m³)				
						W	C	S	G	Adm.ᵃ
Proportion I	20	100 ± 20	4.5 ± 1	40	53.3	168	420	911	805	6.720
Proportion II	20	100 ± 20	4.5 ± 1	50	53.4	160	320	968	853	3.424
Proportion III	20	100 ± 20	4.5 ± 1	60	53.5	160	267	992	874	2.857

ᵃ Air entraining agent.

The diffusion coefficients of chloride and their temperature dependency were obtained by the immersion tests.

Influence of temperature on diffusion coefficient of chloride ion

The equation for evaluation of diffusion coefficient of chloride in concrete under high temperature is given (12). The diffusion coefficients obtained by the equation and the results of tests are shown in Fig. 116.

$$\log (D_p) = -A \cdot X + B \qquad X = 1000 \cdot T^{-1} \qquad (12)$$

Where:
D_p is the diffusion coefficient of chloride ion in noncarbonated concrete ($cm^2 \cdot s^{-1}$);
T is absolute temperature (K);
A is constant (2.27, 1.90 in case of W/C = 40%, 50%, and 1.90 in case of W/C = 60%);
B is constant (0.05, −0.79 in case of W/C = 40%, 50%, and −0.28 in case of 60%).

From Fig. 117, the diffusion coefficient of the chloride ion increases with an increase in temperature, and that there is a linear relation between the logarithm of the diffusion coefficient and the reciprocal of the temperature. Moreover, concrete with a larger water–cement ratio has a tendency to have a larger diffusion coefficient. The results of the tests were used as the basis for proposing a diffusion coefficient evaluation equation; taking into account temperature and the water–cement ratio.
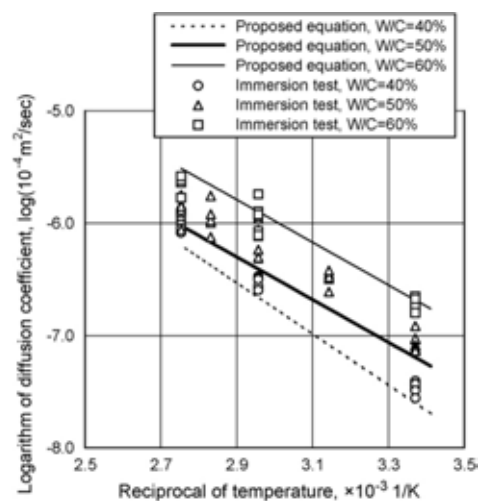
FIG. 117. Proposed equation for evaluation of effect of temperature on chloride ion diffusion coefficient, and data of immersion tests on diagram of Arrhenius plots [117].

139

Corrosion test

Figure 118 shows the relationship between the corrosion incidence ratios and the concentrations of chloride ion in the concrete at room temperature. From the corrosion initiation tests at high temperature, the chloride ion concentration for corrosion initiation was about 1.2 kg·m^{-3} at 65°C, 1.6 kg·m^{-3} at 90°C, and the concentration did not decrease by the temperature rise. Therefore, the value at normal temperature 1.2 kg·m^{-3} can be used at the high temperature up to 90°C as for the limiting chloride ion concentration of corrosion initiation.

The influence of carbonation on the diffusion coefficient of chloride ion has also been evaluated. The results showed that at 40°C the diffusion coefficient was about 1.6 times larger (for the largest water–cement ratio), but there was no increase for the 65°C case.

Proposal of verification method of durability against salt attack

A verification method assuming the initiation of reinforcing steel corrosion to be the limiting factor has been proposed. The chloride ion concentration at the depth of the position of reinforcing steel at the end of the proposed storage duration is evaluated using (13).

$$C_d = C_s \cdot (1 - \text{erf} \cdot (0.1 \cdot c \cdot (2 \cdot (D_d \cdot t)^{1/2}))^{-1} \tag{13}$$

Where:
C_d is design concentration of chloride ion at the reinforcing steel position (kg/m^3);
C_s concentration of chloride ion at concrete surface (kg·m^{-3}) from Table 18;
c   depth of reinforcing steel (mm);
t   design life (s);
D_d is design diffusion coefficient of chloride ion (cm^2·s^{-1}), from (14).

$$D_d = F \times D_p \text{ and here } \quad \log D_p = -A(1/T) + B \tag{14}$$

Where:
D_p is diffusion coefficient of chloride ion of noncarbonated concrete (cm^2·s^{-1});
F   coefficient by which influence of carbonation is considered (=1.6);
T   is absolute temperature (K).

Verification of chloride ion concentration is less or greater than the concentration required for corrosion initiation is determined by using equation (15).

$$C_d \cdot C_{lim}^{-1} \leq 1.0 \tag{15}$$

Where
C_{lim} is limiting chloride ion concentration for corrosion initiation (1.2 kg·m-3).

This verification method can be applied to reinforced concrete structures with a water–cement ratio in the range 40–60% and for temperatures up to 65°C.
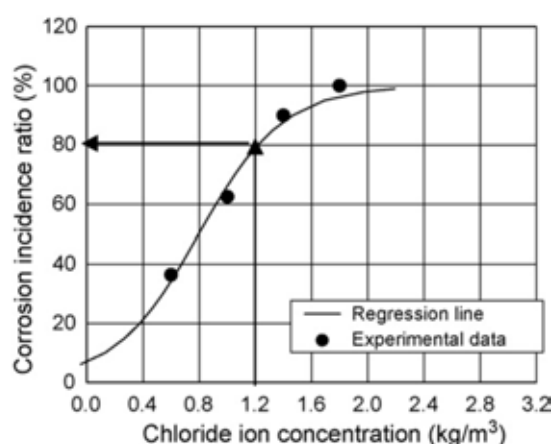
FIG. 118. Relationship between corrosion incidence ratio and chloride ion concentration at room temperature.

TABLE 18. CHLORIDE ION CONCENTRATION AT CONCRETE SURFACE AS A FUNCTION OF DISTANCE FROM THE SEA [117]

	Distance from the sea (km)					
	Splash zone	Seashore	0.1	0.25	0.5	1.0
Chloride (kg·m^{-3})	13.0	9.0	4.5	3.0	2.0	1.5

8.2.2.2. *Neutron shielding casks-French studies*

In service neutron shielding materials properties changes are caused by irradiation or thermal oxidation processes. To our knowledge, however, experimental results show us that oxidation is by far the most predominant process. In France studies have been undertaken into the oxidative mechanisms of thermoset matrix based neutron shielding materials used in French designed casks. The applied methodology was:

- Accelerated ageing tests are carried-out on neutron shielding samples at various temperatures and O_2 partial pressures. The aged samples are then characterized using mostly gravimetry, optical and IR microscopy;
- O_2 permeation tests carried-out in order to estimate both O_2 diffusivity and solubility into neutron shielding films;
- To investigate the long term properties, a non-empirical model is applied. In this regard, oxidation kinetic is coupled with oxygen diffusion. The model simulates very confidently weight losses (which are then converted into hydrogen atoms loss) and oxidation profiles.

The most important results are summarized:

- As expected, a 'diffusion limited oxidation' (DLO) characteristic was observed; as shown in Fig. 119;
- Temperature and O_2 pressure accelerate sample weight loss;

141

- Existence of a linear relationship between hydrogen atom loss with overall weight loss;
- Simulation data are in good agreement with experimental results for all conditions under study. This allowed the in-service Vyal B hydrogen atoms loss over decades to be predicted; as shown in Fig. 120.

8.2.3. Aluminium alloys used in transport/storage baskets-Japanese studies [118–120]

The baskets used in transport and storage casks have many functions including criticality control, heat removal and structural strength. It is preferable that the basket is made from light weight material in order to increase the number of fuel assemblies loaded in the cask for efficient transport and storage. Aluminium alloy is especially suitable as a base material for basket construction due to its low density and high thermal conductivity; for example A5083FH-O and A6061-T6/T651. In addition, the borated aluminium alloys (BC-A6N01SS-T1 and 1%B-A6061-T6/T651) have been developed to enhance the neutron absorbing ability. Generally, the borated aluminium needs properties as follows:

- Uniformly dispersed boron (or boron carbide) particles in the materials to control the criticality;
- Highly thermal conductivity to remove decay heat from spent fuel;
- Keeping the required mechanical strength for long period more than 60 years under high temperature (> 200˚C).

Mechanical properties of the borated aluminium materials considering the heat load have been measured and the life time for service has been evaluated by using Larson-Miller parameter (LMP). The effect of irradiation on the mechanical properties of one of aluminium alloys was shown to be negligible through materials testing in a research reactor.
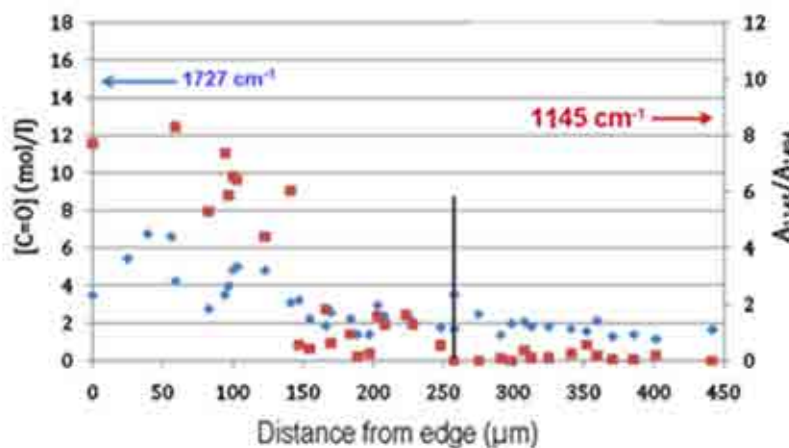
FIG. 119. Vyal B samples exposed to 160°C, 2 bars O₂. Display a superficial layer (roughly 250 μm) while the core is not affected.
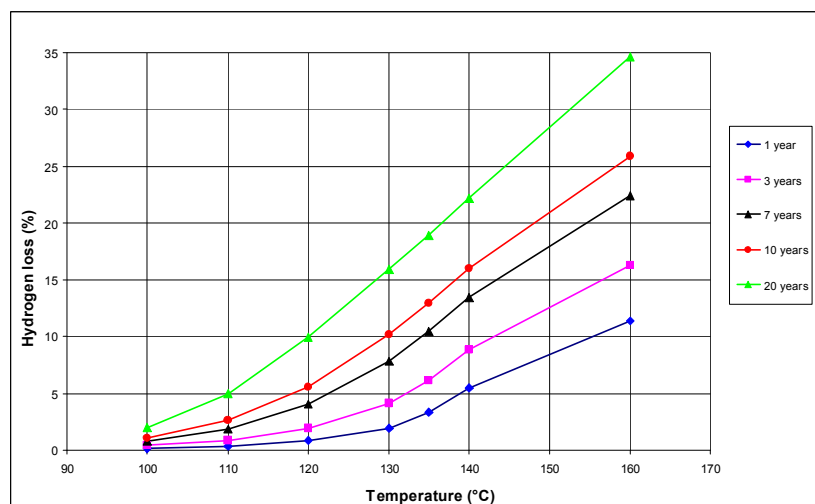
FIG. 120. Plot of hydrogen loss versus temperature and time.

8.2.4. Seals and welds–metal casks

For the technical design and the operation of facilities for the dry interim storage of irradiated fuel assemblies in casks, a large number of guidelines have been established in several countries. According to these guidelines, the design and operation of a storage facility where dry storage and/or transportation casks (dual purpose casks (DPCs)) are stored, must guarantee the safe enclosure of the radioactive inventory in order to ensure that the precautions against damage reflect the state of the art in science and technology. The containment barriers of the cask are, therefore required to remain intact under all conceivable circumstances (hazardous incidents, accidents, aging, impact, etc.) which could occur during its operational life. In order to protect the environment and the people, the release of activity has to be limited to the lowest achievable value and must comply with the legally required limits with a sufficient safety margin.

A cask lid system is normally comprised of two thick metallic lids, which are bolted to the cask body and sealing is achieved with metallic gaskets as shown in Fig. 121.

8.2.4.1. HELICOFLEX® seals-German operating experience

In the case of CASTOR® casks, HELICOFLEX® metallic gaskets have been used for many years and cask applications. The selection of metallic gaskets was based on the requirements for long term stability (40 years) and a high degree of leak tightness ($\leq 10^{-8}$ Pa·m³·s^{-1}) over a broad temperature range from –40°C up to 250°C and even higher for a short time under accident conditions. The cross section of a HELICOFLEX® metallic gasket (Fig. 122.) consists of an inner helical spring, an inner jacket of stainless steel and an outer jacket of aluminum (Al) or silver (Ag).

Metal gaskets of this type are characterized by excellent resilient properties which ensure useful elastic recovery. This is the precondition to accommodate minor distortions in the flange assembly due to changes in internal and external loads, even under accidental conditions of transport. Figure 123 shows the typical compression and decompression cycle of the HELICOFLEX® gaskets.

The first cask, which is still in operation, was loaded in 1983 at the Paul Scherer Institute (PSI) Switzerland. Up to now a total of approximately 1000 casks have been loaded and stored. The use of DPC´s in Germany therefore, is based on the operating experience gained since 1983 from loaded casks in interim storage facilities (see Fig. 124).

The functionality of the lid system is permanently monitored on each cask, using a pressure gauge observing the pressure at the lid interspace, which is significantly above ambient level. This assures the detection of functional impairments and the implementation of existing repair concepts taking the identified degradation mechanism into account. Up to now, there has been no indication that an ageing effect could lead to malfunction of the metallic gaskets, with an increased risk of the release of activity. The current licensing certificate is based on test series with flanges under extremely pessimistic boundary conditions, long-term experiments with measurements of leak rates of prototype casks under storage conditions as well as under accident condition (e.g. leak rates after drop tests).
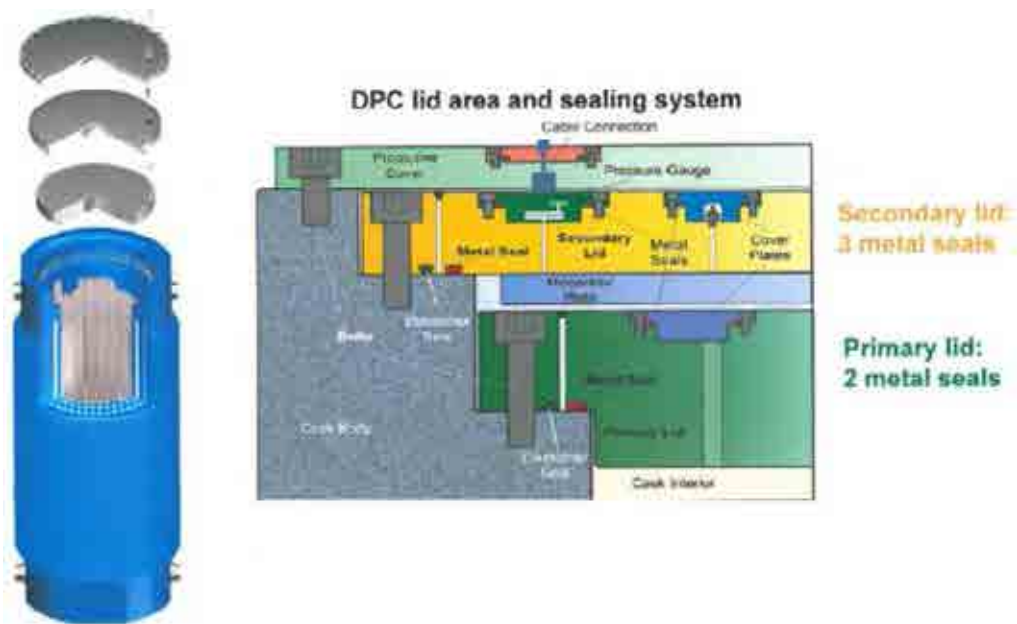
FIG. 121. Cask lid sealing system. Example shown is a dual-purpose cask (DPC, CASTOR®-type) [121].

Fig. 122. Cross-section of a metallic gasket of the type HELICOFLEX® [122].

144
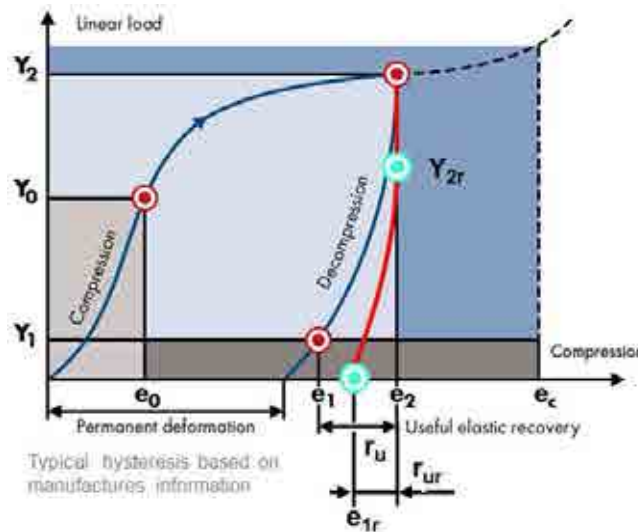
Fig. 123. Load compression behaviour of a HELICOFLEX® metallic gasket of the type [121].
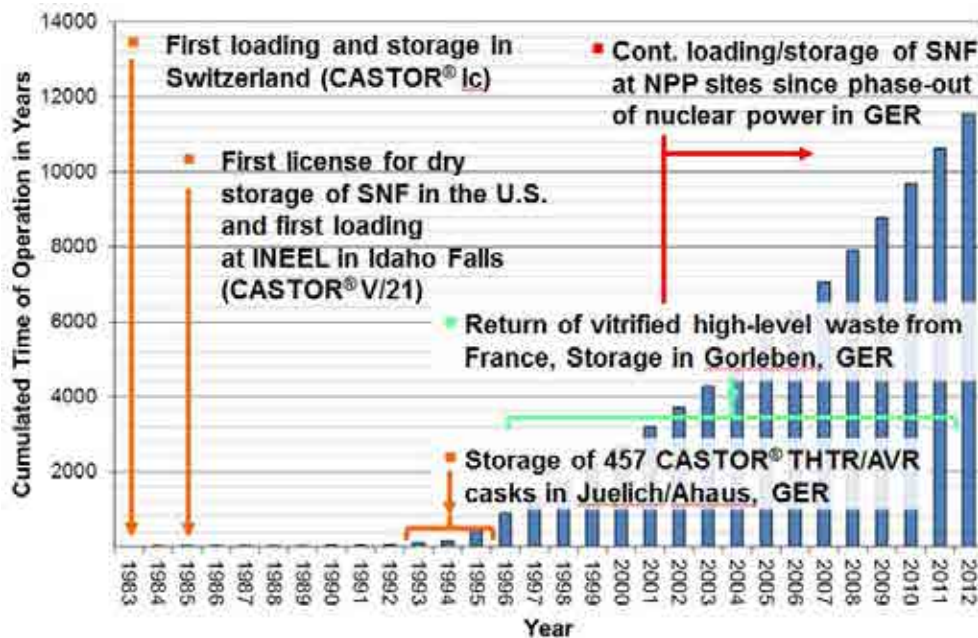
FIG. 124. Accumulated sealing performance-German experience based upon time in operation (status: 08/2012) [121].

8.2.4.2. Metal gaskets–continued operations

Timely considerations should be taken into account to identify needs for additional technical information if a lifetime extension is necessary. Therefore, technical reviews have been undertaken in order to identify the technical gaps between the current level of knowledge and the information that is needed for the future [14], [123]. For metallic gaskets nothing new was found. The creeping due to temperature under mechanical loads is still the dominating degradation mechanism. This leads to changes in the linear load between the gasket, the sealing surface and the elastic recovery. Due to the creep effects, the point of optimum

compression (see Fig. 123) drifts towards the lower load values (Y_{2r}) with time of operation. The additional permanent deformation of the gasket reduces the useful elastic recovery with the time of storage. The reduced useful elastic recovery is of no influence under static loads during storage. But, under the conditions of transport, the lower elastic recovery (r_{ur}) must be considered in the design of the flange assembly. The gapping of the flanges must be limited to less than the elastic recovery remaining after the storage period [121]. This effect could have an influence on the leak tightness over time and during accident conditions.

In order to cover this issue, the performance of further long term tests with gaskets in representative operational configurations with different types of gaskets and different temperature has been proposed [123].

8.2.4.3.   *Long term gasket test-German studies*

The correlation between load compression behaviour and the leak rate is important for any forecast of the cask behaviour with an extended storage period or transportation after long term storage. Therefore, several investigations were initiated in order to examine the changes of the load-compression behaviour of metallic gaskets versus time and temperature.

In Germany, investigations of ongoing laboratory tests with continuous leakage rate measurements during gasket loading and unloading were performed [122, 124]. Different gasket types at different temperatures with holding times since 02/2009 were examined. Both the load values (Y_{2r}) and the elastic recovery (r_{ur}) decrease with time. The decrease occurs more quickly with increasing temperature. On a logarithmic time scale the behaviour appears as a linear function. The extrapolation for a storage period of 40 years confirmed that the gasket has the ability to remain leak tight even at a constant temperature of 150°C; which is above the maximum operational temperature of the gasket directly after loading.

A long term corrosion test [124] with metallic gaskets with enclosed borated pool water between the inner and outer jacket has shown, since 2001 and up to now, no increase in leakage rate. This observation is also valid for gaskets with defects penetrating the outer jacket.

8.2.4.4.   *Long term gasket tests-French studies*

In 2006, the CEA reported on results of experiments with different gasket types, which demonstrate the influence of time and temperature on the lower load values (Y_{2r}) under long term conditions. The presented results reflect an intermediate stage of the test for a period of 25 000 h (2.85 y) [125–126]. The experiments will be continued in cooperation with GNS and CRIEPI up to 100 000 h (11.4 y). It can be concluded that the initial temperature level during cask loading has a large influence on the admissible application period of a gasket. For gasket temperatures below 120°C, a storage period of more than 100 years seems to be feasible.

8.2.4.5.   *Long term sealing system tests-Japanese studies*

The behaviour of the metallic gasket is only one part of the whole system. The ageing behaviour of the lid bolts and state of the sealing surfaces are of importance for the leak tightness of the lid system as well. Because creeping is a thermally activated process, the knowledge of the time dependent temperature profile of the components involved in the sealing system may help to describe the ageing effects more realistically.

In Japan, the use of transport/storage casks for spent nuclear fuel storage is considered rational and economical. Since the storage duration may be 40 to 60 years, the function for sealing the radioactive materials in the casks must be reliable in the long term. Metal gaskets are widely used for this purpose in the industry. Yamamoto and Yokoyama et al. performed thermal relaxation tests on metal gaskets [127–129]. They clarified that larger gasket section diameters have better durability for stress relaxation, investigated the spring back forces of the metal gasket after a relaxation test and determined the relationship between the plastic deformation rate and the Larson Miller parameter. Furthermore, they also measured the leak rate after exposing a flange with relaxed metal gasket to displacement. The results revealed that the small radial and axial displacement of the flange with a metal gasket affected the leak rate. Several studies [130–132] concerning the effect of displacement of the flange or cask lid on leak rate were performed. Sassoulas et al. carried out relaxation tests on four types of metal gaskets for 10 000 h [125]. For silver covered gaskets, the relaxation tests continued for 25 000 h. Two methods were applied to evaluate the long term sealing performance. One was the time extrapolation method, and the other was the time–temperature equivalence method. CRIEPI has accumulated and expanded test data by the long term confinement performance tests on full scale cask lid enclosures.

Tests on cask lid enclosures

In the test at CRIEPI, two full scale cask lid enclosures were tested [133]; as shown in Fig. 125. In both tests, electrical heaters were installed in the cask cavities to maintain a constant temperature and the lids were closed dry.

Enclosure type I, as shown in Fig. 126, was based on a TN-24 cask. The cask body and lid were made of forged carbon steel, while the sealing surface was overlaid with stainless steel welding (SUS304), and a double metal gasket enveloped in aluminium was installed for the lids. The cross sectional diameter of the gasket was 6.1 mm, while the inner and outer linings were made of Inconel and aluminium, respectively.

Enclosure type II, as shown in Fig. 127, was based on the CASTOR cask. The cask body and lids were made of ductile cast iron and stainless steel, respectively, while the sealing surface of the body was plated with nickel. In this enclosure, an inner metal gasket (covered in silver) and an outer silicone rubber gasket were installed. The cross sectional diameter of the gaskets was 10 mm while the inner and outer linings of the metal gasket were made of Inconel and silver, respectively.

Test conditions

Temperature condition of the test was determined by assuming the loading of 21 fuel assemblies (type of fuel: 17 × 17 PWR, burnup: 43 GW·d·t(HM)$^{-1}$). Based on the maximum temperature of the primary gasket calculated by the ABAQUS code, the test temperature of the primary gasket was determined and kept constant at 160°C during the test. After closing the secondary lid, the inner space between the primary and secondary lids was filled with helium gas. The inner pressures between the lids were set to 0.4 and 0.6 MPa for Types I and II, respectively. The measurement of temperature was carried out by thermocouples placed on and in the lid models.
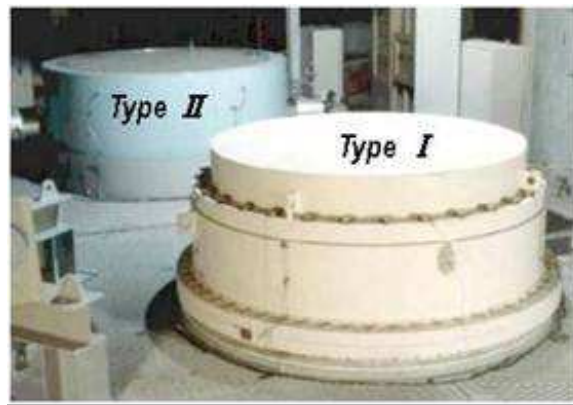
FIG. 125. Type I and II enclosures used in Japanese studies.
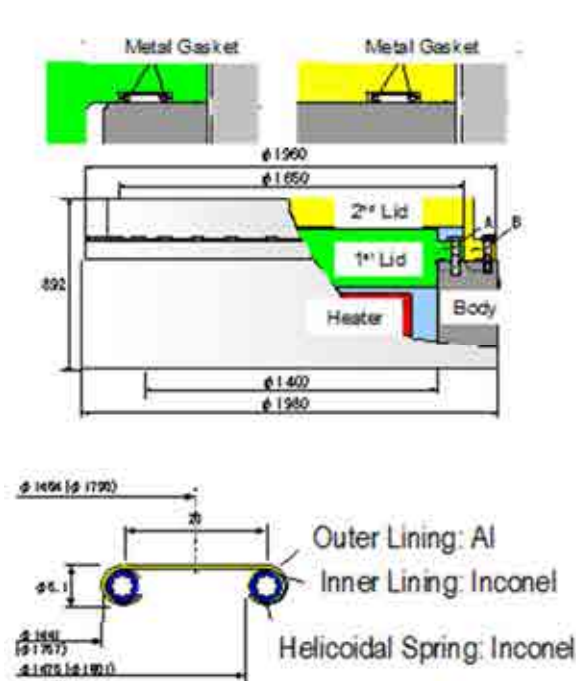
FIG. 126. Dimensions of enclosure type I [133].
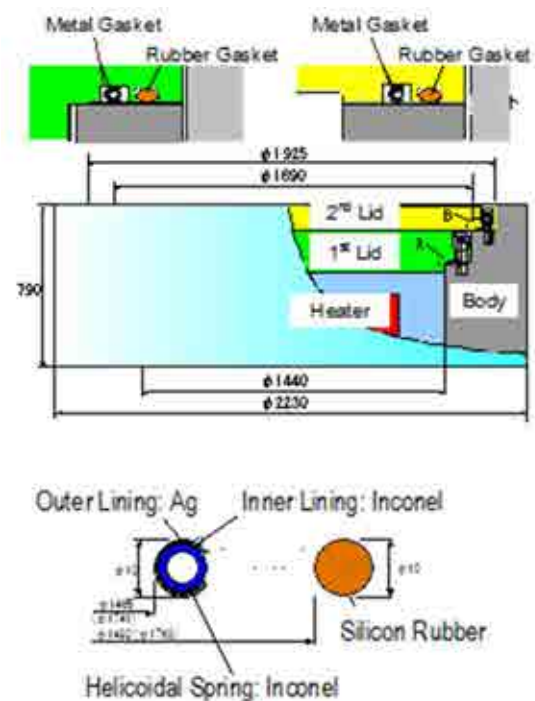
FIG.127. Dimensions of enclosure type II [133].

Test results of leak rate measurements

The temperature of the primary and secondary lids, although affected by seasonal changes of ambient temperature, remains approximately constant. Figure 128 shows the leak rate measurements. The measured leak rates of Types I and II were in the order of 10^{-10} and 10^{-11} Pa· m^3·s^{-1}, respectively.

Evaluation by Larson Miller parameter

According to previous studies [134–135], long term estimation values at a lower temperature might be predicted using the short term results at a higher temperature as leakage from the gasket correlates positively to the Larson Miller parameter (LMP).

Sealing performance evaluation using full scale lid enclosure data

Reliable containment performance has been maintained for more than 19 years at constant temperature. Generally, as the temperature of the cask with spent nuclear fuel decreases over time due to the decay heat, these tests were performed under accelerated conditions. To evaluate the long term integrity of the metal gasket, the period over which sealing performance is assured was calculated using the threshold value (LMP = 8050) at which leakage from the metal gasket occurs; this was based on the test data for the full scale lid enclosures. In this evaluation, it was assumed that the material constant in the LMP equation was 14.

The time history of the cask temperature distribution was calculated using the ABAQUS code. The temperature distribution was dependent on the cask design and the specification of the spent nuclear fuel. The initial temperature of the metal gasket was selected as a parameter. Figure 129 shows the time history curves of the gasket temperature with various initial temperatures, while the horizontal axis shows the storage period. By calculating LMP using the measured temperature, LMP values for Types I and II were 7942 and 7781, respectively. Namely, the sealing performance of the gaskets covered in aluminium were assured until LMP = 7942 while that of the gasket covered by silver was assured until LMP = 7781. Figure 130 shows the LMP values calculated by the time history curves shown in Fig. 128, including two horizontal lines, which designate LMP=7942 and 7781. The points of intersection between the horizontal lines and the time history curves show the period for which sealing performance is ensured. Figure 131 shows the relationship between the initial temperature of the secondary lid gasket and the assured sealing performance period. Assuming a storage period of 60 years, sealing performance is assured for the gasket covered in aluminium, provided the initial gasket temperature is 134°C or less, and for gaskets covered in silver, provided the initial gasket temperature is 125°C or less.

Opening of the lids

During the long term containment test, a decrease in the axial force of the secondary lid bolts was observed. To maintain the good containment condition, it is very important to keep the axial force of the bolts constant during the storage. It is also important to close up the lid until the flange surface of lid contacts to the flange surface of the cask body. Thermal condition of the lid is one of the reasons for loosening of the bolts.

Axial force measurement tests were carried out on the type I enclosure to establish the effect of closure and thermal condition of the lid on the axial force and containment performance. Test cases are shown in Table 19. In each case, new metal gaskets for primary and secondary lids were used. Temperature, pressure between two lids and axial force of the secondary lid bolts were measured during the test. The number of measured bolts was 24. To measure the axial force on the bolt, strain gauges were put on the bolt. Leak rates before and after the test was measured using a helium leak detector. When the lids were closed, the displacement of the lid was measured to check the contact condition of the flange. In the test cases 1 and 2, the

flange surface of the lid contacted to the flange surface of the cask body. In test case 3, the flange surface of lid did not contact with the flange surface of the cask body.

From the test case 1 and 2, the axial force deceased by about 20% as temperature increased. In test case 3, the axial force decreased by about 50%. These results show that it is very important to close up the lid until the flange surface of the lid contacts with the flange surface of the cask body. In all cases, the measured leak rate was less than the order of 10^{-8} Pa·m^3·s^{-1}.
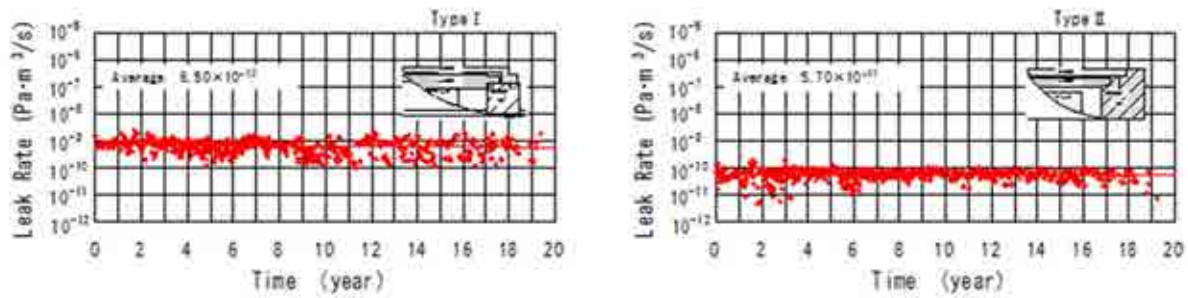
FIG. 128. Leak rate of the type I and II enclosures (Secondary Lid) [133].
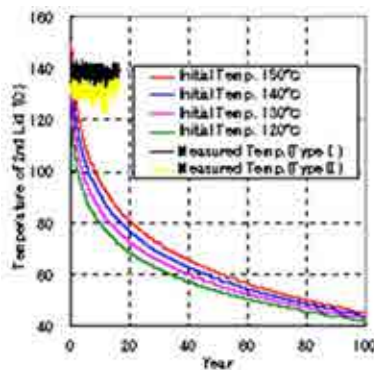
FIG. 129. Time history curves of the lid temperatures [133].
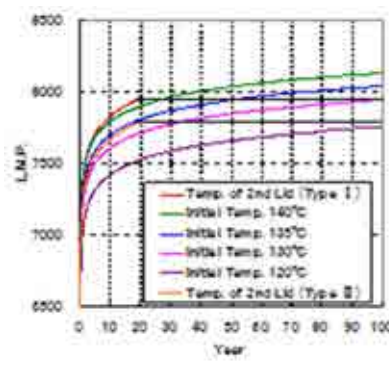
FIG. 130. Time history curves of LMP [133].
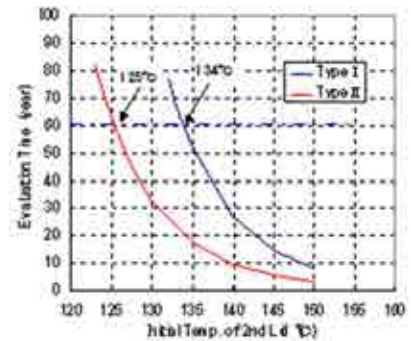
FIG. 131. Relationship between assured initial temperature of the lid and evaluation time [133].

TABLE 19. AXIAL FORCE TEST CONDITIONS ON TYPE I LID ENCLOSURE

Case n°	Cask temperature when the lids were closed	Number of bolt tightening (2nd lid)	Test period
1	Room temperature	Initial torque: 5 cycles Final torque: 10 cycles	10 days
2	High temperature	Initial torque: 8 cycles Final torque: 10 cycles	7 days
3	Room temperature	Initial torque: 1 cycle Final torque: 2 cycles	7 days

8.2.4.6. Detection method for the degradation of welded fuel canisters–Japanese studies

In concrete cask storage systems spent fuel is loaded into stainless steel canisters which are filled with helium gas and then welded leak tight. Whilst the primary role of the helium is to store the fuel in an inert atmosphere, helium also enhances heat removal from the spent fuel. If the helium gas were to leak from the canister, then convection of decay heat from the fuel to the canister surface will be effected; i.e. in principle the temperature at the canister surface would change. In this study, a new detection method has been proposed based on surface temperature difference between an intact and leaking canister [136].

The study evaluated two types of full scale concrete casks. One was a reinforced concrete cask (RC cask) and the other was a concrete filled steel cask (CFS cask); shown in Fig. 132 and specified in Table 20. The difference between the two types of storage systems were structure and basket material.

Helium gas leak tests were performed using the two concrete cask systems described above and using the test matrix as given in Table 21. In cases 1 and 3, the canisters were filled with helium at atmosphere pressure (0 kPa) before heating. When the inner pressure reached 56 kPa (steady state) pressure the heat input was 22.6 kW in the CFS cask; 59 kPa in the RC cask case. In case 2, the canister was filled with helium gas to about 100 kPa before heating, at 151 kPa (steady state) the heat input was 22.6 kW. In each case, tests started when the valve was opened to allow helium to leak out. Figure 133 shows the temperature measurement points on the canister surface.

Helium leak test in CFS cask (Case 1)

The initial conditions were steady state with a heating rate of 22.6 kW and the inner pressure was 56 kPa. The valve of the canister was opened slightly, so that the helium gas leaked and the inner pressure changed from 56 to 5 kPa in 4 days. Finally, the valve was opened completely to reach atmospheric pressure (0 kPa) before closing the valve. It was found that the canister surface temperatures were dependent on the air inlet temperature. It was difficult to judge whether the surface temperature changes were caused by helium gas leak or not.
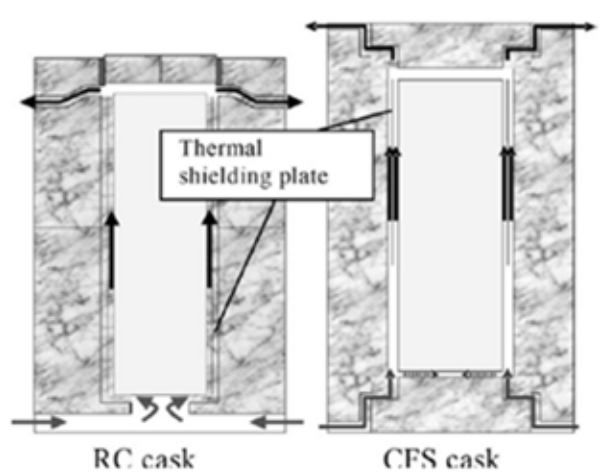
FIG. 132. Concrete cask systems used in the canister degradation detection studies [136].

TABLE 20. CONCRETE STORAGE SYSTEM SPECIFICATIONS

Concrete Cask Specifications		
Item	RC	CFS
Height (mm)	5787	6120
Outer diameter (mm)	3940	3800
Inner diameter (mm)	1850	1838
Weight (t)	150	154
Canister Specifications		
Item	Type I (RC Cask)	Type II (CFS Cask)
Height (mm)	4630	4470
Outer diameter (mm)	1676	1640
Weight (t)	35	30
Body material	Stainless steel	Austenitic-ferritic S.S.
Basket material	Stainless steel	Aluminium alloy

On the other hand, in the helium gas leak condition, the temperature at the center of the canister bottom rises, but the temperature at the center of the top of the canister falls with time or with a decrease in helium content. Figure 134 shows the change in canister surface temperature distribution with time, under normal operations, in relation to the air inlet temperature. In comparison, Figure 135 shows the change in canister surface temperature distribution for a leaking canister. It was found that the temperature difference between the center of canister bottom (T_B) and the center of canister top (T_T) increased by about 8°C after 60 h.

TABLE 21. TEST MATRIX FOR HELIUM LEAK TESTS [136]

Case No.	Cask Type	Initial Pressure (kPa)[#]	Final Pressure (kPa)[#]	Leak Rate (Pa m^3·s^{-1})
1	CFS	56	5	4.86×10^{-1}
2	CFS	151	1	5.16
3	RC	59	1	36.0

Gauge pressure
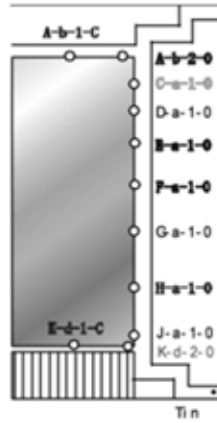
FIG. 133. Temperature measurement points on the canister [136].
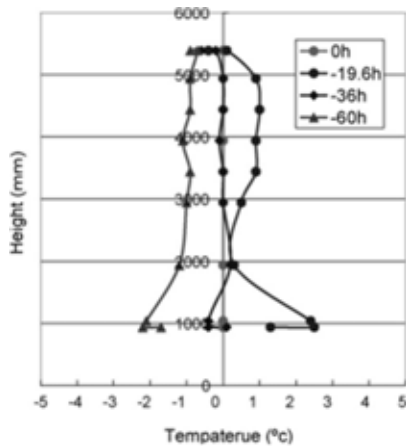
FIG. 134. Change of temperature distribution (normal) [136].
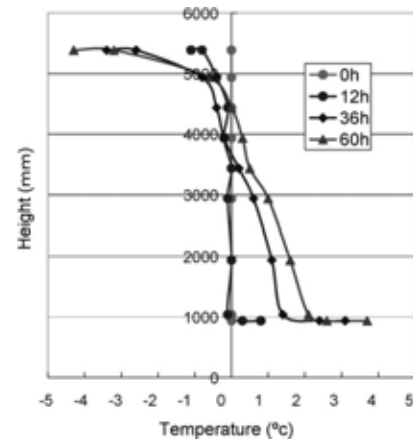
FIG. 135. Change of temperature distribution (leaking) [136].

Figure 136 shows the change in ΔT_{BT} and the inner pressure in the canister with time [136]. It was found that ΔT_{BT} increased as helium leaked from the canister.

High pressure helium leak test in CFS cask (Case 2) and helium leak in RC cask (Case3)

In Case 2, the initial inner pressure was 151 kPa. The pressure was dropped to 36 kPa in 1 day, and dropped to 1 kPa in 3 hours. It was calculated that the rate of helium gas leakage was 7.25 Pa m^3·s^{-1}. After helium leakage, the value of ΔT_{BT} increased by approximately 20 C. In the RC cask test, the inner pressure dropped from 56 kPa to 1 kPa in 2 h. The helium gas leak rate was large as 36.0 Pa m^3·s^{-1}. The canister surface temperature changed slowly after the helium gas leaked rapidly; ΔT_{BT} increasing 8 C in 24h.

In these tests, the principle that the canister surface temperature would change as a result of helium gas leaking from the canister has been confirmed. The greatest effect was observed at the bottom and top of the canister. Defining the temperature difference as ΔT_{BT}, it was found

that ΔT_{BT} increased by up to 20 C as a result of a leak. The value of ΔT_{BT} increases monotonously towards a constant value as gas leaked; even if the inlet air temperature dropped. It is therefore feasible to detect a helium gas leakage in the early stages of storage by monitoring both ΔT_{BT} and the inlet air temperature.
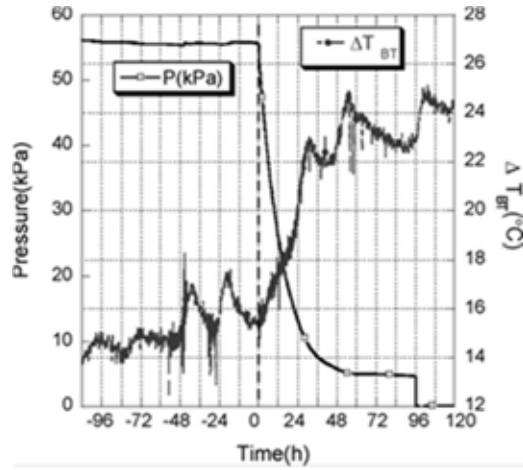
FIG. 136. Change of ΔT_{BT} and pressure (Case 1).

9. EXTENDED (OVER 100 YEARS) STORAGE ISSUES

9.1. GENERIC ISSUES

The likely extension of originally envisioned interim storage durations (or, extended storage) has led to a number of technical gaps analyses to identify and investigate potential fuel and storage system issues. The results of these investigations[21] can vary depending on the focus of the lead organizations. Perceptions of technical gaps and their relative priorities are in an evolutionary state and are likely to be revised as data are collected and evaluated.

In 2012, EPRI published a report [123] by the international subcommittee of the EPRI led 'Extended Storage Collaboration Program' (ESCP) looking into international perspectives on technical data gaps associated with extended storage and transportation of spent nuclear fuel. A summary of the technical gaps identified by this subcommittee are reproduced in Table 22. While many technical gaps were identified, ESCP members agreed that the highest priority should be devoted to providing additional information to close three technical gaps for extended used fuel dry storage and subsequent transportation:

- Long term degradation of high burnup fuel cladding via creep and embrittlement (hydride reorientation);
- Corrosion of the exterior of stainless steel welded canisters containing spent fuel in an inert atmosphere (for example, helium backfilled inside the welded canisters);
- Degradation of concrete used for shielding and structural purposes.

With regard to potential degradation mechanisms of high burnup fuel cladding, gaps generally stem from a paucity of data on the properties and behaviour of high burnup fuel under conditions of extended dry storage. This is particularly true for newer claddings and fuel materials that have been developed to enable operation to higher burnup. Several issues are also based on uncertainties regarding conditions that might or might not affect other aspects of fuel behaviour; for example water in breached rods that could remain after drying and that could lead to corrosion, stress corrosion cracking or hydrogen generation.

Degradation of storage containers and their components during extended storage include corrosion or SCC of the container, seals, bolts or welds (particularly in coastal environments), degradation of the neutron shielding, degradation and cracking of concrete. Those will need to be addressed through appropriate ageing management programmes similar to those established for managing reactor structures and components.

The IAEA CRP on demonstrating performance of spent fuel and related storage systems beyond the long term (DEMO) is currently being run to contribute to the EPRI ESCP. As such some of the technical gaps that have been identified will be addressed as part of the DEMO CRP. DEMO is programmed to report in 2016.

---

[21] For example, in the USA, U.S. NRC's 'Identification and prioritization of the technical information needs affecting potential regulation of extended storage and transportation of spent nuclear fuel', U.S. DoE Office of Nuclear Energy (DoE-NE) 'Used fuel disposition (UFD) program', and U.S. Nuclear Waste Technical Review Board (NWTRB) [14–16].

TABLE 22. SUMMARY OF EXTEND STORAGE TECHNICAL GAPS IDENTIFIED BY ESCP PARTICIPATING COUNTRIES [123]

Structure, system, component	Degradation mechanism	A	B	C	D	E	F	G
Cladding	Annealing		X	X	X	X	X	X
	H$_2$ embrittlement/hydride cracking		X		X	X	X	X
	Oxidation	X	X		X	X	X	X
	Creep	X	X		X	X	X	X
	High burnup fuel, MOX fuel	X						
Pellet	Cracking, bonding			X	X	X		
Assembly hardware	Corrosion		X		X			X
Basket	Corrosion, irradiation	X						
Neutron poison/shielding	Thermal aging				X	X		X
	Creep					X		X
	Embrittlement					X		X
	Corrosion					X		X
Welded canister	Atmospheric corrosion		X	X	X	X	X	X
	Aqueous corrosion		X	X			X	X
Moisture absorber	Irradiation, thermal	X						
Bolted cask	Fatigue of seals, bolts	X		X	X			X
	Atmospheric corrosion	X						X
	Aqueous corrosion							X
Metal gasket	Creep	X						
Overpack/cask	Freeze–thaw	X	X		X	X	X	X
	Corrosion	X	X					X

Where:
A–Germany, B–Hungary, C–Japan, D–Republic of Korea, E–Spain, F–United Kingdom, G–United States of America.

9.2. HELIUM GENERATION

Alpha decay damage and helium accumulation are the key process affecting the evolution of properties and behaviour of spent fuel in extended storage. The dose rates and the temperatures experienced during storage are lower than during in pile operation: however, at relatively low temperature (typically < 650 K), the recombination of point defects generated by the decay process is not favoured; moreover, the duration of the storage is much longer than the in pile life of the fuel. Technical gaps related to fuel–cladding interaction due to helium generation and release, pellet swelling and additional fuel fragmentation have been identified by the U.S. NRC as being among the highest priority areas of research [14]. Cladding stress during storage may be affected by fuel swelling, helium generation due to α decay of actinides, and fuel fragmentation.

The effects of alpha decay damage and helium build up during spent nuclear fuel storage are the object of a multi-year programme of studies carried out at the Joint Research Centre Institute for Transuranium Elements (JRC-ITU); which covers in particular the evolution of physical–chemical and mechanical properties [137–138] as a function of accumulated radiation/decay damage and helium. The goal of these studies is to assess the mechanical integrity of spent nuclear fuel rods after discharge from the reactor and in particular during storage. The experimental characterization covers microstructure alterations, lattice swelling, thermal diffusivity, calorimetry, hardness and mechanical fracture behaviour. Irradiated LWR fuels (UO_2 and MOX) and tailor made materials are studied. The superimposition of alpha-decay effects occurring during storage at relatively low temperature on the fuel configuration as determined by in pile irradiation is evaluated. The investigations address processes and mechanisms from the microstructural level (lattice defects, helium bubbles) up to the macroscopic properties (swelling, impact load resistance), which determine the safety performance of the spent fuel rod during long term storage. The present JRC-ITU contribution is focused on a storage timescale <100 years. Applications to very long term storage concepts will be the subject of a separate study.

Figure 137 shows the mass of helium and the corresponding α-decay/g generated as a function of time in LWR UO_2 and MOX fuels with different burnup (including, as indicative curve, a mixed oxide compound with high Pu content) calculated using the ORIGEN code. The horizontal dashed lines on the diagram represent the cumulative alpha decay damage (dose) in the used fuel expressed as displacements per atom (dpa) spanning over five orders of magnitude. Also plotted on the diagram is the solubility of helium in polycrystalline UO_2 measured by high temperature–pressure infusion and subsequent thermal desorption [139]. The dose rate experienced by the fuel during storage is significantly lower than the level characteristic of in pile conditions; the latter is typically of the order of 1 dpa/day; dominated by neutron and fission damage; characterized by higher temperature; relatively short durations.
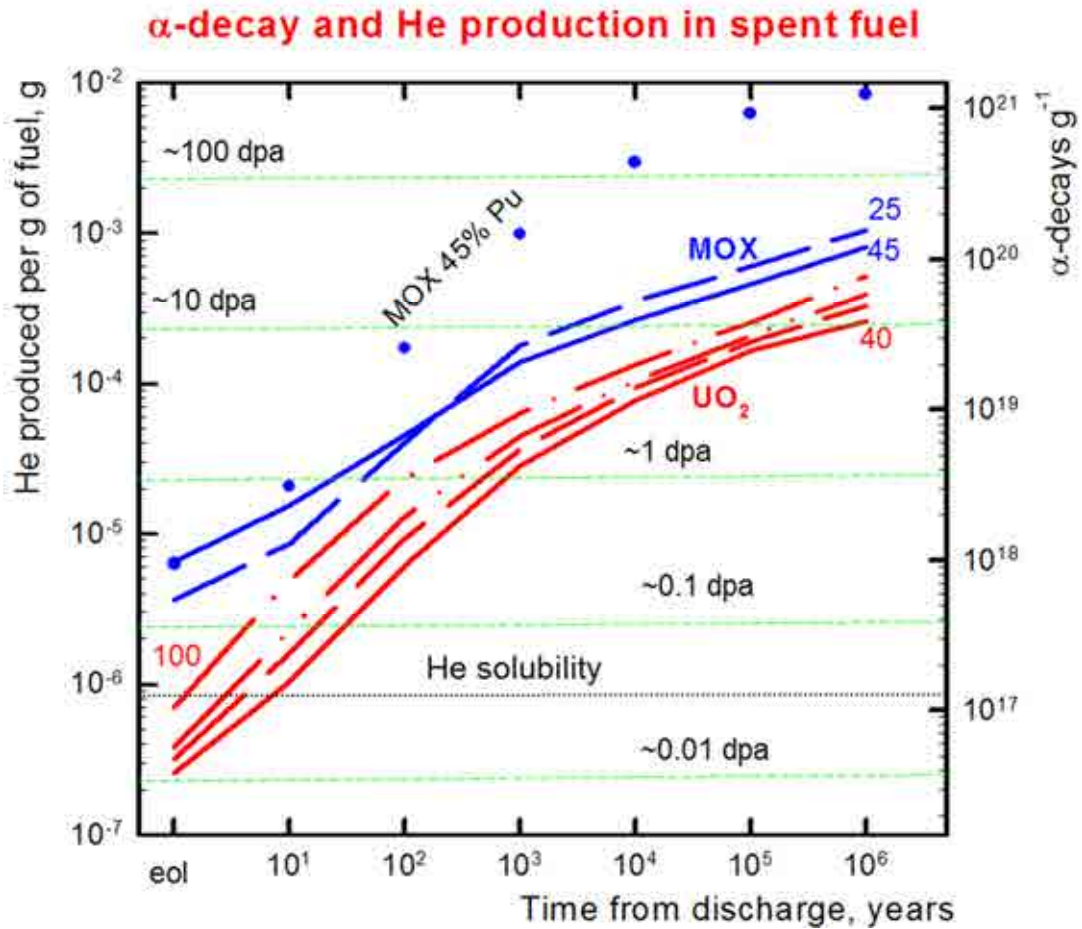
FIG. 137. Cumulative helium and alpha decay generated as a function of time in spent LWR fuel after discharge from the reactor. Data points (blue dots) representing the case of a high Pu content fuel is also plotted for comparison. The horizontal dashed lines represent accumulated damage levels indicatively expressed as displacement per atom (dpa). Also shown is a helium solubility curve from [139].

9.2.1. Pellet swelling

Fuel swelling is a possible effect caused by cumulative alpha decay events (and radiogenic helium) occurring during storage. The importance of this process lies on the possible consequences in terms of increasing stress and pellet cladding mechanical interaction in the used fuel rod. Pellet swelling observed in the reactor is due to: cumulative irradiation damage: the production of fission products; to a large extent characteristic of fuel with a burnup >45 GW·d·t(HM)$^{-1}$; the formation of fission gas bubbles. Once unloaded from the reactor, the cumulative effect of self-irradiation damage together with the changes in the chemical composition and helium production can also lead to swelling and modify the mechanical condition of the pellet.

Figure 138 shows the evolution of the lattice parameter, *a* of alpha doped UO_2 measured by XRD. The percentage fractional increase ($\Delta a/a_0$) is plotted as a function of accumulated dpa. The lattice parameter increases up to a maximum value of ~0.5% at ~1.2 dpa (approximately 4 years of storage under accelerated damage accumulation conditions), corresponding to a volume swelling of ~1.5%. After >~8 years, corresponding to ~2.8 dpa, a/a_0 is ~0.4%. The trends measured in this work are in good agreement with literature values. However, the maximum increase of the lattice parameter here is slightly higher than some reported values at saturation for UO_2 [140]; this is probably due to the fact that the dpa range investigated in the present study goes beyond and covers a wider interval than those typically reported in literature for synthetic materials under alpha decay conditions.

As can be seen in Fig. 138, the $\Delta a/a_0$ of alpha doped UO_2 at 0.2 dpa (the level of damage corresponding to a storage time span <100 years) is in the range 0.2–0.3%, and is in agreement with the reported levels for UO_2 and $^{238}PuO_2$. Although the lattice parameter showed further increase, saturation effects after damage accumulation of approximately 0.2 dpa were observed in the present study with respect to other properties; for example evolution of hardness with time [138] and thermal transport measurements [137]. This behaviour was correlated to the formation of numerous dislocation loops. The factors responsible for the swelling are the formation of point defects and dislocation loops (as evidenced by TEM analysis) in the material and the accumulation and retention of helium. The analysis of helium incorporation in the UO_2 lattice and lattice swelling was addressed by ab initio calculations [141–142] and by experimental and modelling studies [139], [143–147]. The swelling will remain low as long as the quantity of helium remains within its solubility limit. However, this solubility threshold is exceeded relatively soon during storage, leading to the formation of helium vacancy complexes and resulting in a lattice parameter increase.
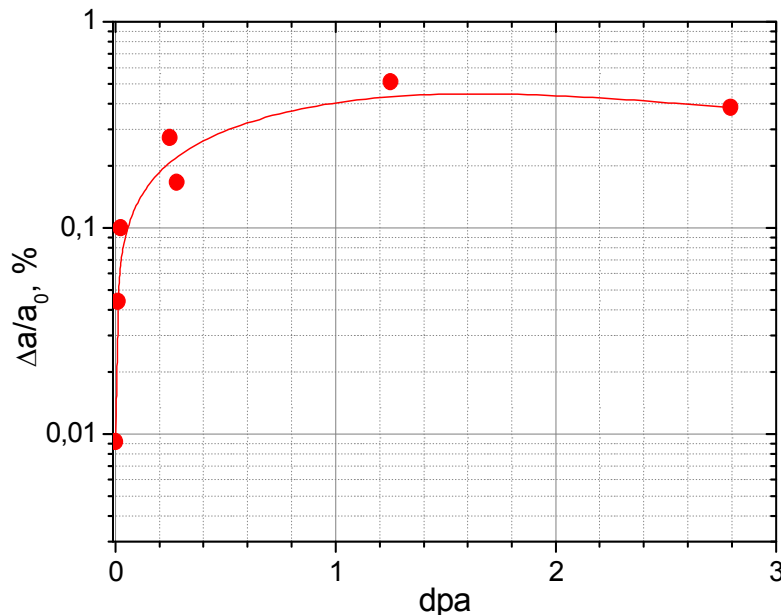
FIG. 138. Lattice parameter variation as a function of cumulated damage dose (dpa) for ^{238}Pu doped UO_2.

9.2.2. Helium release

A significant finding of the helium thermal desorption studies and on quantitative calibration tests on alpha doped UO_2 is that up to a relatively high damage level (corresponding to ~2.8 dpa) all the radiogenic helium is retained in UO_2. As already mentioned, helium retention is likely responsible for the swelling behaviour observed at high dose. The diagrams in Fig. 139 show the helium desorption profile as a function of temperature measured by Knudsen cell effusion tests for two samples: an alpha doped sample with ~1 dpa (a) and a UO_2 sample with 65 GW·d·t(U)$^{-1}$ after 15 years of storage (b). Similar release behaviour (namely, similar temperature release peaks) is observed for the two samples in spite of a large difference in accumulated alpha decay dose. The first significant helium release stage starts at around 1000K and ends at ~1400K for both samples. This first release stage is attributed to helium diffusion from a stable lattice position to the surface through grain boundaries. During this stage part of the helium is trapped into bubbles and other suitable sites. This fraction is released at higher temperatures by de-trapping mechanisms and, at the highest temperature level, by burst release mechanisms. In the case of spent fuel there are many trapping sites formed during in pile irradiation (fission gas bubbles, pores, cavities, defects, etc.). Therefore, the helium release is strongly affected by these types of mechanisms even at low alpha dose level. In the case of alpha doped, unirradiated UO_2, there are no pre-existing sites able to trap helium [141]. Only at relatively high dose and helium concentrations are nano sized helium bubbles formed. The thermal release profile of helium from alpha doped material with comparably low dpa level (< 0.1 dpa) for the spent fuel sample described in Fig. 139(b) typically shows only the first release peak at ~1000 K, without any further significant release at higher temperatures [144].

9.2.3. Fuel fragmentation

The potential occurrence and extent of fuel fragmentation or cracking during long term storage is unknown. Fuel fragmentation may be affected by extreme effects of α decay and of the accumulation of helium in bubbles at inter-granular and intra-granular locations. The mechanism by which fuel fragmentation, as such, could contribute to additional cladding stress is unclear because the fragmentation process would likely be associated with gas release to the plenum. That is, a driving force to cause pellet fragments to strain the cladding is absent. As a result, gaseous swelling in the fuel would be expected to range from non-existent to negligibly small at the low temperatures associated with very long storage. On the other hand, the occurrence of fuel cracking (without complete fuel fragmentation) in the radial direction during storage may cause local stress concentration at the fuel cladding interface [148]. Further work is ongoing to assess the potential relevance of this process.
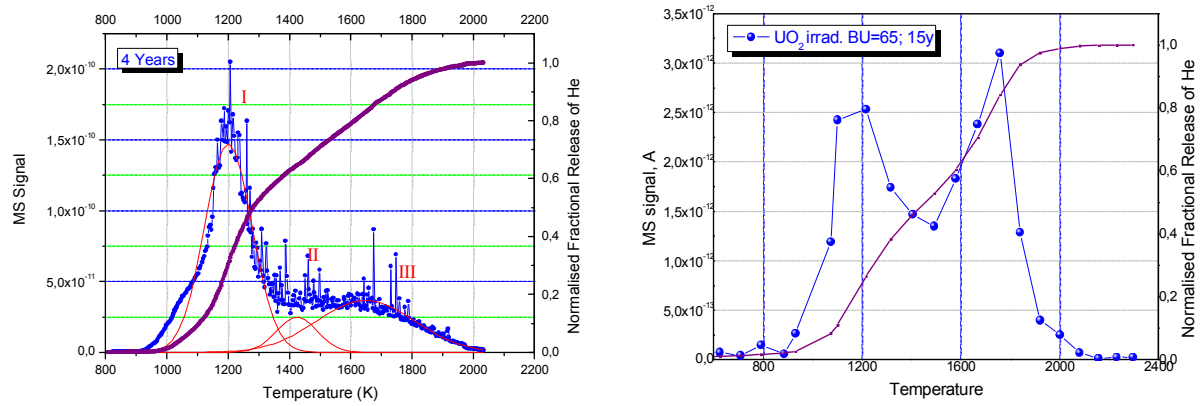
(a) alpha doped UO₂ with an accumulated dose of   (b) 65 GW·d·t(U)⁻¹ after ~15 y of storage (~0.05-
~1 dpa.   0.1 dpa).

FIG. 139. Helium release as a function of temperature measured using a Knudsen cell combined with mass spectrometry. The helium release profile is similar for the two materials in spite of the large difference in accumulated dose. The high temperature profiles (T>1400 K) highlight the effect due the presence of sinks for the helium atoms (bubbles, cavities, etc.), which are a pre-existing feature in spent fuel whereas they are formed only at high dpa level in the case of alpha-doped UO₂.

9.2.4. Implications for spent fuel storage

Information relevant to long term storage of SNF presently shows that saturation of the microscopic swelling in UO$_2$ as a result of α decay is reached for a dose of ~1 dpa (Fig. 138). This damage level could be reached in spent UO$_2$ fuel over a storage period of a few centuries (depending on the fuel burnup, see Fig. 136). The lattice parameter evolution corresponding to higher dose would correspond to time intervals exceeding the expected extended storage time for spent fuel and it may be relevant to assess the very long term evolution of the spent fuel material after disposal in a geologic repository. The direct applicability to spent LWR fuel of lattice swelling data obtained by accelerated decay damage and helium accumulation studies on unirradiated 'alpha doped' UO$_2$ is the subject of ongoing investigations. A relative increase in the lattice parameter corresponding to a ~1% volume increase, would correspond to a diametral strain of about 0.3%, which is about the same as the thermal contraction of fuel pellets relative to their cladding on shutdown. The homogeneous imposition of such strain by fuel pellets would result in a negligible increase of cladding stresses. Possible local effects due to inhomogeneous swelling in different regions of the fuel pellet, combined with the presence of cracks and other heterogeneities in the fuel structure will be investigated in future studies.

Helium produced by α decay during storage is expected to remain in the fuel matrix or accumulate in intra-granular pores. Helium accumulation inside the fuel grains could lead to gas retention and bulk pellet swelling.

Increases in the concentrations of gas atoms at grain boundaries could lead to inter-granular fracture and gas release. The diffusivity of helium in irradiated fuel pellets is very low at the temperatures of dry storage, so release by diffusion based processes is not expected to contribute to the pressure of gas in the free rod volume. The possibility of helium release by

other, non-diffusion processes (micro cracking and grain boundary separation) is unknown and constitutes an area of uncertainty. As a result, increases in the pressure of gas in the intra-space of SNF rods due to accidents and the release of helium, krypton and xenon from intra-granular sites has been identified as a potential issue in dry storage. Helium produced by α decay during storage, however, is estimated to reach a concentration of <0.1 at% in UO_2 irradiated to 60 GW·d·t(U)$^{-1}$ after 300 years, and ~1 % in MOX fuel after 10 000 years [147]. For UO_2, assuming that all the helium produced by α decay over the first 300 years is released, the increase in gas pressure in the free volume of a fuel rod is <5%, which is in the range of variability in fission gas release during in reactor operation and appears to be a negligible factor in cladding stress during storage.

10. CONCLUSIONS

The accumulated reporting of the IAEA's BEFAST and SPAR CRPs now exceeds 30 years.

For zirconium and stainless steel based LWR clad spent fuels there is >50 years wet storage and >30 years dry storage experience. Performance in storage remains excellent with no generic failure mechanism identified or experienced. In the case of stainless steel clad AGR spent fuel there is >30 years of wet storage experience. Storage performance is good provided the fuel is stored in the presence of a corrosion inhibitor. For MAGNOX spent fuel, magnesium alloy clad, there is ~57 years' experience in handling and storage; this includes ~43 years of dry storage operations. The tendency is only to store for relative short periods of time in wet storage, but the fuel will remain intact for longer periods provided optimum pool storage chemistry is maintained. There has been no reported degradation of MAGNOX spent retrieved from dry storage[22].

A considerable number of studies on hydrogen behaviour in zirconium based clad material have been undertaken during this phase of the SPAR project. Whilst studies using empty clad tubes have improved the understanding of hydrogen behaviour in zirconium based clad material, the properties associated with the presence of fuel may be different. A gap in this area remains in establishing experiments under actual storage conditions.

Improving the knowledge base on spent fuel behaviour for retrieval and transport situations has been investigated. The amount of fuel material released upon impact appears to be independent of fuel burnup, test method, is localized to the area of rupture and has been found to be <2 pellets worth of material for all fuel types tested. The studies have enabled establishing reference conditions for safety assessments.

Knowledge of the long term performance of materials used in spent fuel storage systems is required for continued operations and for storage system relicensing. A number of studies on the behaviour of materials have continued or been initiated during this phase of the SPAR project. In some areas, such as the influence of SCC on dry storage canisters in marine environment, studies are still ongoing. In other areas, for example metal seals, the experience to date and ongoing long-term studies have not established limiting factors for their continued use.

In the very long term, helium generation from α decay and the accumulation of helium may become an important mechanism in fuel matrix evolution. Although there remains unknowns in relation to gas retention by the fuel matrix, bulk pellet swelling or release mechanisms to the free volume, even where all the gas generated in the first 300 year of UO_2 spent fuel storage is released, there is a negligible effect on cladding stress during storage. More attention has to be devoted to spent MOX fuel behaviour.

Continued spent fuel storage and future transitions from one phase of the back end of the nuclear fuel cycle to the next require that the operational experience and research results be reported and disseminated to the Member States for input to continued operations safety assessments and the licensing of new facilities. In this respect field experience needs to be collected and reported; especially from the deployment of new technology.

---

[22] Except the small amount of fuel which was affected by water ingress to one of the air cooled dry stores at Wylfa NPP.

REFERENCES

[1]   INTERNATIONAL ATOMIC ENERGY AGENCY, Spent Fuel Performance Assessment and Research, IAEA-TECDOC-1343, IAEA, Vienna (2003).

[2]   INTERNATIONAL ATOMIC ENERGY AGENCY, Spent Fuel Performance Assessment and Research: Final Report of a Coordinated Research Project (SPAR-II), IAEA-TECDOC-1680, IAEA, Vienna (2012).

[3]   INTERNATIONAL ATOMIC ENERGY AGENCY, Storage of Spent Nuclear Fuel, Safety Standards Series No. SSG–15, IAEA, Vienna (2012).

[4]   INTERNATIONAL ATOMIC ENERGY AGENCY, Behaviour of Spent Fuel Assemblies During Extended Storage (BEFAST-I), IAEA-TECDOC-414, IAEA, Vienna (1987).

[5]   INTERNATIONAL ATOMIC ENERGY AGENCY, Extended Storage of Spent Fuel (BEFAST-II), IAEA-TECDOC-673, IAEA, Vienna (1992).

[6]   INTERNATIONAL ATOMIC ENERGY AGENCY, Further Analysis of Extended Storage of Spent Fuel (BEFAST-III), IAEA-TECDOC-944, IAEA, Vienna (1997).

[7]   NUCLEAR DECOMMISSIONING AUTHORITY, Managing Nuclear Material and Spent Fuel – Work Area (2015), http://www.nda.gov.uk/nuclear-materials-and-spent-fuels/

[8]   UNITED KINGDOM DEPARTMENT OF ENERGY AND CLIMATE CHANGE, Long-term Nuclear Energy Strategy, BIS/13/630, (2013), http://www.gov.uk

[9]   NUCLEAR DECOMMISSIONING AUTHORITY, MAGNOX Fuel Strategy: Contingency Options (2014), http://www.nda.gov.uk/publication/magnox-fuel-strategy-contingency-options-january-2014/

[10]   NUCLEAR DECOMMISSIONING AUTHORITY, Oxide Fuels: Credible Options, (2011), http://www.nda.gov.uk/publication/oxide-fuels-credible-options-november-2011/

[11]   NUCLEAR DECOMMISSIONING AUTHORITY, Oxide Fuels: Preferred Option, (2012), http://www.nda.gov.uk/publication/oxide-fuels-preferred-options-june-2012/

[12]   UNITED KINGDOM DEPARTMENT FOR ENVIRONMENT, FOOD AND RURAL AFFAIRS, Managing Radioactive Waste Safely: A Framework for Implementing Geological Disposal, TSO ID5818553, TSO, London (2008).

[13]   UNITED STATES. DEPARTMENT OF ENERGY, Report to the Secretary of Energy - Blue Ribbon Commission on America's Nuclear Future, U.S. DoE, Washington, DC (2012).

[14]   UNITED STATES. DEPARTMENT OF ENERGY, Strategy for the Management and Disposal of Used Nuclear Fuel and High-level Radioactive Waste, U.S. DoE, Washington, DC (2013).

[15]   UNITED STATES. NUCLEAR REGULATORY COMMISSION, Identification and Prioritization of the Technical Information Needs Affecting Potential Regulation of Extended Storage and Transportation of Spent Nuclear Fuel, U.S. NRC, Washington, DC (2012).

[16]   UNITED STATES. DEPARTMENT OF ENERGY, Gap Analyses to Support Extended Storage of Used Fuel, U.S. DoE, Washington, DC (2012).

[17]   ELECTRIC POWER RESEARCH INSTITUTE, Extended Used Fuel and High-level Waste Storage Collaboration Programme – Progress Report and Review of Gap Analyses, ML1022149, EPRI, Palo Alto (2011).

[18]   NUCLEAR NEW BUILD GENERATION COMPANY, Hinkley Point C Pre Commencement Safety Report, HPC PCSR2 sub-chapter 11.5, (2012), http://hinkleypoint.edfenergyconsultation.info/public-documents/hinkley-point-c-pre-construction-safety-report-2012/

[19]   JAPAN NUCLEAR FUEL LTD, Status of Spent Fuel Acceptance, (2013), http://www.jnfl.co.jp/transport-schedule/recycle.html

[20]   JAPAN NUCLEAR FUEL LTD, Active commissioning test schedule, (2013), http://www.jnfl.co.jp/cycle-recycle/testing/active-test.html

[21]   UNITED STATES NUCLEAR REGULATORY COMMISSION, Resolution of Licensing Process Expectations for Pressurized Water Reactor Fuel Assemblies Susceptible to Top Nozzle Stress Corrosion Cracking in Dry Cask Spent Fuel Storage and Transportation, U.S. NRC, Washington, DC (2013).

[22]   JÉGOU, C., CARABALLO, R., DE BONFILS, J., BROUDIC, V., PEUGET, S., VERCOUTER, T., ROUDIL, D., Oxidizing dissolution of spent MOX47 fuel subjected to water radiolysis: Solution chemistry and surface characterization by Raman spectroscopy, J. Nucl. Mater. **399** (2010) 68–80.

[23]   DURBIN, S.G., LINGDREN, E.R., "Investigation of zirconium fires during spent fuel pool LOCAs", paper presented at NEI Used Fuel Management Conference, Baltimore, 2011.

[24]   ZIGH, G., VELAZQUEZ-LOZADA, E.R., "Zirconium fire on pressurized water reactor (PWR) spent fuel pools (SFP)", paper presented at U.S. NRC Regulatory Information Conference, Washington, DC, 2013.

[25]   UNITED STATES. NUCLEAR REGULATORY COMMISSION, Consequence Study of a Beyond - Design Basis Earthquake Affecting the Spent Fuel Pool for a U.S. Mark 1 Boiling Water Reactor, NUREG-2161, U.S. NRC, Washington, DC (2014).

[26]   GRAHN, P.H., WIKSTRŐM, M., "Experiences from the operation of the Swedish central interim storage facility for spent fuel (CLAB)", Storage of Spent Fuel from Power Reactors, IAEA-TECDOC-1089, IAEA, Vienna (1990) 289–295.

[27]   INTERNATIONAL ATOMIC ENERGY AGENCY, Survey of Wet and Dry Spent Fuel Storage, IAEA-TECDOC-1100, IAEA, Vienna (1999).

[28]   PEEHS, M., EINFELD, K., "Effects of long term dry storage of spent fuel", Proc. of IHLRWM 1992, Las Vegas, NV, 1992, ANS, La Grange Park, IL (1992) 1181–1187.

[29]   PEEHS, M., BANCK, J. "Spent fuel storage: a reliable technology in the back end of the fuel cycle", Proc. of the 4th Int. Conf. on Nuclear Waste Management and Environmental Remediation, Prague, 1993, ASME, New York (1993) 259–266.

[30]   KUMANO, Y., "Integrity inspection of dry storage casks and spent fuels at Fukushima Daiichi nuclear power station", paper presented at CRIEPI Int. Conf. ISSF 2010, Tokyo, 2010.

[31]   BRITISH ENERGY GENERATION LTD., The Sizewell B Spent Fuel Management Option Study, BE GEN Ltd., Gloucester (2010).

[32]   ELECTRIC POWER RESEARCH INSTITUTE, Dry Cask Storage Characterization Project – Final Report, EPRI 1002882, EPRI, Palo Alto (2002).

[33]   UNITED STATES. DEPARTMENT OF ENERGY, Examination of Spent PWR Fuel Rods After 15 Years in Dry Storage, NUREG/CR-6831, U.S. NRC, Washington, DC (2003).

[34]   UNITED STATES NUCLEAR REGULATORY COMMISSION, Safety Evaluation Report - Surry Independent Spent Fuel Storage Installation, Docket No. 72-2, U.S. NRC, Washington, DC (2005).

[35]   UNITED STATES NUCLEAR REGULATORY COMMISSION, Cladding Considerations for the Transportation and Storage of Spent Fuel, Interim Staff Guidance 11 Rev. 3, U.S. NRC, Washington, DC (2003).

[36]   ELECTRIC POWER RESEARCH INSTITUTE, Dry Storage of High Burnup Spent Fuel – Responses to Nuclear Regulatory Commission Requests for Additional Information and Clarification, EPRI 1009276, EPRI, Palo Alto (2003).

[37]   SHIRAI, K., TAKEDA, H., SAEGUSA, T., "Confinement analysis of dual purpose metal cask subjected to impulsive loads during handling accidents", Proc. of PATRAM 2007, Miami, Florida, 2007, ISBN 9781622769308, Curran Associates, New York (2013) 538–545.

[38]   TAKEDA, H., SHIRAI, K., WATARU, M., TANI, J., ARAI, T., SAEGUSA, T., "Current status of R&D on spent fuel storage -CRIEPI's perspectives 2008", Proc. INMM Spent Fuel Management Seminar XXV, INMM, Washington, DC (2008).

[39]   SHIRAI, K., NAMBA, K., SAEGUSA, T., "Safety analysis of dual purpose metal cask subjected to impulsive loads to aircraft engine crash", Proc. of Conf. on Nuclear Engineering (ICONE16), Orland, Florida, 2008, Vol. 4, ASME, New York (2008), 25–31.

[40]   KAMIMURA, K., et al, "Thermal creep test of BWR and PWR spent fuel cladding", Storage of Spent Fuel from Power Reactors, IAEA-CSP-20, IAEA, Vienna (2003) 375–385.

[41]   ITO, K., et al, "Evaluation of irradiation effect on spent fuel cladding creep properties", Proc. of 2004 International Meeting on LWR Fuel Performance, Orlando, Florida, 2004, ANS, La Grange Park, IL (2004).

[42]   AOMI, M., et al, "High burnup fuel cladding tube property test for evaluation of spent fuel integrity in interim dry storage", Management of Spent Fuel from Nuclear Power Reactors, IAEA Proceedings Series STI/PUB/1295, IAEA, Vienna (2007) 409–422.

[43]   OTSUKA, A., NAKAMURA, M., KATAYAMA, K., et al., "Demonstration test programme for longterm dry storage of PWR spent fuel", Proc. GLOBAL 2011, JAEA/ANS, Makuhari, Japan (2011) Paper No. 455416.

[44]   UNITED STATES NUCLEAR REGULATORY COMMISSION, Moderator Exclusion under Hypothetical Accident Conditions and Demonstrating Sub-criticality of Spent Fuel under the Requirements of 10 CFR 71.55(e), Interim Staff Guidance 19, U.S. NRC, Washington, DC (2003).

[45]   ELECTRIC POWER RESEARCH INSTITUTE, Development of a Metal/Hydride Mixture Model for Zircaloy Cladding with Mixed Hydride Structure, EPRI 1009694, EPRI, Palo Alto, CA (2004).

[46]   ELECTRIC POWER RESEARCH INSTITUTE, Failure Criteria for Zircaloy Cladding Using a Damage-based Metal/Hydride Mixture Model, EPRI 1009693, EPRI, Palo Alto, CA (2004).

[47]   ELECTRIC POWER RESEARCH INSTITUTE, Spent Fuel Transportation Applications: Fuel Rod Failure Evaluation Under Simulated Cask Side Drop Conditions, EPRI 1009929, EPRI, Palo Alto, CA (2005).

[48]   ELECTRIC POWER RESEARCH INSTITUTE, Spent Fuel Transportation Applications: Global Forces Acting on Spent Fuel Rods and Deformation Patterns Resulting from Transportation Accidents, EPRI 1011817, EPRI, Palo Alto, CA (2005).

[49]   ELECTRIC POWER RESEARCH INSTITUTE, Spent Fuel Transportation Applications: Modelling of Spent-fuel Rod Transverse Tearing and Rod Breakage Resulting from Transportation Accidents, EPRI 1013447, EPRI, Palo Alto, CA (2006).

[50] ELECTRIC POWER RESEARCH INSTITUTE, Spent Fuel Transportation Applications: Longitudinal Tearing Resulting from Transportation Accidents – A Probabilistic Treatment, EPRI 1013448, EPRI, Palo Alto, CA (2006).

[51] DAUM, R. S., MAJUMDAR, S., LIU, Y. and BILLONE, M. C., Radial-hydride embrittlement of high-burnup zircaloy-4 fuel cladding, J. Nucl. Sci. Technol. **43** 9 (2006) 1054–1067.

[52] GEELHOOD, K.J., BEYER, C.E., LUSCHER, W.G., Stress/Strain Correlation for Zircaloy, PNNL-17700, PNNL, Richland, WA (2008).

[53] JERNKVIST, L.0., MASSIH, A.R., Models for Fuel Rod Behaviour at High Burnup, SKI Report 2005:41, Quantum Techologies AB, Uppsala, Sweden (2004).

[54] DAUM, R.S., MAJUMDAR, S., BATES, D.W., MOTTA, A.T., KOSS, D.A., BILLONE, M.C., "On the embrittlement of Zircaloy-4 under RIA-relevant conditions", Zirconium in the Nuclear Industry: 13th Int. Symp., STP 1423, ASTM, West Conshohoken, PA (2002) 702-719.

[55] YAGNIK, S.K., KUO, R-C., RASHID, Y.R., MACHIELS, A.J., YANG, R.L., "Effect of hydrides on the mechanical properties of Zircaloy-4", Proc. of 2004 International Meeting on LWR Fuel Performance, Orlando, Florida, 2004, ANS, La Grange Park, IL (2004).

[56] SINGH, R., KISHORE, R., SINGH, S., SINHA, T., KASHYAP, B., Stress-reorientation of hydrides and hydride embrittlement of Zirconium-2.5Nb pressure tube alloy, J. Nucl. Mater. **325** (2004) 26–33.

[57] SAKAMOTO, K., NAKATSUKA, M., Stress reorientation of hydrides in recrystallized Zircaloy-2 sheet, J. Nucl. Sci. Technol. **43** 9 (2006) 1136–1141.

[58] HARDIE, D., SHANAHAN, M. W., Stress reorientation of hydrides in zirconium-2.5% niobium, J. Nucl. Mater. **55** (1975) 1–13.

[59] CHUNG, H.M., KASSNER, T.F., Cladding metallurgy and fracture behavior during reactivity-initiated accidents at high burnup, Nucl. Eng. Des. **186** (1998) 411–427.

[60] CHAN, K.S., A micromechanical model for predicting hydride embrittlement in nuclear fuel cladding material, J. Nucl. Mater. **227** (1996) 220–236.

[61] SAKAMOTO, K., MATSUOKA, H., TAKAGI, A., KASHIBE, S., "Study on hydride reorientation in Zircaloy-2 fuel claddings during interim dry storage", LWR fuel performance meeting/ TOPFUEL 2007, San Francisco, California, 2007, ISBN 9781604239423, Curran Associates, NY (2007) 472–480.

[62] QUECEDO, M.A., et al.: "Results of thermal creep tests on highly irradiated ZIRLO™", paper presented at TOP FUEL 2008, Seoul, Republic of Korea (2008) Paper 8063.

[63] LLORET, M., et al.: "Results of thermal creep tests on irradiated Zry-2", TOP FUEL 2012, Manchester, UK, 2012, Top Fuel 2012 Transactions – Spent Fuel and Transportations, ENS, Brussels, Belgium (2012) 12–17.

[64] AOMI, M., et al., "Evaluation of hydride reorientation behavior and mechanical property of high burnup fuel cladding tube in interim dry storage", Zirconium in the Nuclear Industry: 15th Int. Symp., STP 1505, ASTM, West Conshohocken (2009) 651.

[65] KIM, Y., KIM, J., KOOK, D., KIM, Y., "Effects of hoop stress on the hydride reorientation in spent nuclear fuel cladding", Trans. Of Korean Nuclear Society Autumn meeting 2012, Gyeongju, Republic of Korea (2012).

[66] ALAM, A.M., HELLWIG, Ch., Cladding tube deformation test for stress reorientation of hydrides, J. ASTM Int. **5** 2 (2008) 635–649.

[67] VALANCE, S., BERTSCH, J., ALAM, A.M., Statistical analysis of hydride reorientation properties in irradiated zircaloy-2, J. ASTM Int. **8** 1 (2011) 523.

[68]   YAGNIK, S.K., et al., Round-robin testing of fracture toughness characteristics of thin-walled tubing, J. ASTM Int. **5** 2 (2008) 1–21.

[69]   BERTSCH, J., VALANCE, S., ZUBLER, R., "Crack resistance determination of irradiated fuel cladding using the cladding tensile fracture test", Proc. of 2010 LWR Fuel Performance/TOP FUEL/WRFPM, Orlando, Florida, 2010, ISBN 9781617828485, Curran Associates, NY (2011) 434–443.

[70]   LEDERGERBER, G., et al., Characterization of high burnup fuel for safety related fuel testing, J. Nucl. Sci. Technol. **43** 9 (2006) 9–11.

[71]   AMERICAN SOCIETY FOR TESTING AND MATERIALS, Standard Specification for Wrought Zirconium Alloy Seamless Tubes for Nuclear Reactor Fuel Cladding, ASTM B811-13, ASTM, West Conshohocken, PA (2013).

[72]   BELL, L.G., DUNCAN, R.G., Hydride Orientation in Zirconium-2.5%Nb; How it is Affected by Stress, Temperature and Heat Treatment, AECL-5110, AECL, Chalk River, Canada (1975).

[73]   WALLACE, A.C., SHEK, G.K., LEPIK, O.E., "Effects of hydride morphology on zirconium-2.5nb fracture toughness", Zirconium in the Nuclear Industry: 8th Intern. Symp., STP 1023, ASTM, West Conshohocken, PA (1989) 66–88.

[74]   COLAS, K., Fundamental Experiments on Hydride Reorientation in Zircaloy, PhD Thesis, Pennsylvania State University, PA (2012).

[75]   KAMMENZIND, B.F., FRANKLIN, D.G., PETERS, H.R. AND DUFFIN, W.J. "Hydrogen pickup and redistribution in alpha-annealed zircaloy-4," Zirconium in the Nuclear Industry: 11th Int. Symp., STP 1295, ASTM, West Conshohocken, PA (1996) 338–370.

[76]   FERRY, C., POINSSOT, C., BROUDIC, V., CAPPELAERE, C., DESGRANGES, L., GARCIA, P., JEGOU, C., LOVERA, P., MARIMBEAU, P., CORBEL, C., MISERQUE, F., PIRON, J.-P., POULESQUEN, A., ROUDIL, D., GRAS, J.-M., BOUFFIOUX, P., Référentiel Scientifique sur l'évolution à Longterme des Combustibles Usés , CEA RT DPC/SECR 04-032 indice B, CEA, Saclay. Paris (2005).

[77]   BILLONE, M.C., BURTSEVA, T.A., EINZIGER, R.E., Ductile-to-brittle transition temperature for high burnup cladding alloys exposed to simulated drying–storage conditions, J. Nuc. Materi. **433** (2013) 431–448.

[78]   RACINE, A., Influence de L'orientation des Hydrures sur les Modes de Deformation, D'endommagement et de Rupture du Zircaloy-4 Hydruré, Ph.D Thesis, l'Ecole Polytechnique, Route de Saclay, 91128, Palaiseau Cedex, Paris, France, (2005).

[79]   BAI, J.B., et. al., Effect of microstructure factors and cold work on the hydride precipitation in zircaloy-4 sheet, Journal of Advanced Science **3** (1994) 188.

[80]   SABOL, G.P., "In-reactor corrosion performance of ZIRLO™ and zircaloy-4", Zirconium in the Nuclear Industry: 10th Int. Symp., STP 1245, ASTM, West Conshohocken, PA (1994) 724–744.

[81]   KEARNS, J.J., WOODS, C.R., Effects of texture, grain size and cold work on the precipitation of orientated hydrides in zircaloy tubing and plate, J. Nuc. Materi. **20** 3 (1966) 241–261.

[82]   MCMINN, A., DARBY, E.C., SCHOFIELD, J.S., "The terminal solid solubility of hydrogen in zirconium alloys", Zirconium in the Nuclear Industry: 12th Int. Symp., STP 1354, ASTM, West Conshohocken, PA (2000) 173–195.

[83]   PULS, M.F., The Effect of Hydrogen and Hydrides on the Integrity of Zirconium Alloy Components, ISBN 978-1-4471-4195-2, Springer, Berlin (2012).

[84]   MCRAE, G.A., COLEMAN, C.E., LEITCH, B.W., The first step for delayed hydride cracking in zirconium alloys, J. Nuc. Materi. **396** (2010) 130–143.

[85]   KIM, Y.S., Comment on 'The first step for delayed hydride cracking in zirconium alloys' by G.A. McRae et.al., J. Nuc. Materi. **396**, (2010) 144–148.

[86]   KEARNS, J.J., Terminal solubility and partitioning of hydrogen in the alpha phase of zirconium, zircaloy-2 and zircaloy-4, J. Nuc. Materi. **22** (1967) 292–303.

[87]   KEARNS, J.J., Diffusion coefficient of hydrogen in the alpha zirconium, zircaloy-2 and zircaloy-4, J. Nuc. Materi. **43** (1972) 330–338.

[88]   KEARNS, J.J., Dissolution kinetics of hydride platelets in zircaloy-4, J. Nuc. Materi. **27** (1968) 64–72.

[89]   ADAMSON, R.B., "Hydrogen solubility and microstructural changes in zircaloy-4", Zirconium in the Nuclear Industry: 12th Int. Symp., STP 1354, ASTM, West Conshohocken, PA (2000) 15–31.

[90]   VIZCAÍNO, P., FLORES, A.V., BOZZANO, P.B., BANCHIK, A.D., VERSACI, R.A., RÍOS, R.O., "Effects of neutron irradiation on microstructure and properties of zircaloy due to neutron irradiation", Zirconium in the Nuclear Industry: 16th Int. Symp., STP 1529, ASTM, West Conshohocken, PA (2011) 754–783.

[91]   VIZCAÍNO, P., BANCHIK, A.D., ABRIATA, J.P., Hydrogen in zirclaoy-4 effects of the neutron irradiation on the hydride formation, Journal of Materials Science **1354** (2007) 15–31.

[92]   VIZCAÍNO, P., BANCHIK, A.D., ABRIATA, J.P., Solubility of hydrogen in zirclaoy-4 irradiation induced increase and thermal recovery, J. Nucl. Mater. **304** (2002) 96–106.

[93]   VERMOLEN, F., VUIK, K., A numerical method to compute the dissolution of second phases in ternary alloys, Journal of Computational Applied Mathematics **93** (1998) 123–143.

[94]   TSAI, H., BILLONE, M.C., Thermal creep of irradiated zircaloy cladding, J. ASTM Int. **3** 1 (2006) Paper JAI112425.

[95]   KAMMENZIND, B.F., BERQUIST, B.M., BAJAI, R., KREYNS, P.H., FRANLKIN, D.G., "The long range migration of hydrogen through zircaloy in response to tensile and compressive stress gradients", Zirconium in the Nuclear Industry: 12th Int. Symp., STP 1354, ASTM, West Conshohocken, PA (2000) 196–233.

[96]   DAUM, R.S., MAJUMDAR, BILLONE, M.C., Experimental and analytical investigation of the mechanical behaviour of high burnup zircaloy-4 fuel cladding, J. ASTM Int. **5** 5 (2008) Paper JAI101209.

[97]   SANDERS, T.L., SEAGER, K.D., RASHID, Y.R., et. al., A Method for Determining the Spent Fuel Contribution to Transport Cask Containment Requirements, SAND90-2406, Sandia Nuclear Laboratories, Albuquerque, (1992).

[98]   KAMIMURA, K., et. al., "Integrity criteria of spent fuel for dry storage in Japan", paper presented at CRIEPI Int. Conf. ISSF 2010, Tokyo 2010.

[99]   INTERNATIONAL ATOMIC ENERGY AGENCY, Regulations for the Safe Transport of Radioactive Material -2009 Edition, Safety Standard Series No. TS-R-1, IAEA, Vienna, (2009).

[100]   PURCELL, P.C., DALLONGVILLE, M., "Testing of LWR fuel rods to support criticality safety analysis of transport accident conditions", presented at PATRAM 2004, Berlin, Germany, (2004) Paper 134.

[101]   ZEACHANDIRIN, A., DALLONGEVILLE, M., PURCELL, P.C., CORY, A., AREVA TN and INS: Description of 'Fuel Integrity Project' methodology principles, RAMTRANS **22** 4 (2011) 179–183.

[102]   RONDINELLA, V.V., WISS, T., PAPAIOANNOU, D., NASYROW, R., "Studies on nuclear fuel evolution during storage and testing of used fuel response to impact loadings", Proc. PSAM11 and ESREL 2012, Helsinki, 2012,
ISBN: 9781622764365, Curran Associated, NY (2012) 3171-3179.

[103]   PAPAIOANNOU, D., NASYROW, R., RONDINELLA, V.V., GOLL, W., WINKLER, H-P., LIEDTKE, R., HOFFMANN, D., "Fuel release experiments on irradiated fuel rodlets under transient impact conditions", Annual Meeting on Nuclear Technology 2009, KTG org., Berlin (2009) 1004.

[104]   OZAWA, M., HIROSE, T., MIURA, H., BABA, T., KAMIMURA, K., AOMI, M., YASUDA, T., MURAKAMI, T.K., SHINOHARA, Y., "Fuel rod mechanical performance under dynamic load condition on high burn-up spent fuel of BWR and PWR", Proc. PATRAM 2013, San Francisco, 2013, INMM, Chicago, IL (2013).

[105]   HIROSE, T., OZAWA, M., MIURA, H., BABA, T., KAMIMURA, K., et al. "Dynamic load impact tests on high burnup spent fuel rods of BWR and PWR", paper presented at NuMat 2012: the Nuclear Materials conference, Osaka, Japan, 2012.

[106]   HIROSE, T., OZAWA, M., MIURA, H., BABA, T., KAMIMURA, K., "Research on integrity of high burnup spent fuel under long term dry storage and transport," paper presented at OECD/NEA International Workshop on Safety of Long Term Interim Storage Facilities, Munich, 2013.

[107]   TORRES, E., RUIZ-HERVÍAS, J., MARTIN-RENGEL, M.A., "Drop-weight ring compression test for evaluating the mechanical behaviour of fuel rods under impact conditions", Proc. PATRAM 2013, San Francisco, 2013, INMM, Chicago, IL (2013).

[108]   SABOL, G.P., ZIRLO™ - An alloy development success, J. ASTM Int. **2** 2 (2005) Paper JAI12942.

[109]   MARTIN-RENGEL, M.A., Integridad Estructural de Vainas de Combustible Nuclear en Condiciones de Almacenamiento Temporal en Seco, PhD thesis, Universidad Politécnica de Madrid, ENRESA technical publication 05-2010 (in spanish), (2009).

[110]   SHIRAI, K., TANI, J., GOTOH, M., WATARU, M., "SCC evaluation of multi-purpose canister in long term storage", Proc. PSAM 11 and ESREL, Helsinki, 2011, ISBN: 9781622764365, Curran Associates, (2012) 3161–3170.

[111]   SCHEEL, J.E., et al., "Mitigation of stress corrosion cracking in nuclear weldments using low plasticity burnishing", Proc. ICONE16, Orland, 2008,
ISBN 0791848167, ASME, NY (2008) 649–656.

[112]   CASERES, L., MINTZ, T. S., Atmospheric Stress Corrosion Cracking Susceptibility of Welded and Unwelded 304, 304L and 316L Austenitic Stainless Steels Commonly Used for Dry Cask Storage Containers Exposed to Marine Environments, NUREG/CR-7030, USNRC, Washington, DC, (2010).

[113]   OBERSON, G., HE, X., MINTZ, T., HE, Z., PABALAN, R., MILLER, L., Assessment of Stress Corrosion Cracking Susceptibility for Austenitic Stainless Steels Exposed to Atmospheric Chloride and Non-Chloride Salts, NUREG/CR-7170, USNRC, Washington, DC, (2014).

[114]   ETO, S., TANI, J., SHIRAI, K., et al., Measurement of concentration of chlorine attached to a stainless steel canister material using laser induced breakdown spectroscopy, Spectrochimica Acta part B **87** (2013) 74–80.

[115]   ETO, S., T. FUJII, T., SHIRAI, K., "Development of measurement technology of chlorine attached on canister using laser –Application of LIBS using collinear geometry", CRIEPI report H11020, CRIEPI, Tokyo, (2012). (in Japanese).

[116] ETO, S., MIURA, Y., TANI, J., et al., Effect of residual stress induced by pulsed-laser irradiation on initiation of chloride stress corrosion cracking in stainless steel, Mat. Sci. Eng. A-Struct. **590** (2014) 433–439.

[117] MATSUMURA, T., SHIRAI, K., SAEGUSA, T., Verification method for durability of reinforced concrete structures subjected to salt attack under high temperature conditions, Nucl. Eng. Des. **238** (2008) 1181–1188.

[118] SAKATA, Y., NAKATANI, T., SHIOTSU, H., Mechanical properties of A5083FH-O used for basket of transport and storage cask, The Japan Society of Mechanical Engineers **77** 780 (2011) 1407.

[119] MATSUOKA, T., ISHIKO, D., MATEGUCHI, T., Mechanical properties of BC-A6N01SS-T1 for basket material of transport and storage cask, The Japan Society of Mechanical Engineers **78** 786, 105, (2012).

[120] SHIMOJO, J., AKAMATSU, H., Mechanical properties of 1%B-A6061-T6/T651 and A6061-T6/T651 used for basket of transport and storage cask, The Japan Society of Mechanical Engineers, **76** 771 (2010) 141.

[121] EICKHOFF, R.S., "Ageing management in the design and operation of dual-purpose casks", Proc. PATRAM 2013, San Francisco, 2013, INMM, Chicago, IL (2013).

[122] VÖLZKE, H., "Dry spent fuel storage in dual purpose casks - Ageing Management Issues", paper presented at INMM Spent Fuel Management Seminar XXVIII, Arlington, VA, 2013.

[123] ELECTRIC POWER RESEARCH INSTITUTE, Extended Storage Collaboration Program International Perspectives on Technical Gaps Associated with Extended Storage and Transportation of Used Nuclear Fuel, EPRI 1026481, EPRI, Palo Alto, CA, (2012).

[124] PROBST, U., et al, Investigation of seal effects according to axial compression variation of metal seals for transport and storage casks, RAMTRANS **19** 1 (2008) 47–52.

[125] SASSOULAS, H., et al., Ageing of metallic gaskets for spent fuel casks: century-long life forecast from 25,000 h Long Experiments, Nucl. Eng. Des. **236** (2006) 2411–2417.

[126] BEZIAT, A., et al., "Ageing of Helicoflex® Metallic Gasket for Spent Fuel Cask: Analysis of Sealing Performance of a 75,000 h Campaign", Proc. PATRAM 2013, San Francisco, 2013, INMM, Chicago, IL (2013).

[127] YAMAMOTO, H., "Dual-purpose metal cask integrity after longterm interim storage", paper presented at PATRAM 2001, Chicago, 2001.

[128] YOKIYAMA, T., et al., "Integrity assessment of dual-purpose metal cask after long term interim storage - seal performance under transport conditions", paper presented at PATRAM 2004, Berlin, 2004.

[129] TAKEDA, H., et al., "Instantaneous leakage evaluation of metal cask at drop impact", Proc. of ICONE14, Miami, 2006, ISBN 0791842444, ASME, NY (2006) 815–821.

[130] SCHUBERT, S., et al., "Behaviour of metallic seals in CASTOR cask under normal and accident conditions of transport: qualification requirements", Proc. of PATRAM 2007, ISBN 9781622769308, Curran Associates, New York (2013) 1827–1834.

[131] MARLIER, R., ISSARD, H., "New metallic gaskets qualification: resistance to accident conditions of transport in TN International casks", Proc. of PATRAM 2007, ISBN 9781622769308, Curran Associates, New York (2013) 1819–1826.

[132] PROBST, U., et al., "Investigation of seal effects according to axial compression variation of metal seals for transport and storage casks", Proc. of PATRAM 2007, ISBN 9781622769308, Curran Associates, New York (2013) 1053–1060.

[133] WATARU, M., et al., "Long-term containment performance test of metal cask for spent nuclear fuel storage", PSAM 11 and ESREL 12, Helsinki, 2012, ISBN: 9781622764365, Curran Associates, (2012) 3143–3152.

[134] KATO, O., et al., Long-term containment performance test facilities for spent fuel transport/storage casks, RAMTRANS **12** 2–3 (2001) 119–122.

[135] ITO, C., et al., Longterm containment performance test for spent fuel transport/storage casks, Trans. At. Energy Soc. Japan **2** 2 (2003) 158–162 (in Japanese).

[136] TAKEDA, H., WATARU, M., SHIRAI, K., SAEGUSA, T., Development of detecting method of helium gas from canister, Nucl. Eng. Des. **238** (2008) 1220–1226.

[137] STAICU, D., WISS, T., RONDINELLA, V.V., HIERNAUT, J.-P., KONINGS, R.J.M., RONCHI, C., Impact of auto-irradiation on the thermophysical properties of oxide nuclear reactor fuels, J. Nucl. Mater. **397** (2010) 8–18.

[138] RONDINELLA, V.V., WISS, T., HIERNAUT, J-P., STAICU, D., "Dose rate effects on the accumulation of radiation damage", Proc. ICEM 07, Bruges, 2007, ASME, NY (2007) 1071–1076.

[139] MAUGERI, E., WISS, T., HIERNAUT, J-P., DESAI, K., THIRIET, C., RONDINELLA, V.V., COLLE, Y-J., KONINGS, R.J.M., Helium solubility and behaviour in uranium dioxide, J. Nucl. Mater. **385** (2009) 461.

[140] WEBER, W.J., In growth of lattice defects in alpha irradiated UO_2 single crystals, J. Nucl. Mater. **98** (1981) 206–215.

[141] PETIT, T., FREYSS, M., GARCIA, P., MARTIN, P., RIPERT, M., CROCOMBETTE, J-P., JOLLET, F., Molecular modelling of transmutation fuels and targets, J. Nucl. Mater. **320** (2003) 133–137.

[142] YUN, Y., ERIKSSON, O., OPPENEER, P. M., Theory of helium trapping, diffusion and clustering in UO_2, J. Nucl. Mater. **385** (2009) 510–516.

[143] RONDINELLA, V.V., COBOS, J., WISS, T., HIERNAUT, J-P., "Studies on spent fuel alterations during storage and radiolysis effects on corrosion behaviour using alpha-doped UO_2", Proc. ICEM 03, Oxford, 2003, ASME, NY (2003) 265–272.

[144] RONDINELLA, V.V., WISS, T., MAUGERI, E., COLLE, J-Y., "Effects of helium build-up on nuclear fuel evolution during storage", Proc. IHLRWMC 2011, Albuquerque, New Mexico, 2011, ISBN 9781617828508, Curran Associates, NY (2011) 230–233.

[145] FERRY, C., PIRON, J-P., Stout, R., "Effect of helium accumulation on the spent fuel microstructure", in Scientific Basis for Nuclear Waste Management XXX, MRS Proc., ISBN 9781107408746, Cambridge University Press, Cambridge (2014).

[146] FERRY, C., POINSSOT, C., CAPPELAERE, C., DESGRANGES, L., JEGOU, C., MISERQUE, F., PIRON, J.P., ROUDIL, D., GRAS, J.M., Specific outcomes of the research on the spent fuel longterm evolution in interim dry storage and deep geological disposal. J. Nucl. Mater. **352** (2006) 246.

[147] FERRY, C., PIRON, J-P., AMBARD, A., Effect of helium on the microstructure of spent fuel in a repository: an operational approach, J. Nucl. Mater. **407** (2010) 100.

[148]   AHN, T., RONDINELLA, V.V., WISS, T., "Potential stress on cladding imposed by the matrix swelling from alpha decay in high burnup spent nuclear fuel", Proc. IHLRWMC 2013, Albuquerque, New Mexico, 2013, ISBN 9781627486446, Curran Associates, New York (2013) 111–117.

LIST OF ABBREVIATIONS

AF   As fabricated
AFR - Away from reactor storage
AR -   At reactor storage
AGR - Advanced gas cooled reactor
BEFAST- Behaviour of spent fuel assemblies in extended storage
BWR - Boiling water reactor
CANDU - Canadian deuterium uranium reactor
CBB - Crevice bent beam
CC -   Concrete canister
CLAB - Central interim storage facility for spent nuclear fuel (Sweden)
CRP - Coordinated research project
CRUD - A deposit on fuel assembly surface (in SPAR context)
CTDT - Cladding tube deformation test
CWSR - Cold worked stress relieved
DBTT - Ductile to brittle transition temperature
DSC - Dry storage container (Canada)
EOL - End of life
FA -   Fuel assembly
FEM - Finite element modelling
FSM - Field signature method
HCC - Hydride continuity coefficient
HLW - High level waste
HTGR - High temperature gas cooled reactor
HWR - Heavy water reactor
ISFSI - Independent spent fuel storage installation
LWR - Light water reactor
MAGNOX- Magnesium no oxidation (magnesium alloy cladding, UK)
MEB - Multi element bottle (UK)
MOX - Mixed oxide fuel
MPC - Multi-purpose canister
MVDS - Modular vault dry storage
NPP - Nuclear power plant
PWR - Pressurized Water Reactor
RBMK - Russian type of graphite modulated water cooled reactor (reaktor Bolshoy Moshchnosti Kanalniy)
RCT - Ring compression test
RHCF Radial hydride continuity factor
RHF - Radial hydride fraction
RHT - Hydride reorientation treatment. Also referred to HRT by some experimenters
RIP - Rod internal pressure
RXA - Recrystalized annealed
SF (A) - Spent fuel (assembly)
SNF   Spent nuclear fuel
SRA - Stress relieved and annealed
SS -   Stainless steel
TAD - Transportation, ageing and disposal
TC -   Thermocouple

t (HM) -   Tons of heavy metal
TEM -   Transmission electron microscopy
THORP -   Thermal oxide fuel reprocessing plant (Sellafield, UK)
TSSD -   Terminal solid solubility for dissolution
TSSP -   Terminal solid solubility for precipitation
WWER -   Russian type of PWR (Wodo-Wodyanoi Energetichecki reactor)
Zr1Nb -   Zirconium niobium alloy fuel cladding (WWER)
Zry -   Zircaloy

REPORTS ON RESEARCH PROJECTS WITHIN THE SPAR-III CRP

TITLE: **Hydride Formation in Neutron Irradiated Material Under In Reactor Conditions**

COUNTRY: **Argentina**   CHIEF SCIENTIFIC INVESTIGATOR: **P. Vizcaíno**

AGREEMENT NUMBER: **15810**   COMPANY: **CNEA-CONICET**

BACKGROUND:

The present is a brief summary of the three reports completed within the framework of the SPAR III project. The following is a resume of our aims, techniques used to achieve the objectives and conclusions attained under the guiding thread of the hydride formation in neutron irradiated zirconium alloys and other reactor in operating conditions.

As is it known, under reactor operating conditions zirconium components go through transformations which affect their original microstructural and thermodynamical properties. Both concerns are starting points of many research lines for the zirconium alloys used in the nuclear power reactors.

Regarding microstructural transformations, one of the most important topics is the phase stability of these alloys. To cite a well-known case, second phase particles of zircaloy-4 shown to be unstable under neutron radiation. Since such phases play a role in the corrosion rate control, this instability became a problem for high burnup fuel claddings design. Similar observations can be made about the β–Zr phase in the Zr-2.5Nb CANDU pressure tubes alloy.

On the other hand, there are issues directly involved with thermodynamics, e.g., hydrogen behaviour and its role in the degradation processes of fuel assemblies and other zirconium alloys components, which showed to be affected by neutron radiation.

Finally, applied stresses and thermal cycling are part of these operating conditions, which can be simulated performing experiments in situ which allows testing hydrogen solubility behaviour and hydride reorientation.

In the context described above, the research topics proposed to SPAR III were aimed to improve the knowledge of these degradation processes. In this scheme, zircaloy-4 which remained more than ten years at full power operation and virgin unirradiated zirconium alloys were suited by the more improved micro analytical techniques to characterize microstructural transformations cited above.

OBJECTIVE:

To improve the knowledge of degradation processes in zirconium alloys.

RESEARCH APPROACH:

Experiments about hydrogen solubility and nature of hydride formation in neutron irradiated zircaloy were approached by differential scanning calorimetry (DSC), synchrotron X ray diffraction (SXRD) at the Brazilian synchrotron and transmission electron microscopy (TEM) techniques.

Experiments studying hydrogen solubility under stress in Zr-2.5Nb were made in situ in a beam line of the 'Advanced Photon Source', Argonne, Illinois, USA by transmission synchrotron X ray diffraction.

RESEARCH RESULTS [A1–A4]:

Regarding neutron irradiated zircaloy-4:

- After the annealing sequence, a TTSSd increased 55°C in average from the first to the last run, showing moderate dependence with the hydrogen content: from 40°C in the low hydrogen side of the interval (60-80 wppm) up to 60°C in the high hydrogen side (150-200 wppm). The precipitation temperature, TTSSp, increased 40°C in average from the first to the last run, but the tendency is strongly dependant on the hydrogen content: from 15°C in the low hydrogen side of the interval (60-80 wppm) up to 65°C in the high hydrogen side (150-200 wppm).
- Optical and TEM observations show that in irradiated material there is a wide hydride size distribution, in the interval [10 nm, 100 μm]. A sub-microscopic population higher than 13% of the observed in the optical range was estimated. These observations give support to the hypothesized interaction between irradiation defects and hydrogen atoms as the cause of the observed solubility increase. The relationship between hydrides and <c> loops was observed in TEM images.
- The classic Williamson Hall X ray diffractograms analysis show that the nature of the hydrides could be understood as strongly distorted objects which are preferably formed in a highly distorted matrix. The deep nature of the hydrides remains obscure yet, but results suggest that new designed experiments in X ray diffraction and TEM observations will reveal it.
- Modified Williamson Hall method and TEM analysis allowed characterizing the dislocation arrangement in the irradiated as received and annealed samples. The results showed to be that the techniques are complementary and the obtained results, compatible. Further experimental work will be performed to confirm the hypothesis about the irradiation defect interaction with hydrogen atoms.
- TEM and SXRD observations indicate a complete amorphisation of the zircaloy-4vsecond phase particles (SPPs) in high fluence material. It was shown that Fe diffusion depends on the irradiation dose and also on temperature: the material which remained at 205°C showed a decrease in the Fe/Cr ratio, with a maximum frequency around 1.3, being the non-irradiated Fe/Cr ratio ~ 1.85. But, the SPPs which remained at 280°C showed a Fe/Cr ratio ~0.13. Finally, the samples annealed 24 h at 600°C showed a Fe/Cr ratio ~1.5, close to the unirradiated SPPs ratio. Based on the TEM, SXRD and DSC data, we found that crystallization temperature is kinetic dependant. T_c rises from 450°C to 500°C increasing the heating rate from 5°C/min to 20°C/min. The measured heat of crystallization was 27.3±2.1 kJ/mol (Fe + Cr).

Regarding in situ experiments on unirradiated Zr-2.5Nb:

- Thermal cycling of Zr2.5%Nb pressure tubes specimens containing $\approx$100 wt ppm H between room temperature and 400°C results in the dissolution and re-precipitation of zirconium hydride, with a distinctive hysteresis between these two processes. We have found that the details of the precipitation and dissolution process depend on the actual orientation of the α-Zr grains in which hydride precipitation takes place. In situ synchrotron X ray diffraction experiments during such thermal cycles have provided information about hydride precipitation specific to the two most important groups of α-Zr phase orientations, namely crystallites having c-axes parallel (m_{Hoop}) and tilted by $\approx$20° (m_{Tilted}) from the tube hoop direction. The results indicate that hydrides precipitate at slightly higher temperatures ($\approx$5°C), and dissolve at consistently higher temperatures ($\approx$15°C) in m_{Tilted} grains than in m_{Hoop} grains.
- Application of a tensile stress along the tube hoop direction results in two noticeable effects in hydride precipitation. Firstly, it shifts hydride precipitation towards higher temperatures, at a rate of $\approx$(0.08±0.02)°C/MPa for hydrides precipitated in the m_{Hoop} grains. Secondly, it produces a redistribution of hydrogen between grains of different orientations, increasing hydride precipitation in those α-Zr grains in which an uniaxial external load is in the same direction as the direction of the grain normal. A detailed analysis of the diffracted signal shows that such redistribution occurs during the precipitation stage and results in differences in the precipitation temperatures for different grain orientations.

TITLE: **Behaviour of LWR Spent Fuel Rods During Storage and Under Accidental Impact Load Conditions**

COUNTRY:**EC**   CHIEF SCIENTIFIC INVESTIGATORS: **V.V. Rondinella**

AGREEMENT NUMBER:**16097** COMPANY: **JRC-ITU**

BACKGROUND**:**

The behaviour of spent fuel rods at various burnup under accidental load conditions is not well known. As a consequence of a transport accident, spent fuel rods could break and fuel could be released into the cask. During an accident, the fuel release from all rod breakages must not endanger the criticality safety even in the worst case of reconfiguration and accumulation of the released fuel assuming the ingress of water into the cask. Accordingly, the mechanical behaviour of the irradiated rod plays a major role when evaluating the criticality safety.

Spent fuel and other high specific activity waste forms experience significant build-up of decay damage and helium during extended storage time. This has an impact on the evolution of properties which are important to define the functionality of the fuel/waste compound, and may, in extreme cases, compromise the mechanical stability of the material. The relationship between microstructure effects and macroscopic property evolution is the key to be able to predict the behaviour of a material under a given set of conditions, hence to determine the safety of a storage concept.

OBJECTIVE:

The scope of this contribution includes the assessment and evaluation of the structural behaviour of cladding and fuel under extreme transient load conditions encountered in hypothetic transport and handling accidents. The investigation focuses on a broad understanding of the failure (brittle rupture), fragmentation, and on the quantification of the fuel amount released per rod breakage corresponding to different burnup levels and fuel types.

Additionally, the contribution aims at characterizing and understanding the evolution of the microstructure subjected to alpha decay and helium build up, in particular to verify extent and stability associated with defects saturation processes occurring at high damage level in the crystalline lattice, and determine if at very high accumulated dose level the decay damage and the radiogenic helium may affect the overall stability of the compound.

RESEARCH APPROACH:

A series of impact tests on irradiated UO_2 fuel segments has been successfully performed, followed by characterization of the debris and released fuel fraction.

Characterization of several compounds, including spent fuel, alpha doped UO_2 and ceramic waste forms, and natural analogues have been carried out to investigate mechanisms and properties evolution as a function of accumulated decay damage. In particular, accumulation of alpha decay damage and helium in the micro- and macro-structure was studied under accelerated dose rate conditions, in order to simulate damage and helium production levels corresponding to long term storage of spent fuel. Scanning and transmission electron microscopy, calorimetry, thermophysical and recovery properties measurement using various tools were performed.

RESEARCH RESULTS [A5–A8]:

The impact load tests causing fracturing of LWR rodlets with a range of burnup showed overall similar behaviour in terms of fuel fragments released. In particular, no enhanced fuel dispersion was observed for high burnup fuel, and no 'flow-out' type of behaviour was observed for low burnup fuel. These tests indicate that the fuel volume directly affected by the rod fracturing is released. The fragments had a maximum size of ~2–3 mm, and included powdered material.

The evolution of thermo-mechanical properties (thermal conductivity, stored heat, hardness, lattice swelling) and of the defect population observable in the microstructure of UO_2 was monitored as a function of accumulating alpha decay damage and corresponding helium generation. The properties showed the typical saturation behaviour corresponding to the accumulation of defects in the fuel (micro)structure. Most properties saturated at a damage level of 0.2–03 displacements per atom (dpa), corresponding to a few decades of storage for LWR fuel. Lattice swelling showed saturation around 1 dpa. The thermal properties and microstructure evolution under accelerated decay damage accumulation regimes show very similar features to the case of spent fuel.

Valuable information for proper predictions of storage behaviour of spent fuel rods will be defined and organized.

TITLE: **Interim Dry Storage of Spent Fuel in Casks**

COUNTRY: **France**   CHIEF SCIENTIFIC INVESTIGATOR: **H. Issard**

AGREEMENT NUMBER: **15894**   COMPANY: **TN International (Cogema Logistics)**

BACKGROUND:

French option for the back end of the fuel cycle is reprocessing of used fuel and recycling the fissile material, except some very specific fuel stored in vaults (dry conditions). Used fuel management solutions studied by AREVA for various countries allow for either direct transport to the reprocessing plant, or interim storage and transport after storage of used fuel. Interim storage solutions are wet storage or dry storage (DSC, metal casks or vault systems). When the decision on used fuel management has been postponed, some extension of interim storage duration is considered, therefore it becomes necessary to study used fuel and cask material behaviour and deterioration mechanisms.

OBJECTIVE:

One objective of this R&D was to review research efforts on spent fuel behaviour and Dry storage experience in casks. Particularly we were interested in the assessment of retrievability of fuel after storage for further use. A review therefore, was made of the effect of storage time/ temperatures and of loading/ drying operation on used fuel integrity. R&D programmes were also carried out on the evaluation of cask materials in long term, especially materials susceptible to degradation.

RESEARCH APPROACH:

First, investigations and tests are carried out by laboratories from French atomic energy commission (CEA) concerning creep and brittle fracture of fuel rod cladding, especially the effect of hydrogen on the embrittlement of the cladding.

Secondly, investigations and tests are carried out by AREVA TN concerning evaluation fuel during and after impact (regulatory tests required in the document IAEA SSR6).

Design and safety analysis by the cask vendor for evaluation of cask materials in long term.

RESEARCH RESULTS:

Study of used fuel behaviour and dry storage experience in casks. CEA is pursuing the PRECCI programme which includes behaviour of LWR fuels in dry storage: thermal creep, embrittlement due to hydrogen effects, function of stress, cladding material, cladding temperature and history. Investigation concerning fuel degradation by CEA on M5® cladding concluded that there is a significant impact of irradiation defect annealing which leads to an increase of cladding ductility and a decrease of the adverse effect of radial hydrides.

Concerning fuel in impact, the fuel integrity project [A9] carried out by TN and INS (UK) included fuel rods testing, with irradiated samples up to 40–50 GW·d·t(U)$^{-1}$ and the development of models. A methodology for the evaluation of the impact of irradiated fuel (transport accident) has been finalized and allow for the assessment of fuel integrity and criticality safety demonstration of the transport packages. Depending on g-load and direction of drop, axial or lateral, fuel assemblies show different level of deformation: deformation of

fuel pin array, fuel rod sliding, fuel rod bending or compression and eventually rupture. The amount of fuel material dispersion in case of cladding rupture has been measured and is limited to a few grams.

With these analysis, it is possible to determine the maximum allowable acceleration for a fuel assembly for hypothetical transport accident.

Concerning storage casks or storage modules, long term behaviour of dry storage materials and equipment have been modelled and tested; both neutron shielding ability and containment seals can be maintained by limiting the temperature.

TITLE: **Spent Fuel Performance and Research in Germany**

COUNTRY: **Germany**   CHIEF SCIENTIFIC INVESTIGATOR: **A. Jussofie**

AGREEMENT NUMBER: **16033**   COMPANY: **GNS**

BACKGROUND:

For the long term management of spent fuel, dry storage in dual purpose casks and direct disposal remain the management policy in Germany. Due to the lacking progress in developing a repository for heat generating waste in deep geological formations the likely extension of the interim storage period beyond 40 years raises issues especially regarding degradation of fuel and the functional reliability of the cask closure system.

OBJECTIVE:

- Investigation of irradiated fuel rods exposed to mechanic stress

- Review of longterm performance of lid systems bolted to the cask body and tightened by Helicoflex® metallic gaskets

RESEARCH APPROACH:

The ongoing trend to increase the target burnup will be reflected by an increasing number of high burnup SFAs which have to be transported after their long term intermediate storage to their final destination. The prerequisite for loading SFA with high burn-up is the evidence of maintaining the criticality safety even under accidental transportation conditions acc. to the international transport regulations. Accordingly, the amount of spent fuel released into the cask due to rod breakage is an issue which has to be addressed by experimental investigations. Therefore, two experimental approaches, a bending test using fuel rod segments with one end fixed and the other end free as well as a hammer drop test on segments with both ends fixed, were initiated in collaboration with power utilities and research institutions (ITU, Studsvik) in order to quantify the amount of fuel released in case of rod breakage in consideration of a wide burnup range.

In order to comply with the requirements of the guidelines established for the dry interim storage of irradiated fuel assemblies in casks, the safe enclosure of the radioactive inventory must be guaranteed. The application of dual purpose casks with metallic gaskets is approved for a 40 year storage period. If lifetime extension beyond 40 years is necessary, the leak tightness of the cask closure system has to be proven for an extended storage period with subsequent transportation and under accident conditions. Operational reliability is estimated on the basis of long term tests with metallic gaskets under static load conditions at different temperatures in order to examine the changes of the load-compression behavior of metallic gaskets versus time and temperature.

RESEARCH RESULTS

No significant variations in the amount of fuel released were observed using a burnup range from 20 to 75 GW·d·t(HM)$^{-1}$ irrespective of the experimental approach applied. For all specimens tested the fuel release per breakage was less than 2 g. No evidence of an increased

fuel release due to high burnup was found. In order to reach a level of significance (p < 0,001) a maximum release of 10 g fuel per breakage has to be assumed.

The study to assess the residual load values for metal gaskets after a thermal ageing period of 100 000 h has been done up to 75 000 h so far in cooperation with CEA, CRIEPI and GNS. It can be concluded that the initial temperature level during cask loading has a large influence on the admissible application period of a gasket. For gasket temperatures below 120°C, a storage period of more than 100 years seems to be feasible. Moreover, the continuous leakage rate measurements during gasket loading and unloading that were performed by BAM in Germany with gaskets partly exposed to holding times since 02/2009 at different temperatures show that the gasket has the ability to remain leak tight even at a constantly high temperature level of 150°C, which is above the maximum operational temperature of the gasket directly after loading.

TITLE: **Spent WWER–440 fuel performance under long-term storage conditions**

COUNTRY: **Hungary**   CHIEF SCIENTIFIC INVESTIGATOR: **F. Takáts**

CONTRACT NUMBER: **15821**   COMPANY: **TS Enercon Kft**.

BACKGROUND:

Paks Nuclear Power Plant is the only NPP in Hungary. It has four WWER–440 type reactor units. The fresh fuel is imported from Russia so far. The spent fuel assemblies were shipped back to Russia until 1997 after about 6 years cooling at the plant. A dry storage facility (MVDS type) has been constructed and is operational since then. By 1 January 2008, there were 5107 assemblies in dry storage.

OBJECTIVE:

- Collection of data on wet AR storage of spent fuel from the NPP Paks:
  - Collection and systematic evaluation of data;
  - Measurements and visual control of storage pool component characteristics;
  - Review questions related to the storage of defective fuel or fuel debris.

- Collection of data on dry AFR(OS) storage at Paks NPP:
  - Collection and systematic evaluation of data;
  - Report results from the MVDS surveillance programme;
  - Review the re-licensing criteria for the storage facility.

RESEARCH APPROACH:

Aiming to evaluate physical and chemical conditions in the storage pools the following parameters are monitored: temperature (^{o}C), pH, optical transparency (%), chemical composition (Cl, H_3BO_3), isotope specific activity (Bq/kg).

The overall limitations (t < 70°C in case of refuelling operations, < 60°C, in case of storage; H_3BO_3 > 12 g/kg) are continuously controlled. Chemical conditions are measured and corrected if necessary minimum daily during refuelling operations, and weekly during storage, except the boron concentration monitored continuously.

As routine measurements the following activity data are measured:

- Corrosion products (^{51}Cr, ^{54}Mn, ^{59}Fe, ^{58}Co, ^{60}Co, ^{110m}Ag);
- Volatiles (^{131}I, ^{132}I, ^{133}I, ^{134}I, ^{135}I,);
- Non-volatile components (^{137}Cs, ^{134}Cs, ^{138}Cs, ^{139}Ba, ^{140}Ba, ^{91}Sr, ^{92}Sr, ^{85}Rb, ^{88}Rb, ^{89}Rb);
- Other components (^{187}W, ^{56}Mn, ^{99}Mo, ^{122}Sb, ^{124}Sb, ^{24}Na, ^{42}K, ^{95}Nb, ^{95}Zr, ^{97}Zr, ^{140}La).

The measurements of activity are carried out, as a rule, once a month; during refuelling they are done more frequently.

RESEARCH RESULTS:

The conclusions drawn are similar to those of the earlier research timeframe, namely:

- On the basis of the measured chemical characteristics, the water quality remains in stable condition. The activity levels can be managed safely using the pool water purification system;

- The main sources of activity in the storage pools are surface and water contaminants. Corrosion during storage period is negligible;
- Dry storage experience is good; temperature of the stored fuel is low, as confirmed by the benchmarked calculations. There were some storage tubes reopened and no unexpected observations were made;
- During the interim storage of bottled damaged spent fuel in the pools no unexpected events were observed, the fuel is being prepared for shipment.

TITLE: **Long term Integrity of Spent Fuel and Construction Materials and Behaviour of Components for Dry Storage Facilities**

COUNTRY: **Japan**   CHIEF SCIENTIFIC INVESTIGATOR**: T. Saegusa**

AGREEMENT NUMBER: **15853**   COMPANY**: CRIEPI**

BACKGROUND:

In Japan, two dry storage facilities at TEPCO and JAPCO sites have been in operation since 1995 and 2002 respectively. The TEPCO dry storage facility was damaged by a Tsunami attack on 11th March 2011. The casks stored in the facility have since been moved to an onsite temporary cask custody area; after confirmation of the integrity of casks. On the other hand, the Tsunami did not attack the dry storage facility at the JAPCO site. The integrity of the storage building and the casks were maintained. In addition, an off-site centralized dry storage facility has been constructed at Mutsu City. Operation of the storage facility is pending a safety re-examination against new safety regulations. Its final storage capacity will be 5000 t(U) and the storage period is up to 50 years. To support storage operations, it is therefore necessary to obtain and evaluate data on the integrity of spent fuels and cask construction materials during long term dry storage.

OBJECTIVES:

Construction materials for dry storage facilities:

- To evaluate long-term reliability of welded stainless steel canisters under stress corrosion cracking (SCC) environment, including the critical salt density deposited on the canister to initiate SCC, monitoring, prevention, and the mitigation method of SCC;
- To detect and analyze the cover gas leak from canisters;
- To evaluate integrity of sealability of metal gasket under long term storage;
- To evaluate influence of the vibration on sealing performance of the ageing gasket.

RESEARCH APPROCH:

The integrity of construction materials used in metal and concrete casks will be verified through a combination of experimental and computational analysis. This includes: 1) SCC evaluation method; 2) Long term sealability test of lid structure; 3) Evaluation of sealing performance of metal gasket under the transport condition considering ageing; 4) Detection method of helium gas leak from canister.

RESEARCH RESULTS:

For the chloride induced SCC on the canister surface. Scenarios to maintain the confinement function of the canister made of the normal UNS S30403 SS materials during storage period were established by keeping the salt density on the canister surface below the critical salt density to initiate SCC or by controlling the crack propagation if any SCC initiated. Furthermore the feasibility of the scenarios were demonstrated by tests defining the critical salt density (0.8 $g \cdot m^{-2}$) for the SCC initiation and by tests of crack propagation based on metrological data of representative coastal sites in Japan [A10–A13].

The welding process results in high tensile residual stresses and cold working in the surface and near surface of the canister material. Surface treatment techniques such as shot peening (SP), laser shot peeing (LSP) and low plasticity burnishing (LPB) can mitigate or impede SCC by inducing compressive residual stresses into the surface material [A14].

Two kinds of cask sealing arrangement, which are part of full scale metal casks, have been tested for more than 19 years at constant temperature. Very reliable containment performance was demonstrated. Moreover, by applying the Larson Miller parameter to the results obtained, and taking into account the decay heat of the spent nuclear fuel over time, provides an indication of the long term sealing performance. After the test had ended, all of the lids were opened and the degradation data of the gaskets were obtained. It was confirmed that it is very important to tighten the lid bolts until the flange surface of the lid contacts with the flange surface of cask body [A15].

Numerical methodology to evaluate sealing performance of metal gasket after long term usage was proposed and applied to evaluation of the opening displacement of the cask lids during sea transportation. The evaluated opening displacement of the primary and secondary lids was less than the estimated spring back distance (0.09mm). Thus the sealing performance will not be lost due to lid opening by the acceleration measured during the sea transportation.

The leakage of helium gas from the canister can be detected by monitoring the change of ΔT_{BT} which is defined as the difference in the temperatures between the bottom and top on the canister surface [A16].

TITLE: **Research on Integrity of High Burnup Spent Fuel Under the Long Term Dry Storage**

COUNTRY: **Japan**   CHIEF SCIENTIFIC INVESTIGATOR**: K. Kamimura**

AGREEMENT NUMBER: **13081**   COMPANY**: JNES**

BACKGROUND

In Japan, spent fuels will be reprocessed as recyclable energy source at a reprocessing plant. The first commercial plant is under construction. It is necessary that spent fuels should be stored in the independent interim storage facilities (ISF) until reprocessing. Mutsu interim spent fuel storage facility (Recyclable Fuel Storage Company) was permitted for construction in May 2010, and the construction has almost been finished up to now. JNES has a mission to support the regulatory body by researching the data of technical standard and regulation. Investigating of spent fuel integrity during long term dry storage is one of them.

JNES had concerns of high burnup fuels from a view point of:

- Increase of hydrogen concentrations in cladding;
- Increase of hydrides precipitated radially;
- Fuel integrity or ductility effect on potential criticality under accident condition during storage and transportation.

OBJECTIVES

Objectives were to acquire the following behaviour data by dynamic load impact tests on high burnup spent fuel rods of BWR and PWR and to improve the guidance of regulation of spent fuel storage and transportation.

(1) The limit of load and strain for high burnup fuel in the cask drop accident.

(2) The amount of deformation of high burnup fuel rods under dynamic load impact.

(3) The amount of fuel pellet material released from fuel rods under dynamic load impact.

RESEARCH APPROACH

Zry-2 (BWR) and MDA (PWR) claddings and segmented rods of around 55 GW·d·t(U)$^{-1}$ irradiated fuel were used for the tests. Elemental mechanical test of cladding and dynamic load impact test of fuel rod were carried out.

   (1) Elemental mechanical test of cladding

Elemental mechanical tests consist of tensile and ring compression tests. Axial tensile yield strength, failure strain, ring compressive strength, and failure fattening ratio were acquired. Maximum strain rate for the tests was 10 per second. The tests were carried out at room temperature as conservative condition from a viewpoint of cladding brittleness.

   (2) Axial dynamic load impact test on BWR fuel rod

Collision weight mass was 3.5 kg same as whole fuel rod weight. Collision speed was a main parameter which varied from 3.7 to 12 m·s^{-1}. Two types of specimen were used. One is fuel section (hard bonding material), and the other is upper plenum part.

(3) Lateral dynamic load impact test on BWR fuel rod

Specimen types were hard bonding material, loose bonding material, and hydride reorientation treatment material with dummy pellets. Weight mass was 0.6 ~ 2.6 kg. Collision speed was 4 and 8 m·s^{-1}.

(4) Lateral dynamic load impact test on PWR fuel rod

Specimen types were as irradiated rodlet and hydride reorientation treatment cladding with dummy pellets. Weight mass was 3 kg. Collision speed was 10.9 at ~12.9 m·s^{-1}.

RESEARCH RESULTS [A17–A20]

(1) Results of elemental mechanical test of cladding

Results of dynamic tensile test (BWR & PWR)

With increase of strain rate, UTS increased and contrary total elongation decreased. Mechanical characteristics of unirradiated Zry-2 and MDA were different, but those of irradiated ones were similar.

Results of Dynamic Ring Compression Test (BWR & PWR)

With an increase in compression speed (<100 mm·s^{-1}), ductility decreased in all claddings.

Hydride reorientation treatment condition of 300 C, 70 MPa, 30 C·h^{-1} had no effect on crosshead displacement ratio; i.e. ductility index of BWR cladding. Influence of hydride reorientation treatment condition of 300 C, 115 MPa, 30 C·h^{-1} was clearly observed PWR cladding ductility.

(2) Axial dynamic load impact test results on BWR fuel rod

Cladding breakage was occurred only in the case of 12 m·s^{-1}. Bowing, but not failure was occurred in the cases of 9 m·s^{-1} and upper plenum. Pellet dispersion was observed in the case of 12 m·s^{-1}.

(3) Lateral dynamic load impact test result on BWR and PWR fuel rods

Lateral dynamic load impact test result showed that strength of fuel rods with pellets was one order higher than that of cladding without pellets.

(4) Dispersed pellet amount and particle size distribution

In BWR fuel rod samples, the amount of dispersed pellet at the breakage by axial dynamic load impact test was equivalent to approximately two pellets and about 60 % of those were very fine powder. In case of lateral load impact test the amount was equivalent to approximately three pellets and about 40 % were very fine powder.

In PWR fuel rod sample, the amount of dispersed pellet was smaller amount of 1.4 g.

It is thought that the cause of the difference between BWR and PWR rod is based on the difference in test apparatus and the difference of the pellet irradiation condition and pellet cladding contact condition. It might be caused by the difference of microstructure between BWR and PWR fuel pellets.

TITLE: **Long Term Integrity of PWR Spent Fuel in Dry Storage**

COUNTRY: **Republic of Korea**   CHIEF SCIENTIFIC INVESTIGATOR**: J-W. Choi**

AGREEMENT NUMBER: **15964**   COMPANY**: KAERI**

BACKGROUND

The newly established organization KRMC (Korea radioactive waste management corporation) which is responsible for all kinds of radioactive waste generated in the Republic of Korea launched the PWR spent fuel dry storage research project in June 2009. This project has objectives to develop a storage system and evaluate the integrity of PWR fuel in dry storage.

The project consists of three steps. At first step, it would develop own degradation models by referring to pre-exist good models and develop the hot test scenarios. Second step, test facilities would be constructed and used for testing the degradation behaviour in each mechanisms and in total. As a final step, total evaluation code would be developed by integrating each degradation model produced in the first step and the test data produced in the second step. All the activities would be summarized into a report and applied to licensing work.

The Republic of Korea PWR spent fuels have unique characteristics of various fuel types (array type, clad material) and high capacity factor (maximum usage of fuel which is bad for integrity). These facts could impact on the research ranges of experimental data needed for degradation evaluation. In this research, spent fuel performance data concerning long term dry storage will be analysed and the major degradation mechanisms like creep and hydride behaviour will be studied and proposed for Korean PWR spent fuels.

OBJECTIVES:

- To acquire hot test data on spent fuel;
- To characterize Korean PWR spent fuel properties;
- To develop the degradation mechanism models for spent fuel integrity evaluation;
- To analyse spent fuel performance data in long-term dry storage.

RESEARCH APPROACH

Year 1

Undertake a literature survey on foreign operating experience and research into spent fuel degradation mechanisms.

Year 2

Develop degradation models for spent fuel integrity through evaluating cladding creep, hydride reorientation, delayed hydride cracking, cladding and pellet oxidation etc.

Year 3–5

Undertake hot tests evaluating the major degradation mechanisms in dry storage.

RESEARCH RESULTS

KAERI has deployed the techniques of tube and ring tests to evaluate the impact of hydride reorientation [A21].

A test vessel DRYSIM has also been manufactured and is undergoing performance tests at the manufacturers prior to be being loaded with spent fuel and monitored in at reactor storage pool. The vessel will be used to support the deployment of dry PWR storage in the Republic of Korea, because of lead time to get a licence to undertake dry storage the tests are being done in wet storage. This has adds complexity to the project.

TITLE: **WWER–440 Spent Fuel and Structural Materials Performance in Jaslovke Bohunice Wet Storage Facility**

COUNTRY: **Slovakia**   CHIEF SCIENTIFIC INVESTIGATOR: **Ľ.Kupča**

CONTRACT NUMBER: **15705**   COMPANY: **VUJE Inc.**

BACKGROUND:

Spent fuel from four units of WWER–440 operated in Slovak Republic as well as the fuel from stopped two units of NPP V-1 is stored in wet storage condition in spent fuel storage interim facility (SFIS) in JAVYS Jaslovske Bohunice. According to the fact that was changed the philosophy of storage from short (ten years) to long term (50 years), there was need to enlarge the capacity of SFIS storage.

OBJECTIVE:

The long term storage of spent fuel needs the monitoring of safety related SFIS component corrosion stability. That is why was prepared and realized the surveillance specimen programme for Jaslovské Bohunice spent fuel interim storage.

Except this there was designed in VUJE the sophisticated project of special remote controlled apparatus which enables the control of spent fuel by several NDT methods, as well as the destructive methods application for individual spent fuel assemblies in special conditions by demand.

RESEARCH APPROACH:

Based on the VUJE long term experience in the field of NPP WWER components corrosion monitoring, was designed the special surveillance specimen programme realized in Jaslovske Bohunice SFIS pools.

Basic philosophy of this monitoring program is to support the reliable operation of SFIS during its life time. Very important issue is to prepare for corrosion stability analyses the special samples made from original archive structural materials of SFIS components.

RESEARCH RESULTS:

The main goals of actual stage of this long-term project are:

- Analyses of the seventh set of specimens No.116/2 from ATABOR steel after 7, 5 eventually 4 years of exposition in the Bohunice spent fuel interim wet storage environment using the following methods:
  - Documentation of sample surfaces after removal from storage pool;
  - Microstructure evaluation for the base and weld metal;
  - Analysis of corrosion media influence to the structure of ATABOR steel using the light microscopy;
  - Scanning electron microscopy and microanalysis of exposed samples;
- The optimization of database structure on the base of experience from the second stage of SPAR-III contract;
- On the basis of the analysis results to prepare the new optimized set of specimens prepared from the specific heat of ATABOR steel.

Present situation is:

The second phase of the contract renewal between IAEA and VUJE was successfully finished. Planned activities were the complete analysis of the sixth set of specimens after 7, 5 eventually 4 years of exposition in the wet storage environment using the following methods:

- Documentation of samples surfaces after removal from storage pool (finished);
- Microstructure evaluation for base and weld metal (finished);
- Analysis of influence of corrosion media to the structure of ATABOR steel using the light microscopy (finished);
- Scanning electron microscopy and microanalysis of exposed samples (finished).

We hope that this project will continue in the next year with detail analysis of the seventh set of exposed samples.

On the base of the analysis results there was prepared the new optimized set of specimens from the specific heat of ATABOR steel used as the structural material for the new type of compact spent fuel racks. This set of specimens was added to the previous sets for long term exposition in the SFIS monitoring system.

The realization of planned programme was fulfilled according to the schedule.

TITLE: **Spent Fuel Behaviour During Interim Storage**

COUNTRY: **Spain**   CHIEF SCIENTIFIC INVESTIGATOR: **P. Zuloaga**

AGREEMENT NUMBER: 15719   COMPANY: **ENRESA**

BACKGROUND:

According to the '6th General Radioactive Waste Plan', spent fuel in Spain shall have to be gathered in a centralized temporary storage (CTS) for some decades prior to any further decision. The CTS technology has already been chosen, namely, a vault type building based on dry storage. ENRESA is actively supporting, alone or with other partners, a number of R&D programmes on interim dry storage, mostly concerned about high burnup fuel issues and new cladding materials.

OBJECTIVE:

Review of spent fuel data relevant for future storage in Spain

Perform destructive and non-destructive examinations on irradiated and non-irradiated fuel rods relevant to Spanish spent fuel management.

RESEARCH APPROACH:

Among the programmes initiated in the last years (finished or about to be finished) one may highlight the following ones:

- Isotopic measurements on high burnup fuels: up to 75 GW·d·t(U)$^{-1}$ PWR and 53 GW·d·t(U)$^{-1}$ BWR peak values;
- Mechanical tests on high burnup PWR (ZIRLO) cladding and BWR (Zry-2) cladding samples;
- Mechanical tests on unirradiated ZIRLO rods. Influence of hydrides content;
- Modelling of mechanical tests with unirradiated claddings;
- Interim storage creep modelling;
- Burnup measurement equipment;
- Fuel database.

RESEARCH RESULTS [A22–A23]:

Spent fuel management is an important issue for fuel cycle costs. Any method for optimizing the storage and transport of spent fuel produces increasing profits to nuclear industry. Many of the limits in the regulatory guidance related to spent fuel have not followed the evolution of increasing fuel burnup discharge and designs. An example of this is the criticality analysis with burnup credit for reactivity determination based on isotopic calculations. These calculations involve high uncertainties. A reduction of uncertainties, and the associated conservatism, can be obtained through experimental measurements, which help closing knowledge gaps and validating calculation codes. ENRESA and her partners have obtained isotopic measurements on PWR (high burnup and high enrichment samples) for isotopes representative of shielding, gas production, reactivity, residual heating and burnup determination. A different approach has been followed concerning BWR samples. Although the BWR samples burnup used in these tests is lower, the aim is to highlight the void effect and the different neutron spectra of a BWR compared to a PWR. PWR samples have been

included in the NEA database (SFCOMPO). BWR measurements will follow a similar objective.

Concerning mechanical testing of irradiated materials, five high burnup PWR (ZIRLO) samples were creep tested and characterized to investigate the behaviour of advanced cladding materials under dry storage conditions. The results were reported in the previous SPAR II report. The results have been consistent with the expected behaviour from reference CWSR material, Zry-4. The higher hoop stress and temperature, the greater creep deformation. The samples kept significant ductility during tests. Only one sample had a leak after 17% engineering strain of the tube. Metallographic tests performed afterwards showed significant hydride reorientation (due to cooling after test procedure). However, no specimen failure was observed during cool down. Hardness measurements showed partial recovery in some of them.

Another set of five BWR (Zry-2) samples were creep tested and characterized. The test matrix was chosen to be easily comparable to PWR samples. Creep tests showed lower creep rates for RX material than those obtained in the past for ZIRLO, consistent with published data. In order to reorient different fractions of hydrides, special procedures for cooling have been implemented at the end of each test. The radial fraction increased with the stress and some degree of reorientation has been observed even at 70 MPa hoop stress, consistent with published data. Axial tensile tests show the effect of the irradiation damage annealing on mechanical properties.

Other tests on unirradiated ZIRLO rods have been performed to obtain the mechanical properties and behaviour of this type of cladding, at ambient temperatures and at other temperatures representative of in pile or storage conditions. A cohesive fracture model has been chosen for its modelling. A hydrogen charging method has been developed to show the effect of hydrides. A method of hydrides reorientation was developed to obtain the influence of reoriented hydrides on the cladding mechanical behaviour. Mechanical tests included axial tensile, ring tensile and ring compression tests. The results have let the researchers develop an iterative model that is also considered for irradiated samples, and a failure criteria proposal has been developed.

Another programme consists in developing a cladding mechanical model for interim storage, considering the few codes actually adapted to this step. A commonly used code, such as FRAPCON, is being adapted for this. The mechanical model included in the code has been shown not to be suitable for interim dry storage. So, a simpler code has been included in it to evaluate the cladding creep during interim storage, based on open data. Preliminary results confirm that, by keeping the allowed limits imposed on ISG-11 Rev. 3, most fuel is not expected to be damaged due to creep, including high burnup fuel. The same team is currently developing a fuel and cask thermal model to be coupled to the mechanical code described above.

ENRESA is also supporting the development of a burnup measurement equipment, in order to reduce uncertainties on measurement results, which will be helpful to confirm burnup reactor records. A measurement campaign is expected in the near term.

Finally, ENRESA has worked closely with NPPs to develop an agreed fuel database. Although not directly related to R&D, this database will add much more information about fuel currently used in Spanish NPPs which, in turn, will help developing further R&D programs directed at more specific issues.

TITLE: **Corrosion Inhibition Studies in Support of the Long Term Storage of AGR Fuel**

COUNTRY: **UK** CHIEF SCIENTIFIC INVESTIGATOR: **J. Kyffin**

AGREEMENT NUMBER: **N/A** COMPANY: **Sellafield Ltd.**

BACKGROUND:

Thorp receipt and storage (TR&S), Sellafield, UK has been chosen as the optimum facility to be used for the long term, interim wet storage of Advanced Gas Reactor (AGR) fuel.

TR&S is currently a demineralised water pond due to a materials compatibility issue. However, a proportion of AGR spent fuel is known to be susceptible to corrosion through inter-granular attack (IGA). To avoid this, the chosen interim storage regime for AGR fuel is sodium hydroxide dosed pond water to pH 11.4. Some fuel has been safely stored in these conditions for 24 years in other Sellafield fuel ponds.

For the period until the materials that are incompatible with pH 11.4 have been removed from the pond, a temporary pond water chemistry will be introduced to offer some corrosion protection. Lead container studies have been used to evaluate sodium nitrate (10 ppm) and 'Low Dose' sodium hydroxide (pH 9). 'Low Dose' conditions have been chosen for implementation.

OBJECTIVES:

- To underpin and implement temporary pond water chemistry for AGR storage;
- To develop and deliver a programme of work to support the transition and safety case delivery for interim storage of AGR fuel.

RESEARCH APPROACH

The temporary pond water chemistry for AGR storage is underpinned by lead container studies to evaluate the impact of increasing chloride concentrations on the ability of pH9 sodium hydroxide to inhibit IGA corrosion. Materials compatibility corrosion trials are also being performed.

The development of a programme of work to support the transition to interim storage of AGR fuel is based on identified gaps in the outline safety case that has been agreed with the regulatory community. The principle areas of interest are: increase confidence in the storage regime; demonstrate that corrosion models are applicable to cladding after higher irradiation and to changes in fuel design; understand the efficacy of corrosion inhibition at higher temperatures than previously studied; characterise failed fuel; and develop methods for fuel condition monitoring.

RESEARCH RESULTS [A24]:

- The principle result from the lead container studies is that sensitised AGR fuel has been stored in pH 9 sodium hydroxide with 1 ppm chloride without evidence of cladding failure for >800 days. The study has been expanded to study chloride concentrations up to 2.5 ppm;
- New results for activities identified on the programme of work to complete the technical basis for AGR fuel storage are not yet due. However, current research activities include:

- Post irradiation examination of high irradiated and long dwell cladding;

- Scoping experimental work to support development of novel fuel inspection / corrosion sensing techniques, including ultrasonic testing, electrochemical noise sensors, in pond inspection of irradiated brace material;

- Theoretical studies of the effect of increased storage temperatures on the ability of sodium hydroxide to inhibit IGA corrosion and the evolution of uranium oxide fuel exposed to pond water conditions;

- Preparatory activities for a programme of post storage examination of long stored intact and failed fuel, and more recent, shorter stored higher burnup fuel.

TITLE: **US Industry Spent Fuel Management (R&D and Operating Experience)**

COUNTRY: **USA**   CHIEF SCIENTIFIC INVESTIGATORS: **A. Machiels**

AGREEMENT NUMBER: **15749**   COMPANY: **EPRI**

BACKGROUND**:**

In the USA, it is highly likely that commercial spent nuclear fuel will need to be stored at the reactor sites for many decades until centralized interim storage or final disposal becomes available. Given the economic and worker dose involved in transferring spent fuel from wet (spent fuel pools) to dry storage, it would be desirable to continue to store and eventually ship spent fuel in the original dry storage systems rather than incurring the additional economic and radiological penalties associated with repackaging. Currently available information on long term ageing have allowed several utilities to obtain license extensions for their existing dry storage installations for up to 60 years after initial fuel loading. Given the uncertainty about the eventual readiness of options for ultimate disposal, it may be necessary to store spent fuel at reactor sites for periods well beyond 60 years. In addition, risk information assessment of criticality risks during transportation, including improvements in criticality methods (burnup credit), are being developed to provide more rational bases for future improvements in operations and regulations.

OBJECTIVE:

1. To identify the needs for enhancing existing technical bases for extended storage and transportation of commercial spent nuclear fuel.

2. To initiate work on high-priority ageing management topics.

3. To advance the state of the art in assessing criticality safety for wet storage and transportation applications.

RESEARCH APPROACH:

1. EPRI established the Extended Storage Collaboration Program (ESCP) in 2009 to investigate ageing effects and mitigation options for the extended storage and transportation of spent nuclear fuel. An ESCP's 'International Subcommittee' has developed a summary of the regulatory status, operational status, fuel inventory, and technical gaps.

2. Work has been initiated toward the development of a chloride induced stress corrosion cracking susceptibility assessment for austenitic stainless steel canister based storage systems. Inspection of canisters deployed at power plants has been initiated.

3. Probabilistic assessments of (a) a generic bolted storage system and (b) a nuclear criticality event during transportation by rail of a spent PWR package have been completed. Criticality benchmarks based on PWR operational data have been established for use in criticality applications using full burnup credit

RESEARCH RESULTS [A25–A29]:

Detailed results of the research are available in EPRI reports that are downloadable from the EPRI web site (refer to EPRI report numbers).

1. For extended storage, two areas stand out as being of high importance for potential degradation:

Hydrogen embrittlement of fuel cladding

Corrosion of welded canisters

From a broader perspective, data gaps deemed to be of high importance were identified for each component of the dry storage system. For fuel, the concern is the hydride effects on fuel cladding and retrievability after storage; for the canister, general canister corrosion and stress corrosion cracking of canister closure welds (particularly in marine environments); for the bolted closure, degradation of bolts and seals; and for the over pack, concrete degradation. Several cross cutting needs, such as thermal modelling, have been identified and been generally assessed to be of high importance.

2. A roadmap has been developed with regard to assessing the stress corrosion cracking susceptibility of stainless steel canisters to marine environments. By the end of 2013, an updated literature survey and a failure mode and effects analysis (FMEA) have been completed in draft form.

3. Within the limits of cases analyzed, there are no credible combinations of accident events, accident locations, and fuel misloading or reconfiguration that would result in a critical configuration during the transportation of spent nuclear fuel. The non-mechanistic criticality evaluation performed in as loaded or as designed configuration can be considered the bounding case for all conditions of transportation for spent PWR fuel because this case bounds normal and hypothetical accident cases that can credibly exist for spent fuel transportation packages. Criticality during hypothetical transportation accidents should be a regulatory non-issue, given that misallocation of regulatory requirements can lead to greater overall risks, specifically by increasing the number of shipments if overly restricting spent-fuel transportation payloads.

TITLE: **US Government Spent Fuel Research Experience**

COUNTRY: **USA** CHIEF SCIENTIFIC INVESTIGATORS: **R. Einziger**

AGREEMENT NUMBER: **15841** COMPANY: **NRC**

BACKGROUND:

1- Data to determine effects of hydride reorientation in zirconium based cladding. The 'Division of Spent Fuel Storage and Transportation' interim staff guidance (ISG)–11 Rev 3 ('Cladding Considerations for the Transportation and Storage of Spent Fuel') establishes maximum cladding temperatures for the storage and transportation of low burnup spent fuel (<45 GW·d·t(HM)$^{-1}$). While the limit may be applied to the storage of high burnup fuel, it is stated that transportation of fuels stored at or above this limit would be considered on a case by case basis due to additional technical concerns about the potential effects of hydride reorientation during storage on the cladding's mechanical properties. Significant effects of reorientation might compromise the ability of the cladding to support all regulatory requirements. The US NRC, in cooperation with the EPRI, and the US DoE established a programme at the ANL to generate data that could be used by each programme sponsor to independently determine the ramifications of reorientation on cladding behaviour.

The ANL programme has two major differences from other national programmes: 1) It subjects samples to a reorientation treatment that has both decreasing temperature and stress typical of what might be seen during vacuum drying for dry storage; 2) After hydride reorientation, the cladding samples are subjected to limited displacement tests at typical transportation temperatures to determine the cladding residual ductility. From these data, a three axis map of hydrogen content, peak stress, and displacement test temperature can be developed. These data will show regions where ductility is preserved, and other regions where cladding cracks dominate. This map can be compared to potential stresses and hydride levels in a variety of spent fuel types to determine potentially adverse behaviour during transport.

2- Analysis of effects of high burnup fuel properties on containment source term. NUREG/CR-6487 and ISG–5 provide guidance on source terms to use when evaluating the ability of spent fuel storage casks to meet containment regulations in 10 CFR Part 72. The current guidance is intended to be bounding and is based on the properties of lower burnup (<45 GW·d·t(HM)$^{-1}$) fuel. The current guidance for the number of failed fuel rods is the same for both storage and transportation casks, while in fact the normal and accident conditions are quite different.

Currently fuel is being driven to much higher burnup (current limit is 62.5 GW·d·t(U)$^{-1}$ peak rod average) that has changed the properties of the fuel. The change in the mechanical properties of the cladding will increase the potential for multiple fracture sites in a rod. The formation of a fuel rim at higher burnup may change the propensity of the fuel to fracture under impact and the resulting particulate size distribution. Previous analysis accounts for fuel fracture that occurs during an accident event and removal of particulates from the cask cover gas prior to the gases release from the cask. This project continues to re-evaluate the particulate release fractions using high burnup fuel properties. Uncertainties in the release fractions due to uncertainties in the fuel properties data base are also evaluated.

3- Behaviour of storage system components exposed to external conditions or postulated events. The United States government has numerous ongoing projects to study technical issues related to the long term storage system behaviour. Representative issues include coastal

salt spray corrosion of canisters, high temperature behaviour of metal and polymer seals, fuel pellet swelling effects on the cladding stress and behaviour during accidents and in extended storage. Since the start of this work additional issues such as fuel rod vibration fatigue during normal transport and aging management during extended storage have arisen. All these issues have one thing in common they must be addressed to determine that the storage and transportation meet the safety regulations.

OBJECTIVE:

1. Obtain data to determine the effects of hydride reorientation in zirconium based cladding.
2. Analyze the effects of high burnup fuel properties on containment source term.
3. Determine the behaviour of storage system components exposed to external conditions or postulated events.

RESEARCH APPROACH:

The NRC does not do research to solve issues, but rather to determine if there is a regulatory issue. As a result there is no intent of doing sufficient testing to answer questions with a certain degree of quantized uncertainty. Research takes the form of gathering and interpreting of laboratory data, and modelling analysis, depending on the nature of the issue. The method used to approach each issue can be found in the individual documents listed in the research references.

RESEARCH RESULTS:

- Hydride reorientation [A30];
- Vibration testing [A31];
- Drying [A32–A34];
- Welded storage canisters chloride induced stress corrosion cracking [A35–A37];
- Behaviour of cask seals [A38–A40];
- Ageing management [A41].

BIBLIOGRAPHY TO THE ANNEX

[A1]   VIZCAÍNO, P., FLORES, A.V., BOZZANO, P.B., BANCHIK, A.D., VERSACI, R.A., RÍOS, R.O., "Hydrogen solubility and microstructure changes in zircaloy-4 due to neutron irradiation", Journal of ASTM International, Vol. 8, No 1, Paper ID JAI102949, West Conshohocken, Pennsylvania, (2011).

[A2]   SANTISTEBAN, J.R., VICENTE-ALVAREZ, M.A., VIZCAINO, P., BANCHIK, A.D., VOGEL, S.C., TREMSIN, A.S., VALLERGA, J.V., MCPHATE, J.B., LEHMANN, E., KOCKELMANN, W., 'Texture imaging of zirconium based components by total neutron cross-section experiments' Journal of Nuclear Materials, Vol. 425, Issues 1–3, 218–227, (2012).

[A3]   VICENTE-ALVAREZ, M.A., SANTISTEBAN, J.R., VIZCAINO, P., FLORES, A.V., BANCHIK, A.D., ALMER, J., 'Hydride reorientation in Zr2.5%Nb studied by synchrotron X-ray diffraction' Acta Materials, Vol. 60 Issue 20, 6892–6906, (2012).

[A4]   VIZCAINO, P., SANTISTEBAN, J.R., VICENTE-ALVAREZ, M.A., BANCHIK, A.D., ALMER, J., 'Effect of crystallite orientation and external stress on hydride precipitation and dissolution in Zr2.5%Nb', Journal of Nuclear Materials, Vol. 447, Issues 1–3, 82–93, (2014).

[A5]   RONDINELLA, V.V., WISS, T., PAPAIOANNOU, D., NASYROW, R., Studies on nuclear fuel evolution during storage and testing of used fuel response to impact loadings, PSAM11-ESREL 2012, June 25-29, 2012, Helsinki; Vol. 1, 3171-3179, IAPSAM & ESRA, ISBN: 978-1-62276-436-5, (2012).

[A6]   MAUGERI, E., WISS, T., HIERNAUT, J-P., DESAI, K., THIRIET, C., RONDINELLA, V.V., COLLE, Y-J., KONINGS, R.J.M. ., Helium solubility and behaviour in uranium dioxide, J. Nucl. Mater. 385, 461, (2009).

[A7]   AHN, T., RONDINELLA, V.V., WISS, T., Potential stress on cladding imposed by the matrix swelling from alpha decay in high burnup spent nuclear fuel, Proc. 14th International High-Level Radioactive Waste Management Conference (IHLRWMC), Albuquerque, New Mexico, April 28—May 2, Paper 6830, (2013).

[A8]   RONDINELLA, V.V., WISS, T., MAUGERI, E., COLLE, J-Y., Effects of helium build-up on nuclear fuel evolution during storage, Proc. 12th International High-Level Radioactive Waste Management Conference (IHLRWMC), Albuquerque, New Mexico, Apr 10—14, paper 3458, (2011).

[A9]   ZEACHANDIRIN, A., DALLONGEVILLE, M., PURCELL, P.C., CORY, A., 'AREVA TN and INS: Description of Fuel Integrity Project methodology principles', Packaging, Transport, Storage & Security of Radioactive Material (RAMTRANS), 22, 4, (2011).

[A10]   ETO, S., TANI, J., SHIRAI, K., et al., "Measurement of concentration of chlorine attached to a stainless steel canister material using laser induced breakdown spectroscopy", Spectrochimica Acta part B, 87, 74—80, Elsevier, London, (2013).

[A11]   ETO, S., T. FUJII, T., SHIRAI, K., "Development of measurement technology of chlorine attached on canister using laser –Application of LIBS using collinear geometry-", CRIEPI report H11020, Japan, (2012). (in Japanese).

[A12]   ETO, S., MIURA, Y., TANI, J., et al., "Effect of residual stress induced by pulsed-laser irradiation on initiation of chloride stress corrosion cracking in stainless steel", Mat. Sci. Eng. A-Struct., 590, 433—439, (2014).

[A13]   MATSUMURA, T., SHIRAI, K., SAEGUSA, T., "Verification method for durability of reinforced concrete structures subjected to salt attack under high temperature conditions," Nuclear Engineering Design, 238, 1181—1188, (2008).

[A14]   SHIRAI, K., TANI, J., GOTOH, M., WATARU, M., SCC Evaluation of Multi-Purpose Canister in Long Term Storage, in Proceedings of PSAM 11, 25—29 June, 2012, Helsinki, Finland, ISBN: 9781622764365, Curran Associates, (2012).

[A15]   WATARU, M., et al., 'Long term Containment Performance Test of Metal Cask for Spent Nuclear Fuel Storage', PSAM, 25-29 June, 2012, Helsinki, Finland, (2012).

[A16]   TAKEDA, H., WATARU, M., SHIRAI, K., SAEGUA, T., "Development of detecting method of helium gas from canister", Nucl. Eng. Design, 238, 1220—1226, (2008).

[A17]   KAMIMURA, K., et. al., "Integrity Criteria of Spent Fuel for Dry Storage in Japan", International Seminar on Spent Fuel Storage (ISSF) 2010, Central Research Institute of Electric Power Industry, 15—17 November, Tokyo, Japan, (2010).

[A18]   OZAWA, M., HIROSE, T., MIURA, H., BABA, T., KAMIMURA, K., AOMI, M., YASUDA, T., MURAKAMI, T.K., SHINOHARA, Y., Fuel Rod Mechanical Performance Under Dynamic Load Condition on High Burn-up Spent Fuel of BWR and PWR, PATRAM 2013, 18—23 August, San Francisco, USA, (2013).

[A19]   HIROSE, T., OZAWA, M., MIURA, H., BABA, T., KAMIMURA, K., et al. "Dynamic Load Impact Tests on High Burnup Spent Fuel Rods of BWR and PWR", NuMat 2012: the Nuclear Materials conference, Osaka, Japan, 22—25 October, (2012).

[A20]   HIROSE, T., OZAWA, M., MIURA, H., BABA, T., KAMIMURA, K., "Research on Integrity of High Burnup Spent Fuel under Long Term Dry Storage and Transport," OECD/NEA International Workshop on Safety of Long Term Interim Storage Facilities, Munich, Germany, May, (2013).

[A21]   KIM, Y., KIM, J., KOOK, D., KIM, Y., 'Effects of hoop stress on the hydride reorientation in spent nuclear fuel cladding', Trans. of Korean Nuclear Society Autumn meeting, Gyeongju, Korea, Ocotober 25—26, (2012).

[A22]   TORRES, E., RUIZ-HERVÍAS, J., MARTIN-RENGEL, M.A., Drop-weight ring compression test for evaluating the mechanical behaviour of fuel rods under impact conditions. PATRAM 2013, 18—23 August, San Francisco, USA, (2013).

[A23]   MARTIN-RENGEL, M.A., Integridad estructural de vainas de combustible nuclear en condiciones de almacenamiento temporal en seco, PhD thesis, Universidad Politécnica de Madrid, ENRESA technical publication 05-2010 (in Spanish), (2009).

[A24]   STANDRING P. N., HANDS B. J., MORGAN S., BROOKS A., Development of an alternative corrosion inhibitor for the storage of advanced gas cooled reactor fuel, In Press Proc. International Conference on Management of Spent Fuel from Nuclear Power Reactors, 31 May–4 June, Vienna, Austria (2010).

[A25]   ELECTRIC POWER RESEARCH INSTITUTE, Extended Storage Collaboration Program International Perspectives on Technical Gaps Associated with Extended Storage and Transportation of Used Nuclear Fuel, EPRI, Palo Alto, CA, EPRI 1026481, (2012).

[A26]   ELECTRIC POWER RESEARCH INSTITUTE, Failure Modes and Effects Analysis (FMEA) of Welded Stainless Steel Canisters for Dry Cask Storage Systems, EPRI, Palo Alto, CA, EPRI 3002000815, (2013).

[A27] ELECTRIC POWER RESEARCH INSTITUTE, Criticality Risks During Transportation of Spent Nuclear Fuel, EPRI, Palo Alto, CA, EPRI 1016635, (2008).

[A28] ELECTRIC POWER RESEARCH INSTITUTE, Transportation of Commerical Spent Nuclear Fuel, EPRI, Palo Alto, CA, EPRI 1016637, (2010).

[A29] ELECTRIC POWER RESEARCH INSTITUTE, Benchmarks for Quantifying Fuel Reactivity Depletion Uncertainty, EPRI, Palo Alto, CA, EPRI 1022909, (2011).

[A30] BILLONE, M.C., BURTSEVA, T.A., EINZIGER, R.E., "Ductile-to-brittle transition temperature for high burnup cladding alloys exposed to simulated drying—storage conditions", Journal of Nuclear Materials, 433, 431—448, (2013).

[A31] WANG, J-A., WANG, H., BEVARD, B.B., HOWARD, R.L., FLANAGAN, M.E., "Reversible Bending Fatigue Test System for Investigating Vibration Integrity of Spent Nuclear Fuel during Transportation', Proceedings of the 17th International Symposium on the Packaging and Transportation of Radioactive Materials - PATRAM 2013, August 18 — 23, San Francisco, CA, USA, (2013).

[A32] MILLER, L., et.al, Vacuum Drying Test Plan - Public Version, U.S. Nuclear Regulatory Commission, Contract No. NRC–02–07–C–006, ML13192AA127, (2013).

[A33] MILLER, L., et.al., Overview of Vacuum Drying Methods and Factors Affecting the Quantity of Residual Water After Drying – Public Version, U.S. Nuclear Regulatory Commission Contract No. NRC–02–07–006, ML13192A125, (2013).

[A34] JUNG, H., et.al. Extended Storage and Transportation: Evaluation of Drying Adequacy, U.S. Nuclear Regulatory Commission Contract NRC–02–07–006, ML13169A039, (2012).

[A35] OBERSON, G., et.al., U.S. NRC Sponsored Research on Stress Corrosion Cracking Susceptibility of Dry Storage Canister Materials in Marine Environments, 2013 Waste Management Symposium, February 24— 28, Phoenix, AZ, (2013).

[A36] AHN, T., OBERSON, G., DEPAULA, S., Chloride-Induced Stress Corrosion Cracking of Austenitic Stainless Steel for Dry Storage of Spent Nuclear Fuel, PRiME 2012, The Electrochemical Society, Honolulu, Hawaii, October 7 – 12, (2012).

[A37] CASERES, L., MINTZ, T.S., Atmospheric Stress Corrosion Cracking Susceptibility of Welded and Unwelded 304, 304L, and 316L Austenitic Stainless Steels Commonly Used for Dry Cask Storage Containers Exposed to Marine Environments, NUREG/CR-7030, (2010).

[A38] GONZALEZ, F., BAJWA, C., EASTON, E., EINZIGER, R., YANG, J., HNETKOVSKY, E., "Spent Nuclear Fuel Transportation Package Seals in Beyond Design Basis Temperature Excursions" in Proceedings of the ASME 2012 Pressure Vessels & Piping Division Conference-PVP2012, July 15 — 19, Toronto, Ontario, Canada, (2012).

[A39] GONZALEZ, F., BAJWA, C., EASTON, E., EINZIGER, R., YANG, J., HNETKOVSKY, E., "Transportation Package Seal Performance in Beyond Design Basis Thermal Exposures",– in Proc. Waste management 2012 Confer., Phoenix, AZ, paper 12472, (2012).

[A40] YANG, J., HNETKOVSKY, E., "Performance of Metal and Polymeric O-Ring Seals in Beyond-Design-Basis Temperature Excursions", NUREG/CR-7115, (2011).

[A41]   EINZIGER, R., "An Aging Management Plan for Spent Fuel Storage and Transportation", Radwaste Solutions, Vol. 20, No. 1, p. 38, (2013).

CONTRIBUTORS TO DRAFTING AND REVIEW

Brezina, M.	Department of Structural Analysis, VUJE a.s., Trnava, Slovakia
Dus, J.	Eidgenőssisches Nuklearsicherheitsinspektorat (ENSI), Brugg, Switzerland
Einziger, R.	United States Nuclear Regulatory Commission (NRC), Washington, DC, United States of America
Fernandez, J.	Empresas Nacional de Residuos Radioactivos, S.A. (ENRESA), Madrid, Spain
Hillier, A.	Spent Fuel Management Department, Sellafield Ltd., Seascale, United Kingdom
Issard, H.	AREVA NC, St. Quentin En Yvelines, France
Jussofie, A.	Gesellschaft fuer Nuklear Service m.b.H (GNS), Essen, Germany
Kamimura, K.	Safety Standards Division, Japan Nuclear Energy Safety Organization (JNES), Tokyo, Japan
Kook, D-H.	Korea Atomic Energy Research Institute (KAERI), Daejeon, Korea
Kyffin, J.	Spent Fuel Management Department, Sellafield Ltd., Seascale, United Kingdom
Kupca, L.	Department of Structural Analysis, VUJE a.s., Trnava, Slovakia
Machiels, A.	Electric Power Research Institute (EPRI), Palo Alto, CA, United States of America
Rondinella, V.	Institute for Transuranium Elements, European Commission - Joint Research Centre, Eggenstein-Leopoldshafen, Germany
Saegusa, T.	Central Research Institute of Electric Power Industry (CRIEPI), Chiba, Japan
Sasahara, A.	Central Research Institute of Electric Power Industry (CRIEPI), Komae, Japan
Standring, P.	International Atomic Energy Agency
Takats, F.	TS Enercon Kft. International Consulting, Budapest, Hungary
Vizcaino, P.	Centro Átomico Ezeiza, Comisión Nacional de Energía Atómica, Buenos Aires, Argentina

Research Coordination Meetings

Tokyo, Japan: 6–10 November 2010
Charlotte, United States of America: 14–18 May 2012
Busan, Korea of Republic: 4–8 November 2013

Consultants Meetings

Vienna, Austria: 14–16 December 2009;
18–20 March 2013; 8–11 May 2014

ORDERING LOCALLY

In the following countries, IAEA priced publications may be purchased from the sources listed below or from major local booksellers.

Orders for unpriced publications should be made directly to the IAEA. The contact details are given at the end of this list.

AUSTRALIA
DA Information Services
648 Whitehorse Road, Mitcham, VIC 3132, AUSTRALIA
Telephone: +61 3 9210 7777 • Fax: +61 3 9210 7788
Email: books@dadirect.com.au • Web site: http://www.dadirect.com.au

BELGIUM
Jean de Lannoy
Avenue du Roi 202, 1190 Brussels, BELGIUM
Telephone: +32 2 5384 308 • Fax: +32 2 5380 841
Email: jean.de.lannoy@euronet.be • Web site: http://www.jean-de-lannoy.be

CANADA
Renouf Publishing Co. Ltd.
5369 Canotek Road, Ottawa, ON K1J 9J3, CANADA
Telephone: +1 613 745 2665 • Fax: +1 643 745 7660
Email: order@renoufbooks.com • Web site: http://www.renoufbooks.com

Bernan Associates
4501 Forbes Blvd., Suite 200, Lanham, MD 20706-4391, USA
Telephone: +1 800 865 3457 • Fax: +1 800 865 3450
Email: orders@bernan.com • Web site: http://www.bernan.com

CZECH REPUBLIC
Suweco CZ, spol. S.r.o.
Klecakova 347, 180 21 Prague 9, CZECH REPUBLIC
Telephone: +420 242 459 202 • Fax: +420 242 459 203
Email: nakup@suweco.cz • Web site: http://www.suweco.cz

FINLAND
Akateeminen Kirjakauppa
PO Box 128 (Keskuskatu 1), 00101 Helsinki, FINLAND
Telephone: +358 9 121 41 • Fax: +358 9 121 4450
Email: akatilaus@akateeminen.com • Web site: http://www.akateeminen.com

FRANCE
Form-Edit
5 rue Janssen, PO Box 25, 75921 Paris CEDEX, FRANCE
Telephone: +33 1 42 01 49 49 • Fax: +33 1 42 01 90 90
Email: fabien.boucard@formedit.fr • Web site: http://www.formedit.fr

Lavoisier SAS
14 rue de Provigny, 94236 Cachan CEDEX, FRANCE
Telephone: +33 1 47 40 67 00 • Fax: +33 1 47 40 67 02
Email: livres@lavoisier.fr • Web site: http://www.lavoisier.fr

L'Appel du livre
99 rue de Charonne, 75011 Paris, FRANCE
Telephone: +33 1 43 07 50 80 • Fax: +33 1 43 07 50 80
Email: livres@appeldulivre.fr • Web site: http://www.appeldulivre.fr

GERMANY
Goethe Buchhandlung Teubig GmbH
Schweitzer Fachinformationen
Willstätterstrasse 15, 40549 Düsseldorf, GERMANY
Telephone: +49 (0) 211 49 8740 • Fax: +49 (0) 211 49 87428
Email: s.dehaan@schweitzer-online.de • Web site: http://www.goethebuch.de

HUNGARY
Librotade Ltd., Book Import
PF 126, 1656 Budapest, HUNGARY
Telephone: +36 1 257 7777 • Fax: +36 1 257 7472
Email: books@librotade.hu • Web site: http://www.librotade.hu

INDIA

Allied Publishers
1st Floor, Dubash House, 15, J.N. Heredi Marg, Ballard Estate, Mumbai 400001, INDIA
Telephone: +91 22 2261 7926/27 • Fax: +91 22 2261 7928
Email: alliedpl@vsnl.com • Web site: http://www.alliedpublishers.com

Bookwell
3/79 Nirankari, Delhi 110009, INDIA
Telephone: +91 11 2760 1283/4536
Email: bkwell@nde.vsnl.net.in • Web site: http://www.bookwellindia.com

ITALY

Libreria Scientifica "AEIOU"
Via Vincenzo Maria Coronelli 6, 20146 Milan, ITALY
Telephone: +39 02 48 95 45 52 • Fax: +39 02 48 95 45 48
Email: info@libreriaaeiou.eu • Web site: http://www.libreriaaeiou.eu

JAPAN

Maruzen Co., Ltd.
1-9-18 Kaigan, Minato-ku, Tokyo 105-0022, JAPAN
Telephone: +81 3 6367 6047 • Fax: +81 3 6367 6160
Email: journal@maruzen.co.jp • Web site: http://maruzen.co.jp

NETHERLANDS

Martinus Nijhoff International
Koraalrood 50, Postbus 1853, 2700 CZ Zoetermeer, NETHERLANDS
Telephone: +31 793 684 400 • Fax: +31 793 615 698
Email: info@nijhoff.nl • Web site: http://www.nijhoff.nl

Swets Information Services Ltd.
PO Box 26, 2300 AA Leiden
Dellaertweg 9b, 2316 WZ Leiden, NETHERLANDS
Telephone: +31 88 4679 387 • Fax: +31 88 4679 388
Email: tbeysens@nl.swets.com • Web site: http://www.swets.com

SLOVENIA

Cankarjeva Zalozba dd
Kopitarjeva 2, 1515 Ljubljana, SLOVENIA
Telephone: +386 1 432 31 44 • Fax: +386 1 230 14 35
Email: import.books@cankarjeva-z.si • Web site: http://www.mladinska.com/cankarjeva_zalozba

SPAIN

Diaz de Santos, S.A.
Librerias Bookshop • Departamento de pedidos
Calle Albasanz 2, esquina Hermanos Garcia Noblejas 21, 28037 Madrid, SPAIN
Telephone: +34 917 43 48 90 • Fax: +34 917 43 4023
Email: compras@diazdesantos.es • Web site: http://www.diazdesantos.es

UNITED KINGDOM

The Stationery Office Ltd. (TSO)
PO Box 29, Norwich, Norfolk, NR3 1PD, UNITED KINGDOM
Telephone: +44 870 600 5552
Email (orders): books.orders@tso.co.uk • (enquiries): book.enquiries@tso.co.uk • Web site: http://www.tso.co.uk

UNITED STATES OF AMERICA

Bernan Associates
4501 Forbes Blvd., Suite 200, Lanham, MD 20706-4391, USA
Telephone: +1 800 865 3457 • Fax: +1 800 865 3450
Email: orders@bernan.com • Web site: http://www.bernan.com

Renouf Publishing Co. Ltd.
812 Proctor Avenue, Ogdensburg, NY 13669, USA
Telephone: +1 888 551 7470 • Fax: +1 888 551 7471
Email: orders@renoufbooks.com • Web site: http://www.renoufbooks.com

United Nations
300 East 42nd Street, IN-919J, New York, NY 1001, USA
Telephone: +1 212 963 8302 • Fax: 1 212 963 3489
Email: publications@un.org • Web site: http://www.unp.un.org

Orders for both priced and unpriced publications may be addressed directly to:

IAEA Publishing Section, Marketing and Sales Unit, International Atomic Energy Agency
Vienna International Centre, PO Box 100, 1400 Vienna, Austria
Telephone: +43 1 2600 22529 or 22488 • Fax: +43 1 2600 29302
Email: sales.publications@iaea.org • Web site: http://www.iaea.org/books